
Adhesion of Polyurethane-Steel Hybrids and Influence of Annealing on its Durability and Lifetime



TECHNISCHE UNIVERSITÄT
CHEMNITZ

Von der Fakultät für Maschinenbau der
Technische Universität Chemnitz

genehmigte

Dissertation
zur Erlangung des akademischen Grades

**Doktor-Ingenieur
(Dr.-Ing.)**

vorgelegt von

MSc.-Ing. Jaime Alejandro Puentes Parodi
aus Bogotá, Kolumbien

Eingereicht am: 04. Januar 2018
Tag der mündlichen Prüfung: 20. Juni 2018

Gutachter: Prof. Dr.-Ing. Michael Gehde
Prof. Dr.-Ing. Udo Wagenknecht

Bibliografische Beschreibung

Puentes-Parodi, Jaime Alejandro

Thema: Adhesion of Polyurethane-Steel Hybrids and Influence of Annealing on its Durability and Lifetime

Dissertation an der Fakultät für Maschinenbau der Technischen Universität Chemnitz, Professur Kunststoffe, Chemnitz den 20.06.2018

154 Seiten, 127 Abbildungen, 31 Tabellen, 162 Literaturzitate

Referat:

Heutzutage decken Polymer-Metall-Hybride eine breite Palette von fortschrittlichen Anwendungen ab, insbesondere in der Automobil- oder Luftfahrtindustrie, wo hochleistungsfähige und leichte Komponenten sehr gefragt sind. Hybridbauteile ersetzen hier vorrangig Metallstrukturen in diversen Anwendungen. Diese reichen von Gerätegehäusen über Fahrradrahmen bis hin zu komplexen elektromechanischen Montageteilen, die eine Kombination von Eigenschaften erfordern. Beispielsweise in elektrischen Servolenkungen, Xenonbeleuchtungen oder Sensoren [1,2]. Hybride können zusätzliche Funktionalität in Bezug auf Festigkeit, Haltbarkeit, Stoßfestigkeit und Verschleißfestigkeit bieten, ohne dabei die Größe oder das Gewicht der gesamten Komponente zu beeinträchtigen. Es bestehen jedoch immer noch Herausforderungen hinsichtlich der Verbesserung der Haftung zwischen unterschiedlichen Materialien, wie z.B. Metallen, gegenüber polymeren Verbundwerkstoffen. Es besteht ein Mangel an Forschung über den Einfluss einer Wärmebehandlung auf Adhäsion und Haltbarkeit in Polymer-Metall-Hybriden, die durch Umspritzen von Einlegern im Spritzgießprozess hergestellt werden. Weiter existiert auch ein Forschungsbedarf für die Verwendung von Haftvermittlern, die gleichzeitig als Korrosionsschutz für metallische Substrate dienen um den Lebenszyklus der Komponenten zu verlängern, wenn sie verschiedenen Umgebungsbedingungen ausgesetzt werden.

Ziel war es, den Einfluss der Wärmebehandlung auf die Haftfestigkeit und Haltbarkeit des Metall-Kunststoff-Verbundes unter Berücksichtigung physikalisch-chemischer und mechanischer Wechselwirkungen zu untersuchen. Versagensarten und Lebensdauern wurden nach der hygrothermischen Alterung abgeschätzt, bei der verschiedene Temperaturen und Feuchtigkeitsgrade unabhängig voneinander bewertet wurden. Somit war es möglich die Variable zu identifizieren, welche den Lebenszyklus des Hybridteils am stärksten beeinflusst. Lebenszeitvorhersagen, berechnet aus kinetischen Parametern für die Zersetzung (aus der thermogravimetrischen Analyse), wurden experimentell mit starren Polyurethan-Stahl-Hybriden validiert, die üblicherweise als Fernwärmerohre verwendet werden. Methoden wie Konfokal-, Rasterkraft- (AFM) und Rasterelektronenmikroskopie (REM) wurden zur Bewertung der verschiedenen Oberflächen eingesetzt. Um die Veränderungen der organischen Strukturen zu untersuchen wurden verschiedene Techniken wie Fourier-Transformations-Infrarotspektroskopie (FTIR), Röntgenphotoelektronenspektroskopie (XPS) und energiedispersive Röntgenstrahlung (XDS) verwendet. Der Einfluss des Temperns auf die Haftfestigkeit, die Versagensarten und die Haltbarkeit des Hybrids wurde durch Schäl- und Zugversuche, thermische Analyse (TGA, DSC) und Permeationsuntersuchungen bestimmt.

Abstract

Nowadays, polymer-metal hybrids are covering a broad range of advanced applications, especially in the automotive or aerospace industries where high performance and lightweight components are highly demanded. Hybrid parts may offer additional functionality regarding strength, durability, impact and wear resistance without sacrificing size or weight of the full component. However, there are still challenges regarding improving the adhesion between dissimilar materials such metals to polymers and its composites. There is a lack of research about the influence of a post heat treatment on adhesion and durability in polymer-metal hybrids manufactured through an overmolding processing chain. There is also a need for using adhesive promoters that may offer simultaneous corrosion protection to metallic substrates in order to extend the lifecycle of the part when subjected to diverse harsh environments.

In this work, two organic coatings used as adhesive promoters on steel substrates were investigated: the first one is a polyester-based powder-coat adhesive developed in the Leibniz-Institute in Dresden. The second one is a high performance anti-corrosive electrophoretic paint that has never been reported in the literature as an intermediate adhesive layer in a thermoplastic-polyurethane (TPU) overmolding processing chain. A TPU was overmolded on both pre-coated steel substrates, and the adhesion of the polymer to the metal substrate was investigated after a heat treatment (annealing), and a subsequent hygrothermal aging at different temperature-humidity conditions. The influence of the annealing process on the adhesion and durability of the multilayered specimen was investigated in depth; similarly, failure modes and lifetimes were evaluated after the hygrothermal aging. Lifetime predictions calculated from kinetic parameters for solid decomposition -obtained from thermogravimetric analysis- were validated experimentally with polyurethane-steel hybrids commonly used as district heat pipes.

Adhesion of TPU on the steel substrate using both organic coatings as adhesive promoters was successful due to the contribution of new physical-chemical and mechanical interactions at the polymer-coating interface, especially after annealing at 100 °C for 20 h. Additionally, heat treated hybrids exhibited a much better performance because of the apparent increased in the anchoring density at the polymer-metal interfaces. It is conclusive that progressive failure of the multilayered specimen is strongly dependent on water diffusion rather than thermolysis of any of the components, as it was detected by FTIR, and observed in the micrographs on the artificially-aged hybrid surfaces.

Finally, accelerated aging was used to correlate lifetime predictions throughout the analysis of the kinetics of degradation using TGA experiments and mechanical tests. The calculated values of the activation energy evidence that durability of the polyurethane-based polymers is affected by temperature and humidity at the conditions described in this work. Lifecycle is directly related to kinetic parameters, and especially to the activation energy, E_A . This kinetic parameter for pre-aged specimens, and particularly for those subjected to higher temperature conditions, were lower when compared to the fresh polymer; as it was demonstrated that TGA analysis is a primary tool to predict lifetime for thermoplastic and thermosetting polyurethanes.

Keywords: TPU, polymer-metal hybrid, injection molding, adhesion, annealing, hygrothermal aging, thermal degradation, lifetime.

Acknowledgement

First and foremost, I want to thank Dr. Ines Kühnert for accepting me in her research group at the Leibniz-Institute in Dresden. Her remarkable support, help, and advices in these 4 years in Dresden, not only in scientific matters but also in administrative and day-to-day issues were primordial to have reached this stage of my professional career. I also appreciate the opportunities and motivation she gave me to attend international conferences overseas where I growth my knowledge and expertise.

Special thanks to my co-supervisor, Dr. Andreas Leuteritz, for all fruitful and interesting discussions, for his suggestions and guidance on the scientific and experimental work, and his friendly character and patience. I would like to thank also Prof. Gert Heinrich and Prof. Udo Wagenknecht in Dresden for opening me the doors of the Leibniz-Institute. I will never forget my very first interviews with them and their friendly and openness attitude.

In the TU Chemnitz, I would like to express my gratitude to Prof. Michael Gehde for allowing me to be part of his outstanding Polymer Materials Department and his cooperation and assistance in the academic and administrative issues that allow me to take this work to a successful end.

I have to express my gratitude to all members of the “Formgebungsprozesse und Simulation”. My thanks go with more appreciation to Leandro Santoro for his enormous help in the preparation of specimens and taking care of experiments; to Matthieu Fischer for his interesting and worthy discussions and his help in solving day-to-day issues at the IPF; finally to Martin Zimmermann for setting up the experimental devices and his cooperation in the experimental part.

In the Processing Department, I also like to deliver my sincere appreciation to Dr. Regine Boldt, Andreas Scholze, Maria auf der Landwehr, Anna Ivanov and Bernd Kretzschmar for their support in the preparation of specimens and development of my experimental work. Many thanks also to the secretary Anne Hofmann who always had a very friendly and supportive disposition in all administrative issues.

I must also extend my thankfulness in the Reactive Processing group in particular to Dr. Michaela Gedan-Smolka for all her knowledge and discussions concerning to the adhesive powder-coating, to Marcel Tuschla, Antje Schneider, and Lisa Ziegler for their help in the preparation of the coating and assist in the setup of experimental tests.

I am truly grateful also to people in other Departments at IPF, especially to Dr. Mikhail Malanin and Dr. Lottar Jakisch for their experimental setup concerning spectroscopy, Dr. Astrid Drechsler and Matthias Holzschuh for interfacial evaluation, Dr. Ulrike Staudinger for the electrical resistivity measurements, Liane Häußler and Sabine Krause for thermal analysis, and last but not least, to Holger Scheibner and Kristina Eichhorn for all mechanical tests to hundreds of specimens.

For the financial support, I am really thankful to the “Verein zur Förderung des Leibniz-Institutes für Polymerforschung Dresden e. V.” for its support in all international Conferences. Great thanks to Colciencias in Colombia for its generous scholarships to encourage young people to go out and learn all new technologies and scientific methods to transfer them back to the country.

Last but not least, I am indebted to my beloved family in Colombia and New Zealand for being always there to give all support and affection.

Jaime Alejandro Puentes Parodi
Dresden, December 2017.

Table of Contents

1.	Introduction and Motivation	1
2.	Theoretical Background on Polymer-Metal Hybrids	3
2.1.	Importance of Polymer-Metal Hybrids	3
2.2.	Applications and Properties	3
2.3.	Components of a Polymer-Metal Hybrid	5
2.3.1.	Metal Substrates	5
2.3.2.	Polymers.....	5
2.4.	Trends in Polymer-Metal Joining Technologies	6
2.5.	Adhesion and Physical-Chemical Interactions at Polymer-Metal Interfaces.....	12
2.6.	Thermoplastic Polyurethane-Steel hybrids	17
2.6.1.	Steel as Substrate	17
2.6.2.	Thermoplastic Elastomer Urethane (TPU).....	21
2.6.3.	Polymer-Steel Adhesion Promoters	25
2.6.4.	Influence of Annealing on Adhesion of a Polymer-Steel Hybrid.....	27
2.7.	Durability and Long Time Performance of a Polyurethane-Steel Hybrid	28
2.7.1.	Aging in Metal Substrates.....	28
2.7.2.	Aging in TPU	29
2.7.3.	Aging in Adhesive Coatings.....	31
2.7.4.	Aging in Polymer-Metal Hybrids.....	33
2.7.5.	Lifetime Estimations in Polymer-Metal Hybrids	36
2.8.	Conclusive Remarks (Challenges) and Aims of the Work	37
3.	Experimental	39
3.1.	Materials	39
3.1.1.	Steel Substrates.....	39
3.1.2.	Thermoplastic Polyurethane, TPU	40
3.1.3.	Adhesive Powder Coating.....	41
3.2.	Composite Preparation	41
3.2.1.	Steel Sheet Preparation.....	42
3.2.2.	Powder Coating	42
3.2.3.	The Overmolding Process	43

III Table of Contents

3.2.4.	Annealing	44
3.2.5.	Summary of Prepared Specimens	44
3.2.6.	Summary of Adhesion Mechanisms in the Polymer-Metal Hybrid.....	45
3.3.	Characterization Methods and Equipment	47
3.3.1.	Mechanical Test	47
3.3.2.	Thermal Analysis	48
3.3.3.	Surface Analysis.....	50
3.3.4.	Infrared Spectroscopy Examination - FTIR.....	52
3.3.5.	Permeation of Gases through the TPU.....	53
3.3.6.	Accelerated Hygrothermal Aging	54
EXPERIMENTAL RESULTS AND DISCUSSION.....		56
4.	Surface Analysis of Steel Substrates.....	56
4.1.	Microscopic Surface Characterization of Steel and Coated Substrates	56
4.2.	Dynamic Contact Angle Measurement	57
4.3.	Surface Chemical Characterization	58
4.3.1.	Fourier Transformed Infrared Spectroscopy - FTIR	58
4.3.2.	X-Ray Photoelectron Spectroscopy - XPS	59
4.4.	Metal Surface Resistivity Measurements.....	61
5.	Effects of Annealing on Adhesion and Mechanical Performance of the Hybrid.....	62
5.1.	TPU Performance	62
5.1.1.	Molecular Mechanisms of Deformation of the Neat Polyester-based TPU.....	62
5.1.2.	Effects of Different Annealing Temperatures on Mechanical Performance.....	64
5.1.3.	Analysis of Thermal Properties.....	64
5.2.	Adhesion of TPU to the Metal Substrate	65
5.2.1.	Adhesion of TPU Through the in-house Adhesive Coating.....	65
5.2.2.	Adhesion of TPU Through the e-coat	67
5.2.3.	Interactions at TPU/in-house and TPU/e-coat Interfaces	68
5.3.	Influence of Annealing on Adhesion Strength.....	68
5.3.1.	Failure modes of Annealed Hybrids	70
5.3.2.	Effects of Different Annealing Temperatures on Adhesion: Thermal Analysis.....	71
5.4.	Thermal Analysis of Adhesive Coatings.....	73

5.4.1.	On in-house Coating	73
5.4.2.	On e-coat	75
5.5.	Chapter Summary	76
6.	Hygrothermal Aging and Failure Modes of TPU-Steel Hybrids	81
6.1.	Annealing and Hygrothermal Aging on Neat TPU Strips: Mechanical Performance	81
6.2.	Failure Modes at the Polymer-Metal Joints After Annealing and Aging	84
6.3.	Influence of Hygrothermal Aging on Adhesion Strength	89
6.4.	Thermal Analysis of Hygrothermally Aged TPU in Contact with the Adhesive Promoters.....	90
6.5.	Effects of Hygrothermal Aging at the TPU-Steel Interface – FTIR Analysis	91
6.6.	Corrosion of the Metal Substrate and Effects at the Polymer-Metal Joint	99
6.6.1.	Thermal Properties of Hygrothermally-Aged Adhesive Coatings	103
6.7.	Chapter Summary	105
7.	Durability and Lifetime Predictions of the Polymer-Metal Composite	108
7.1.	Permeation and Diffusion	108
7.1.1.	Influence of Annealing on the Diffusion of Water Vapor in TPU: Water Uptake	108
7.1.2.	Influence of Annealing on Permeation of Gasses in TPU	109
7.1.3.	Water Vapor Diffusion in the Polymer-Metal Composite	111
7.1.4.	Diffusion Time of Water Vapor and Lifetime Estimations	113
7.2.	Chapter Summary	115
8.	Durability and Lifetime of Polyurethane-Metal Joints Under Thermal Loads	118
8.1.	Case I: Durability And Lifetime Of Overmolded Tpu On Steel Substrates	119
8.1.1.	Thermogravimetric Analysis of Aged TPU	119
8.1.2.	Thermogravimetric Analysis of Coatings in Contact with TPU	125
8.2.	Case II: Durability And Lifetime of Rigid Pur In Direct Contact With A Steel District Heat Pipe. Failure Analysis And Validation Of The TGA Method	129
8.2.1.	Materials and Methods	129
8.2.2.	Results and Discussion	131
8.3.	Chapter Summary	141
9.	Relevant Conclusions and Outlook.....	142
10.	References.....	146

1. INTRODUCTION AND MOTIVATION

Nowadays, it is found that polymer-metal hybrids are covering a wide range of advanced applications, especially in the automotive or aerospace industries where high performance and lightweight components are required [1]. Some other interesting examples [2] include hybrid joints in electric or hydrogen-powered vehicles for low electrical resistivity components; in power generation devices, strong adhesion of polymer composites to metal pieces is required for turbine blades, solar panels or fuel cells. In medical applications, it is also essential the joining of high-performance materials for orthopedics or medical devices. The main goal of hybrid components is to have the best possible functionality regarding strength, durability, impact resistance, abrasion and wear resistance without sacrificing size or weight of the full component [3]. However, there are still challenges regarding improving the adhesion between dissimilar materials such as metals to polymers and its composites. For instance, there is a very few literature [4,5] dealing with the analysis of adhesion after a post-thermal treatment in polymer-metal hybrids manufactured in an overmolding processing chain. There is also a need for using adhesive promoters that also may offer corrosion protection to the metal substrate and, therefore, a longer lifecycle for hybrid systems are expected.

It is indispensable as well that hybrids withstand all kinds of mechanical and thermal loads at diverse environmental conditions, especially under unpredictable scenarios that may lead to premature failure. Metals, in particular, steel, despite its relatively high density and low corrosion resistance, is still one of the most used materials in engineering applications due to its high mechanical strength and versatility regarding adjusting mechanical properties depending on the final use [6]. Polymers in the other hand, offer remarkable low densities but low mechanical properties that limit their functions, especially components subjected to high temperatures, high stresses or high rate impacts [7]. Nowadays, there is special interest in thermoplastic polyurethanes due to their outstanding resistance to abrasion, versatility in terms of mechanical properties, and large thermal expansion coefficients making them suitable for hybrid components where it is required to balance thermal expansion of dissimilar materials.

For all those reasons, it is necessary to combine the right materials to optimize the performance of a final product regarding mechanical properties and low weights. It is also essential an in-depth understanding of the adhesion mechanisms in the composite, especially because hybrid components are complex multilayer systems where failure may occur in any of the interfaces involved. Therefore, it will be possible to infer the failure mechanisms and predict the lifetime of the composite more accurately.

In this work two organic coatings, as adhesive promoters, on steel substrates will be investigated: the first one is a polyester-based powder-coat developed in the Leibniz Institute für Polymerforschung Dresden e. V. The second one is a high performance anti-corrosive electrophoretic paint that has never been reported in literature as an intermediate adhesive layer in a thermoplastic-polyurethane overmolding processing chain. A TPU will be overmolded on both coatings and the adhesion of the polymer to the metal substrate will be examined. Adhesion, failure modes and durability at the polymer-metal joints of the hybrid after a thermal treatment will be investigated as well. Lifetime is going to be calculated after an artificial hygrothermal aging in which temperature and humidity will be evaluated independently to identify the variable that will affect the most the durability and life cycle of the multilayered part. It is expected that this work will contribute to the polymer-metal hybrid community in the sense of giving new tools and insights with the main purpose of manufacturing much more reliable and durable hybrid components that may be used in diverse high-performance applications.

2. THEORETICAL BACKGROUND ON POLYMER-METAL HYBRIDS

2.1. IMPORTANCE OF POLYMER-METAL HYBRIDS

Polymer – metal composites or polymers in combination with non-organic materials have been used extensively for the last 20 years in sporting goods, aerospace, transportation, construction, and other engineering applications [8]. A polymer – metal composite consists of a metal substrate, generally an adhesive promotor, and the polymer component that can be adhered to the substrate. The main idea behind hybrid parts is to combine the high modulus and ultimate strengths of metal substrates with the low density and versatility of polymeric materials. The best of each material's properties will end up in a synergy of excellent performance in a final composite [6] as listed in Figure 1.

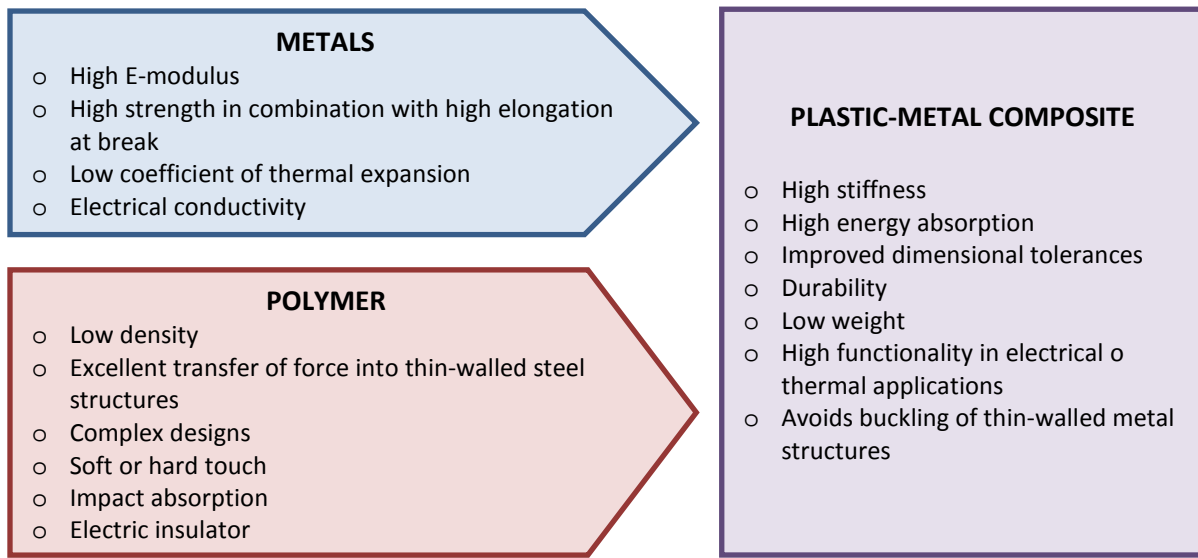


Figure 1. Polymer-metal properties combination [20].

2.2. APPLICATIONS AND PROPERTIES

The applications of Polymer-Metal Hybrids, or referred as PMH elsewhere [9], are growing in the last few years, especially in the automotive or aeronautical industry. PMH are becoming now strong competitors for applications where high mechanical loads or structural components are required. The combination of specific properties of plastics and metals in a single part can provide structural functioning that cannot be achieved in the individual constituents. Table 1 highlights the most relevant single properties of metals and polymers that could be combined to enhance the final performance of hybrid components.

Property	Steel	Al alloys	Mg alloys	Unreinf. PA	Reinf. PA (PA6GF30)	TPUs	Rigid PUR
Youngs modulus [GPa]	200	70	42	0.2 to 3.2	6.2	0.1-0.8	-
Tensile strength [MPa]	1000	455	300	10 to 100	110	50	50
Density [g/cm ³]	7.8	2.7	1.8	0.9 to 1.4	1.4	1.19	0.08
Thermal conductivity [W/mK]	30	237	62	0.1 to 0.5	0.3	0.19 to 0.25	0.023
Heat distortion temperature [°C]	+600	+100	+200	+40 to +200	+200	+60 to +180	174
Thermal expansion [K ⁻¹ · 10 ⁻⁶]	12	22	25	40 to 250	30	120 to 180	5

Table 1. Main mechanical properties of selected metals and polymers. Taken from [10–12].

Audi, in 1996, was the first automotive company that started to use a front end based on a polymer-metal hybrid structure that was fabricated by Ecia, in France. In this component, a steel sheet was combined with an elastomeric polyamide, Durethan BKV 130 from Bayer [13]. Current uses and applications of PMH can also be seen in instrument panels, bumpers, cross-beams and door modules, damping or sealing elements, door modules, among others, as displayed in Figure 2.

Nowadays, hybrid systems have been developed worldwide by companies like Lanxess [14], Dow Automotive [15], BASF Performance Polymers [16] and Evonik [17]. Non-automotive applications, from appliance housings to bicycle frames, are also growing in the market [18]. There are even applications in complex electromechanical assembled parts which require designs of electrical or electronic connectors or other combine parts in electrical servo steering, xenon lighting or sensors [19], where the polymer plays a role mainly as an isolator.

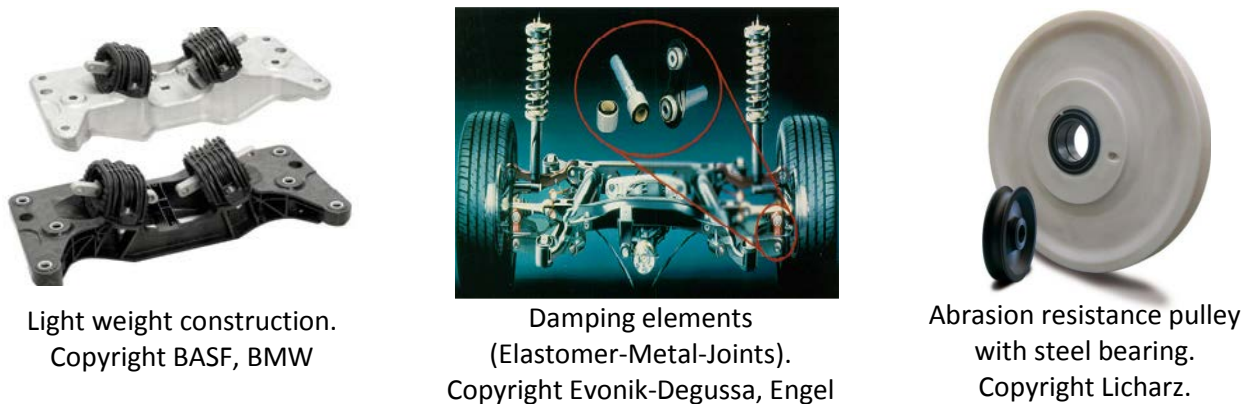


Figure 2. Examples of high performance polymer-metal composites.

2.3. COMPONENTS OF A POLYMER-METAL HYBRID

2.3.1. Metal Substrates

The preferred materials for hybrids as substrates are steel, aluminum and magnesium alloys because they offer high mechanical properties and could be used in structural parts in the automotive or aeronautical industry [18–20]. Hybrids based on steel substrates will be treated in numeral 2.6.1.

- Aluminum

Polymer-metal composites with Al alloys substrates offer relatively lower densities than steel alloys: 2,7 g/cm³ vs. 7,9 g/cm³ [6], higher electrical and thermal conductivities, and more corrosion resistance when exposed to normal environments. Applications of polymer-Al composites are limited by the low mechanical strength of Al, which requires additional processing steps -like cold working or alloying- to enhance its fatigue and tensile strengths [6].

- Magnesium

Magnesium-based hybrids are characterized by the lowest density of any structural metal, i.e. 1,7 g/cm³; consequently, it is the best option when light weight is a decisive factor. On the other hand, Mg is soft and has the lowest E-modulus of all structural metals. Another drawback is that Mg and its alloys are difficult to deform at room temperature and only a very few percentage of deformation can be achieved without cracking the metal. Regarding chemical stability, it has an excellent corrosion protection at normal conditions, but it oxidizes easily in marine applications [6,21].

2.3.2. Polymers

Among the polymeric materials used in hybrid components, the most common are the structural glass-fiber-reinforced-polymers and rubbery-like thermoplastic elastomers, TPE [22–24]. TPEs may play a role in laminate composites as intermediate material that offers shock and vibration absorption, they can also act as strain equalizers between parts with different thermal expansion coefficients; they may also bring a soft touch or grip to structural components especially in automotive industry [25]. The recent range of materials used in overmolded parts has grown considerably and includes more TPE families such as thermoplastic polyurethanes, TPU; thermoplastic vulcanizates, TPV, and styrenic block copolymers referred as SEBS. In this work a commercially available polyester-based TPU was used, and it will be described in more detail in numeral 2.6.2.

2.4. TRENDS IN POLYMER-METAL JOINING TECHNOLOGIES

There are several methods for joining dissimilar materials as in polymer-metal composites. Among the most common technologies reported are mechanical fastening, adhesive bonding, and welding processes. There are, of course, combinations of different techniques such as adhesive joining with mechanical fastening or welding and injection over molding in metallic parts [3]. Other joining methods are treated in depth in [3,8,26–31] and are summarized in Figure 3.

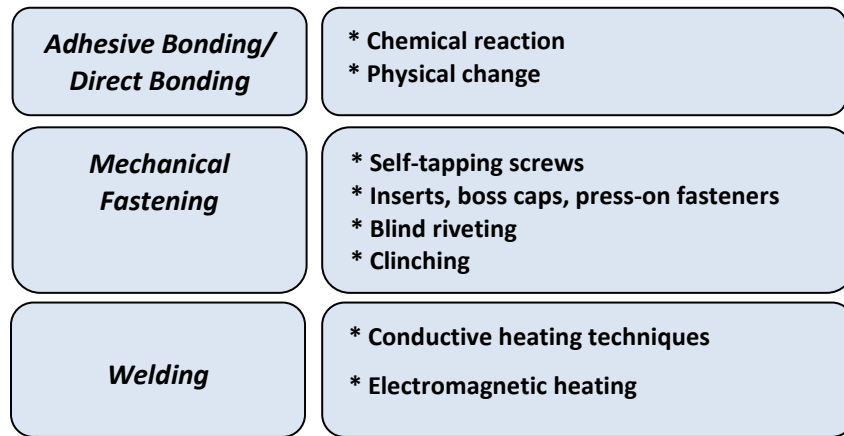


Figure 3. Common joining methods in polymer-metal composites. Adapted from [3,32,33].

In this work, the joining method of the polymer to the steel component is performed by combining adhesive bonding and injection molding technology. Adhesion is carried out by using a functionalized intermediate layer on which the polymer is injected; such a process is denominated “polymer overmolding”. Joining technologies in polymer-metal composites by overmolding have been recently described in detail by Grujicic et al. [13,22,24] and are resumed into three categories: overmolding, metal overmolding process combined with subsequent joining operations, and adhesively bonded hybrids. There is an additional category related to direct adhesion (without coupling agents) in polymer-metal hybrids that will be described in numeral 2.4.

- Metal Overmolding

Overmolding is the injection molding process, patented by Bayer in 1996, where one material, usually, is injected onto a metal insert with flared holes which allow the melted polymer penetrate through the metal structure. Then, the solidified plastic interlocks the metal substrate mechanically by a “shrink-fit” phenomenon, as seen in Figure 4.

The main purpose is to obtain a seamless combination of multiple materials into a single part or product. The overmolding process also shortens the number of steps involved in the manufacturing of a combined part, as the total part cost is reduced when compared to parts that are traditionally injected and require a further assembly step; it could also eliminate further secondary finishing processes like painting, trimming, polishing or similar [25,34,35].

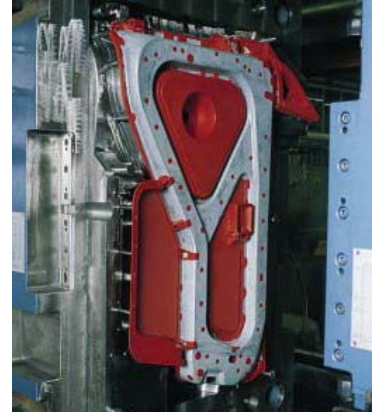


Figure 4. Overmolding of a polymer onto a stamped metal sheet. LANXESS.

Final overmolded parts have advantages to single material products due to the versatility of characteristics that can be obtained regarding design, ergonomics, vibration damping, water resistant seal, sound absorption and thermal or electrical insulation [20,25,35,36]. The overmolded polymer must be strongly bonded to the metal either by mechanical interlocking and/or by physical-chemical means, which turns to be critical for the durability and mechanical performance of the part; otherwise, even small differences or incompatibility between the materials can compromise the joint and end up in premature delamination. The use of primers or adhesives can also be essential [25] to achieve an optimal bond between two dissimilar materials, as it was done in this work.

The overmolding process is made by two commonly used techniques: single-shot and two-shot or multiple-shot technique.

Single-shot or insert molding technique

The substrate has to be placed in the mold cavity as an insert, and then the polymer is subsequently injected in a standard single-shot injection molding machine, as in Figure 5. This process is the most common in the industry because traditional machines and molds can be used, tooling costs are also lower, but it is effective only when there are short production runs. Especial care has to be taken with the inserted substrate due to impurities that can adhere to the surface and, eventually, may cause premature failure; for this reason, it is recommended utilizing gloves or special equipment when placing the substrate into the mold cavity [34].

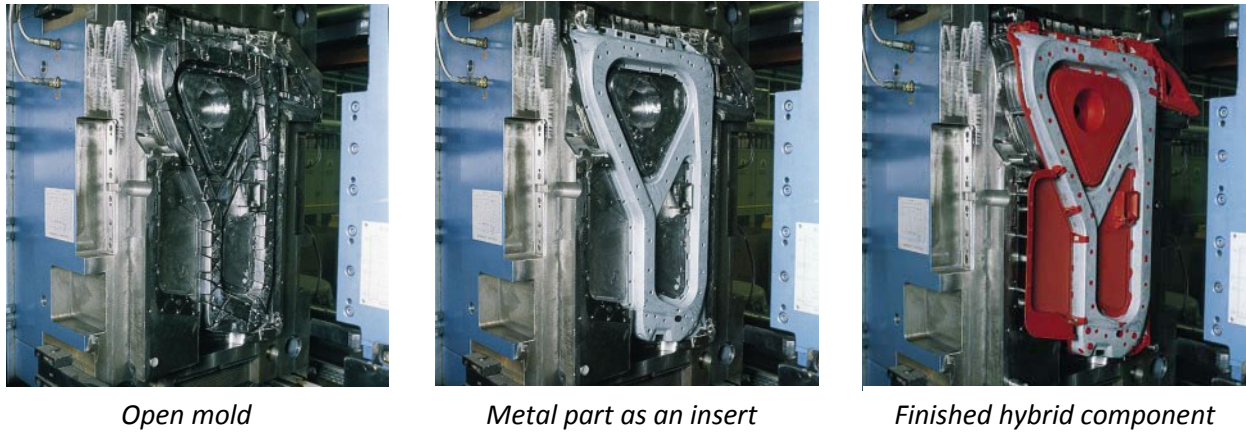


Figure 5. Industrial overmolding of plastic on a metal substrate through the single-shot/insert molding technique. Adhesion of the polymer to the metal is by mechanical interlocking. LANXESS [14].

Metal Overmolding Combined with Secondary Joining Operations.

The technology was patented by Rhodia and produced it for the front-end module of a light truck [13]. It consists of a stamped metal sheet that is coated with a thin thermoplastic reinforced polymer, generally nylon. In a subsequent step, a polymeric subcomponent structure already injected is bonded to the metal substrate by ultrasonic welding; adhesion can also be improved by designing holes in the metal sheet that eventually will allow the melted polymer to pass through, increasing the mechanical interlocking. To ensure good mechanical performance, the plastic part should have columns or crossed-beams sections as in Figure 6 a).

Metal Overmolding on Intermediate Adhesion Promoters

Adhesion of a polymer on a metal substrate by injection molding using an intermediate adhesive was patented and applied on a prototype front-end module of a Volkswagen in 2003. A glass fiber reinforced polypropylene and a low energy surface acrylic-epoxy adhesive manufactured by Dow were employed for this purpose. The hybrids manufactured under this technology bring some advantages like a reduction in the stress concentration between both dissimilar components; the adhesive also contributes to absorbing energy between the polymer and the metal surfaces, as sketched in Figure 6 b).

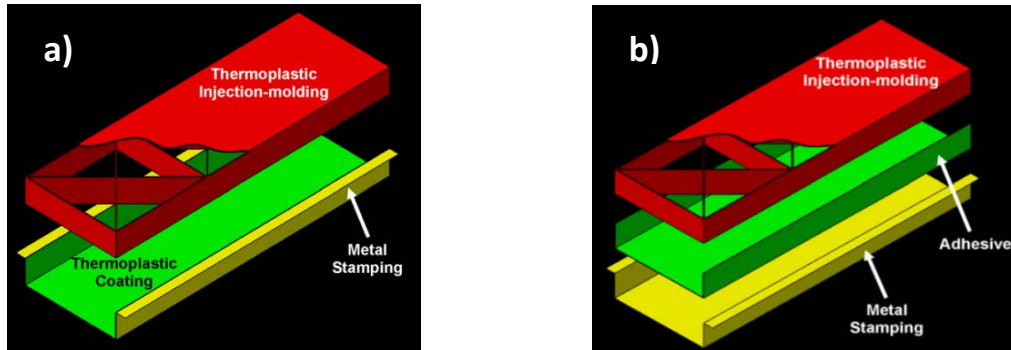


Figure 6. a) Sketch of the metal overmolding process and b) an adhesively bonded metal sheet with a thermoplastic structural component. Published with permission from Elsevier [13].

- Adhesives

The use of adhesives is the most common method to bond dissimilar materials [37]. Adhesive bonding is a versatile bonding technology due to its ease regarding bonding dissimilar materials like ceramics, plastics, metals or wood. It consists of a primer or intermediate compound which is applied superficially to a substrate or adherent. The structural joint between the two surfaces is formed after the adhesive is cured or hardened, or after a chemical reaction which takes place due to external stimuli, like heat or UV radiation. In any case, the developing of structural properties is expected [38]. As summary, Figure 7 displays a broad classification of adhesives by setting mode [66].

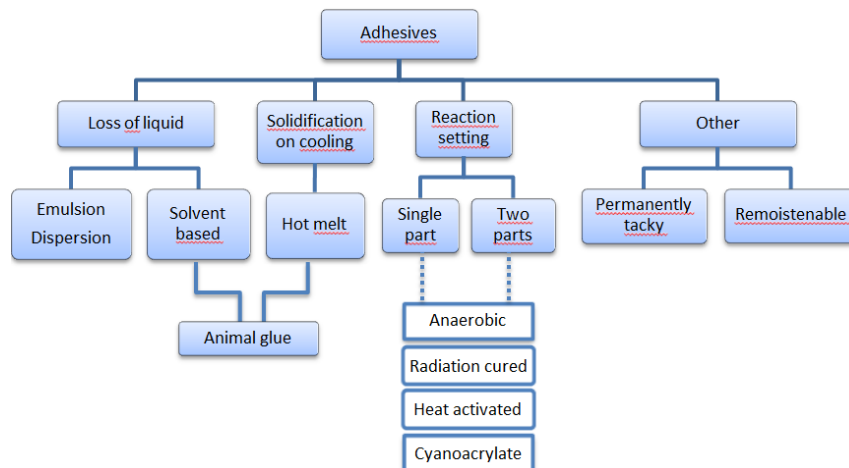


Figure 7. Classification of adhesives by setting mode [66].

In general, the most efficient adhesives are those crosslinked by chemical reactions such as epoxies, polyurethanes, silicones and phenolics. The less efficient types are those hardened by cooling from a melt, evaporation of a solvent or physical alteration. In this group, one can find hot-melts, plastics, rubber adhesives and polyvinyl acetate [33].

The most important factors for strong and durable joints are the generation of clean and rough surfaces for mechanical interlocking, good wetting of the substrate, low viscosity of the adhesive for intimate interaction and appropriate curing time [39].

Some advantages of adhesive bonding, when compared to other joining methods, are the ability to bond dissimilar materials with different thickness and surfaces. Homogeneity of the bond provides a better stress distribution and consequently a better fatigue resistance, flexibility in the design of the product and of course a very good cost/effectiveness relationship [40].

- Joining by Friction

Recent joining-by-friction technologies were developed by the Helmholtz Research Center in Geesthacht, Germany.

The first technology is denominated “Friction Spot Joining”. It is a complex technique in which the metal sheet is softened by friction generated by a specialized tool on top of the metal part. The heat flows underneath the sheet and melts a thin superficial layer at the thermoplastic interface. During the joining process, the softened metal is deformed by a tool that forms a geometrical undercut with the shape of a metallic nub. The joining of the metal to the polymer or composite is achieved mainly by mechanical interlocking and secondary adhesion forces due to the metallic nub geometry at the metal-polymer interface. Detailed information about this joining technology is explained in [41].

The second technology by friction is named “Friction Riveting”. It consists of joining a cylindrical metallic rivet inserted in a polymeric base plate. The heat generated by the high rotational speed rivet and axial pressure melts the polymer at the tip of the rivet. Local temperature increases at the tip of the metal rivet and by a forging pressure, the tip is deformed increasing its original diameter. After the consolidation pressure, the bonding at the interface is by a mechanical interlocking between the deformed rivet tip and the melted polymer [42].

Other similar joining-by-friction technologies for polymer-metal hybrid laminates, also patented by the Helmholtz Research Center, are found in [3].

- Direct Adhesion

Direct adhesion is the joining of the polymer to the metal substrate without adhesives or using interlocking holes or rivets on the metal substrate. It can be accomplished either by modifying the surface of both materials or by an in-situ reaction of the polymer on the surface of the metal. Direct

adhesion technologies are based on modifications on the surface of the metal or polymer with the main goal of increasing the roughness and hence gaining mechanical interlocking. The adhesion mechanisms here relied on the penetration of the melted polymer onto the modified metal surface at micro size level. Direct adhesion of polymers on metal parts can also be realized by a chemical modification of the polymer or by using reactive polymers, especially thermosetting plastics or elastomers that can polymerize onto the inorganic surface. A common example in

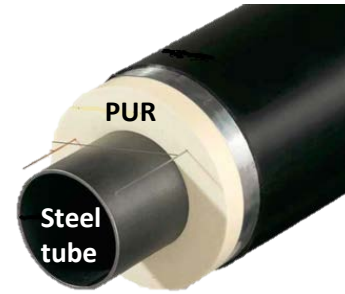


Figure 8. PUR direct adhesion on steel surface [159].

the industry are elastomers bonded directly to the metal; this technique was developed and patented by Charles Sanderson in 1862 and consisted in vulcanizing natural rubber on brass plating. In further research, it was found that the adhesive strength depended strongly on the composition of brass and the degree of vulcanization of the elastomer, as well as the surface preparation (chemical or mechanical) of the metal. This adhesive process, which occurs during the vulcanization reaction, is still the basis for the most of the rubber bonding today, and it is widely used in the automotive industry for applications that require mainly anti-vibration or shock absorber components [43,44].

Another common case of direct adhesion of a reactive polymer on metal substrates is the rigid polyurethane, PUR, bonded directly in steel tubes like the ones used in district heat pipes like the one in Figure 8. The reactivity of the PURs is attributed to the isocyanate group, which makes them very useful in adhesive applications; it is difunctional, meaning that there are at least two isocyanate groups per molecule that are very reactive in the polymerization process. Mohamed et al. [45] and Gaehde et al. [46] found a strong chemical bonding between an aromatic polyurethane that was cured on the surface of the mild steel. The explanation for the strong adhesion forces was evaluated through X-ray Photoelectron Spectroscopy (XPS) at the interface of both components. It was found that the reaction of the isocyanate groups ($R - N = C = O$) with the iron oxide layers at the metal surface ($O \cdots Fe$) produced covalent bonded carbamates ($R - NH - CO - OFe$) at the steel side as sketched on Figure 9.

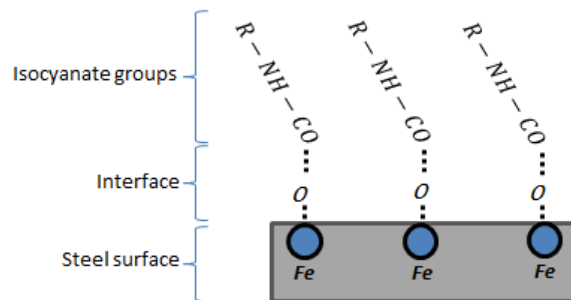


Figure 9. Chemical interaction of polyurethanes at steel surface, adapted from [45,46].

2.5. ADHESION AND PHYSICAL-CHEMICAL INTERACTIONS AT POLYMER-METAL INTERFACES

Adhesion is defined as the molecular interaction at the interface between two or more materials; it involves an adherent or substrate with an adhesive which generates an intermediate surface or an adhesive joint [39]. The thermodynamic work of adhesion can be defined mathematically as [40,47–50]:

$$W_A = \gamma_1 + \gamma_2 - \gamma_{12}$$

Equation 1. Work of adhesion

Where γ_1 is the surface energy of the substrate, γ_2 is the surface energy of the adhesive and γ_{12} corresponds to the interfacial tension between the two surfaces.

Adhesion depends on a large degree on the wettability of the adhesive on the substrate. Wettability may be explained with the real example of a liquid drop on a rigid substrate as seen in Figure 10; where γ_{SV} indicates the surface energy between solid-vapor, γ_{LV} surface energy between the liquid-vapor and γ_{SL} represents the surface energy between the solid-liquid interface.

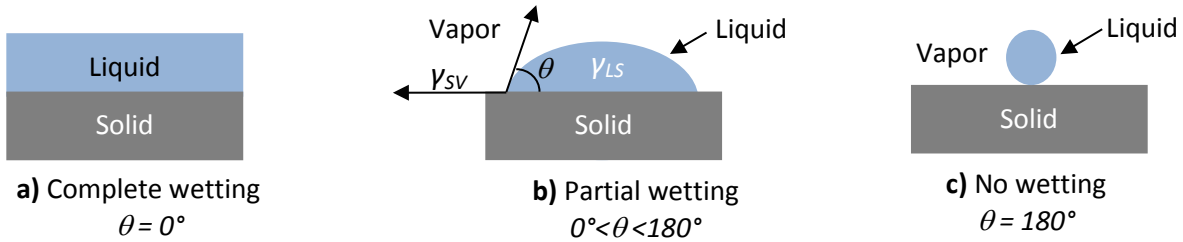


Figure 10. Interactions between liquid, solid and vapor phases and wetting of a liquid drop on a rigid surface. a) Complete hypothetical wetting on a rigid substrate, b) partial wetting with a contact angle θ , and c) no wetting occurs when the contact angle $\theta = 180^\circ$.

It could be assumed that there will be a complete wetting of the adhesive when $\gamma_{LV} + \gamma_{SL} < \gamma_{SV}$, meaning that the net free energy is reduced when the γ_{SV} is replaced by γ_{LV} and γ_{SL} together; inversely when $\gamma_{SV} + \gamma_{LV} < \gamma_{SL}$ no wetting will occur. In the case of partial wetting, which is the most common case in adhesives, equilibrium of forces must take place between the solid, liquid and the interfacial tension, so it may be expressed thermodynamically with Young's equation as follows [51]:

$$\gamma_{SV} = \gamma_{SL} + \gamma_{LV} \cos \theta$$

Equation 2. Young's equation

Where θ represents the contact angle of the drop on the substrate. Smaller angles referred to good wettability, which could mean a better bonding.

A good wettability is not necessarily an indication of good bonding forces, the final joint strength in a polymer-metal composite can be modified, positively or negatively, by a number of factors such as the electrostatic interaction between both surfaces, mechanical interlocking, primary or secondary chemical bonds, and by the formation of weak boundary layers in the region immediately adjacent to the joint interface [48].

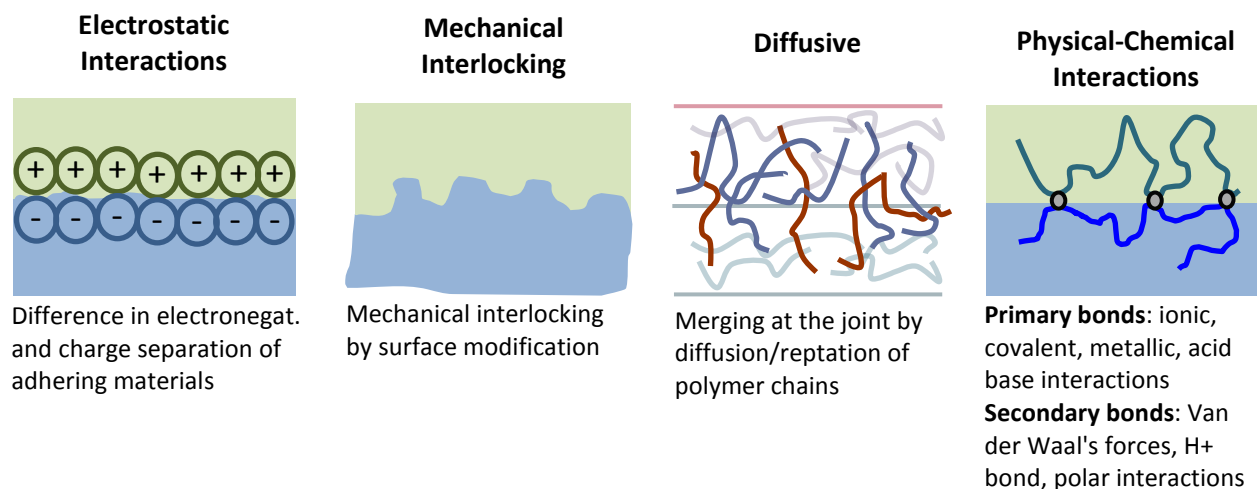


Figure 11. Principal adhesion mechanisms in polymer-metal hybrids. Adapted from [3,47,49,52,53].

- Electrostatic Interactions

Electrostatic interaction phenomena occur when the surfaces of dissimilar materials interact with each other: a double layer of ions develops at the interface of both materials creating an electrostatic charge. In a simplified manner, the attraction forces take place when one surface carries a net positive charge and the other surface a net negative charge as in the case of acid–base interactions and ionic bonding. Different electrostatic charges at the interface lead to the force of attracting bonding, and the bonding strength will depend on charge density. This kind of interaction is the most common between incompatible materials, as seen in polymers that adhered to a metallic substrate [51–53].

- Mechanical Interlocking Mechanism

The mechanical interlocking between dissimilar materials depends on the cavities, pores, and asperities of a solid surface and it is an important parameter in adhesive strength. The increase in adhesion forces is attributed to a high superficial area, which brings an extended roughness; this also depends on the wetting conditions of the substrate which eventually will allow penetration of the adhesive into the cavities or pores [50,54].

It has been demonstrated in diverse studies [13,48,51,52,55–57] the importance of roughness in the magnitude of the adhesive strength, especially in metal substrates with modified surfaces containing fibrous oxides as in Figure 12.

Other authors [50,58] indicate that mechanical interlocking does not necessarily come from a simple physical hooking between two surfaces, but rather, the superficial roughness can also increase the viscoelastic or plastic energy dissipation at the crack tip at failure. So, it is evident now that the energy loss is the major factor of adhesive strength [54].

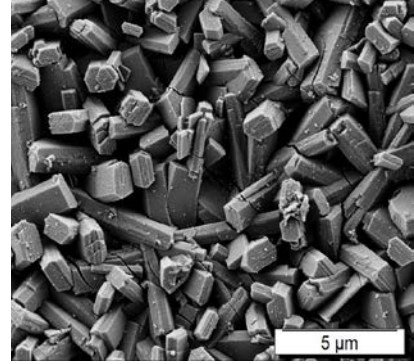


Figure 12. Modified surface of the steel used in this work. Hexagonal protrusions are Zinc oxides, which eventually improve adhesion by mechanical interlocking.

Islam et al. [59] presented in their extensive work the influence of metal roughness on the work of adhesion of a glass fiber/epoxy resin on a low carbon steel composite. They used seven different methods to modify the steel surface, and it was found that the best adhesion was obtained by using a garnet grit blasting technique with different grit sizes.

Salin et al. [60] studied the adhesion properties of EPDM rubber that was vulcanized directly on as-received stainless steel. The surface of the metal was modified with different surface treatments, and their corresponding micrographs are shown in Figure 13. A summary of the measured interfacial peel strength is displayed in Table 2, where is clear that adhesion of rubber on the sandblasted metal exceeded the cohesive strength of the rubber component; on the other hand, adhesion could not be measured in specimens where rubber was bonded on the dry brushed surface.

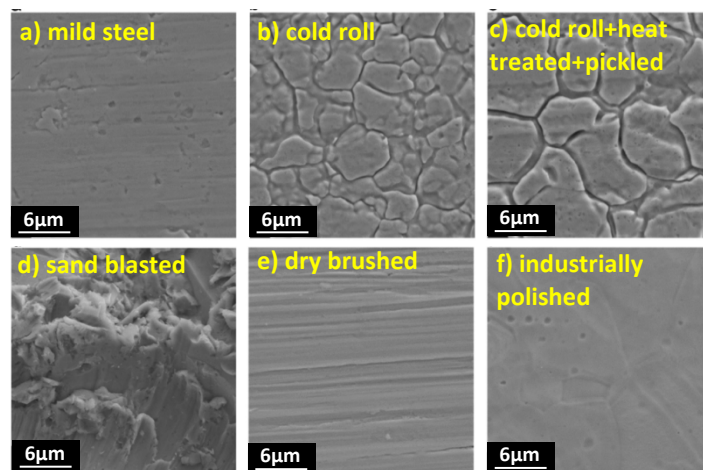


Figure 13. Different steel surfaces from E. Sarlin et al. [60]. Published with permission from Elsevier.

Substrate	Surface Pretreatment	Interfacial peel strength [N/mm]
Stainless steel AISI 304	- Cold roll steel heat treated and pickled	90
	- Sandblasting	269
	- Cold roll steel: heat treated + pickled + skin passed	7.4
	- Dry brushed	no measurable adhesion
	- Industrially polished	no measurable adhesion
Mild steel EN 10130	- No pretreatment	exceeds cohesive rubber strength

Table 2. Direct adhesion of EPDM rubber vulcanized on differently pretreated steel surfaces [47].

- Diffusive

Diffusion mechanism takes into account a mutual diffusion or reptation of polymeric chains through the interface producing a new interphase as shown in Figure 11. Adhesion through interfaces is accomplished when two macromolecules are brought in intimate contact, and interdiffusion of the molecules occurs in the superficial layers of each material. A process of auto diffusion of identical polymers may also occur, and it is referred as autohesion; this process is a function of temperature and contact time after Fick's law [61].

To achieve an optimum diffusion process at the interfaces, some conditions have to be fulfilled: both the adhesive and the substrate must be polymers that have similar or equal solubility characteristics. Additionally, the length of the macromolecule, the glass transition temperature, the curing time and processing temperature play a major role in the interdiffusion process and subsequently, in the adhesive force.

As reported by Cognard [62], the strong adhesion of an amorphous thermoplastic polysulphone (PSU) with an epoxy-amine resin relies on the penetration of the adhesive into the polymer which was measured at around 3 μm thick. For a polyimide that was bonded with another type of epoxy-amine that was cured 4 hours at 130 °C, and then annealed 4 hours at 220 °C, the same interpenetration network increased to over 80 μm .

In the case of adhesion between different components, as in a polymer-metal hybrid, the diffusion would come when the metal is evaporated onto polymeric substrates, as seen in a physical vapor deposition process [53]. Regarding the polymer-metal composites used in this work, the diffusion theory of adhesion will not be suitable for this specific type of bonding, and it will be better explained through electrostatic interactions and mechanical interlocking [62].

- Physical-Chemical

Bonding or adhesion of materials cannot be defined as a single mechanism or theory; even in simple components, and due to the variety of materials involved, many simultaneous adhesion phenomena could take place. Nevertheless, the physical and chemical interactions are the most common due to the intimate contact at the interface, they also contribute, to a wider extent, to the final adhesion strength of the composite which also will be influenced by interlocking, interdiffusion and electrostatic interactions [54].

The physical-chemical contributions to the adhesion strength are related to the action of combine forces like polar, dipolar and primary bonding that work on atoms and molecules that are in intimate contact. Table 3 lists different physical or chemical bonding energies that may take place in interfaces of polymer-metal hybrids.

One of the most significant interactions in adhesion of materials corresponds to the London dispersion forces, or the so-call adsorption theory, which is related to attractive temporal forces that results from electrons in adjacent atoms that occupy temporary positions generating dipolar attractions. They are easily created because they depend only on the existence of nuclei and electrons[50]. These forces are also combined from contributions of primary bonding, dipolar and polar interactions of atoms or molecules [63].

Bond type	Bond energy [kJ mol ⁻¹]	Bond length [nm]
<u>Primary, chemical</u>		
Ionic	600-1000	0.2 - 0.4
Covalent	60-800	0.1 - 0.3
Metallic	100-350	0.2 - 0.6
<u>Secondary, physical</u>		
Hydrogen	~50	0.3
Van der Waals		
Dipole interactions	5 - 20	0.4
London	1 - 40	<1

Table 3. Different physical and chemical bonding energies between atoms and molecules [32].

Secondary interactions are the most common in composite joints; they result from weak interactions between molecules close together; a typical example is the hydrogen atom in the proximity of electronegative atoms like nitrogen or oxygen from neighborhood chains. In contrast, the chemical or primary bonds created at the adhesive-substrate interface are expected to bring in strong adhesive forces of two materials using ionic or covalent bonding [61]. In literature, there are several examples of

primary adhesion between two dissimilar materials such as the bonding of vulcanized rubber with sulfur on a brass surface by the formation of polysulfide bonds [54].

Industrial bonding of dissimilar materials is achieved mainly by using primers or promoter molecules. These compounds can react physically or chemically with the organic and inorganic surfaces, hence, creating a bridge at the interface. The most common adhesion promoters are molecules based on silanes which have been widely used recently in polymeric components that adhered to metals or silica substrates, as reported in the literature [13,53,57,64–66].

In this work, adhesive primers based on urethane crosslinkers were used to achieve a strong adhesion between the polymer and the metal substrate. This mechanism will be discussed in numeral 3.2.2.

2.6. THERMOPLASTIC POLYURETHANE-STEEL HYBRIDS

2.6.1. Steel as Substrate

Hybrid components manufactured on low carbon steel substrates (less than 0.30% of weight in Carbon) can take advantage of steel alloys in terms of its excellent ductility and toughness; it can be easily processed in conventional machines and respond easily to welding processes [11]. Due to the versatility of adjusting final mechanical properties, steel alloys are still the most widely used metals in the Industry. Steels have higher E-modulus and tensile strength if compared to Al or Mg, and are the least expensive to process [67]. The typical applications for this category of metals are found in the automotive industry like automotive body parts, structural beams like I-beams, sheets required to manufacture pipes, buildings and tin cans [6]. Table 4 sums up the most common low-carbon steels used in the industry and their applications. Due to the wide range of structural and engineering applications, and also to the open challenges regarding long-term durability, it was decided to use a low carbon plain steel as a substrate with two different anti-corrosive treatments, which will be described in the lines below.

Designation		Composition			Mechanical properties			Typical applications
AISI/SAE	DIN	C [%wt]	Mn [%wt]	Other [wt%]	Tensile strength [MPa]	Yield strength [MPa]	Ductility [%elong. in 50mm]	
1010	CK10	0.10	0.45	-	325	180	28	Automotive bodies, wire, pipe
1020	CK22	0.20	0.45	-	380	205	25	Pipes, structural sheet steel
A36	Fe360D2	0.29	1.00	0.20 Cu	400	220	23	Structural beams
A516 Gr. 70	19Mn6	0.31	1.00	0.25 Si	485	260	21	Low temp. vessels

Table 4. Designation, composition and mechanical properties of plain low-carbon steels [6].

A major challenge of polymer-steel composites is the low resistance to oxidation, even in normal environments. Therefore, it is recommended to passivate its surface by either anticorrosive treatments or special coatings. Among the most common treatments are the Zinc phosphate conversion coating and the electrophoretic layer (e-coat). Steel substrates with both anti-corrosive treatments were used in this work, and they will be described in more detail in the next lines.

2.6.1.1. Anti-corrosive superficial treatments: Zinc Phosphate

One of the most common conversion coatings available in the metal Industry is the Zinc phosphate conversion coating. The purposes of phosphated coatings are to protect steel, iron, aluminum, copper and magnesium and its alloys against corrosion, lubricity, or as a base for further coatings or painting. Phosphate conversion coatings consist of insoluble metal phosphates, $Me_3(PO_4)_2 \cdot xH_2O$, where *Me* is a divalent metallic cation of metal compounds.

It is a chemical process where the metal surface is converted into the coating with an electrochemical process. Baths of phosphoric acid and phosphated salts react at the surface of the steel forming a layer of insoluble crystalline phosphates. This layer is less reactive than the metal surface, serves as a paint absorber, and decreases the delamination between the painting and the metal significantly. The Zinc phosphate conversion coating also increases the resistance to blistering when exposing to corrosive environments [68].

The standard processing stages of the Zinc phosphated conversion coatings is realized in a continuous way by immersing the part in different baths that contain different aqueous solutions. It is crucial to monitor temperatures, times and chemical quantities in all stages of the processing chain to control the quality of the coating. Figure 14 illustrates a conventional conversion coating process in steel substrates [69,70].

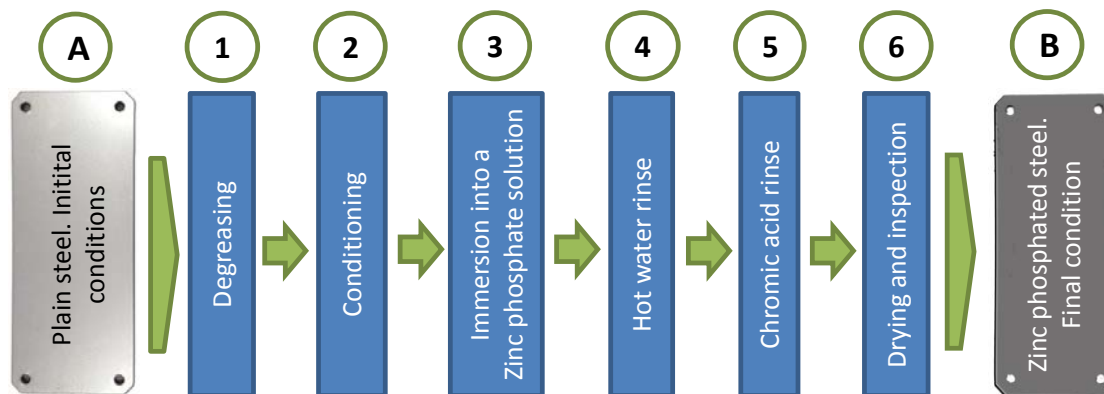
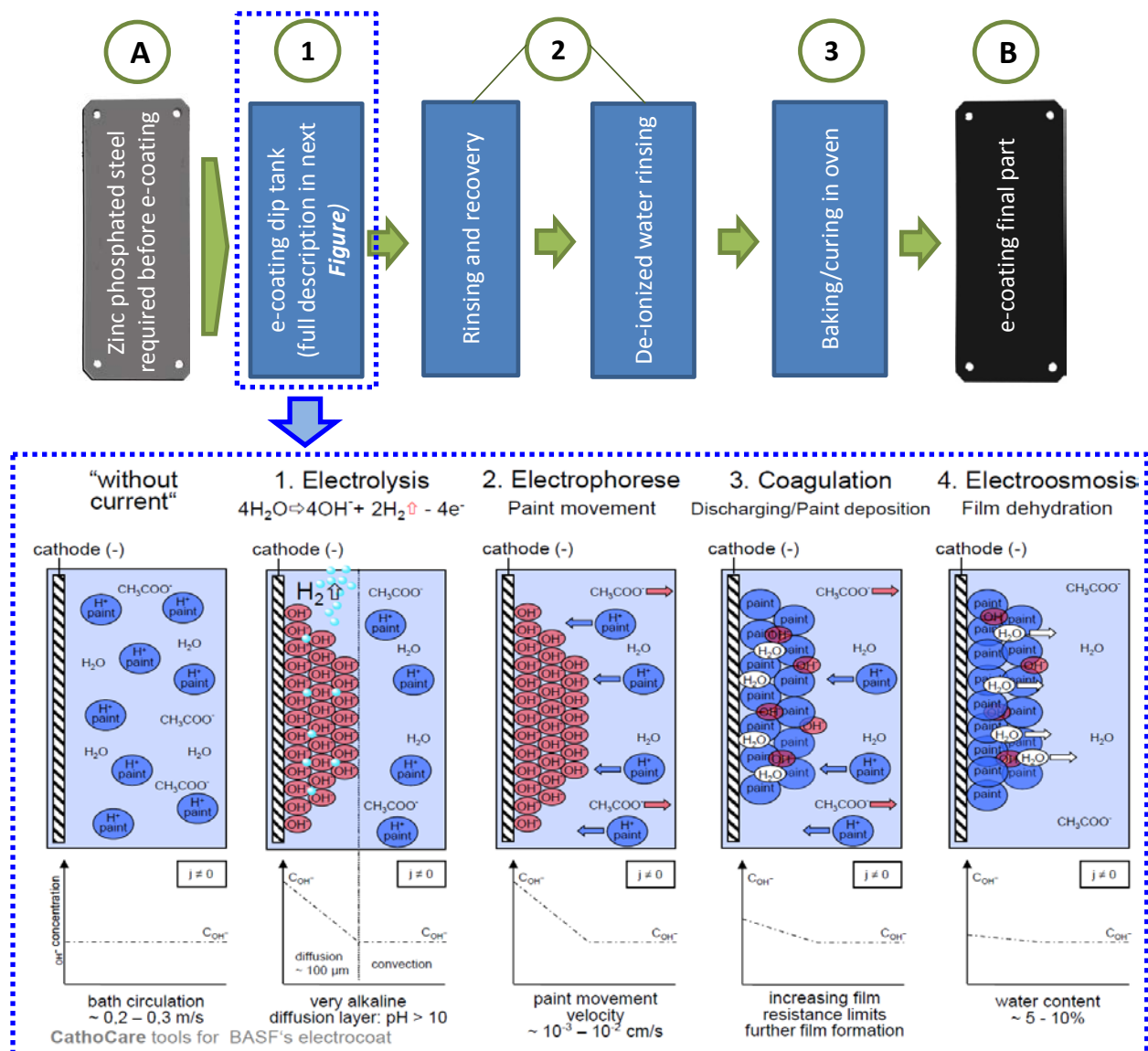


Figure 14. Steps for the Zinc conversion process in plain steel. Pictures tagged as A and B corresponds to the specimens used in this work.

2.6.1.2. Anti-corrosive superficial treatments: e-coat

Electrophoretic Deposition Coating, e-coat, is a relatively modern protective coating metal finishing alternative that started its development in the 80's in the automotive industry. Electrocoating provides significant corrosion protection advantages over conventional coating processes such as homogeneity of coating in complex geometries and sizes, uniform thickness in the final product, and substantial reduction in paint or coating waste [71]. The e-coating process in a steel substrate is summarized as follows and depicted schematically in Figure 15.

- A- Before the e-coating takes place, a pretreatment has to be realized in the part to clean and prepare the surface. A Zinc phosphating conversion coating, as described in 2.6.1.1, may be applied to the metal component to ensure proper adhesion and superior corrosion protection.
- 1- The pretreated part is immersed in a water bath solution that contains a paint emulsion of organic resins. When an electric D.C. voltage is activated across the bath, which also incorporates two immersed electrodes, the suspended particles are deposited onto the substrate's surface as described in detail in Figure 15. The desired thickness of the electrodeposition is controlled by the amount of applied voltage.
- 2- Following the electrodeposition tank, several rinse containers remove the residual emulsion from the part, and the solution is then recycled back to the processing line.
- 3- The final stage in the processing chain is the baking of the freshly e-coated substrate in a conventional oven to crosslink the organic compound.
- 4- Final e-coated steel ready to further painting or coating processes. The pictures A and B in Figure 15 corresponds to the actual sheet substrate used in this work.



- Crosslinking of e-coat During Baking

The fresh particles attached to the metal substrate are placed in an oven at 165 °C for 15 min. At those conditions, the polyester urethane crosslinker is activated as follows [72]:

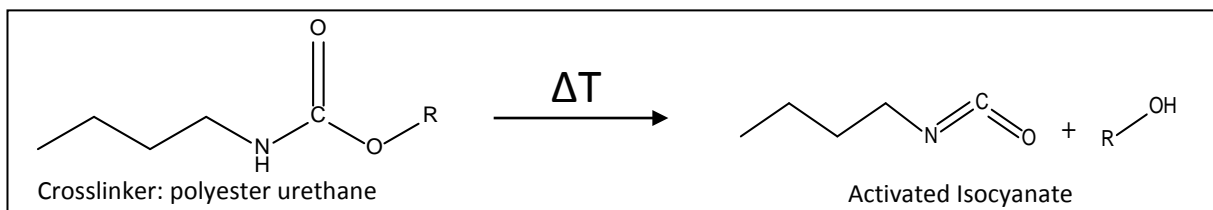


Figure 16. e-coating activation of the urethane crosslinks during baking in oven. BASF [72].

Then, the activated isocyanate group reacts with the OH^- and NH^- groups of the epoxy-amine compounds of the matrix creating a 3D network:

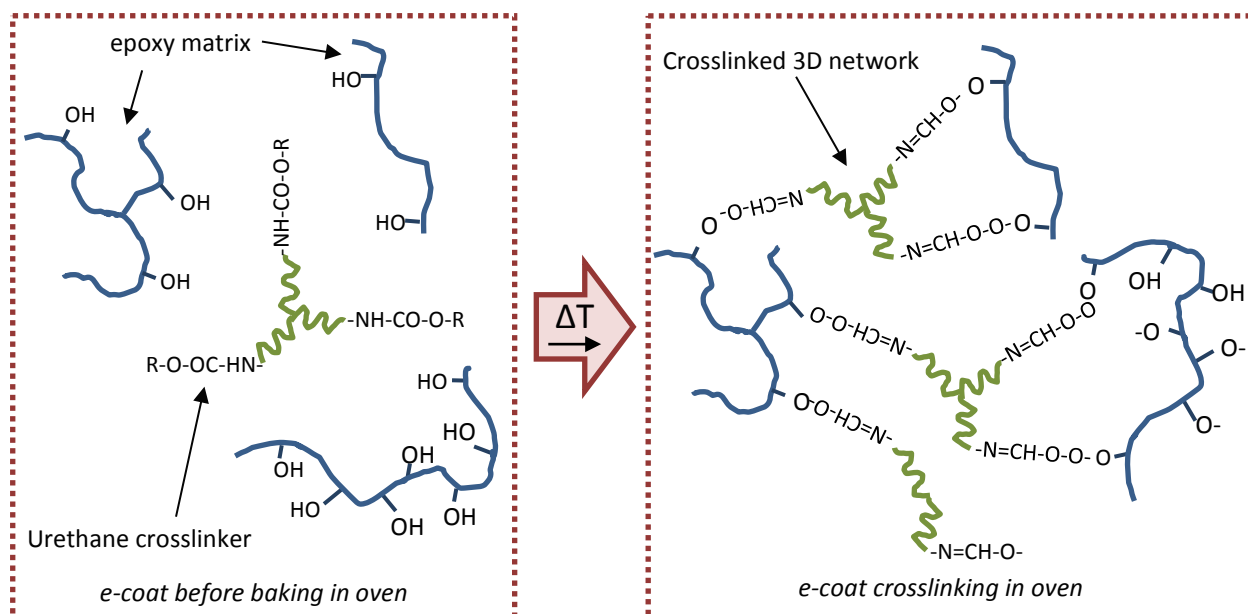


Figure 17. Schematic representation of crosslinking in e-coating. Modified from BASF [72].

2.6.2. Thermoplastic Elastomer Urethane (TPU)

The commercial development of TPU started in the 1950s by Bayer and Goodrich in Germany and U.S. respectively. TPUs are polymers that have similar properties of rubbers, but they can be injected or extruded as standard thermoplastics, making them ideal for components requiring special functions like non-slip grips or soft and comfortable touch. TPUs may reduce shock impacts and vibrations, they can contribute to electrical insulation and provide a high resistance to wear and abrasion as well. In medical or food processing applications, TPUs surface also works as a barrier against environmental factors, like moisture and oxygen [34]. The characteristic properties of thermoplastic elastomers include high elongation and tensile strengths, abrasion resistance, and the capability of withstanding oil, grease, solvents and chemicals [12,55].

Currently, there are three main types of TPUs available in the market; they depend on the chemical linkage in the polymer main chain, and they are classified as Polyester-based, polyether-based and polycaprolactone-based TPUs. A summary of the characteristics is shown in Table 5.

Polyester-based TPU	<ul style="list-style-type: none"> ○ Compatible with PVC and other polar plastics ideal for polyblends ○ High resistance to oils and chemicals ○ Excellent abrasion resistance ○ Good balance of tensile strength and elongation
Polyether-based TPU	<ul style="list-style-type: none"> ○ Slightly lower density than polyester types ○ Low-temperature flexibility ○ Good abrasion and tear resilience ○ Excellent resistance to microbial attack ○ Excellent resistance to hydrolysis
Polycaprolactone-based TPU	<ul style="list-style-type: none"> ○ Inherent toughness and mechanical resistance of polyester-based TPUs ○ High performance at low temperatures ○ Relative high resistance to hydrolysis. Used for hydraulic or pneumatic seals

Table 5. Categories and Properties of Thermoplastic Elastomer Urethanes (TPU) [73].

There are also two subcategories depending on the type of isocyanates used in the polymerization reaction. The most common TPUs available in the market are obtained from aromatic compounds like Methylene diphenyl diisocyanate (MDI) which can be used in applications that require flexibility, strength, and toughness. The second category is based on aliphatic isocyanates like hexamethylene diisocyanate (HDI) and Isophorone diisocyanate (IPD), which are characterized by their stability under the light, optical clarity, adhesion, and surface protection. The common application is in the automotive glass industry as laminated films that bond glass and polycarbonate together.

2.6.2.1. TPU Chemistry

A Thermoplastic Polyurethane is a multiphase block copolymer obtained by a polyaddition reaction, which consists of a polyol or long-chain diol, a chain extender or short-chain diol, and di-isocyanate as sketched in Figure 18. The final architecture of the polymer is rather complex, consisting of immiscible hard and soft segments that form a two-phase microstructure. The intrinsic incompatibility between hard and soft domains is caused by the polar molecules in the hard segments, which may form interchain carbonyl to amino hydrogen bonds that cause the ordering in the hard domains. On the other hand, the soft phase consisting of either polyether or polyester glycols, form amorphous regions [74] and work as an elastomeric matrix, as schematically illustrated in Figure 19. The phase separation is incomplete because some of the hard segments remain isolated or immersed in the soft or rubbery phase [75]. The conformation of the hard segments is a major issue regarding mechanical properties of the polymer; they form physical crosslinks similar to the ones in vulcanized rubbers and convey the elastomeric behavior to the bulk material. Hard domains are also stiffer than soft domains and thus act like nanofiller in the rubbery phase [76].

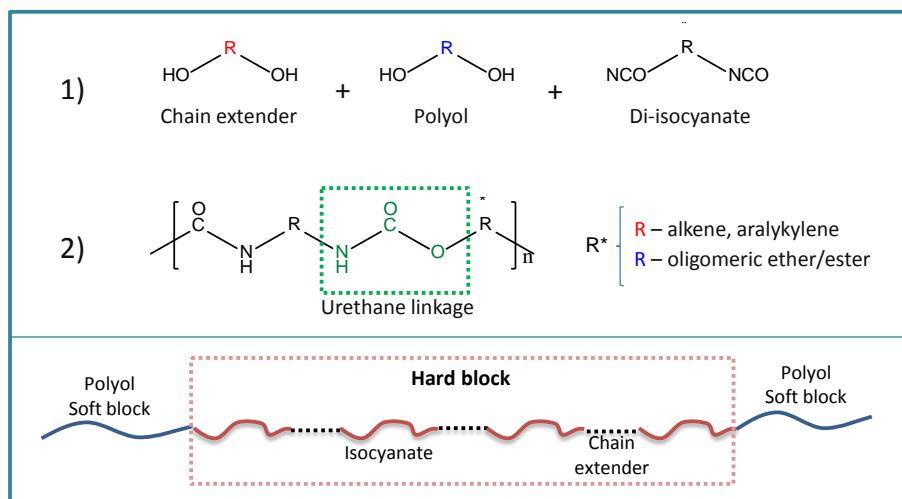


Figure 18. Poly-addition polymerization of a conventional TPU. 1) monomers and 2) TPU polymerized chain [35].

Below the melting equilibrium temperature, soft segments exist above their T_g and contribute to the rubber-like behavior; hard segments instead are below their melt transition temperature and are responsible for the high modulus, permanent deformation, and tensile strength. The combination of molecular weights between soft and hard segments, the variation of their ratios, and the chemical type make possible to have versatility regarding mechanical properties of the polymer [74]. However, the final properties of the TPU are determined not only by the chemical structure and by composition, but also by the synthesis conditions and thermal history, as it will be described in the next numeral.

*Hard segments as
Physical crosslinks
(thermally reversible)*

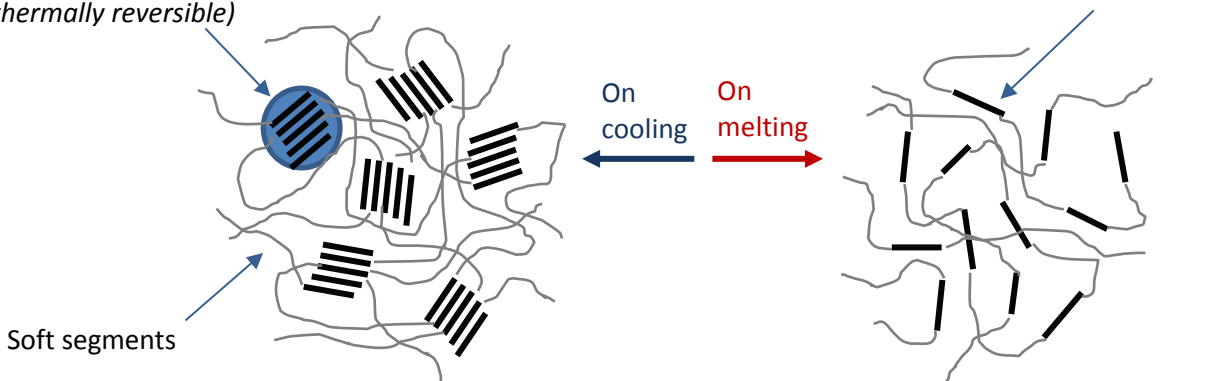


Figure 19. Chain morphology of TPU at room and melting equilibrium temperature [73].

2.6.2.2. Influence of Annealing on TPU Morphology

During the melting stage of the TPU, the hard segments dissolve into the soft domains until equilibrium; the thermodynamic process is very fast above melting temperature. On cooling from the melt, the thermally reversible phase separation occurs again, but the mobility at this stage decreases and the phase separation is then hindered. The final morphology of the hard and soft domains depends now on the cooling rate and post-annealing conditions. Reaching the molecular equilibrium requires a long-term annealing at room temperature or a post-annealing treatment near to the melting point of the hard segment phases [77]. Morphology of TPUs based on MDI diisocyanate has been studied widely in the literature [14,16,17]. Thermal evaluation under DSC analysis shows multiple endothermic peaks: first small melting peaks that occur at around 80 °C, then, two temperature ranges of endothermic behavior at about 170 °C and the last, at a temperature range from about 190 to 230 °C. Endothermal at lower temperature ranges are attributed to the disordering of hard segment phases with relatively short-range order and the high-temperature range melting peaks refer to long-range order segments [75,78,79] as sketched in Figure 20.

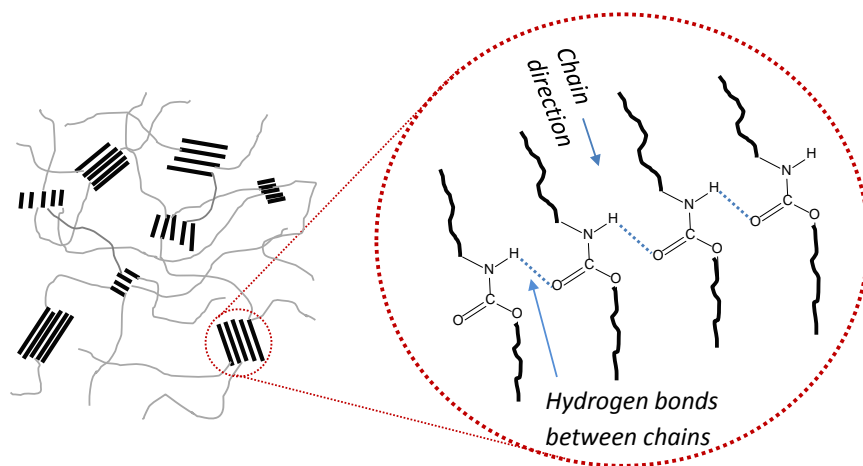


Figure 20. a) Illustrative sketch of different degrees of ordering of MDI TPU hard-segments, and the corresponding amino-hydrogen bonds between urethane groups in hard domains [76].

Frick and Rochman [79] investigated under DSC the morphology of two engineering TPU grades, one TPU based on MDI and the other one using a dimethyl-biphenyl diisocyanate (TODI). Both polymers were subjected to two annealing conditions, at 80 °C for 48 hours and at 110 °C for 24 hours. They found that the annealing process leads to a reorganization of the polymer chains in the direction of processing due to the enlargement of endothermal peaks at about 175 °C when compared to the untreated sample. The conditions of annealing determine the thickness of crystallites as measured by thermal analysis: the size of the crystal thickness increased when the annealing temperature increased. They also mention that the

annealing temperature can be detected on the thermograph as an endothermal peak at the annealing temperature +30 °C. Klauesler and Pompe [75,80] also reported that mechanical properties, specifically the tensile strength and modulus of elasticity, of a segmented TPU increased after a redrying or annealing thermal step after processing. Klauesler attributed the reversible changes in the ultimate strength to the physical interactions of H bonds inside the hard domains of the polymer as illustrated in Figure 20. Yilgor et al.[81] mentioned that due to the hygroscopic nature of the polymer, the water molecules influence significantly the physical interactions between the amino-hydrogen bonds between urethane groups in hard domains and so the morphology by microphase separation. So the change in mechanical properties due to thermal treatments may be explained by the reduction of moisture content, which after an annealing process, allows a rearrangement of the hard and soft segments due to re-bonding of H interactions between chains also allowing to increase polar interactions and diisocyanate symmetry. Klauesler [80] also cited that the effect of post thermal treatments on the mechanical behavior of segmented TPUs could be likewise assigned to post-crosslinking reactions between residual isocyanate groups boosted by water vapor interactions. As widely reviewed in the literature [75,76,78,79], the resulting morphology, and thus the mechanical properties, are strongly dependent on the thermal history and annealing conditions of the thermoplastic elastomer.

2.6.3. Polymer-Steel Adhesion Promoters

In literature, there are reports about various adhesion promoters on steel substrates. Munkert et al. [82] researched the interaction and failures by delamination of a polymer-metal composite in which a one-component epoxy resin was used as an adhesive between stainless steel and polymeric layers of PP and PE. The laminate was manufactured by a process denominated roll bonding, using the epoxy resin that had to be activated at 260 °C on the steel surface before the roll bonding with the PE-PP films. Pethrick [83] made an extensive review of adhesives for structural bonding of carbon fiber composites to metal substrates. In his paper, it is mentioned that the most common structural bonding systems are based on epoxy resins: Another adhesive system providing high toughness to the final hybrid component is manufactured by combining two molecules such as a neat phenolic resin with a poly (vinyl formal) resin with low molecular weight. This type of structural bonding is achieved by coating both surfaces with the polymeric mixture, letting the paste to settle for a certain time (which could take hours), and then bring the substrates together and heat under pressure. Pethrick cites additionally other resin systems that are resumed in Table 6.

Resin system	Applications
Cyanoacrylates	Fast bonding capability but poor resistance to moisture and temperature
Acrylic adhesives	Tolerate oily surfaces and are used for bonding glass to metal
Polyurethane - based adhesives	Good flexibility at low temps and resistance to fatigue, impact resistance and durability, but the load capacity is limited
Silicone resins	Sealants for low-stress applications and flexibility but poor tear strength
Polyimides/Bismaleimides	High temp applications but difficult to process

Table 6. Polymer-metal resin systems and their corresponding applications [83].

Another well-known polymer-metal adhesion promoter is a silane-based compound that is applied on the surface of the metal. The compound consists of amino and vinyl functional groups that serve as a coupling agent between the organic and inorganic components. The metal substrate must be coated just before the overmolding of the polymer to ensure that the organo-reactive molecules must be in contact with the polymer and metal, as explained in Figure 21.

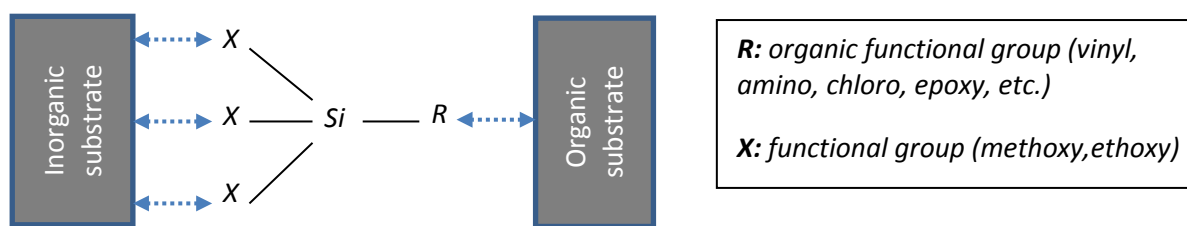


Figure 21. Adhesion between organic and inorganic materials through a silane coupling agent. It is expected that the functional group *R* interacts chemically with the organic material and, simultaneously, the *X* group reacts at the surface of the inorganic component [160].

Honkanen et al. [84] investigated the adhesion of a thermoplastic elastomer (TPU) on a stainless steel substrate using as a coupling agent an amino-functional silane that was applied on the metal sheet. Before the silane treatment, the surface of the steel inserts was modified by electrolytic polishing and different grades of surface oxidation. Subsequently, the TPU was overmolded onto the metal sheets. They found that adhesion improved the joining between the silane layer to steel and simultaneously between the TPU to the steel, and the failure modes of the hybrids occurred adhesively at silane/steel and TPU/silane interfaces. The failure mode of the hybrids with electrolytic and oxidized steel substrates was more cohesive in the TPU if compared to the as-received metal insert; that indicates a better silane bonding to the pretreated surface steel as shown in Table 7.

Substrate	Pre-treatment	Interfacial peel strength [N/cm]	Failure mode
Stainless steel 4301	As-received	109	Adhesive at silane/steel and TPU/silane interfaces
	Electrolytic polishing	106	Mostly cohesive at the TPU
	Electrolytic polishing+5 min oxidized	148	
	Electrolytic polishing+100 min oxidized	129	
	Electrolytic polishing+300 min oxidized	117	

Table 7. Peel strength of overmolded TPU on stainless steel inserts using a silane coupling agent [84].

Currently, companies like Dow Automotive [15], BASF Performance Polymers [16] and Evonik [17] are developing adhesion promoters for polymer-metal automotive applications. These liquids or powder promoters are applied on the metal substrates by coil or electrostatic spray coating. Subsequently, the two coated part has to be baked in the oven to cure the corresponding molecules. Then, the structural polymer (PA6-GF30, PP-GF30, PBT, ABS) is injected on the metal substrate creating strong bonds between the polymer and the metal substrate.

2.6.4. Influence of Annealing on Adhesion of a Polymer-Steel Hybrid

It is not possible to find conclusive results in the literature about how the thermal history of the polymer, or a thermal annealing process, may influence the adhesion and durability of a polyurethane-steel hybrid. From the scarce literature on the topic, it is worth to cite Jiang et al. [67] who reported that higher adhesion forces and improvement of bond quality of a thermally-treated epoxy-steel hybrid could occur due to a post-curing process, together with an alignment of the polymer molecules that consequently enhanced bonding density at the interfaces. Hoikkanen et al. [64] also reported a gain of bond strength of overmolded TPU on different metal substrates pretreated with silane compounds. Specimens were subjected to isothermal treatments at high temperatures, and after the peel test, the adhesion force and the fraction of cohesive failure increased. The positive adhesion was referred to an increase in the interaction between the adhesive layer and the TPU without giving specific details. Co-workers [4] described similarly a step-up in the adhesion strength after annealing of a TPU overmolded on steel substrates.

In these order of ideas, one of the main goals of this work is to contribute to the understanding of how an annealing process influences the adhesion and durability at the polymer-metal joints of the hybrid component.

2.7. DURABILITY AND LONG TIME PERFORMANCE OF A POLYURETHANE-STEEL HYBRID

2.7.1. Aging in Metal Substrates

Deterioration and aging of metal substrates occur on metal components by two mechanisms: firstly, by corrosion, which it is, in a general manner, material dissolution from the surface that is interacting with the environment; secondly, by the formation of a non-metallic oxidized layer [6]. Corrosion is a complex chemical or electrochemical process that takes place in a wide variety of conditions depending on specific material/environment combinations. Deterioration of metal parts occurs due to the interaction of a metal surface with a liquid electrolyte or with gaseous atmospheres [68]. When the metal is exposed to a liquid electrolyte, like water, it will cause a so-called aqueous corrosion; and when exposed to a gaseous environment it will induce oxidation or, in a most general way, gaseous corrosion [85]. Broadly, corrosion on metal substrates depends on variables in the environment such as temperature, surrounding gasses or fluids, and last but not least the composition of the metal. The most common forms of corrosion are resumed as follows [6,68]:

- Oxidative corrosion: usually happens on surfaces exposed to diatomic oxygen dissolved in water or air. It is a uniform electrochemical attack over the entire exposed surface with equal intensity, leaving in most of the cases an oxide deposit.
- Intergranular corrosion occurs at grain boundaries because of bigger interstitial spaces which facilitates diffusion of external elements.
- Chemical corrosion: it is due to a chemical attack by the action of strong acids or alkalis.
- Pitting corrosion: small holes or pits on the surface of the metal induce a difference in concentration of ions or oxygen atoms. The oxidation occurs inside the pit and grows downward.
- Galvanic corrosion: In this case, the metal is corroded when it is in electrical contact with a different (nobler) metal. The less noble metal will corrode whereas the more inert metal will be protected from corrosion.

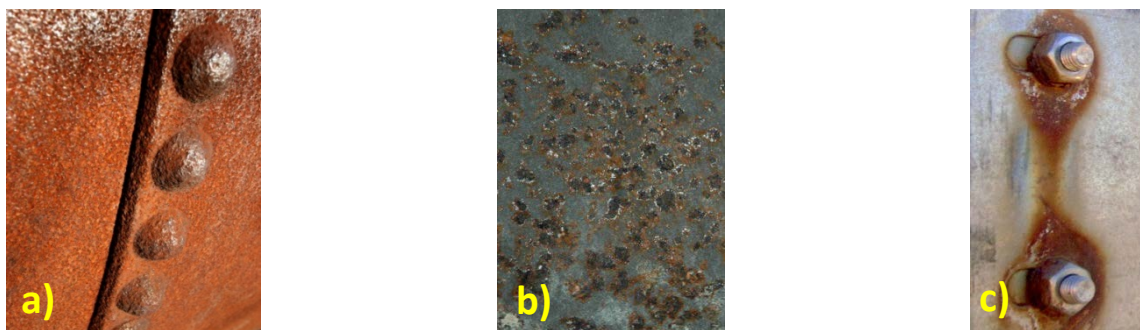


Figure 22. Aging in metal substrates: a) oxidation, b) pitting and c) galvanic corrosion. Public domain images.

2.7.2. Aging in TPU

Several authors have reported the influence of aging on the TPU as it will be described in the lines below. Table 8 summarizes as well similar artificial aging experiments by other authors.

Effects of UV and hydrothermal aging conditions were conducted for five months in a polyester-based TPU by Aglan et al. [86]. They subjected the polymer to UV irradiation for 8 hours at 70 °C, followed by 4 hours condensation at 50 °C in the dark, without water spray. The accelerated hydrothermal aging was done following the ASTM D1183-05, which consists of several cycles of different temperature and humidity conditions, each cycle last one week. It was found that UV radiation caused a much severe degradation than the specimens that were subjected to temperature and moisture cycles. After five months of exposure, TPU strips reduced their tear energy in about 98%; meanwhile, specimens exposed to environmental test reduced it only 35%. The tear strength and storage modulus were also reduced in a proportional manner. Aglan attributed the dramatic reduction in tearing properties of the polymer exposed to UV radiation to the breakage of urethane bonds, as it was detected by DSC and SEM. On the other hand, for the hygrothermally aged samples it was not possible to detect endothermal peaks that could have suggested a breakage of the urethane bonds; and micrographs by SEM showed almost no changes in appearance when compared to the virgin material.

Boubakri et al. [78,79] artificially aged a commercial polycaprolactone copolyester-based TPU by immersing the specimens at 25, 70 and 90 °C for 270 days. In that work, they determined the mechanical properties by determining the tensile strength and the elastic response by DMTA analysis. They found that samples submerged at 70 °C after nine months decreased the tensile strength and ultimate strain significantly: 23% and 70% respectively. TPUs under water at 90 °C failed catastrophically just after 24 days of testing. Opposite, the specimens submerged at 25 °C, presented an increased in the mechanical behavior, after 60 days of exposure. The higher tensile strength was attributed to the reorganization of

plasticized molecules and possibly an intermolecular crosslinking after a long immersion time. Similarly, Braun et al. [89] studied the durability of polyether-based urethanes that are used in medical applications. Some of the samples were submerged in a tub of distilled water at 95 °C, and other specimens were exposed to air at 90 °C for 56 days. The polymers immersed in water decreased their tensile strength by a quarter at 10% of elongation just after the first hour of exposure to hot water. For samples artificially aged under air, there was no significant change in the properties and remain relatively constant.

Thermal decomposition of polyurethanes was treated in depth by Herrera [90] and Simon [91]. Simon classified it in three categories: pure thermal decomposition, thermo-oxidation and thermo-hydrolysis.

Pure thermal decomposition was investigated by thermogravimetric analysis to evaluate the rate of heat degradation, individual volatile compounds, and chain in molecular weight distribution. The weakest link in all types of polyurethanes is the urethane group, oligomer polyols (ether or ester-based) have similar thermal stability but it is higher than that of the urethane links. Basically, the decomposition of urethanes occurs in three steps: first, dissociation to constituents; second, decomposition to primary amine and olefin and third, decomposition with secondary amine formation. Decomposition temperatures depend on aromatic and aliphatic groups from the isocyanate and alcohol molecules of the urethane group.

Simon et al. [91] describes also that in the thermo-oxidative decomposition of polyurethanes the weakest bond depends on the oxidation sensitivity of the corresponding groups. In the case of ether and ester-based polyurethanes, the higher “thermal bond strength” takes place in the urethane group, followed by ester links, and the ether bond in this scenario is the weakest of all.

Thermo-hydrolysis decomposition, which takes place at elevated temperatures in the presence of water, may be explained firstly by hydrolytic degradation that occurs faster in the polyols of ester urethanes and urethane bonds. High temperature accelerates decomposition reaction and depending on the environmental conditions, the thermal processes will take advantage on the thermo-hydrolytic decomposition, and so the lowest thermo-hydrolytic stability of the chemical compounds is in the ester bonds, followed by urethane linkages. As a summary, the stability of chemical groups in polyurethanes is illustrated as follows [91]:

ester ≈ ether >> urethane → pure thermal decomposition
urethane > ester > ether → thermo-oxidation
ether >> urethane > ester → thermo-hydrolysis

Author	Material	Accelerated aging	Aging conditions	time of exposure	Performance after aging
Agilan et al. [86]	PU Elastomer, Baytec MS-242	UV and hygrothermal	ASTM D1183: weekly heating and cooling cycles with various degrees of %RH	5 months	50% reduction of tearing energy. 15% decreased of the storage modulus
Boubakri et al. [87,88]	polycaprolact. copolyester-based TPU. Merquinsa D11T92EM	Hygrothermal aging test for dried and fresh samples	Submerged samples in distilled water at 25, 70 and 90 °C	9 months	at 25 °C: increase in tensile strength after 60 days. at 70 °C: Approx. 20% reduction in tensile strength at 200% strain. at 90 °C: catastrophic failure after 24 days of test
Braun et al. [89]	polyether-based TPU for medical applications	Hot water immersion and air circulating in oven	Immersion in distilled water: 95 °C. Hot air: 90 °C in air circulating oven	56 days	Samples submerged in hot water: decrease of tensile strength by a quarter after 1 hour of test. Samples in air: N/A
BASF [92]	Elastollan C85A	Immersion in water	Immersion at different temperatures	until tensile strength drops to 20 MPa	at 90 °C: Approx. 80 days at 70 °C ≈ 2,3 years at 60 °C ≈ 10 years
BASF [92]	Elastollan C85A	Long-term aging under air	Exposure to air at different temperatures	until tensile strength drops to 20 MPa	at 140 °C: Approx. 1,4 months at 120 °C ≈ 4 months at 100 °C ≈ 13,5 months at 90 °C ≈ 4,5 years

Table 8. Summary of similar hygrothermal accelerated aging test in TPUs.

2.7.3. Aging in Adhesive Coatings

At this point, it is necessary to evaluate aging on the adhesive coatings of the composites so one can conclude how the adhesion strength of the hybrid is influenced directly or indirectly when exposed to certain environmental stresses. It is also essential to know how corrosion or other electrochemical processes may affect the lifetime of the hybrid part. So far, there are no previous works that can give information about the behavior of the in-house coating when subjected to harsh surrounding conditions.



Figure 23. Localized blistering on a coated metal structure. Amtec [161].

In order to evaluate the degree of failure in coatings, the Standard ISO 4628 [93] classifies the degradation of coatings by appearance depending on the quantity, size and uniform changes of defects. The defects found on the coating surface are due to blistering, rusting, cracking, flaking, or delamination.

Osmotic blistering is one of the most common cases of failure in coatings of all nature, especially in high humidity conditions, as seen in Figure 23. It takes place in organic coatings due to the permeation nature of polymers to gasses and moisture. Even small amounts of permeated gasses with soluble contaminants, such as corrosion products like $\text{Fe}(\text{OH})_2$, may be the causal agent for osmotic blistering [94]. The mechanisms of osmotic blistering, illustrated in Figure 24, are fulfilled when there is a permeable film, a structural and impermeable substrate, water dissolved with impurities and a concentration gradient, which is the driven force for the nucleation and growing of the blisters. When water vapor permeates the film, it reaches and dissolves soluble compounds on the substrate surface creating a concentrated solution of low osmotic pressure. The rate of degradation depends on the type of metal and the passivating pre-treatment, the temperature will accelerate the permeation and solubilization processes underneath the coating. The diffused water may also react with water-soluble materials on the metal or adhesive surfaces. At that point, the water solution with impurities, underneath the coating, has a higher concentration than outside. In order to reach equilibrium, water from outside penetrates into the areas with higher concentration of water soluble materials and dilutes the solution. Because the flow of water vapor penetrating from outside is greater than the water flowing out, an increase in the internal pressure at the interface grows forming dome-like blisters that growth bigger, inducing the separation of the coating from the metal substrate. With time, blisters break from the high internal pressure forming pinholes or cracks on the surface of the coating. The rate of permeability and degradation depends on the type of organic coating, thickness, environmental conditions, coating processing and barrier characteristics of the materials involved [94,95].

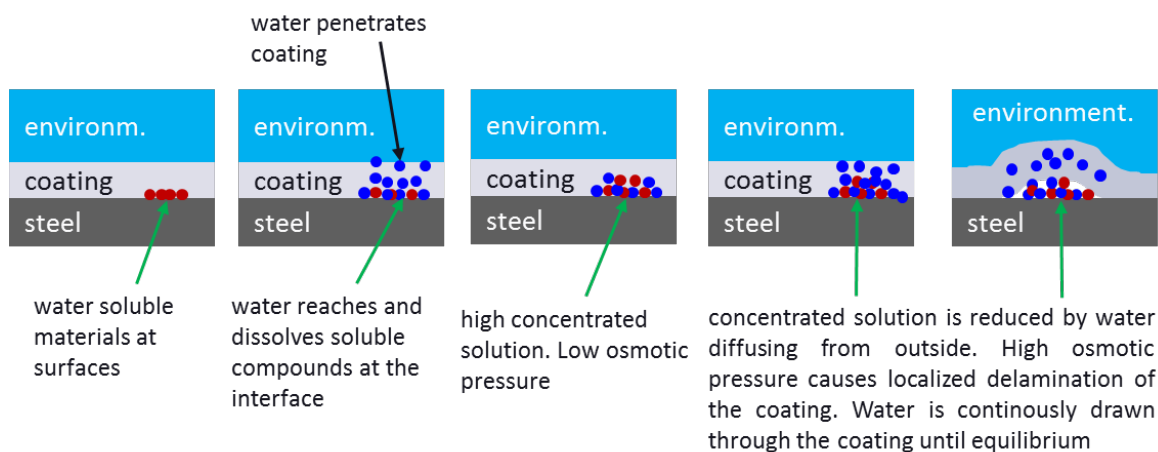


Figure 24. Mechanism of osmotic blistering on the adhesive coating. Adapted from [94,95].

Yang et al. [96] investigated morphological changes of polyurethane coatings on an aluminum substrate when immersed into a dilute Harrison's solution (3) during 30 weeks. After the accelerated corrosion tests, filiform threads were found on the coating surface. The mechanism of formation of the filiform microstructures took place after the solution penetrated into the coating with a subsequent formation of osmotic cells under the polyurethane layer. Osmotic voids were originated by the solution of impurities on the coating that concentrated in the solution, promoting water absorption towards the coating. Coalescence of blisters ended up in filiform-shaped structures on the coating surface. The aging effects on thermal, mechanical and tribological properties of high-density polyethylene coatings used for pipeline applications were investigated by Guermazi et al. [97]. Artificial aging was conducted on samples that were submerged in the sea and distilled water at 70 °C for six months. In terms of thermal properties, it was found that the T_g of the HDPE coating decreased between 2 and 3 °C for the specimens aged under synthetic seawater and distilled water, respectively. The reduction of the T_g is ascribed to the plasticization of polymer chains during the test, as it was also demonstrated by an increase of the solvent diffusion and the flexibility of the polymer chains. About mechanical properties, coating samples in synthetic sea water reduced their elastic modulus and tensile strength by 14% and 13,5% respectively. On the other hand, sample immersed in water presented a higher degradation by the drop of 33,5% and 21% in the elastic modulus and ultimate strength, respectively. Guermazi suggested that degradation in artificial sea water is less dramatic due to the "decrease of chemical potential of water in the solution, followed by the reduction of penetration capacity in aged polymeric coatings".

2.7.4. Aging in Polymer-Metal Hybrids

Several and recent research on hygrothermal aging of polymer-metal composites can be found in the literature [64,65,67,83,98–102]. It is considered generally, that composites using epoxy resins as adhesives, failed after the artificial aging in a brittle manner in the adhesive layer. In other cases, the surface treatment on the metal substrate defines the failure mode, which occurred in some situations as a delamination or as an adhesive failure [103]. In all artificial aging experiments, a significant reduction of the tensile strength and elastic modulus is reported, as listed previously in Table 8. Hoikannen and Jiang [64,67] also reported that specimens that were subjected only to thermal aging increased their bond strength. Hoikannen attributed the higher bonding forces between the metal and the polymer to a number of metal oxides that eventually would dissolve into the silane intermediate layer. Table 9 resumes the most recent publications on hygrothermal aging in polymer-metal composites regarding the material used as a substrate and adhesive, the respective adhesive and aging test, and the failure modes encountered after the accelerated aging.

As a conclusion of the hygrothermal aging in hybrid composites, it is clear that bond strength between the polymer and metal is greatly influenced by the presence of water. Cognard [62] in an extensive work, enounces that diffusion of water into the polymer depends on the polarity of its chains. Water can enter to the polymer, and as long as its quantity is lower or equal to the free volume of the polymer, it will not hydrolyze or affect the polymer or the bonded interface. Diffusion of water could also take place at the interface, especially in joints that are not densely bonded. Cognard also reported that when the free volume of the polymer is occupied, additional water absorption will generate an H-bonding displacement, following a swelling of chains, with a decrease of the T_g and elastic modulus. However these processes are reversible in the polymer [9]. Additionally, at saturation, water will condense through the pores or voids of polymer chains, especially on amorphous regions. At low bonding densities at the interfaces, there will be microcavities that will let water diffuse faster. At this point, the condensed water dissolves soluble compounds of the metal and adhesive faces that will increase the osmotic pressure leading to the formation of cracks and blisters until the metal oxide is fractured, delaminating the coating from the metal substrate. It is also mentioned that water displaces the origin of the failure in such way that the fracture will converge from cohesive to the adhesive in the interface. That effect is more severe in composites under stress as it was described for polymer-metal composites with an EVA hot melt between stainless steel plate and sapphire, and also in epoxy-nylon-sapphire hybrids. Finally, Cognard cites that water in the interface lowers the fracture energy by vaporizing in the cavities that growth laterally along the interface. As an important remark, one of the main purposes of adhesives or intermediate layers must be to increase the anchorage density to reduce a number of microvoids at the interfaces.

Author	Material	Adhesive Test	Aging conditions	Failure mode and comments
Leger et al. 2013	Adhesive: commercial rubber toughened epoxy/amine used in auto. industry. Substrate: galvanized steel	Single lap joint	Immersion in distilled water at 70 °C for 14 days	Initial crack occurred at the interface near to extremities of overlaps. Fracture modes evolved from mainly cohesive to adhesive
Sugiman et al. 2013	Adhesive: epoxy film adhesive. Substrate: Al alloy 2024-T3	Single lap joints and laminated loaded in bending	Immersion in distilled water at 50 °C for 2 years	Single lap joints: failure cohesively. Laminated bending: failure in the bondline between lamianta and stringer. Elastic modulus and tensile strength degraded linearly with moisture content. Degradation of tensile strength is higher than of the elastic modulus
Williams et al. 2012	Adhesive: carbon-fiber epoxy laminates. Substrate: Plasma activated 410 stainless steel	Lap shear	60 °C/98 %RH for 7 days	Plasma activated steel: 97% cohesive. Untreated steel: 30% cohesive failure. Plasma treatment removed contamination from steel surface and carboxylic acid functional groups were formed as well
Heshmati et al. (review of state of the art) - 2015	Polymer-metal composites for civil engineering applications. Fiber reinforced polymer. Substrate: steel	Single lap, double-lap shear, laminated, I beams with lay-up CFRP	Several tests are described	Strength degradation of joints that failed at adhesive/steel interface is around 90% of the cases. Other failure modes is less than 25%
Sarlin et al. 2014	Stainless steel/rubber/GFPR	Floating roller peel test. Sample dimensions: 100 x 12 mm	25 °C/85 %RH 85 °C/atm. cond. 85 °C/85 %RH. Exposure time: 500 h	Adhesion strength exceeded cohesive strength of the rubber even after aging in severe environments.
Hoikkanen et al. 2012	TPU overmolded on copper, stainless steel an Al using a silane coupling agents	180 °C Peel test	25 °C/85 %RH 85 °C/atm. cond. 85 °C/85 %RH. Exposure time: 500 h	Silane coupling is sensitive to hydrolysis so resistance in humid conditions is very low on Cu and steel. High Temp. exposure increased bond strength and the fraction of cohesive failure in Cu, Al and polished steel-TPU hybrids.
Jiang et al. 2015	FRP to steel adhesively bonded joints. Adhesive: epoxy-based	90° shear. 0° tension	40 °C for 4 months	Brittle failure, cohesively in the adhesive layer. Hygrothermal aging decreased significantly the ultimate failure loads of aged adhesives joints under shear and tensile test

Table 9. Recent research on hygrothermal aging in polymer-metal composites.

Grujicic in extensive works [9,13,22] mentioned that a thermal annealing process cannot remove completely residual water absorbed by the polymer due to the high interactions in the polar groups of the chains. Polar interactions are directly related to the reduction of the bonding strength because of the chemical reactions between the excess of water molecules and the OH groups of the polymer or adhesives. This induces a premature destruction of intermolecular H bridging, followed by a displacement of absorbed OH groups from the polymer-metal interface. In general, the durability of a polymer-coating-metal hybrid relies on the polarity of the plastic and the adhesives. For this reason a polymer with functional groups are preferred. On the other hand, the same functionality will lead to absorb excessive amount of water that, as mentioned above, may create defects at the reactive interface such as internal stresses, swelling and cracks.

2.7.5. Lifetime Estimations in Polymer-Metal Hybrids

Lifetime of polymer-metal hybrids reported in literature concentrates mostly in analyzing failure modes or modelling bonding mechanisms of components subjected to certain hygrothermal conditions, as it was cited in numeral 2.7.4. Nevertheless, lifetime estimations of a polymer in proximity of a the metal interface are scarce, mainly because failure depends on many variables such as mechanical loads, environmental conditions, base materials, manufacturing chain, among others [22]. Some of those variables are unpredictable during the lifecycle of the part, making estimations inaccurate. Leuteritz et al. [104,105] researched about accelerating aging of plastic jacket pipes for district heating and failure at the polyurethane-metal joint. The pipes consisted of a steel tube surrounded by polyurethane insulation and a casing of polyethylene. The axial shear strength was determined after service life, and a recalculation of the physical life equivalent to a continuous operation temperature of 120 °C, showed that the lifetime ended earlier than it was required in the Standard EN253. It was also found that premature failure at the polymer-steel joint occurred due to corrosion at the metal surface. Additionally, the author contributed to that research [106] by estimating the lifetime of those pipes, assuming that failure takes place in the polyurethane near to the steel surface, by applying three thermogravimetric methods that are generally used to calculate kinetic parameter of solid decomposition [107–109]. The three different TGA-methods evaluated were: Ozawa-Flynn, Friedman and Chang method. Tests were conducted at four different heating rates, 2, 5, 10 and 20 K/min and kinetics parameters were obtained; then, lifetime was predicted. From the methods evaluated, the lifetime prediction following the Chang method gave the best approximation when compared to results of the previous mechanical test [106] as it will be discussed in detail in chapter 8.1.1.1.

2.8. CONCLUSIVE REMARKS (CHALLENGES) AND AIMS OF THE WORK

From the literature survey, it is clearly seen that joining of dissimilar materials, like polymers and metals, has been a relevant topic in automotive and aeronautical industry and, therefore, researching has progressed over the last years, with many challenges still to be overcome. Much literature has been focused on hybrids based on diverse metal substrates in combination with glass-fiber-reinforced-polymers and their corresponding failure modes, but there is still a need for enhancing adhesion strength in terms of reliability and durability of hard-soft combinations, and more specifically, in thermoplastic elastomers overmolded on steel substrates.

The enhancement and durability of hybrid joints depend mostly on the substrate's surface treatment, on the functionality of the polymeric material, on the processing chain and type of adhesive promoters used to enhance bonding, and on the resulting physical-chemical interactions at the interfaces. It is for this reason that an in-house powder-coating applied on the metal substrate will be used as a main adhesive promoter in the hybrids. However, it is not clear if an adhesive promoter, either a paint or a coating, would contribute to a full protection of corrosion on the metal plate. From literature survey, there is not enough information about dual intermediate coatings that may provide, simultaneously, adhesion and corrosion protection in a steel-based substrate.

Similarly, bonding strengths and reliability at the polymer-coating and/or at the coating-metal interfaces of hybrid systems may be influenced by a post-thermal treatment. Although there is enough literature assessing the effects of annealing treatments on raw TPU specimens, as referred in numeral 2.7.2, there is not yet scientific research available about the influence of thermal treatments on polyurethane-steel hybrids and their impact on adhesive bonding at the interfaces and the corresponding long-term durability.

With respect to long-term durability, there are various papers dealing with ultimate failure and lifetime estimations for the hybrid component, as highlighted in numeral 2.7.4; however, durability and lifetime predictions are tasks that are not yet fully resolved and need to be improved, especially because there are several variables that influence the final performance and reliability of the hybrid part. In a certain way, lifespan calculations depend mostly on the type of materials, the processing chain and the final application. Hence, one of the main aims in this work is to determine precisely the most probable failure modes of a polyurethane-steel hybrid, and from there, calculate as accurate as possible the ultimate failure when the component is subjected to certain hygrothermal conditions.

With the idea of overcoming some of the extensive challenges above described, two adhesive organic coatings applied on the steel surface were investigated: the first one is a novel adhesive powder-coat developed in the Leibniz Institute für Polymerforschung Dresden e.V. The second one is a high performance anti-corrosive electrophoretic paint that has never been reported in literature as an intermediate adhesive layer in a thermoplastic-polyurethane overmolding processing chain. A TPU was overmolded on both coatings and the adhesion of the polymer to the metal substrate was examined. The influence of an annealing post-treatment of the hybrid on adhesion and durability was investigated as well. Failure modes and lifetime were estimated after annealing and artificial hygrothermal aging in which temperature and humidity were evaluated independently to identify the variable that affected in a greater proportion the lifecycle of the hybrid component. In such a way, it may be possible to estimate with higher accuracy the lifetime of the multimaterial part under thermal loads. It is expected that this work will contribute to the polymer-metal engineering community in a way that theories and methods may be applied to new hybrid systems.

3. EXPERIMENTAL

3.1. MATERIALS

3.1.1. Steel Substrates

Three different sets of metal substrates: plain, zinc phosphated and e-coated steel sheets were used as the material base for the hybrid composites. Sheet dimensions are displayed in Figure 25. All metal sheets were obtained directly from an industrial partner, and the description will follow in the next lines.

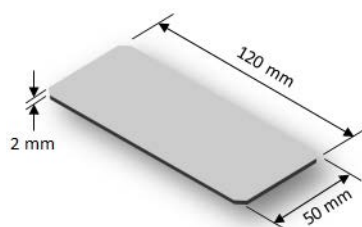


Figure 25. Steel substrate dimensions.

- Plain Steel

A commercial low-carbon, non-alloy steel sheets, grade DC01, of 2 mm thickness, are used as metal substrates. The cold rolled steel sheet is suitable for drawing and forming applications [110]. The main mechanical properties are shown in Table 10.

Material	Youngs modulus [GPa]	Tensile strength [MPa]	Elong. at break [%]	Density [g/cm ³]	Heat distortion temp. [°C]	Thermal expansion [K ⁻¹ · 10 ⁻⁶]
DC01 Steel	200	270-410	min. 28	7,8	600	12

Table 10. Mechanical properties of the DC01 steel substrate [3].

- Standard Zinc-Phosphated Steel

The second set of metal substrates consists of DC01 plain steel sheets that were superficially pretreated with a Zinc-phosphating conversion coating as described in numeral 2.6.1.

Material	Coating weight [g/m ²]	Thick. [μm]	Conditioning	Primary use	Limitations	Applicat. method	Process temp. [°C]
Standard-zinc phosphate	1-7	3-8	Titanium phosphate	Temporary corrosion protection; paint base for high corrosion environments	Poor unpainted corrosion resistance	Spray and immersion	32-60

Table 11. Characteristics of the Standard-zinc phosphating coating [68].

- Electrophoretic coated steel, e-coat

The last set of metal substrates consists of sheets of DC01 steel that were pretreated with an electrophoretic coating described in more detail in numeral 2.6.1.2. The organic coating used in the electrophoretic process is based on epoxy-amine compounds and a polyester-urethane crosslinker [72].

Material	Ref.	Thick. [μm]	Conditioning	Primary use	Limitation	Application method	Compos. of organic coating in wt.%
e-coat	CathoGuard® Electrocoat BASF	40-50 max	Zinc-phosph.	High perform. corrosion protection in automotive parts and other industry manufactured products	Cost	Electrophoret. deposition by immersion	65-90 of organic hardener: Epoxy-amine compounds with polyester crosslinkers. 10-35 pigments

Table 12. Characteristics of the e-coating [72].

3.1.2. Thermoplastic Polyurethane, TPU

The commercial TPE is a polyester-based Thermoplastic Elastomer Urethane, TPU, ref. Elastollan C85A10 from BASF. It is characterized by its excellent tensile strength and high elongation at break, good damping characteristics, high resilience performance and excellent wear resistance [79], as listed in Table 13. The specific mechanical properties of TPUs are attributed to its multiphase chemistry, with soft and hard segments. The manufacturer of the TPU recommends a post-thermal treatment, annealing, that leads to higher mechanical properties in shorter time [112].

Material	Youngs modulus [GPa]	Tensile strength [MPa]	Elong. at break [%]	Hardness [Shore A]	Density [g/cm ³]	T _g [°C]	Heat distortion temp. [°C]	Thermal expansion [K ⁻¹ ·10 ⁻⁶]
TPU C85A10	0,1-0,8	50	650	85	1,19	≈ -40	+60 to +180	120 to 180

Table 13. Main physical properties of TPU C85A10 [92,113].

Elastollan grade C85A10 TPU is formed basically from the combination of three components: the long chain polyester-based polyols, methylene diphenyl diisocyanates (MDI), and short diol chains. The linear polyurethane is formed by a polyaddition polymerization between the polyols and the short chain diols that react with the diisocyanates. The combination of a diisocyanate with the short chain diol produces the rigid component [92] as illustrated schematically in Figure 26. The TPU used in this work, based on polyester polyols, is characterized by its higher mechanical properties, higher heat resistance and higher resistance to mineral oils when compared to the TPUs based on polyether polyols.

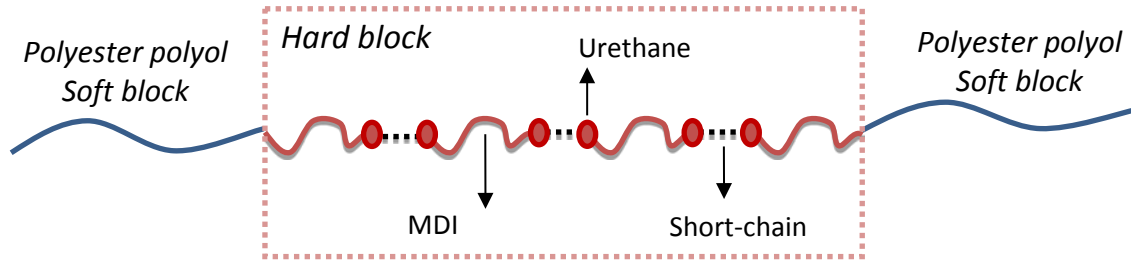


Figure 26. Schematic representation of C85A10 TPU [92].

3.1.3. Adhesive Powder Coating

The adhesive powder coating used in this research was developed in the Leibniz-Institute by using a special catalyst. It consists of a commercially available low molecular weight polyester resin and a commercially available uretdione crosslinker as matrix components. The powder coating is applied to the metal substrate by electrostatic charging gun, and it is baked in an oven at 150 °C for 15 min. Table 14 describes the main properties and processing conditions.

Material	Matrix Components	Appearance	Molecular structure	Tg [°C]	Curing Process	Required Thickness [μm]
In-house Adhesive Powder Coating	low Mw polyester resin, Uretdione crosslinker, pigments	white pigment	Semicrystal.	≈50	150 °C for 15 min	50-80

Table 14. In-house adhesive powder coating characteristics.

3.2. COMPOSITE PREPARATION

The fabrication process of the hybrid specimens is summarized in Figure 27, and it will be explained in detail in the following lines.

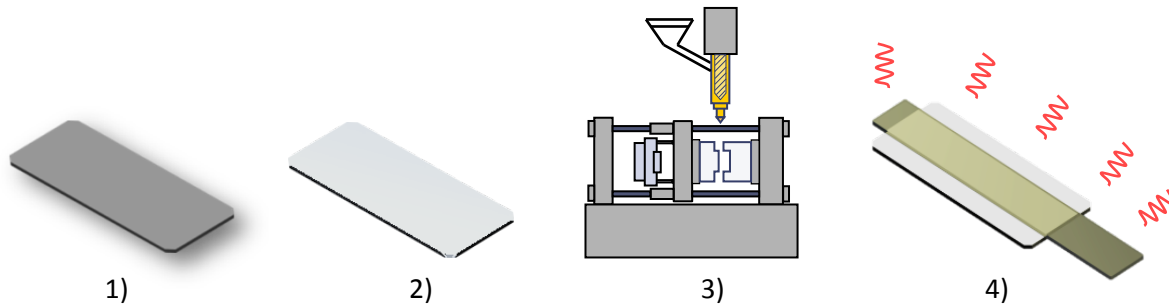


Figure 27. Manufacturing stages of polymer-metal hybrids. 1) Steel sheet preparation. 2) Powder-coating of the metal substrate through a corona charging gun and crosslinking in oven. 3) Overmolding of TPU on a vertical injection unit. 4) Annealing in an air circulating oven at different temperatures for 20 hours.

3.2.1. Steel Sheet Preparation

Plain steel sheets were cleaned and degreased with a solution of acetone, benzene and ethyl acetate to remove the industrially applied grease, oil, and any pollution before applying the adhesive coating. Zinc phosphated and e-coated steel plates did not require a prior cleaning procedure, but they were stored in temperature and humidity controlled rooms, and handled with care using cloth gloves through the whole process to avoid any pollution on the surface.

3.2.2. Powder Coating

The in-house powder is sprayed onto the plain and Zinc-phosphated metal sheets through a corona charging gun that joins the powder electrostatically to the steel substrate, as in Figure 28. The e-coated substrates could not be powder-coated due to the higher resistivity of the e-coating organic layer.

The corona charging method is realized by a high potential created at an electrode that is located in the powder stream. The powder particles are crossing the high potential electrode at the exit of the gun, become charged and are attracted to the grounded metal substrate. The charged particles remain adhered to the grounded substrate until the powder-coated sheet is placed in an oven where it flows into a continuous coating [114]. The freshly crosslinked substrates are then stored at room temperature for 24 hours until the next step in the processing chain.

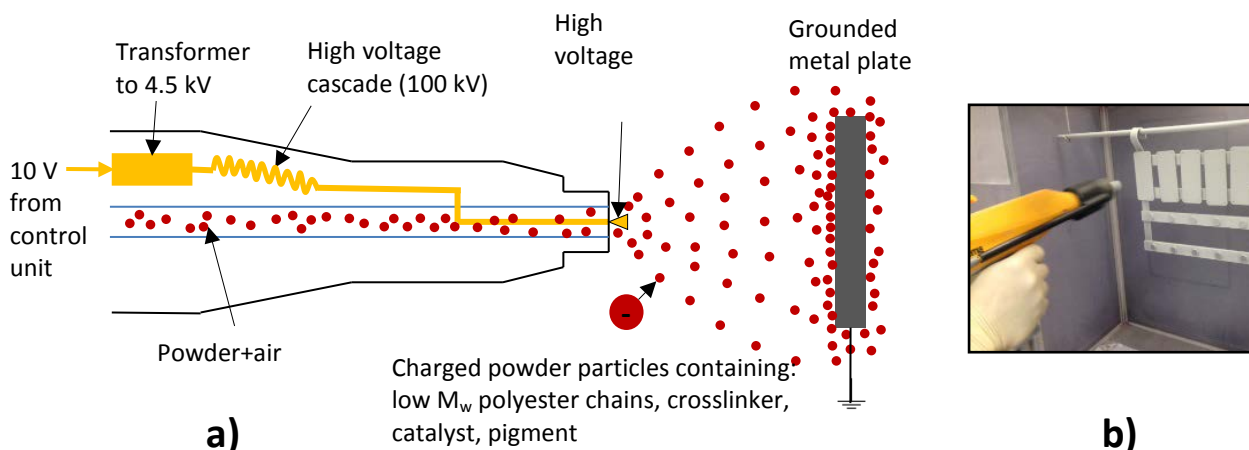


Figure 28. a) Powder coating corona charging principle and b) application of the powder to the steel substrates.

The final controlled thickness of the coating is between 50-80 μm . However, because it is a manual process which depends -to some extent- on the skill of the person applying the coating, the roughness' homogeneity, R_a , is difficult to achieve through the whole surface, as it was measured in a wide range by AFM: $R_a=0.06 - 0.5 \mu\text{m}$.

- Crosslinking Process during Baking in the Oven

The freshly sprayed particles contain as matrix components a commercial low molecular weight (\overline{M}_W) polyester resin and an uretdione crosslinker. Additionally, a $\text{Zn}(\text{acac})_2$ catalyzer and a white pigment based on Titanium Oxide were incorporated in the powder material. Immediately after the powder coating process, the steel sheets are placed in an oven at 150 °C for 15 min. At those conditions, the catalyst, $\text{Zn}(\text{acac})_2$, starts the reaction by opening a dimerized isocyanate ring that allows the crosslinking with the $-\text{OH}$ functionalized group from the low \overline{M}_W polyester chains, as illustrated in Figure 29. A complete crosslinking is ensured by controlling the curing temperature inside the oven, and a final polyallophanate network is kept from the molten film.

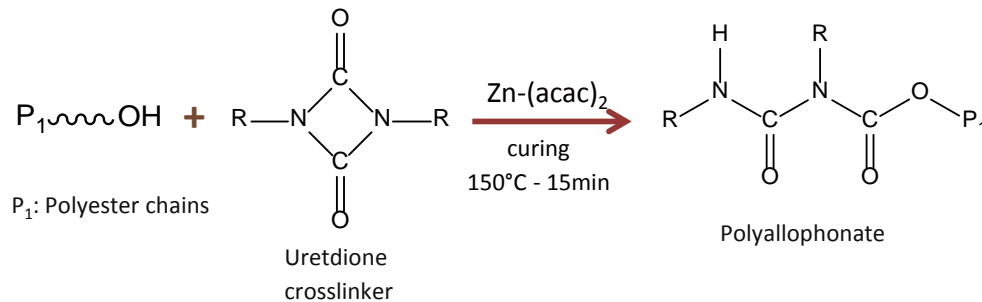


Figure 29. Reaction of Uretidion as crosslinker and OH-groups from polyester and $\text{Zn}(\text{acac})_2$ as catalyst [18].

3.2.3. The Overmolding Process

The overmolding of the TPU on the pre-coated metal was made in an Engel Victory 80 vertical injection unit. The overmolding parameters for the TPU were investigated in detail in previous works of the polymer processing group of the Leibniz-Institut [4,115] and are illustrated in Figure 30.

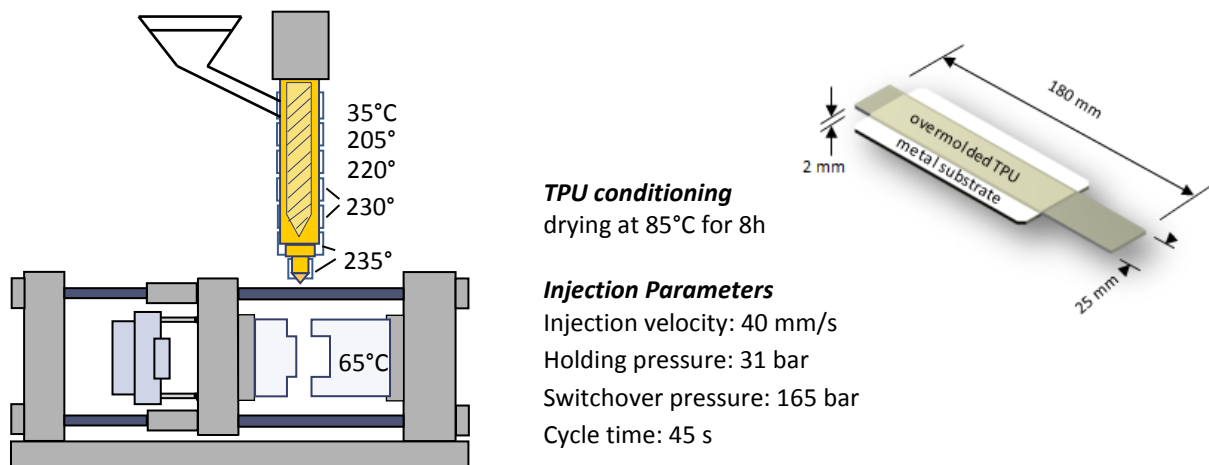


Figure 30. TPU Injection parameters and dimensions of the overmolded TPU on the metal substrate.

- Crosslinking Process of the in-house Coating during the Overmolding Process

When the TPU is overmolded on the pre-coated plate, an additional chemical reaction occurs between the polymer and the polyallophanate film at temperatures higher than 160 °C. It is expected that OH groups of residual polyester oligomers, from the already crosslinked adhesive coating, react with the urethane groups of the TPU forming a polyurethane network at the interphase; the overall reaction is displayed in Figure 31.

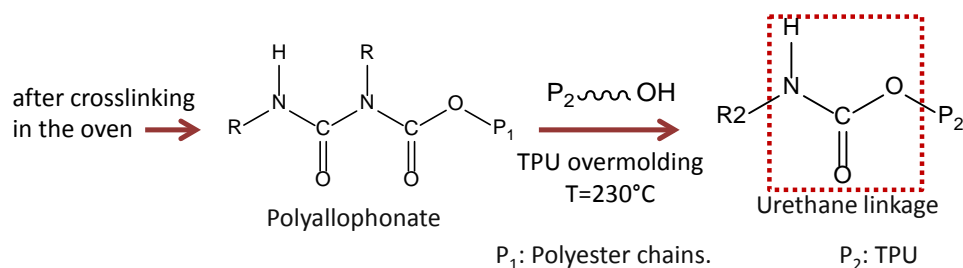


Figure 31. Expected reaction of the adhesive coating with the urethane groups of the TPU during overmolding [18].

3.2.4. Annealing

Immediately after the overmolding process, the hybrids are placed inside a convection oven. Three batches were annealed for 20 hours at different temperatures: 50, 70, and 100 °C. The lower annealing temperature was decided based on the glass transition temperature, T_g , of the in-house adhesive coating, which is around 50 °C. The highest annealing temperature was chosen following the recommendations of the TPU manufacturer, who suggests an annealing temperature of 100 °C for 20 hours in order to reach faster equilibrium conditions and thus, higher mechanical properties. It is not found in literature how an annealing thermal treatment could affect the adhesion and durability of a polyurethane-steel hybrid; neither information about the stability and lifetime of the adhesive coating when subjected to an additional thermal load: ongoing reactions cannot be excluded at this stage.

3.2.5. Summary of Prepared Specimens

Figure 32 illustrates hybrid specimens prepared for this work. The basis for the steel substrates is a low carbon, plain steel on which different surface treatments were applied: phosphated and e-coat. These substrates were received directly from an industrial partner. On top of the plain and phosphated substrates, the in-house adhesive powder-coat was applied, represented in Figure 32 in white color. Subsequently, the TPU was overmolded on the pre-coated substrates, including the e-coated steel, here displayed in black color. Immediately after the overmolding process, samples were annealed at different temperatures for 20 hours; then, the hygrothermal aging took place in various conditions. Hybrids and

individual materials were examined at every step of the processing chain to analyze structural changes in the single components or the polymer-metal joints.

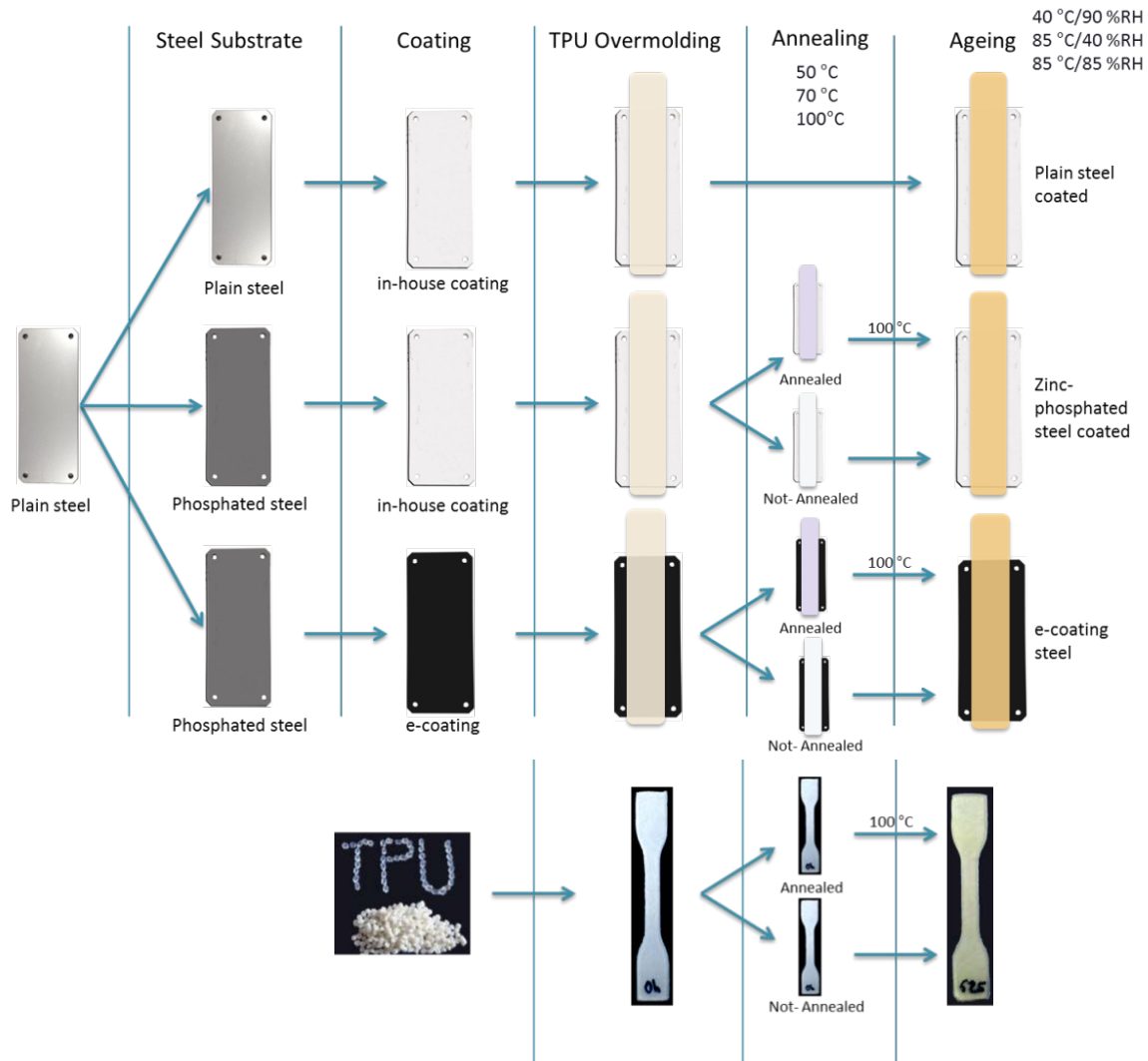


Figure 32. Summary of hybrids and parameters used in this work.

3.2.6. Summary of Adhesion Mechanisms in the Polymer-Metal Hybrid

Figure 33 depicts the activation of the adhesive coating during the production stages and the corresponding adhesion mechanisms that occur between the different materials that take part in the hybrid specimen. During the powder coating process, the negatively charged powder particles, are adhered to the surface of the steel substrate by electrostatic interactions with the cations at the metal surface. Mechanical interlocking plays a role in such a way that the adhesion force between the in-house coating and the metal substrate depends on a greater extent on the superficial roughness on the steel part.

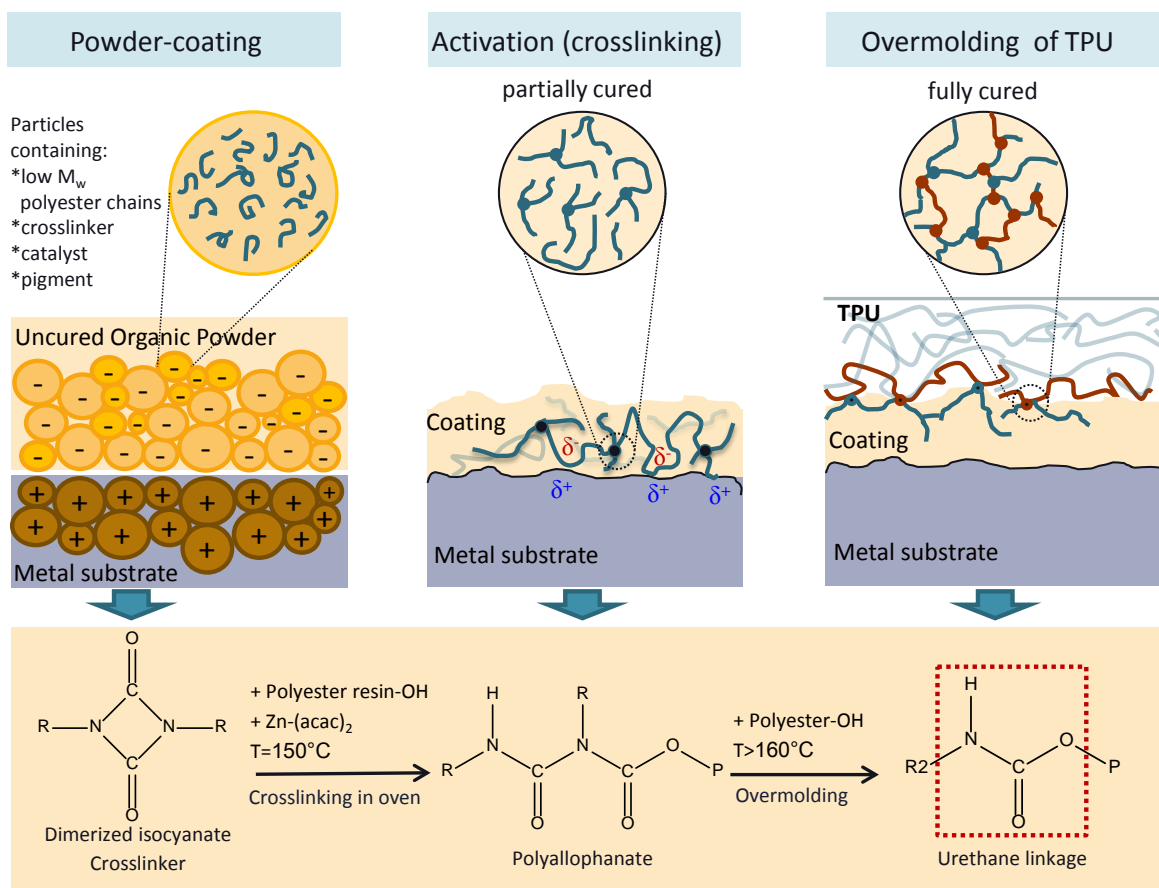


Figure 33. Summary of adhesion mechanisms during the composite production stage.

During the activation stage in the oven, the powder melts and forms a continuous polymeric layer. When the crosslinking process finishes, the organic coating adheres to the metal substrate by mechanical interlocking, by polar and secondary interactions between the ions and OH^- groups of the steel part and the polar NH groups of the urethane in the adhesive coating [48]. Additionally, Dillingham and Moriarty [116] in an extended work based on FTIR analysis, concluded that the adhesion between isocyanate-based polymers to steel is by covalent bonds of the metal oxides and urethane linkages. The existence of this type of organic-metal bonding explains the strong adhesion and durability of coatings and primers based on isocyanate groups.

During the overmolding process, the adhesion between the injected polymer and the coating is intended to be by covalent bonds between the urethane groups of the coating and TPU. It is also expected, that the melted polymer may inter-diffuse through the coating due to the high injection temperatures and pressures on the surface of the pre-coated steel.

3.3. CHARACTERIZATION METHODS AND EQUIPMENT

3.3.1. Mechanical Test

- Tensile Test

Tensile test in single TPU strips was performed following the Standard DIN EN ISO 527-2/S2, whose sample dimensions are displayed in Figure 34. The experiments were made using a 1kN Force Zwick Roell, ref. Zwick 1456, with an extensometer MultiXtens. The deformation speed was 100 mm/min. Specimens were extracted with a cutter-die from injected strips that were subsequently annealed and/or hygrothermally aged.

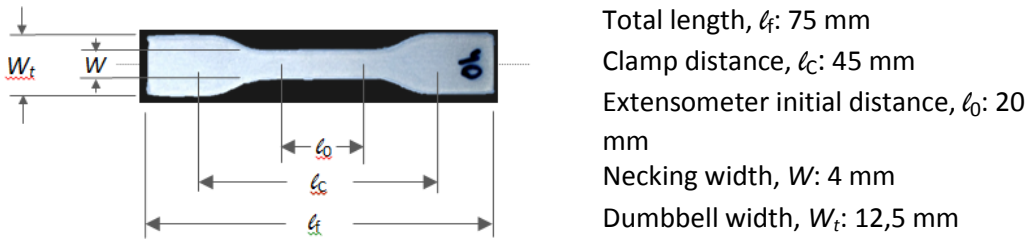


Figure 34. Standard tensile dumbbell specimens for TPU after DIN EN ISO 527-2.

- Peel Test

The main mechanical examination conducted in this work is a peeling test, which allows the direct evaluation of the adhesion of the polymer to the steel substrate. The test was made with a Zwick/Roell BZ2.5/TH1S. The peeling evaluation was performed following the Standard from the *Verein Deutscher Ingenieure*, VDI 2019 [117]. 5 to 6 repetitions per batch were made to evaluate initial conditions, and for the aged specimens, one sample per reference due to size restrictions in the weathering chamber. The overmolded hybrid composite was placed horizontally, the ending part of the overmolded polymer was grabbed by the upper crosshead of the universal testing machine as displayed in Figure 35.

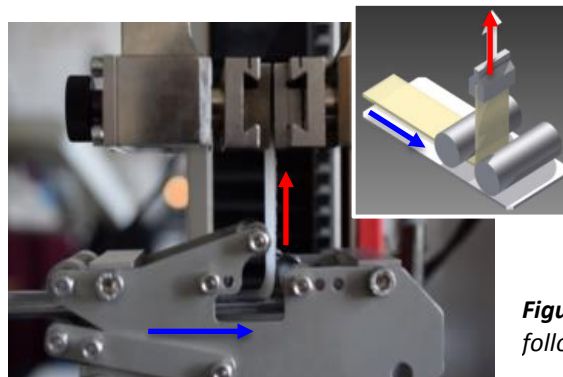


Figure 35. Setup of the peeling test following the standard VDI 2019.

The measured adhesion force, F_{ave} , is considered as the average force measured immediately after the yield point, which occurs at the debonding of the TPU at the edge of the, as indicated by letter A in Figure 36. The steadiness of the adhesion force through the metal plate was also an indicator of a successful bonding between the involved materials. The total work of adhesion (W_{adh}), also indicated in Figure 36, may be obtained experimentally by summing the areas under the curve of the initial Work of deformation (W_{D1}) until the yield point, as indicated by A; plus the Work of peeling (W_S) that is calculated as the area under the F_{ave} curve, and illustrated by B; and the Work of deformation of the polymer during peeling (W_{D2}), which is obtained from the polymer stress-strain deformation curve.

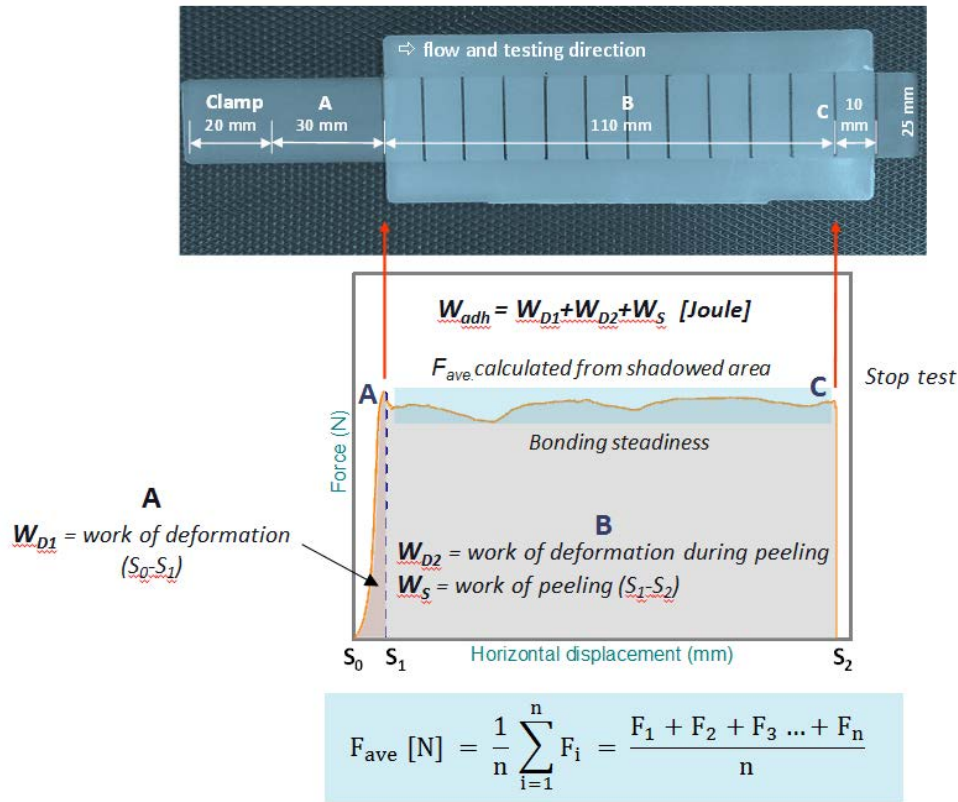


Figure 36. Average adhesion force, F_{ave} , determined from the peeling test.

3.3.2. Thermal Analysis

DSC on TPU

Thermal analysis was realized using a differential scanning calorimeter (DSC), model Q1000 from TA Instruments. DSC curves were obtained heating the samples from -80 °C to 230 °C, then cooling them down to -80 °C, and heating them up again to 230 °C. All steps were realized at 10 K/min under N_2 . Changes in the melting peak were examined in the first heating in order to evaluate the influence of

thermal history on crystallinity, and the T_g was measured in the middle point of the sloped region in the second heating step. Specimens were cut from a clean portion of the TPU stripe after the respective overmolding and annealing and their weight was in average 5.0 ± 1.0 mg.

DSC on Adhesive Coat

Thermal analysis of the in-house adhesive coat was realized by cooling the material to -80 °C, then heating it up to 230 °C at a rate of 10 K/min under N_2 . The second heating step was setup from -80 °C to 230 °C at 10 K/min. The weight of the fresh-powder samples was 6.0 ± 0.5 mg, and 2.5 ± 0.5 for coating samples scratched directly from the surface after curing/aging. The thermal analysis was performed after simulating real processing conditions directly in the DSC device under N_2 . The processing conditions and their thermal cycles were programmed as follows:

Curing stage: from 20 °C to 150 °C at 50 °C/min, holding for 15 min, cooling to 20 °C at 10 °C/min. Then, the evaluation of thermal properties of the adhesive coating was done by cooling down the sample to -80 °C and heated it up again to 230 °C at a rate of 10 K/min. A second heating step from -80 to 230 °C at 10 K/min was also programmed.

- Overmolding stage: includes the continuous DSC cycle of curing (described above), plus the next cycle: from 20 to 230 °C at 100 °C/min - holding for 0.5 min - cooling to 20 °C at 100 °C/min. Then, the evaluation of thermal properties of the adhesive coating was done by cooling down the sample to -80 °C and heated it up again to 230 °C at a rate of 10 K/min. A second heating step from -80 to 230 °C at 10 K/min was also programmed.

- Annealing stage: includes the continuous DSC cycles of curing and overmolding (described above), plus the next cycle: from 20 to 100 °C at 50 °C/min - holding for 20 hours - cooling to 20 °C at 10 °C/min. Then, the evaluation of thermal properties of the adhesive coating was done by cooling down the sample to -80 °C and heated it up again to 230 °C at a rate of 10 K/min. A second heating step from -80 to 230 °C at 10 K/min was also programmed.

DSC on e-coat

Thermal analysis of the e-coat was realized by cooling the sample to -80 °C, then heating it up to 230 °C at a rate of 10 K/min under nitrogen. The second heating step was setup from -80 to 230 °C at 10 K/min. The weight of the powdered samples varied from 2.0 ± 0.5 mg, and they were obtained from peeling out the already coated steel sheet.

Thermogravimetric Analysis, TGA

The TPU and adhesive promoter coats that were in direct contact were evaluated through thermogravimetric analysis was performed by a TGA Q5000 of TA Instruments, from room temperature to 800 °C, under nitrogen and oxygen at three different heating rates: 5, 10 and 15 K/min. The examination was conducted on hygrothermally aged composites as well. Figure 37 describes the location of the specimens from where the polymer was extracted for examination.

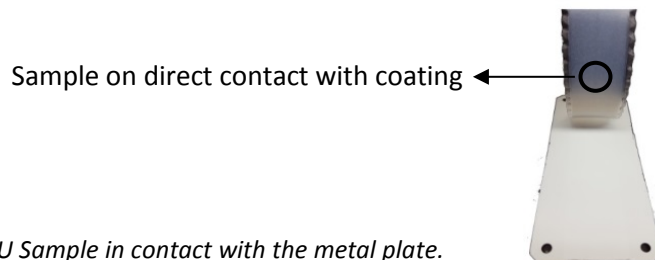


Figure 37. TPU Sample in contact with the metal plate.

3.3.3. Surface Analysis

Dynamic Contact Angle Measurement

In order to evaluate the wettability of the metal substrates, a contact angle measurement was conducted on the different metal surfaces used in this work. The measurements were performed using an OCA 35 XL (DataPhysics Instruments GmbH, Germany). Before the measurement, samples were rinsed with ethanol. The measurement was done with water droplets. Initially the volume was 5 μl , and then it was increased to 15 μl to measure the advancing contact angle, Θ_a . Afterwards, it was reduced again for measuring the receding contact angle, Θ_r , as illustrated in Figure 38.

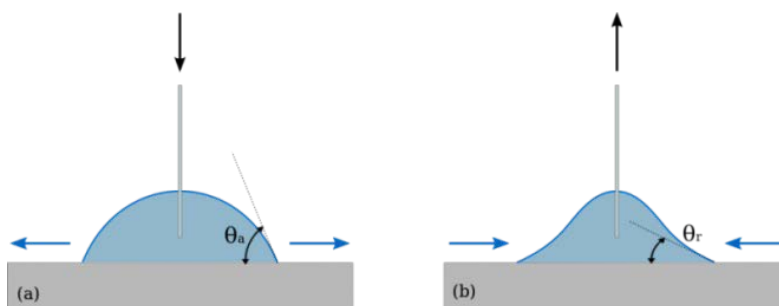


Figure 38. Dynamic contact angle to measure advancing contact angle, Θ_a , and receding contact angle, Θ_r [118].

AFM.

Surface analysis of the coated and uncoated metal substrates was performed by atomic force microscopy, AFM, using a Dimension 3100/NanoScopeV from Bruker.

SEM

Surface evaluation and chemical characterization of the metal plates and TPU in direct contact with the adhesive coatings were performed using a scanning electron microscope (SEM), SEM-Ultra Plus from Zeiss, coupled with energy dispersive X-ray spectroscopy components. Before the investigation, samples were sputtered with 3nm PT to avoid charging.

X-Ray Photoelectron Spectroscopy – XPS

Surfaces of adhesive coatings were analyzed at the atomic level using an XPS AXIS Ultra from Kratos, UK. With this spectroscopic method it is possible to produce chemical maps of the respective surface and bonding of surface species in a depth profile analysis up to ~10 nm. The samples were placed in the device holder and a monochromatic X-ray source excited the electrons in the surface of the substrate. Two lenses-systems were used: one is electrostatic to project them to the detector; the other is a magnetic system to bring more electrons to the electrostatic lens. In case of magnetic surfaces, like in the plain phosphate and plain steel sheets, it was not possible to perform the measurements due to additional forces that acted on the sample and disturbed the automatic sample movement. To analyze the kinetic energy of the ejected electrons, a spherical mirror analyzer and a delay line detector were used. By using a higher value (160 eV) a high signal was acquired, but lower spectral resolution. This mode was use in order to characterize the general chemical spectrum. By using smaller pass energy (20 eV) better spectral resolutions are obtained, so with this mode we got detailed measurement of atomic lines to see chemical shifts.

Digital Microscopy

Examination of aging in coatings was performed in a digital microscope Keyence ref. VHX-2000, from Japan. The microscope has specialized software that allows, by contrast, quantification of corrosion spots on the surface of the in-house coating.

Metal Surface Resistivity

In order to determine the powder-coating feasibility on steel substrates, electrical resistivity characterization had to be conducted following the Standard IEC 61340 [119], using the corresponding devices:

- Electrometer Loresta from Mitsubishi: suitable for resistivities $< 108 \Omega$.
- Electrometer Hiresta von Mitsubishi: Suitable for resistivities between $104 - 1013 \Omega$.

3.3.4. Infrared Spectroscopy Examination - FTIR

An Spectrometer Tensor 27, from Bruker, with a standard sample cell, Pike Miracle single-bounce (ATR) cell, equipped with a ZnSe single crystal was used. Fourier Transform-Infrared Spectroscopy (FTIR) is an analytical method that allows characterizing or identifying organic materials or compounds. When an IR beam passes through a sample, some radiation is absorbed by the sample, and some is transmitted. The final signal received by the detector is a spectrum representing the molecular vibrations and structures from the chemical groups that constitute the polymer. The absorbed infrared radiation excites molecules into a higher vibrational state. The frequency of the absorption peak is determined by the vibrational energy gap, so the number of absorption peaks is referred to the number of vibrational freedom of the individual molecules. A computer must transform the signal obtained by the detector into a single beam IR spectrum by a Fourier transformation [120,121]. Specimens were examined using an Attenuated Total Reflectance (ATR) technique, which allows measuring in the solid state without special preparation. In this method, a total internal reflection from an IR beam, which passes through the ATR crystal, reflects at least once from the inner surface in contact with the sample, as in Figure 39. The corresponding reflection creates an evanescent wave within the sample. The penetration depth is between $0,5 - 2 \mu\text{m}$.

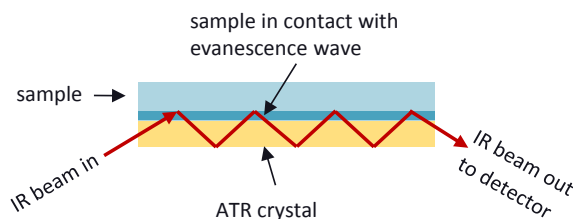


Figure 39. Standard principle of IR beam with an organic sample by FTIR [162].

Figure 40 is displaying the Spectrometer Tensor 27, with the ATR cell, and the setup of the TPU stripe covering the crystal surface.

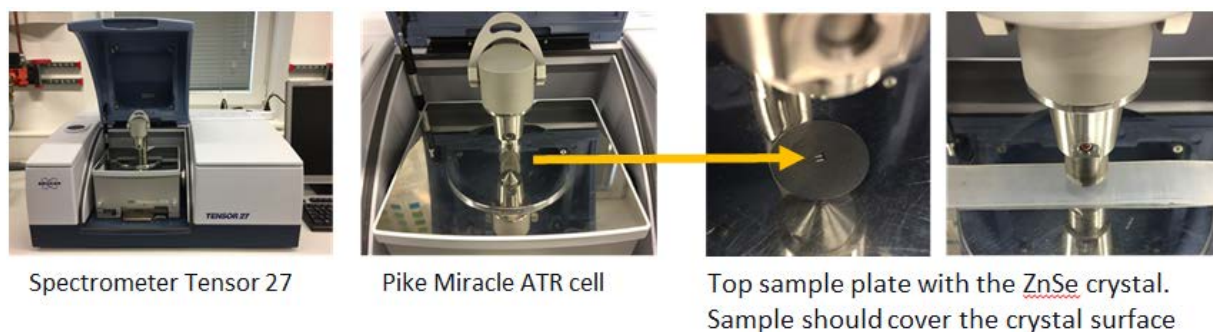


Figure 40. Experimental setup for analysis of TPU stripes used in this work in the FTIR device.

To understand better the degradation and failure mechanisms of the polymer-metal composite, fresh overmolded TPU specimens were examined with and without annealing at 100 °C for 20 hours. Subsequently, artificially aged samples, annealed and not annealed, were analyzed after different hygrothermal aging times and conditions. To remove any impurities from the surfaces, samples were cleaned carefully with ethanol. Measurements were taken on top and on the bottom surface of the polymer that was in direct contact with the coating, as illustrated in Figure 41. Examination of change in the polymer molecular structure by FTIR was conducted immediately after the peel test.

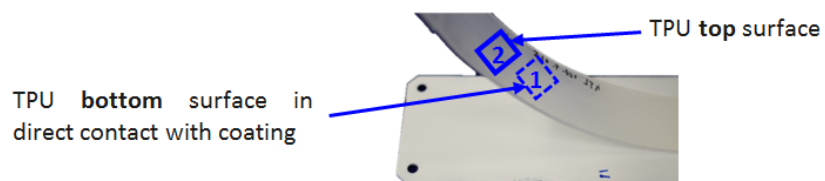


Figure 41. Specimen top and bottom schematic representation for FTIR examination in the overmolded TPU.

3.3.5. Permeation of Gases through the TPU

Permeation evaluation to determine diffusivity of O₂, N₂ and CO₂ in fresh and annealed TPU was conducted in a gas permeability tester, ref. GDP-C from Brugger, Germany. Permeation examination was performed at 40 °C and 20 °C for all samples. The device determines the diffusion parameters according to manometric measurements. The TPU sample, which has to be in the order of micrometers in thickness, was extruded ensuring a uniform thickness of 300 µm, as it was measured in a conventional film thickness profiler. Then, squared-shaped specimens were cut by approximately 6 x 6 cm and stick to an aluminum foil with a hole in the center of 2.5 cm, as described in Figure 42.

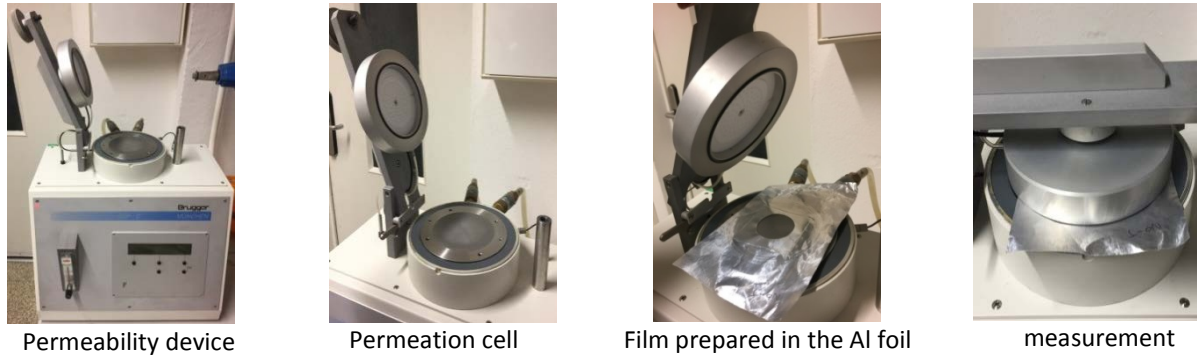


Figure 42. Permeation of gases through a TPU film.

The sample is placed inside the permeation cell, as illustrated in Figure 43. Before the test starts, the upper and lower chambers are under vacuum for 24 hours in order to evacuate any gas inside the polymer film. After this time, the top chamber is filled with the test gas that permeates the film creating a pressure increase in the bottom part of the permeation cell. The device computes the Gas Transmission Rate (GTR) by evaluating the growth of pressure in relation to time and the device specific volume. In the measurement stage, the GTR value increases until equilibration remaining constant. At this point, not only the GTR can be calculated but also the diffusion constant [122].

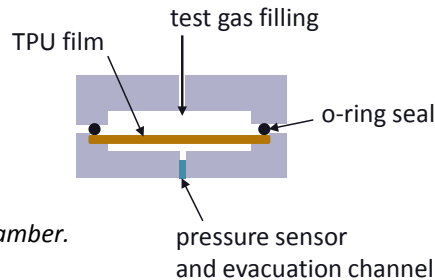


Figure 43. Permeation measurement chamber.

3.3.6. Accelerated Hygrothermal Aging

The accelerated aging test was conducted to evaluate failure modes of the multilayer hybrid under severe environmental conditions. The aging test is a fundamental part of this work because it is unknown until now why, how and where the multilayered part will fail, as sketched in Figure 44. Due to the several materials and components that make up the composite, it is difficult to predict the failure mode so it could be assumed that the main causes that shortened the lifetime of the composite are related to the hydrolysis or thermal degradation of the polymer or the adhesive coatings. Corrosion on the metal substrate may play a significant role on the part's endurance; and last but not least, it is essential to establish if the catastrophic failure will occur adhesively or cohesively or a combination of both. For this reasons, it was decided to evaluate the influence of the temperature and humidity on the adhesion of the composite separately after 1000 hours of exposure as follows: the first batch of specimens was

subjected for 1000 hours to 40 °C/90 %RH, which exemplify an extreme tropical weather. To evaluate in detail the influence of temperature on the adhesion of the polymer to the metal substrate, a second set of samples was subjected to a relatively high temperature and low humidity conditions: 85 °C/40 %RH. The last batch was aged under severe environment conditions to accelerate the lifetime of the hybrid to determine and correlate the failure mode of the multilayered part with the other weathering tests.

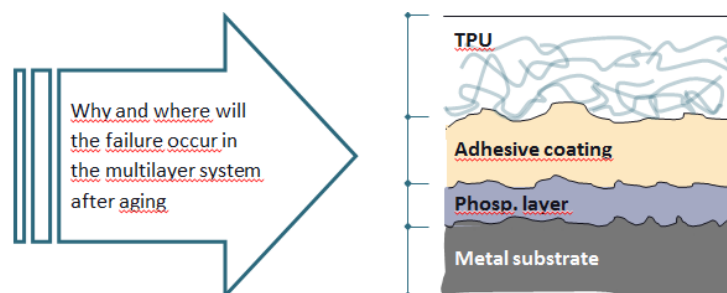


Figure 44. Illustration of the different layers that build up the hybrid specimen.

The accelerated aging was conducted in a weathering chamber ESPEC LHL-114 from Japan, which is suitable to work from +5 to +85 °C and from 40 to 95 %RH. The setup of samples inside the chamber is shown below in Figure 45. The aging test was performed on hybrid composites and neat TPU strips, in both cases with and without annealing. Samples subjected to 40 °C/90 %RH and 85 °C/40 %RH were taken out of the chamber for in-depth analysis after 50, 145, 218, 304, 385, 458, 530, 625, 700, 850, 925 and 1000 hours of exposure. Specimens exposed to a harsh environment, i.e. 85 °C/85 %RH, were analyzed at 49, 145, 218, 304, 385, 456, 530 and 625 hours. It was decided not to do further accelerated aging at this conditions because the premature failure of hybrids occurred after 145 hours of exposure, as it will be seen in detail in chapter 6.

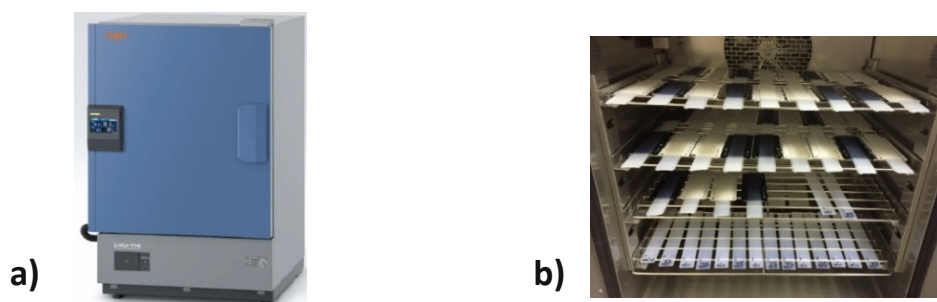


Figure 45. a) Constant climate cabinet ESPEC LHL-114, Japan. b) Setup of specimens ready to be artificially aged.

EXPERIMENTAL RESULTS AND DISCUSSION

4. SURFACE ANALYSIS OF STEEL SUBSTRATES

4.1. MICROSCOPIC SURFACE CHARACTERIZATION OF STEEL AND COATED SUBSTRATES

In Figure 46, the steel sheets used in this work exhibit different optical appearance defined by the superficial pretreatment: the zinc-phosphated has a mate-gray aspect due to the phosphate compounds on the surface, as seen in the corresponding SEM micrograph. The e-coat substrates are black due to the organic compounds and inorganic pigments. In this case, the black color also protects the organic coating from UV radiation.

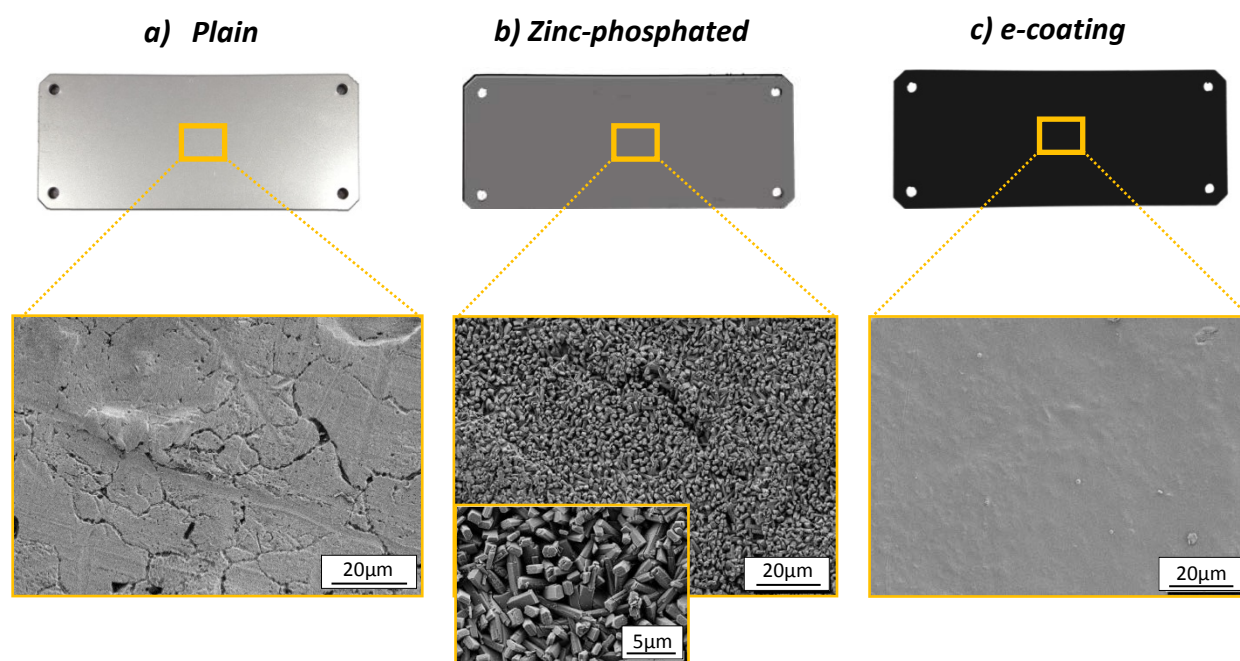


Figure 46. The three different steel sheets used in this work and their respective SEM surface analysis. a) Plain steel after solvent cleaning, b) Zinc-phosphated and c) e-coated steel pretreated sheets

In Figure 47, the AFM images of a 20x20 µm² surface sections with their arithmetic mean roughness, R_a , of a) plain degreased steel, b) as-received zinc phosphatized steel, c) cured in-house powder-coating on the phosphatized metal, and d) e-coat on phosphatized steel. The higher mean roughness of the zinc-phosphatized metal substrate is due to the presence of phosphate crystals on the metal surface as in micrograph in Figure 46 b). These crystals are non-conducting and thus essential for the corrosion protection of the steel; additionally, the high porosity between crystals, observable also by SEM in Figure

46 b), is beneficial for anchoring the powder coating that is applied in the subsequent step. R_a indicates the average superficial roughness range measured by confocal microscopy.

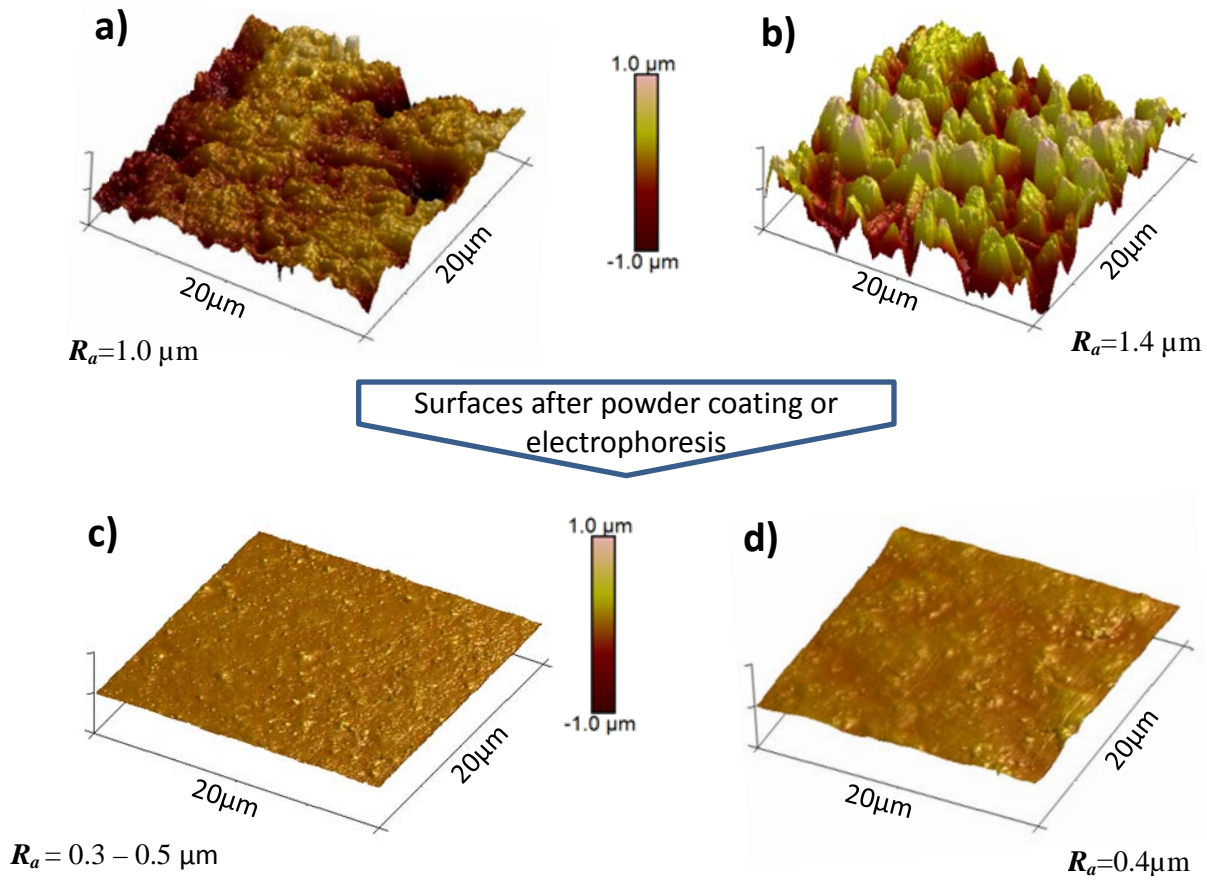


Figure 47. AFM analysis of metal surfaces and their corresponding arithmetic mean roughness R_a of a) plain steel after solvent cleaning, b) zinc phosphated steel, c) zinc-phosphated steel sheet with the in-house adhesive coating in the polyallophanate state on top, and d) zinc phosphated steel with e-coat.

4.2. DYNAMIC CONTACT ANGLE MEASUREMENT

Table 15 enlisted the advancing (Θ_a) and receding (Θ_r) contact angles and the corresponding deviations (d), measured for the different steel substrates used in this work. The dynamic contact angle measurement for the phosphated metal sheet presents a high contact angle hysteresis (difference between advancing and receding contact angles) due to its high roughness, as displayed in Figure 47 b). The phosphatized surface also had the highest high contact angle, corresponding to a low wettability ($>90^\circ$) [123]. High wettability was measured on the in-house and e-coat steel sheets, as listed in Table 15. Wetting properties of substrates are essential in the overmolding process and subsequent adhesion of the polymer to the metal substrates.

	Plain steel				Phosp. Steel				Phosp. + in-house coating				e-coat			
Drop number	Θ_a	d	Θ_r	d	Θ_a	d	Θ_r	d	Θ_a	d	Θ_r	d	Θ_a	d	Θ_r	d
1	88.6	0.5	28.0	0.6	103.6	1.3	11.3	3.2	76.6	0.4	48.4	0.2	82.6	0.2	43.2	0.3
2	87.7	0.3	23.3	1.0	103.9	1.1	16.9	3.5	77.3	0.1	47.8	0.6	82.6	0.2	45.5	0.9
3	88.1	0.4	28.1	0.8	110.3	0.5	18.9	5.4	75.1	0.1	46.1	0.4	82.9	0.3	46.6	1.0
4	88.9	0.2	27.4	1.0	112.9	0.6	19.8	2.6	77.3	0.2	49.3	0.2	82.7	0.2	45.1	0.5
5	86.4	0.7	23.9	2.6	110.1	1.2	16.7	5.7	76.8	0.2	48.4	0.5	82.6	0.2	44.5	0.4
Ø	87.9	0.9	26.1	2.1	108.2	3.7	16.7	3.0	76.6	0.8	48.0	1.1	82.7	0.1	45.0	1.1

Table 15. Advancing Θ_a and receding, Θ_r , contact angles, and their corresponding deviations, d, measured on different metal substrates.

4.3. SURFACE CHEMICAL CHARACTERIZATION

4.3.1. Fourier Transformed Infrared Spectroscopy - FTIR

Figure 48 displays the IR internal reflected beam from the a) in-house, and b) e-coat surfaces on the steel substrates. The frequency of the reflected IR beam in the inner surface is measured as Attenuated Total Reflectance (ATR) vs. wavelength number (cm^{-1}). It is found that in both coatings there are characteristic absorption bands between $3500 - 3300 \text{ cm}^{-1}$ corresponding to primary amines (NH) and hydroxyl groups (O-H). This approximation demonstrates the similarity between the two systems: the in-house coating consisting of a low molecular weight polyester resin crosslinked with urethane compounds; and the e-coat, which is based on epoxy-amine groups and a polyester-urethane crosslinker. The spectrum is broader for e-coat specimens indicating larger intermolecular interactions of OH and NH groups. The fingerprint region of both adhesive promoters is between $1500-400 \text{ cm}^{-1}$ of the spectra, and it is difficult to characterize due to the different vibrations that take place, such as single bond stretches and another types of bending vibrations.

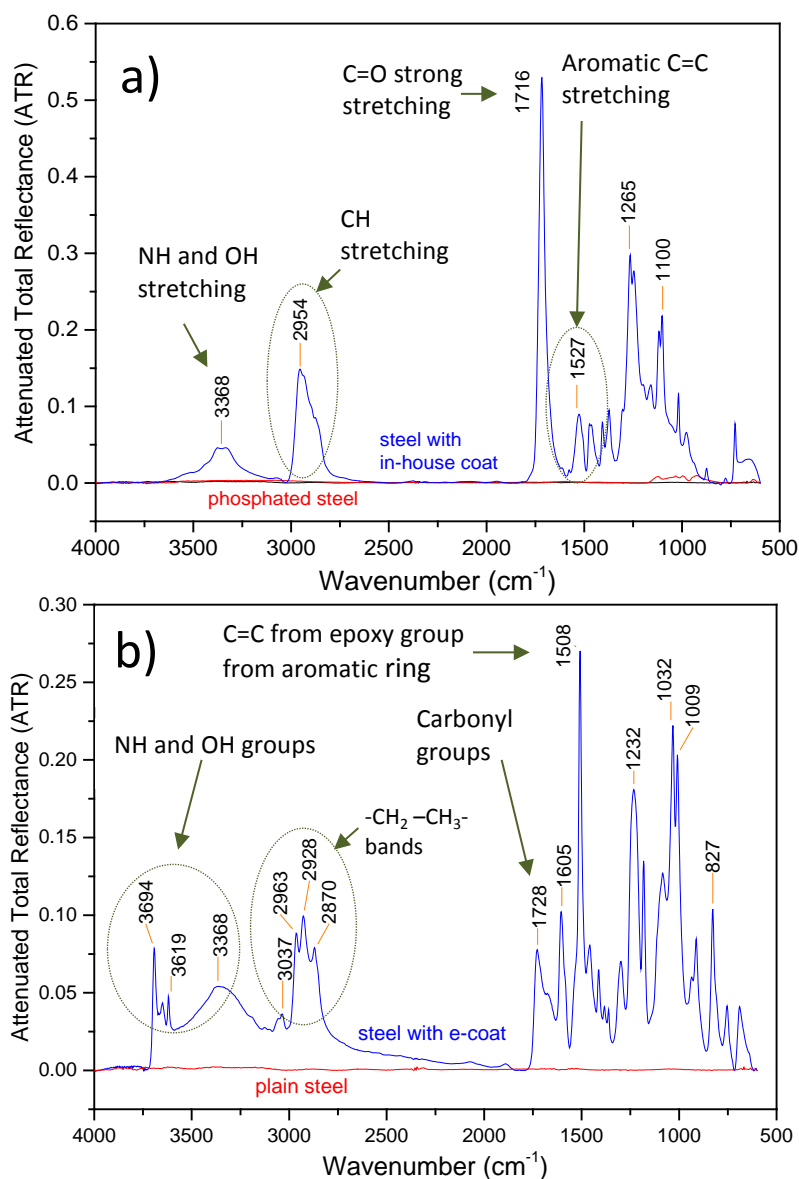


Figure 48. FTIR spectra of a) in-house adhesive promoter cured on the steel substrate and b) e-coat steel

4.3.2. X-Ray Photoelectron Spectroscopy - XPS

Figure 49 presents the general chemical composition of the e-coat and the in-house surfaces obtained by X-Ray Photoelectron Spectroscopy (XPS). The chemical survey is represented as the rate of counts per unit time (counts per second, CPS) of ionizing radiation vs binding energy. From Figure 49 it is visualized that the most predominant molecules for both coatings are N, O, and C. C and O intensities of the in-house coating are sharper because of slightly higher concentrations of those atoms in the crosslinked adhesive promoter. Similarly, Nitrogen atomic concentration in the e-coat doubles the one measured for the in-house compound. 1s Peaks indicate spectrum of electrons near to the nucleus. KLL spectrum

represent the energy of electrons ejected from the atoms due to the filling of the 1s state (K shell) by an electron from an L shell coupled with the ejection of an electron from an L shell [124].

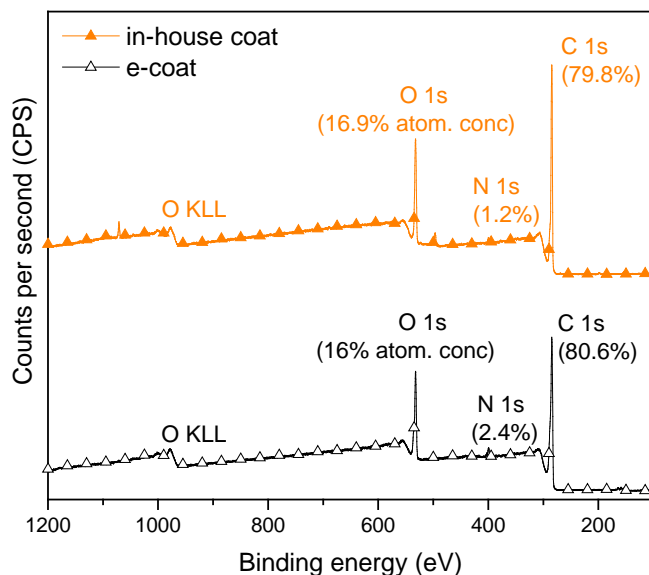


Figure 49. XPS counts per second (CPS) vs binding energy data for the in-house and e-coat surfaces

Also from XPS analysis, a high-resolution structure of the carbon 1s peak for both coatings is displayed in Figure 50. The different chemical interactions of the C with the surrounding molecules are presented as different peaks. Peak 1, represents C in the aromatic ring; peak 2 corresponds to aliphatic groups $R-CH_2-R$; peak 3, indicates aromatic-N bonds; peak 4 and 5 show the C on the alcoholic side of ester and the carboxylic groups, respectively. There is a remarkable concentration of C-O bonding in the e-coat when compared to the IPF coat, indicated below in peaks 4. The higher concentration of these bonds may later influence the interactions/adhesion at the interface. The XPS analysis of the e-coat evidenced an excess of the C-O atomic concentration of 33%, while in the in the IPF coating it sums up around 9%.

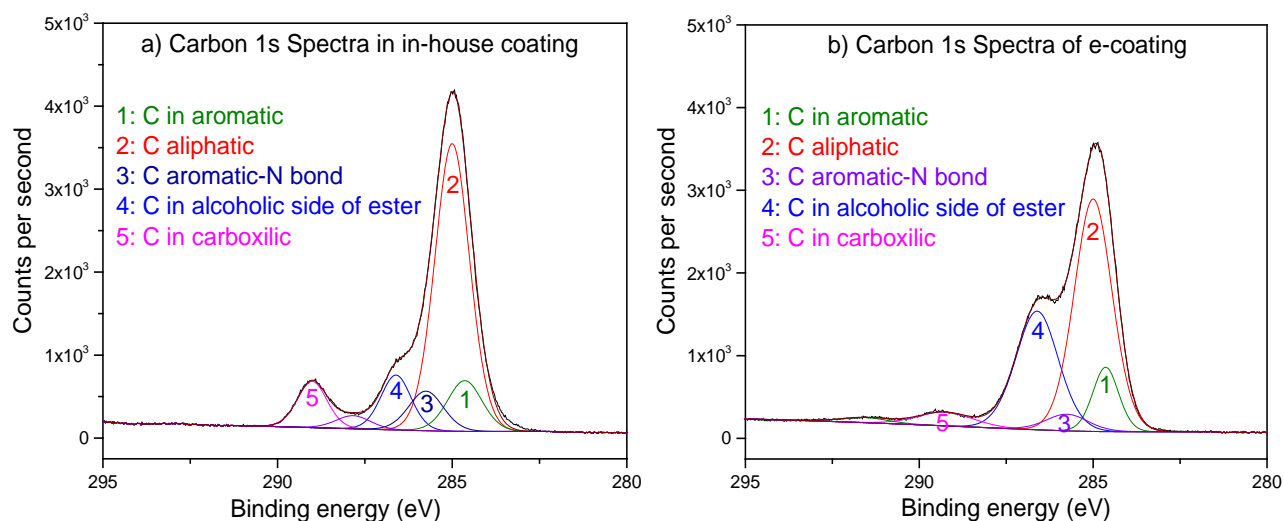


Figure 50. Carbon 1s high resolution spectra of the surface of the a) in-house coating and b) e-coating

4.4. METAL SURFACE RESISTIVITY MEASUREMENTS

In order to determine the applicability of the in-house powder coating on the different steel substrates, the surface resistivity was measured for all the pre-treated metal sheets. The electrical surface resistance in an electrostatic discharge process (powder coating) must be maximum in the order of 10^9 Ohm. The surface resistivity was measured in 8 different points through the whole surface, and the average values for each pretreated sheet are listed in Table 16. For the e-coated specimen, it was not possible to measure the resistivity because it is too high and exceeds the available range of the instruments. This high electrical resistivity, makes the e-coated steel not suitable for powder coating, is attributed to the relatively thick (≈ 40 μm) organic layer that ensures a high degree of corrosion protection.

Average Electrical Resistivity of Different Metal Substrates [Ohm]		
Plain	Zinc-phosphated	E-coating
1,12E-04	4,84E+07	Electrical resistivity is too high and cannot be measured with the instruments, $\rho > 10^{13} \Omega$

Table 16. Electrical resistivity on the different metal substrates

5. EFFECTS OF ANNEALING ON ADHESION AND MECHANICAL PERFORMANCE OF THE HYBRID

5.1. TPU PERFORMANCE

5.1.1. Molecular Mechanisms of Deformation of the Neat Polyester-based TPU

A typical mechanical performance of the thermoplastic polyurethane (TPU) used in this work, is shown in the stress vs strain tensile curve displayed in Figure 51. It consists of 4 different stages driven by the molecular architecture of the rubbery-like TPU [74,76]. In the first stage of deformation, the amorphous and soft domains are stretched in such a way that strain-induced crystallization occurs. In the second stage, the stretching of already deformed amorphous segments happens homogenously and can be seen in the stress-strain curve as a plateau. When the soft segments cannot stretch any longer, the hard and crystalline domains will start to deform in the direction of the applied force; in this situation, there will be an increase in the strength of the material as sketched in the third stage of the curve below. The fourth and final stage corresponds to the final plastic deformation and ultimate strength of the polymer, which is explained by the separation of crystalline block segments and orientation with the tensile axis.

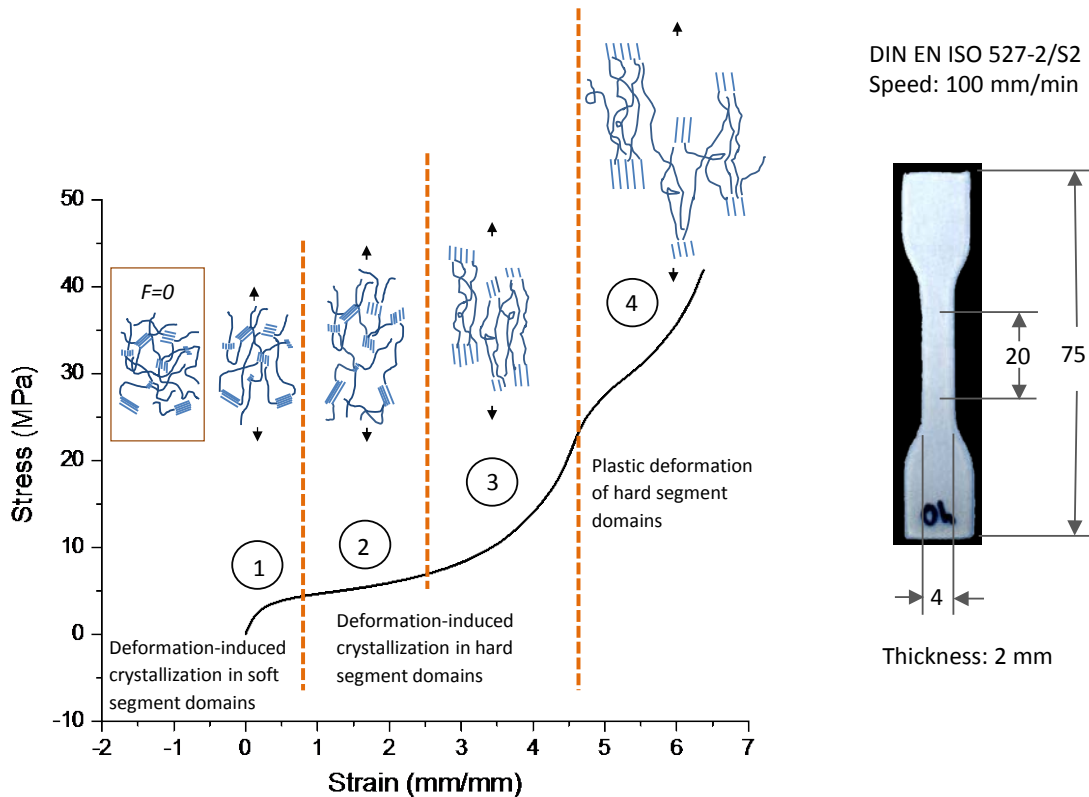


Figure 51. Stages of polymer chain strain in the plastic deformation of fresh TPU used in this work. Picture to the right is the dumbbell following the Standard DIN EN 527-2/S2.

The manufacturer of the Elastollan TPU remarks that injected parts necessitate several weeks of storing at room conditions to reach final mechanical properties, and therefore, a heat treatment (i.e. annealing) is recommended to attain final properties in shorter time [112]. Although the suggested annealing conditions, 100 °C for 20 hours, are mentioned in the processing recommendations, there is no indication about how the mechanical performance changes for that specific material. In this order of ideas, an evaluation of mechanical properties was realized, and it is shown in Figure 52. Part *a)* exhibits stress vs strain curves of injected TPU stripes after storing at room conditions after certain times. It is clearly seen that the ultimate strength increases at longer storing times with a consequent reduction of the final deformation. Figure 52 *b)* summarizes some important mechanical properties obtained in the tensile test: toughness, tensile strength and strain.

Toughness is defined as the ability of the material to absorb energy up to total failure, and it was calculated as the area under the stress-strain curves in part *a)*; its units are in $\text{J}\cdot\text{m}^{-3}$. Tensile strength or ultimate strength, in MPa, stands for the maximum stress that the material can bear on the engineering stress-strain curve at a certain strain. The strain is dimensionless, or more specifically its units are in mm/mm [6]. From Figure 52, one can conclude that the tensile strength is the only mechanical parameter that is clearly affected by storage time. There is a steady increase, passing from 35 MPa for the fresh TPU, to 40 MPa just after nine days of storing. The highest tensile strength was reached after nine months of storage, reaching 55 MPa, which corresponds to a step-up of approximately 60%. Regarding toughness, there is an apparent increase after 15 days of storage, and it stabilizes after one month, reaching approximately 108 J/m^3 , this gaining in toughness is attributed to the higher tensile strengths attained just after two weeks of storing. About the strain, it remains unaltered after nine months of keeping the polymer in room conditions.

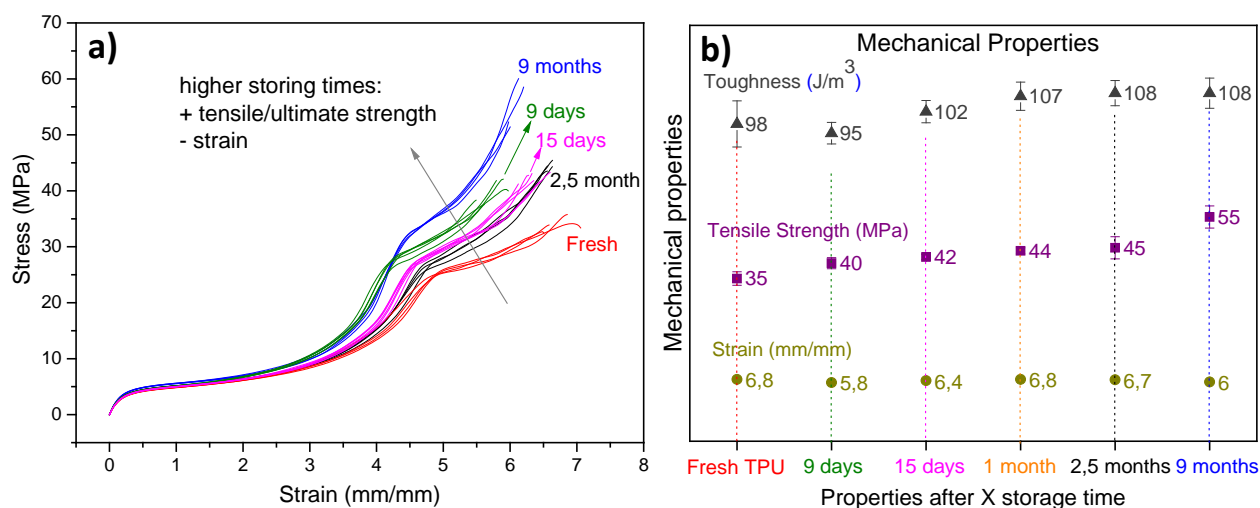


Figure 52. a) Strain-stress tensile curves of TPU Elastollan C85A10 stored at different times and b) a summary of the main mechanical properties after a certain storage time.

5.1.2. Effects of Different Annealing Temperatures on Mechanical Performance

Figure 53 a) displays stress vs strain curves of freshly injected and annealed TPU stripes. Annealing process was conducted at various temperatures (50, 70, 85 and 100 °C) for 20 hours in an air circulating oven to evaluate the influence of the thermal treatment on the mechanical properties of the polymer. As showed in Figure 53 b), annealing at 100 °C increased the toughness of the material; this is attributed to the proportional increment of the ultimate strength, passing from 35 to 46 MPa, which is equivalent to more than 30% increment in that property. The tensile strength of the heat-treated material, even at the lower annealing temperature, i.e. 50 °C, stepped up to 43 MPa, an increase equivalent to 22% when compared to the untreated polymer. This mechanical property remains steady at other thermal treatments with a slight improvement at 85 and 100 °C, jumping to 46 MPa in both cases. Heat treatments at 50, 70 and 85 °C did not influence the ultimate deformation of the polymer as indicated by the strain of the material. Properties of a freshly annealed TPU at 100 °C, are more or less equivalent to those of samples that were stored more than two months as illustrated in the figure below with “X” marks.

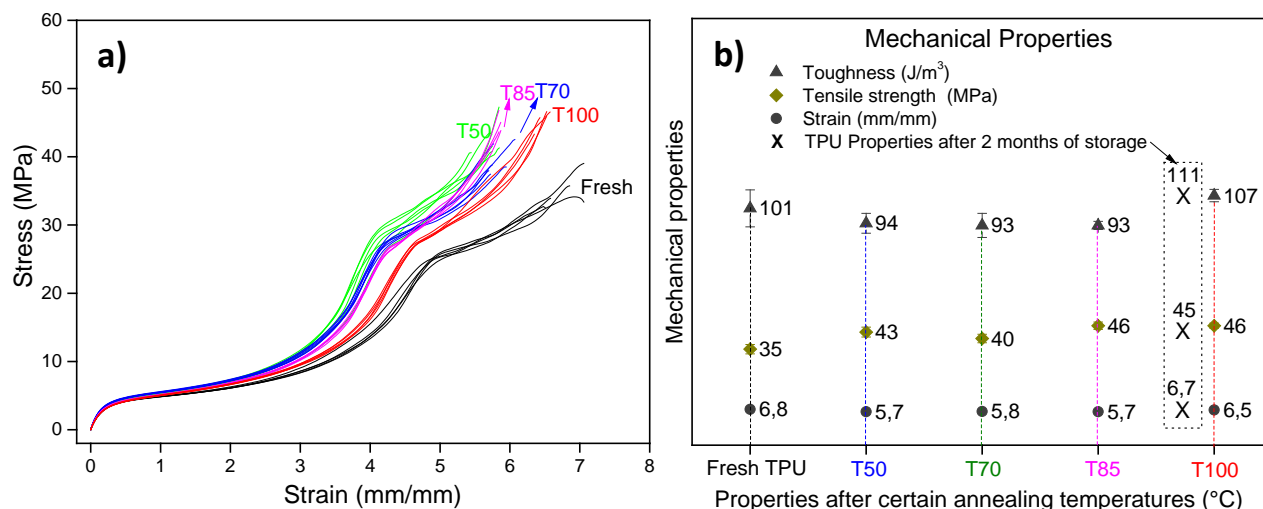


Figure 53. a) Stress-strain curves of the TPU used in this work after different annealing temperatures. b) Influence of different annealing temperatures on mechanical properties of TPU. The “X” marks illustrate the equivalence of properties obtained in polymer samples after two months of storage as displayed in Figure 52 b).

5.1.3. Analysis of Thermal Properties

Figure 54 exhibits the TPU thermographs of dried pellets before processing, and after injection of stripes. DSC curves were obtained in the first heating step, from -80 to 230 °C at 10 K/min under N₂. Thermal analysis display the influence of processing conditions on the molecular structure of the polymer, which

it is explained in detail in the literature [75,78]. The T_g for the freshly injected polymer increased slightly when compared to the unprocessed pellets, and it was detected at -46°C . At higher temperatures, the sharp endothermal peaks of the dried pellets disappeared when the polymer is processed. A new wide endothermic region appears between 25°C and 125°C and may be explained by the re-arrangement of short-range hard segments crystallites. At higher temperatures, a new melting area is observable between 130°C and around 200°C . This may be referred to the melting of the long-range hard segments crystallites, which are also an indication of the broad melting temperature range of the polymer as seen in T_{m2} and T_{m3} . As stated by Brunette et al. [125], N-H intermolecular bonding influences polyurethanes properties such as melting temperatures and mechanical properties when compared to analogous polyurethane esters. In that sense, annealing at 100°C is likely affecting the arrangement of urethane bonds with neighbor chains ($\text{R-N-H}\cdots\text{O=R}$), favoring uniformity and strength with a reduction of the intermolecular distance within hard segments, as also reported by Petrovic et al. [76].

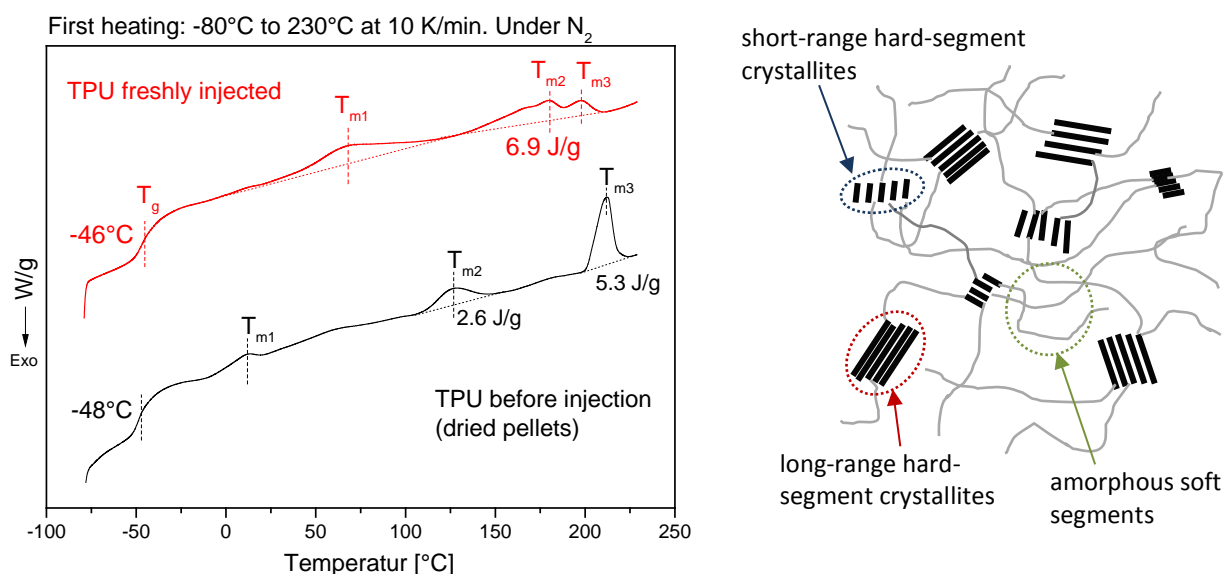


Figure 54. DSC thermograph of a TPU dried pellet before injection and a freshly injected TPU sample. Sketch to the right hand side illustrates the molecular architecture of the TPU used in this work.

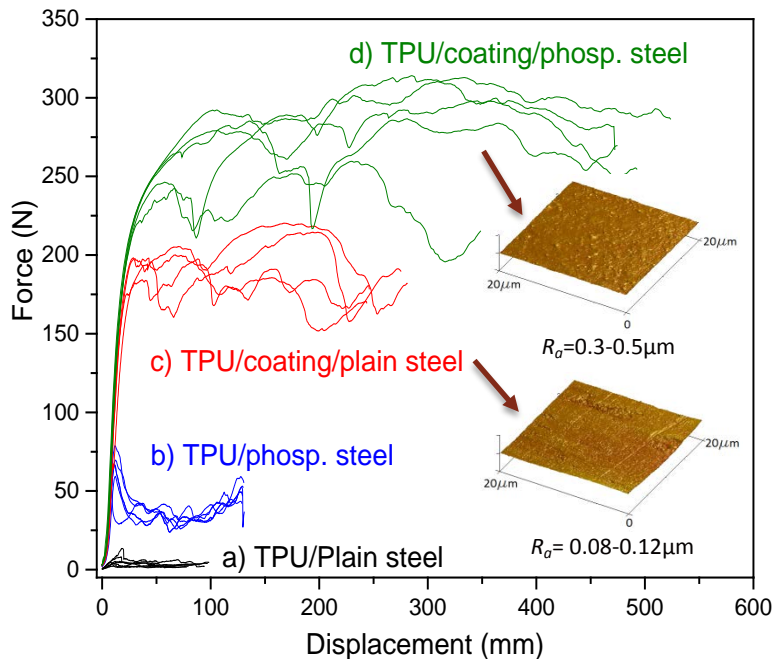
5.2. ADHESION OF TPU TO THE METAL SUBSTRATE

5.2.1. Adhesion of TPU Through the in-house Adhesive Coating

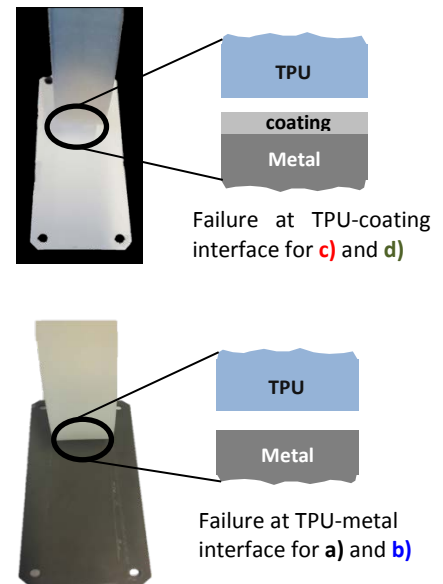
Initial peeling experiments of TPU overmolded on different steel substrates are plotted in Figure 55. The adhesion behavior of the polymer to the metal was determined as the practical adhesion force (N) vs displacement (mm), as it was described in Figure 36. First peel tests were carried out on samples on which the TPU was overmolded directly to the plain and zinc-phosphated steel surfaces without any

adhesive promoter. In this manner, the influence of metal roughness on the direct adhesion of the injected polymer was evaluated, as in Figure 55 b): the increase of nearly 40 N in the joint strength for specimens processed on phosphated steel sheets may be attributed to the mechanical interlocking from the higher surface area as seen in Figure 47.

Mechanical tests for specimens where the TPU was overmolded on the reactive coating are also plotted in Figure 55 c) and d). As expected, the crosslinked polyallophanate coating, as described in numeral 3.2.2, is playing an important role in the bonding of the polymer to the metal substrate. The gain in adhesive force is more than 500% when compared to the direct adhesion of the TPU to the phosphated steel, as in b). The average adhesion force is roughly 200 N for samples coated on a plain metal substrate, and between 250 and 300 N for samples coated on zinc phosphated steel as indicated in c) and d), respectively. The superior adhesion forces measured on the pretreated steel substrates may be attributed to the higher roughness measured by AFM as shown in the AFM images in Figure 55 d). The failure mode of hybrids, on which the polymer was overmolded on the adhesive coating, was purely adhesive at the TPU/coating interface, and for specimens on which the polymer was injected directly on the metal surface, the failure occurred at the TPU/metal interface, as schematically illustrated respectively in Figure 55-B.



A



B

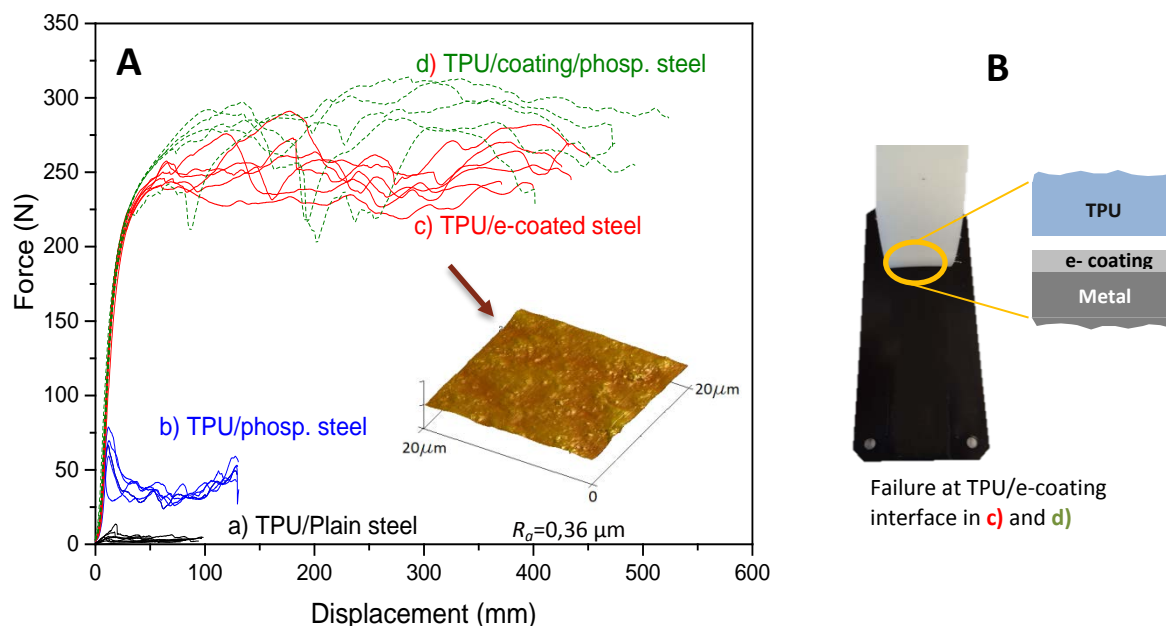
Figure 55.

A- Adhesion force of overmolded TPU on metals substrates: a) direct adhesion on plain steel, b) direct adhesion on zinc-phosphated steel sheet, c) on adhesive coating on a plain metal substrate, and d) on adhesive-coating on a zinc-phosphated steel sheet. AFM images of the metal surfaces are also shown with their respective mean roughness, R_a .

B- Two types of failure modes occurred in the referred composites: Adhesive failure at the TPU/metal interface for samples on which the TPU was injected directly on the metal substrate. b) Adhesive failure at the TPU/coating interface for hybrids on which the TPU was overmolded on the in-house adhesive coating.

5.2.2. Adhesion of TPU Through the e-coat

The peel force of the TPU overmolded directly on the steel sheet pretreated by electrophoresis process is displayed in Figure 56. The adhesive forces are slightly lower to those obtained for the phosphated sheets that were coated with the in-house adhesive powder as indicated by green dotted lines. The adhesive strength of the polymer on the e-coated steel substrate may be attributed to two contributions: first, the mechanical interlocking between the interfaces: the mean roughness, calculated by confocal microscopy, is approximately $0,36\ \mu\text{m}$, and it is equivalent to the superficial roughness obtained for the zinc-phosphatized metal substrate coated with the in-house adhesive. Second, physical and secondary interactions are expected between the $-\text{NH}-$ groups of the overmolded TPU and the epoxy-urethane groups from the e-coat, as detected by FTIR in Figure 17 and following [72], which are equivalent to the interactions described in Figure 57.

**Figure 56.**

A- Adhesion force of the overmolded TPU on e-coat steel sheet and AFM micrograph of the pre-coated metal surface and the calculated mean roughness. The green dotted curves indicate the slightly better adhesion of the TPU to the in-house adhesive coating.

B- Adhesive failure mode at the TPU/e-coating interface.

5.2.3. Interactions at TPU/in-house and TPU/e-coat Interfaces

The significant gain of peeling strength in the hybrid parts that were processed on coated substrates may be explained by the new adhesion mechanisms that take place in the polymer-metal composites. They are rather complex due to the physical and chemical interactions that happen at different processing stages and different layers of the hybrid. It is expected that the overmolding of the polymer on the intermediate coating form chemical and physical interactions at the TPU/coating interfaces. Figure 57 summarizes interactions between the referred materials after the final processing stage.

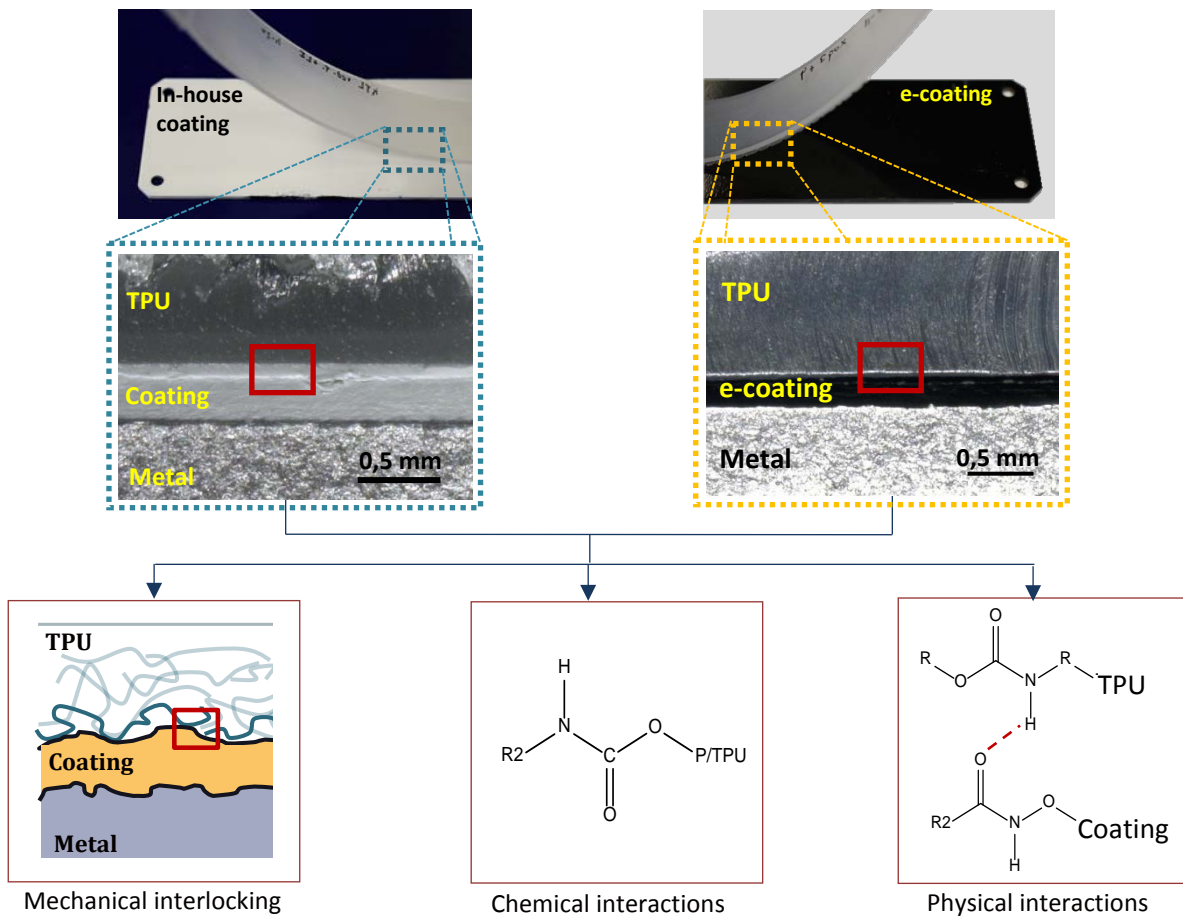


Figure 57. Expected physico/chemical interactions of the TPU with the adhesive promoters at the interface after overmolding the polymer on the metal substrate.

5.3. INFLUENCE OF ANNEALING ON ADHESION STRENGTH

Figure 58 depicts peel forces require for debonding the overmolded TPU from the steel substrates in fresh and annealed hybrids. Specimens thermally treated at 100 °C have higher and steadier bonding forces through the entire substrate when compared to the untreated or annealed composites at 50 °C and 70 °C. The average adhesive force, F_{over} , for fresh specimens that were overmolded on the in-house

coating was around 264 N, while the values of annealed composites processed on the same substrate jumped to 311 N, as illustrated in Figure 58 a). On the other hand, in Figure 58 b), fresh TPU injected on e-coat steel, presented lower F_{ave} , as compared to the annealed specimens shown in part b).

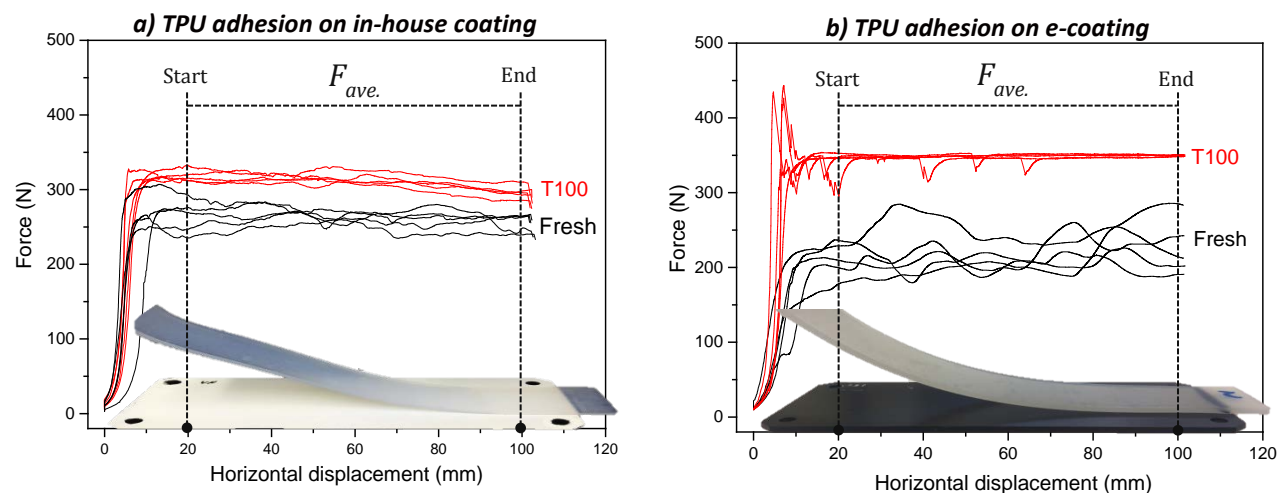


Figure 58. Adhesive test for annealed at 100 °C and not-annealed coated hybrids. a) In-house coated on zinc-phosphatized steel sheet. b) on e-coated steel. The average adhesive Force, F_{ave} , was calculated in a length range from 20 mm to 100 mm on the metal sheet.

The influence of annealing at lower temperatures than 100 °C on the practical adhesion is not significant and remained similar to the thermally untreated specimens, as in Figure 59.

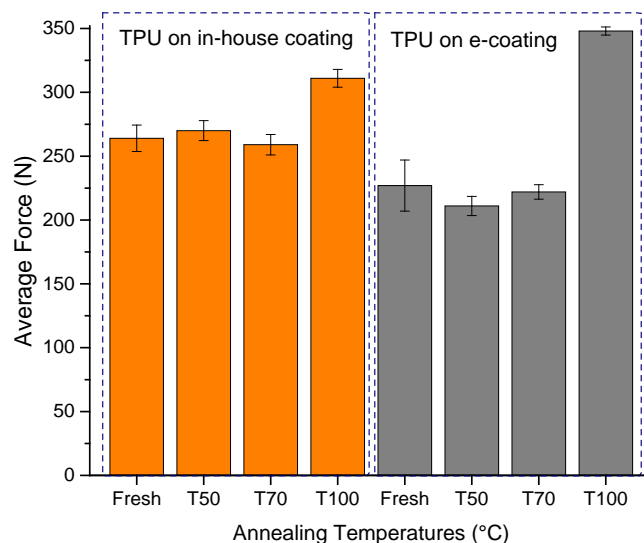


Figure 59. Average adhesion forces at different annealing temperatures of TPU overmolded on: in-house adhesive coating, represented here in orange bars; and on e-coating steel substrate, presented in gray bars.

5.3.1. Failure modes of Annealed Hybrids

It was found that the failure mode for fresh composites or those annealed at 50 °C and 70 °C, experienced a purely adhesive failure at the TPU/coating interface, as displayed in the SEM micrographs in Figure 60. For all annealed samples at 100 °C, there was a combination of adhesive/cohesive failure mode, as observed on the SEM images of the TPU surface that was in direct contact with both intermediate layers, as seen in Figure 61.

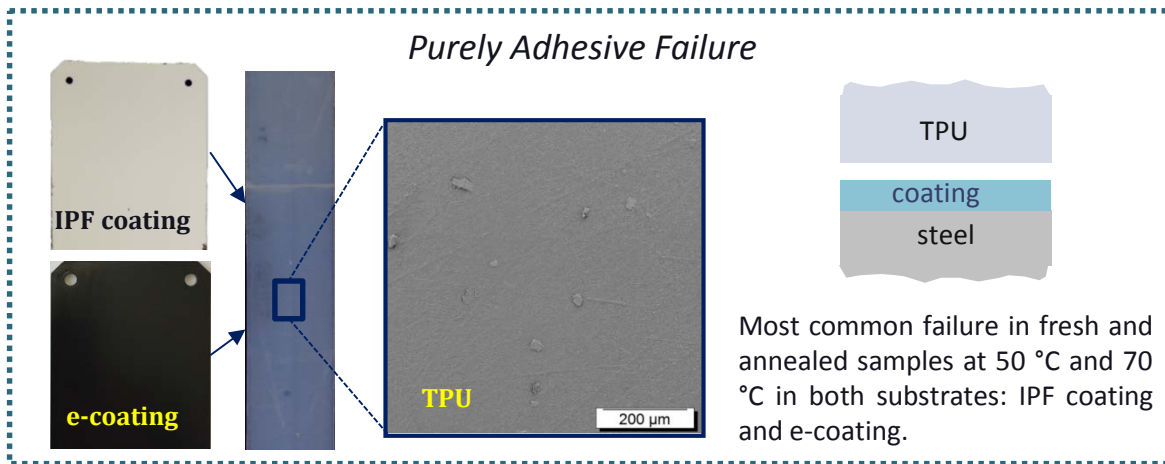


Figure 60. SEM micrographs displaying a pure adhesive failure of a fresh and annealed hybrid at 50 °C and 70 °C for 20 hours. Images were obtained from the TPU surface that was in direct contact with the coating.

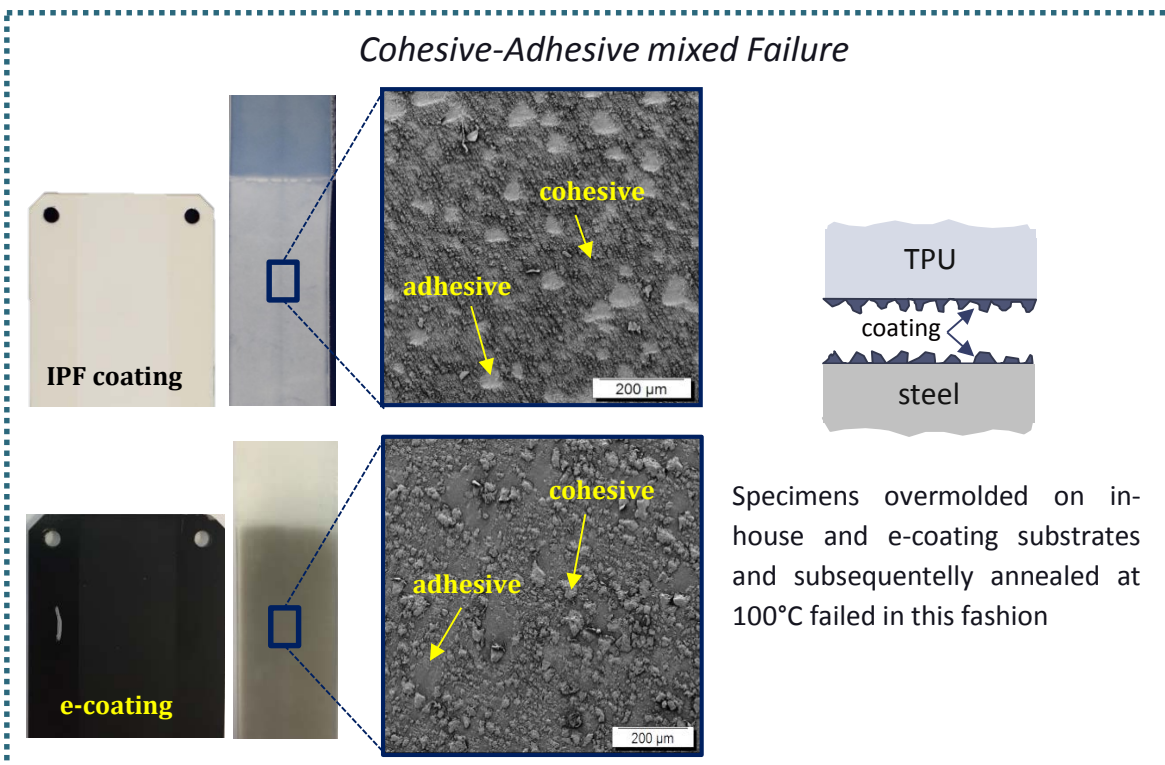


Figure 61. SEM micrographs displaying a cohesive/adhesive mixed failure for hybrids annealed at 100 °C for 20 hours. Images were obtained from the TPU surface that was in direct contact with the coating.

5.3.2. Effects of Different Annealing Temperatures on Adhesion: Thermal Analysis

In order to understand better the higher adhesion forces of annealed hybrids at 100 °C, thermal analysis was performed on the TPU that was in direct contact with the polyallophanate coating. DSC thermographs in Figure 62 display different endothermal peaks after the annealing of specimens at different temperatures for 20 hours. The glass transition temperature, T_g , measured at the first heating, occurs at around -46 °C and decreases slightly when annealing temperatures increase; this little reduction of the T_g is negligible and could be explained by some water vapor uptake after annealing in the convection oven.

The occurrence of endothermic peaks at higher temperatures, i.e. $T > 50$, are extensively explained by Pompe et al. [75]. They identified the broad peaks as hard segments (HS) crystallites that have short and long-range orders, as depicted in Figure 54 b). The fresh specimen has an endothermic peak, T_{m1} , at around 70 °C, which corresponds to the melting of short-range hard segment crystallites (*HS-sr*) of the TPU. As evidenced in the samples that were subjected to thermal treatment, the melting peak of *HS-sr* varies depending on the annealing temperature, and it is proportionally shifted to higher temperatures, suggesting a redistribution of crystals from short-range order into long-range order crystallites that eventually melt roughly at 200 °C (T_{m3}).

The calculated enthalpy of the endothermic peaks that occurs at higher annealing temperatures (100 °C) was around 11 J/g. Fresh and post-treated specimens annealed at 70 °C and 50 °C display a nearly unchanged endothermic peak, whose enthalpy was calculated at approximately 6 J/g. From this, it is clear that the fusion temperature of long-range hard segment crystallites (*HS-lr*), represented in the thermograph as T_{m2} and T_{m3} , is invariant and does not depend on post-processing conditions.

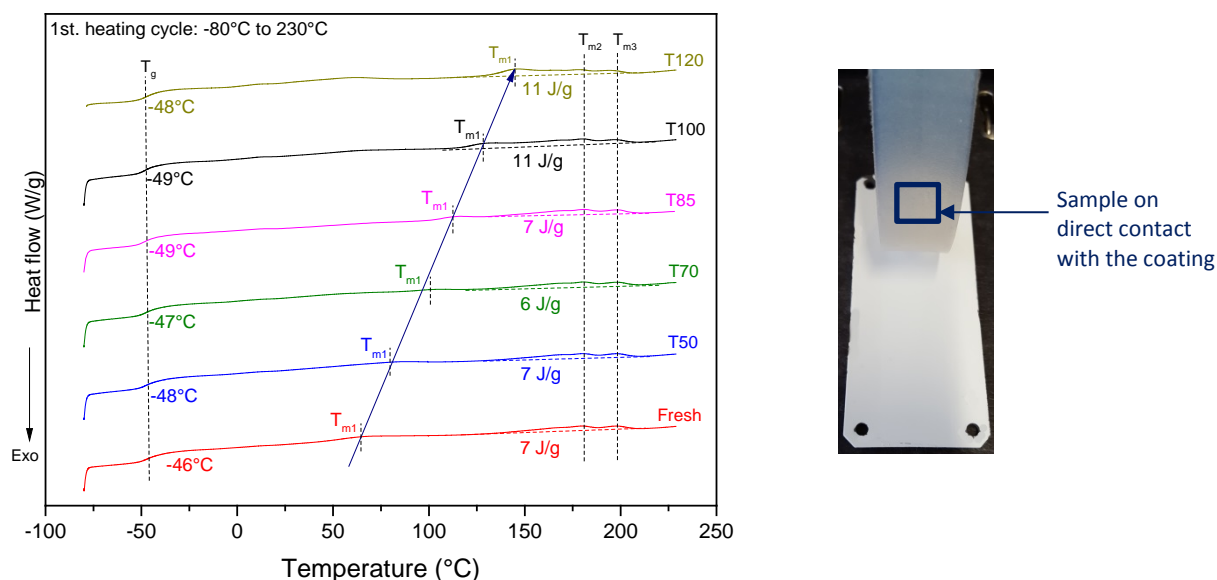


Figure 62. DSC curves of TPU that was in direct contact with the in-house coating at the 1st. heating step and different annealing temperatures.

Additionally, Achim [79] mentioned that the annealing process in TPUs leads to the alignment of chains in the direction of processing with a subsequent increase of the lamellae thickness. This definition is in accordance to the widening of the endothermal peak that took place at higher temperatures in the polymer stripes that were thermally treated at 100 °C and displayed in Figure 62. From the thermal analysis, it is observed that the relative size increment of the melting enthalpy (melting of hard domains) of the polymer after annealing at 100 °C, correlates also with the higher mechanical properties of the TPU, as exhibited in Figure 53. This rearrangement of hard domains by distribution of N-H intermolecular bonds, described in numeral 5.1.3, likely increases molecular interactions at the TPU/coating joints, as sketched in Figure 63.

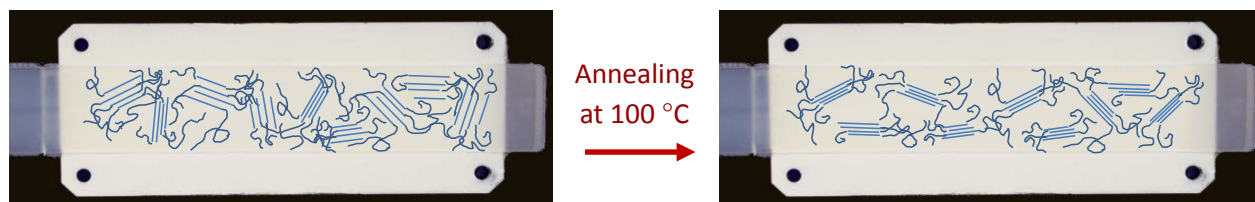


Figure 63. Schematic representation of the thermal treatment effect on the overmolded TPU. Left side illustrates a fresh TPU lamellae and right side depicts a more compact lamellae due to annealing at 100 °C for 20 h.

After the second heating run, from -80 °C to 230 °C at 10 K/min, the thermal history of the material, and the influence of processing on the molecular arrangement is erased, and no relevant information can be obtained. However, the T_g measured at the second heating step is close to -40 °C and remains nearly unchanged for all other annealing temperatures, as in Figure 64. Melting peaks of HS-sr crystallites,

tagged in Figure 62 as T_{m1} , are not detected, but final melting peaks of *HS-Ir* crystallites, T_{m2} and T_{m3} , are nearly unchanged when compared to the thermographs obtained at the first thermal run.

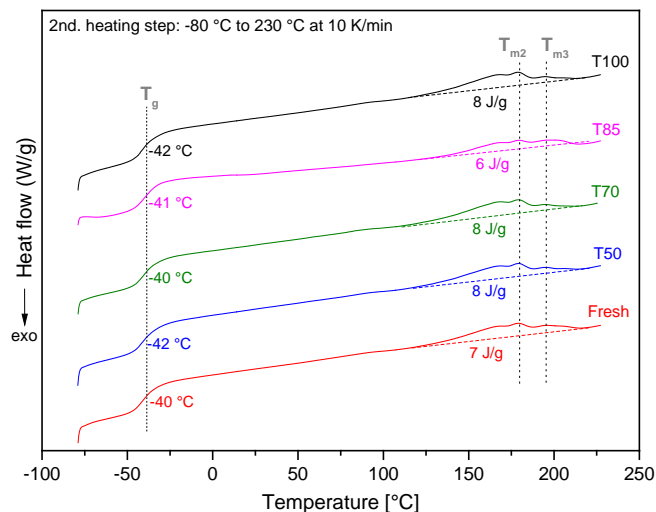


Figure 64. DSC curves of TPU at 2nd. heating step at different annealing temperatures.

5.4. THERMAL ANALYSIS OF ADHESIVE COATINGS

5.4.1. On in-house Coating

Figure 65 depicts the full thermal cycle for the powder-coating during the processing chain of the hybrid part. Thermal analysis was realized simulating, in the DSC device, the different processing stages of the preparation of the hybrid. The first stage corresponds to the curing of the coating inside the oven, after spraying the powder on the metal substrate. The baking occurs at 150 °C for 15 minutes. The second stage is similar to the overmolding of the TPU on the coated metal sheet. The melted TPU makes contact with the coating at around 230 °C, and then, it is immediately cooled down to room temperature. The third stage, which is referred to the annealing of the composite, is simulated in the DSC device as an isothermal process at 100 °C for 20 hours. After each processing stage, the specimen was subjected to conventional DSC heating ramps in order to evaluate how the thermal properties and molecular structure of the crosslinked coating were affected by the corresponding thermal loads.

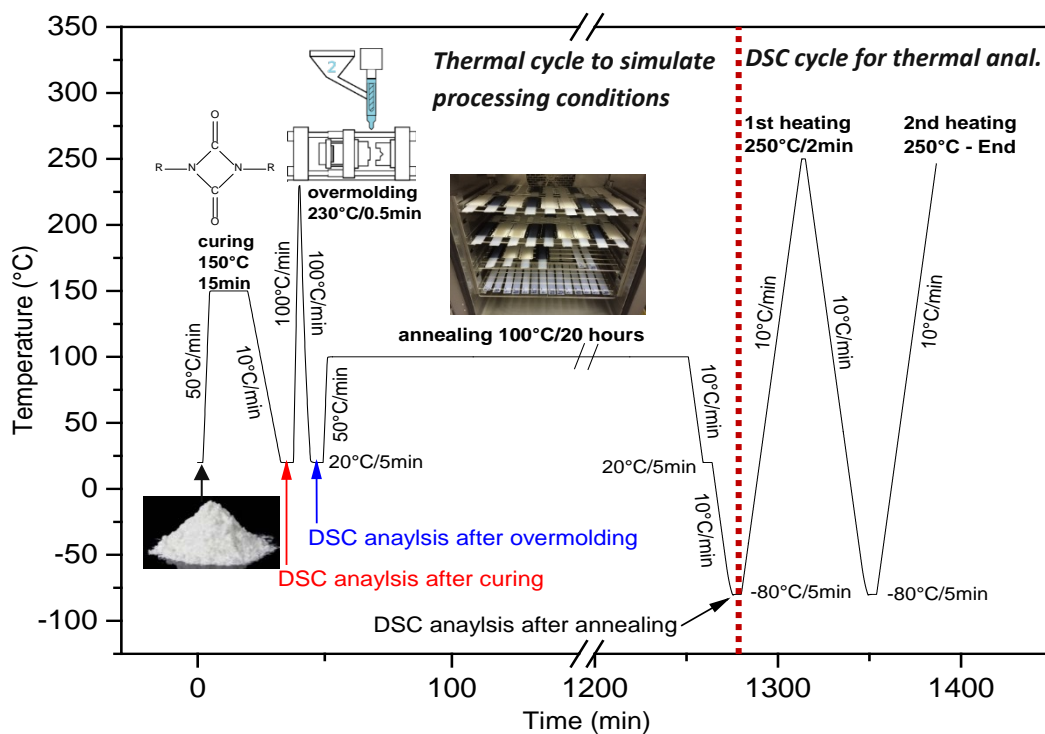


Figure 65. Thermal cycle simulating processing conditions to evaluate the influence of annealing on the in-house adhesive coating. The thermal cycle to the right was used to measure the thermal properties of the coating.

Thermographs in Figure 66 were obtained directly from the first heating ramp (-80 °C to 230°C at 10 K/min) after simulating processing conditions in the DSC device as shown in Figure 65. It is clear that, after curing and overmolding, the exothermal peak of the reactive coating at around 170 °C disappears, indicating that there is not anymore further residual reactivity in the film, and it can be assumed that almost the complete bulk phase of the coating film was transformed into a polyurethane network. After annealing, the respective thermograph exhibits a similar behavior than the sample that was just overmolded. There is no evidence of degradation of the coating or change in the amorphous regions due to annealing at 100°C.

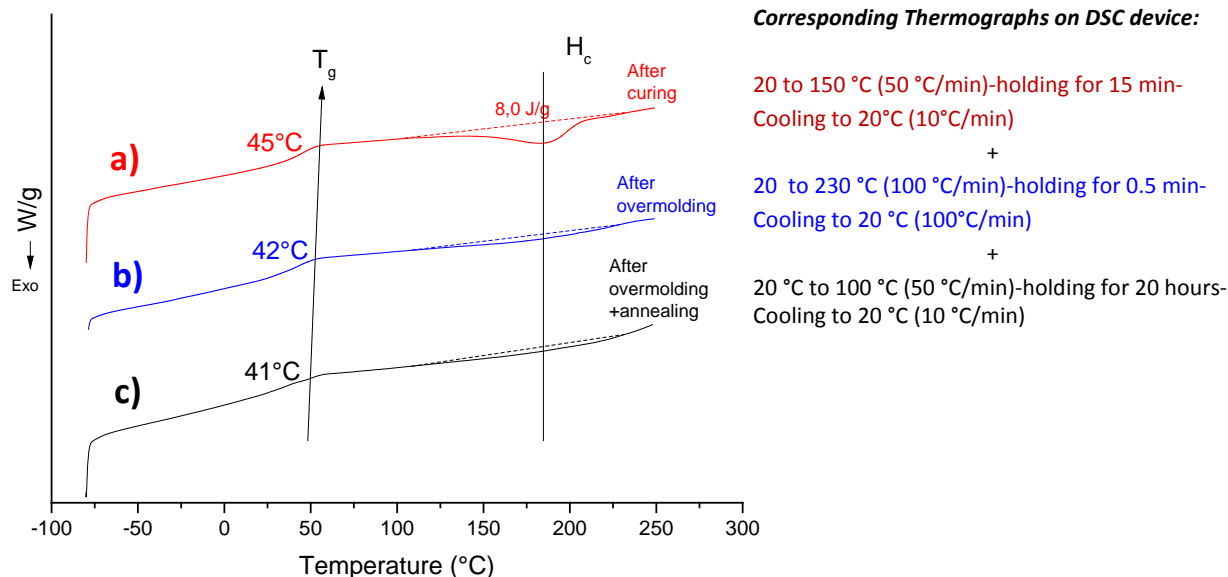


Figure 66. First heating ramps of the in-house coating after different processing stages: a) after curing of the coating, b) overmolding of TPU on the coating and c) annealing of the hybrid.

5.4.2. On e-coat

Thermal evaluation of the e-coat was conducted on metal sheets on which the TPU was just overmolded, and in sheets where the TPU was overmolded and subsequently annealed. For the preparation of the samples, coated surfaces were scratched from the steel substrate carefully in order not to have metal impurities on the measurements. As observed in Figure 67, there are no changes on the molecular structure of the coating. Exothermal peaks were neither detected indicating that no further reactivity of the coating proceeded when subjected to overmolding or annealing. This result suggests that the reactive epoxy groups of the e-coating were totally crosslinked in the baking process.

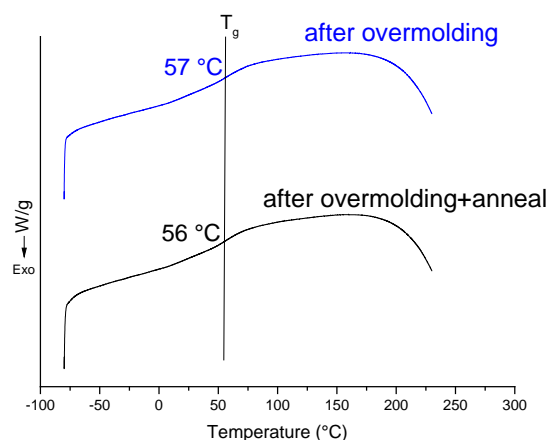


Figure 67. First heating ramps of the e-coat after a) overmolding of TPU, and b) after annealing. Picture to the right illustrates the area where the e-coating was scratched from the surface of the sheet

5.5. CHAPTER SUMMARY

Adhesion of TPU on the metal substrate, using as adhesive promoters the in-house and e-coat layers, takes place by physical-chemical interactions at the polymer-coating interface, as in Figure 69. Overmolding of TPU at 230 °C triggers functional groups at the interface of the organic coatings allowing physical and chemical bonding between functional groups of the polymer, i.e. *OH* and *NH*, and the adhesive layer. Recalling the main components of the e-coat, specifically the urethane crosslinker, it is likely that interactions at the TPU/e-coat interface are similar to the ones determined for the TPU/in-house coat and represented also in Figure 69.

The increase of the practical adhesive force in the hybrid after annealing at 100 °C for 20 hours occurs likely by the combination of two different contributions: first, the increase or rearrangement of the long-range hard segment crystallites of the TPU, as it was measured by the widening of the polymer's melting enthalpy in DSC analysis. It was also found that the tensile strength of single TPU strips increased after the heat treatment at 100 °C for 20 hours. Annealing at lower temperatures did not represent a significant change in the mechanical or thermal properties, as summarized in Figure 68. The alignment of hard segment crystals in the direction of processing, as stated by Achim [79] and Pompe [75], may increase the adhesion strength of the polymer to the substrate due to higher tensile stresses required to remove the polymer from the adhesive layer at the interface.

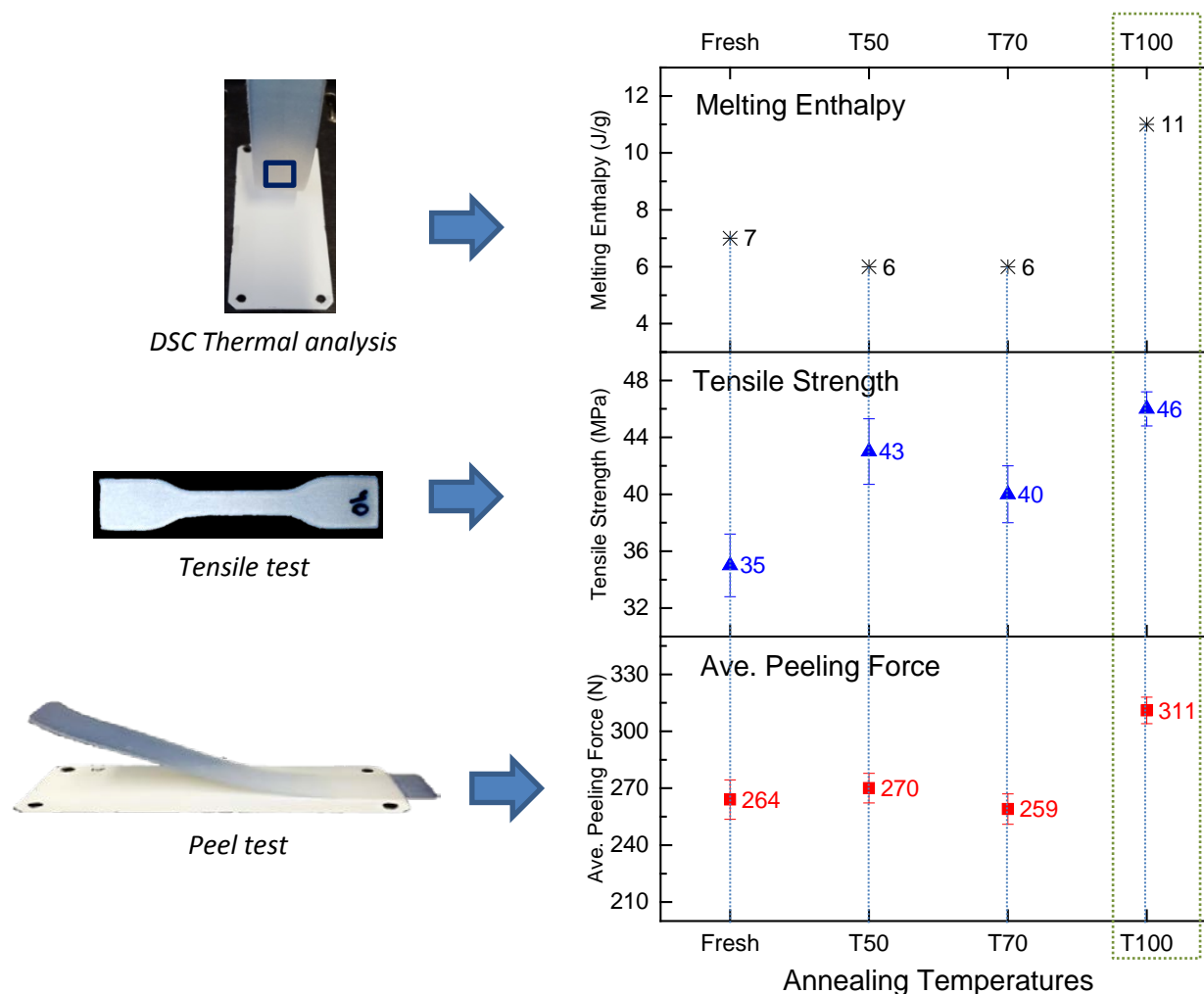
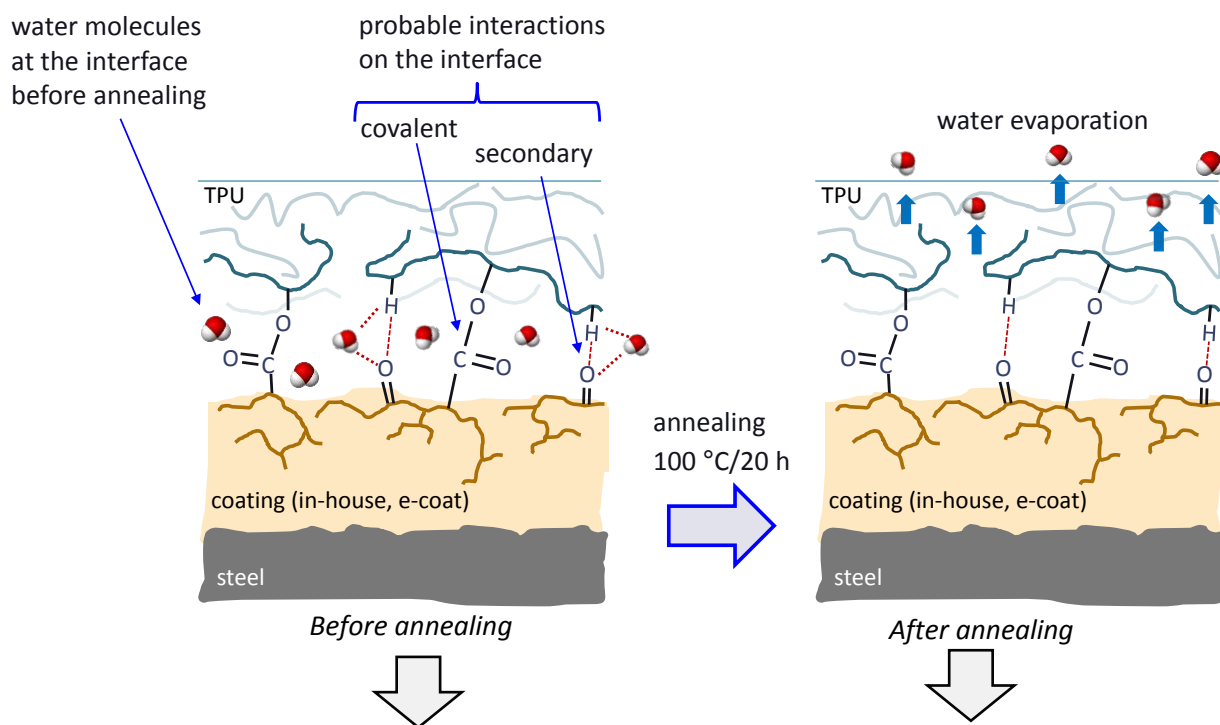


Figure 68. Summary of effects of different annealing temperatures on the mechanical and thermal properties of TPU-coating-metal hybrid.

The second contribution may be assigned to the increase of the anchoring density at the polymer-coating interface. As explained above, the enlargement and re-arrangement of the long-range HS crystallites in the direction of processing may increase the density of intermolecular interactions at the interface, as it was sketched in Figure 63. It is also feasible that the higher adhesion of TPU on the substrate after annealing takes place due to evaporation of water molecules at the polymer-metal joints, with a consequent increase of the anchoring density at the interface as sketched in Figure 69. That hypothesis is correlated to the weight reduction of single components detected after annealing, as listed in Figure 69. It is assumed that water adsorption takes place on the substrates and it is particularly high in the e-coated steel when compared to the in-house coated sheet. Water molecules on the surface are depleted when specimens are thermally treated at 100 °C decreasing the final weight of components. The higher weight loss measured in e-coat substrates may be attributed to the highly polar epoxy-based matrix that facilitates water adsorption. It was found by X-ray Photoelectron Spectroscopy analysis (XPS)

that surface of the e-coat has an excess of up to 33% of C-O bonds which may contribute to the interactions at the interface, meanwhile the in-house coating has between 9 and 10% of C-O and carboxylic bonds, as exhibited in 4.1 (carbon 1s XPS). On the other hand, desorption due to annealing, increases physical-chemical interactions at the TPU-coating interface, enhancing adhesion and durability of joints. Additionally, the failure mode on the hybrid switched from purely adhesive at the polymer-coating interface, to a mix adhesive-cohesive failure type after annealing, as in Figure 71.

Individual contributions to adhesion by the higher mechanical strength of the TPU and the increase of anchoring densities at the polymer-coating interface are difficult to quantify individually, and it is beyond the scope of this work to perform detailed research to specify such contributions.



single component	Initial wt. (g)	wt. (g) after annealing	wt. loss (mg)	av. wt. loss (mg)
e-coat sheet 1	89.8785	89.8694	8.9	8.9 ± 0.5
e-coat sheet 2	89.7062	89.6969	9.3	
e-coat sheet 3	89.7802	89.7720	8.2	
in-house sheet 2	89.5426	89.5386	4.0	4.1 ± 0.1
in-house sheet 3	88.6098	89.6055	4.3	
in-house sheet 4	88.5110	88.5069	4.1	
TPU stripe 1	10.5780	10.5604	17.6	18.4 ± 0.8
TPU stripe 2	10.5761	10.5580	18.1	
TPU stripe 3	10.5747	10.5552	19.5	

Figure 69. Illustration of water evaporation after annealing at the polymer-coating interface with a subsequent increase in the anchoring density. Table exhibits weight reduction of hybrid's single components after annealing, which is attributed to water desorption from the surface.

Manufacturing of coatings may also influence interactions at the interface: the in-house coating was sprayed on the steel manually; therefore, surface roughness homogeneity is difficult to achieve. In this work, a microscopic homogeneous film between 50 and 80 μm is the main precondition for the procedure. By automatic powder application, it is possible to reach a film thickness variation of $\pm 10 \mu\text{m}$ depending on the powder particle size. On the other hand, e-coat was applied industrially, ensuring a homogeneous thickness of around $\pm 5 \mu\text{m}$, as measured in the ultrasonic thickness gauge. The homogeneity of the coating most probably increases anchoring density between the TPU and coating. Figure 70 presents SEM micrographs of the different superficial roughness of metal surfaces coated with the in-house and e-coat treatments.

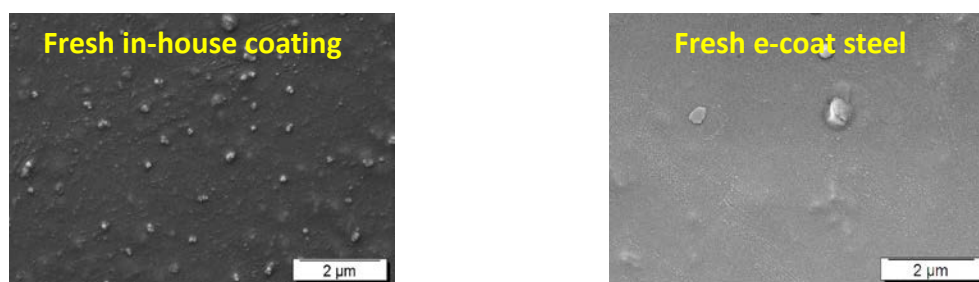


Figure 70. SEM micrographs of the superficial roughness of metal substrates prepared with the in-house coating and e-coat.

Finally, Figure 71 and Figure 72 illustrate failure modes in hybrids prepared on in-house and e-coat substrates respectively. In the case of TPU overmolded on the in-house and e-coat sheets, it was found that the most common failure mode was fully adhesive at the polymer-coating interface. For most of the annealed samples, failure occurred as a mixture of adhesive-cohesive at the coating. Adhesive failure at the coating-metal interface took place seldom on TPU/in-house coating/plain steel, and it is attributed to a bad cleaning procedure at the plain steel surface before spraying the powder. Lastly, hybrids manufactured and hygrothermally aged on plain steel failed cohesively in the metal substrate due to premature oxidation.

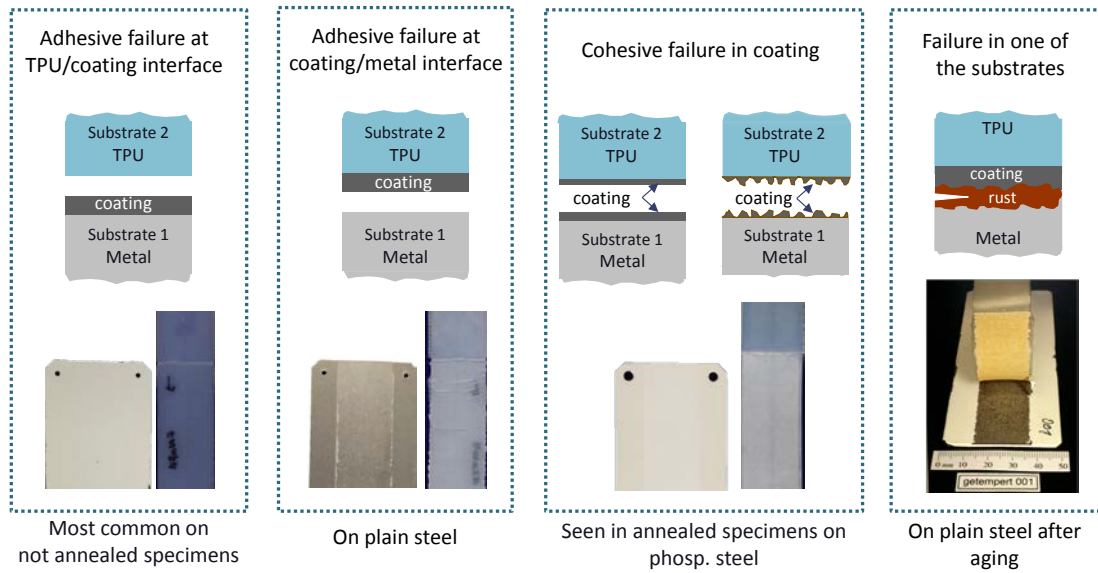


Figure 71. Failure modes in hybrids prepared on in-house coating

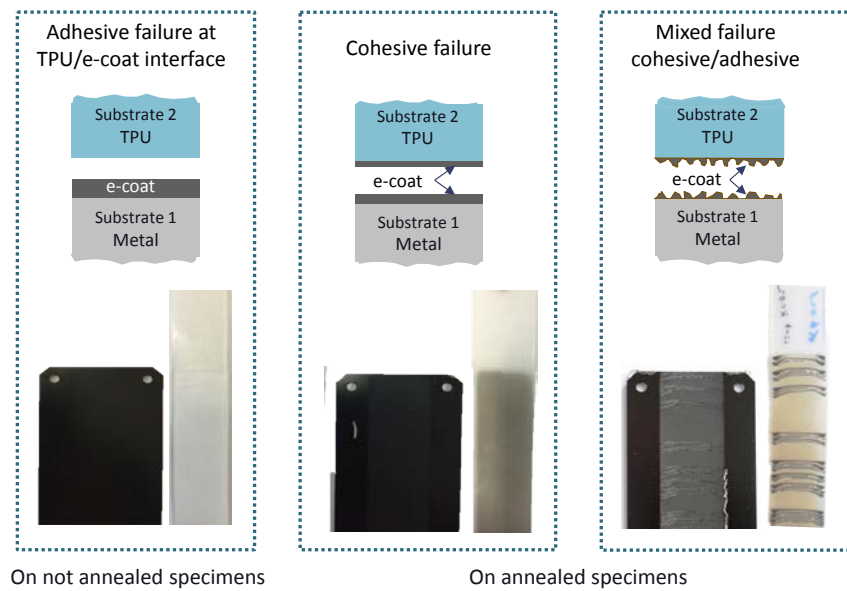


Figure 72. Failure modes in hybrids prepared on e-coat

6. HYGROTHERMAL AGING AND FAILURE MODES OF TPU-STEEL HYBRIDS

6.1. ANNEALING AND HYGROTHERMAL AGING ON NEAT TPU STRIPS: MECHANICAL PERFORMANCE

The mechanical tensile test, as described in 3.3.1, was performed on fresh and annealed (@100 °C for 20 hours) TPU strips that were injected and artificially aged for 1000 h at 40 °C/90 %RH, 85 °C/40 %RH and 85 °C/85 %RH. The respective stress-strain curves of accelerated-aged polymer strips at different weather conditions are shown in Figure 73 to Figure 75. In the figures, the black and red curves represent polymer samples with and without annealing, respectively.

For fresh specimens (without annealing) subjected to 40 °C/90 %RH, the ultimate strength increased significantly with a decreased of the final strain. It is clear that this change in the mechanical behavior is expected in “naturally aged” TPU, as exhibited in Figure 52. For the thermally post-treated strips at 100 °C, there is no evidence of degradation or changes in the tendency of the mechanical properties, as displayed in the strain-stress curve in Figure 73 on the right-hand side. These curves indicate that the annealed process freezes the thermodynamic process related to the molecular arrangement of the hard segment crystallites in the molecular configuration of the TPU.

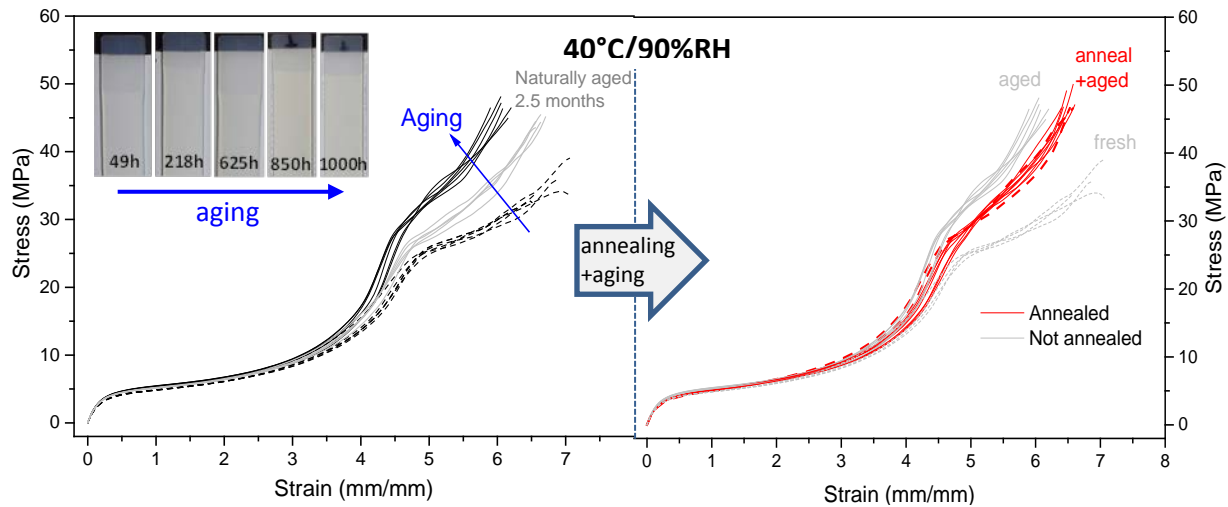


Figure 73. Strain-stress curves for fresh TPU strips hygrothermally aged at 40°C/90%RH. Curves on the right hand side display the mechanical behavior of annealed + hygrothermally aged strips.

Figure 74 show the strain-stress curves of TPU strips subjected to 85 °C/40 %RH. It is observed that for untreated strips there is a slight shift to the left in the final properties, without affecting either the ultimate deformation or the tensile strength. The heat treated specimens in the right-hand figure, indicate a shift of properties to the right, consequently with a reduction of the ultimate strength and an

increase of final strain. This mechanical behavior may indicate a thermo-oxidative degradation as also displayed in the progressively yellowed strips. Nevertheless, for polymers subjected to both environments, i.e. 40 °C/90 %RH and 85 °C/40 %RH, properties remain stable after 1000 hours of exposure, and there are no signs of degradation or catastrophic failure as it was expected initially, as reported by Hoikannen [64].

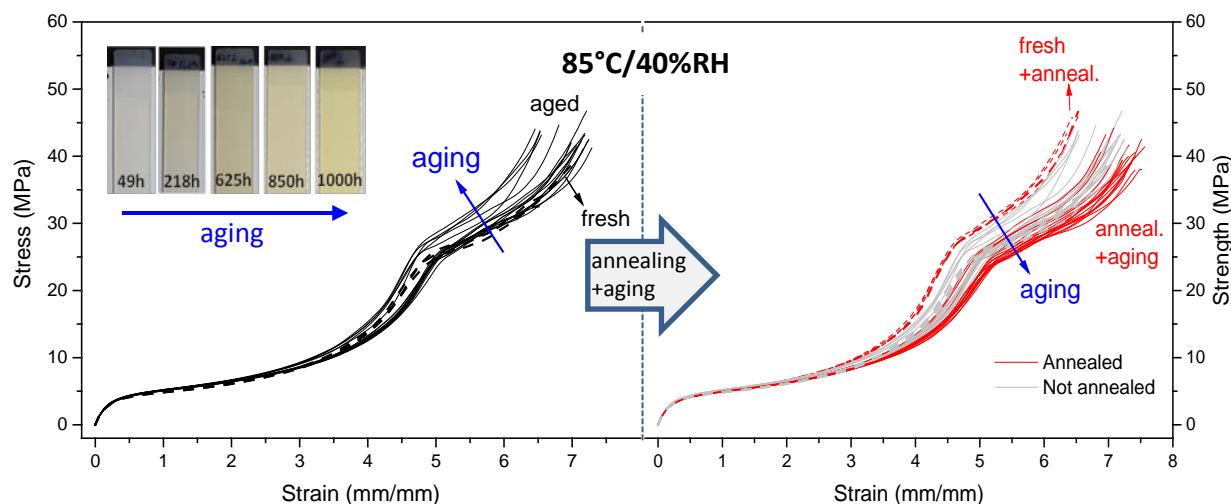


Figure 74. Strain-stress curves for fresh TPU strips hygrothermally aged at 85 °C/40 %RH. Curves on the right hand side display the mechanical behavior of annealed + hygrothermally aged strips.

For specimens subjected to the most severe climate, 85 °C/85 %RH, the mechanical behavior differs significantly from previous conditions. As seen in Figure 75, the ultimate strength decays but the plastic deformation of the polymer increased. This behavior may be explained by a plasticization process occurring in the polymer due to the high temperature and humidity.

The yellowness of the artificially aged strips was evident in polymers that were subjected to higher temperatures. This discoloration is related to an over oxidation and/or subsequent formation of chromophoric groups, due to chemical interactions, of phenol groups used as antioxidants or stabilizers in the polymer [126]. Phenol compounds are also found as mayor components in the molecular structure of urethane-based polymers (methylene diphenyl diisocyanate, MDI). In any case, yellowness is not an indicative of thermal decomposition of the polymer [127].

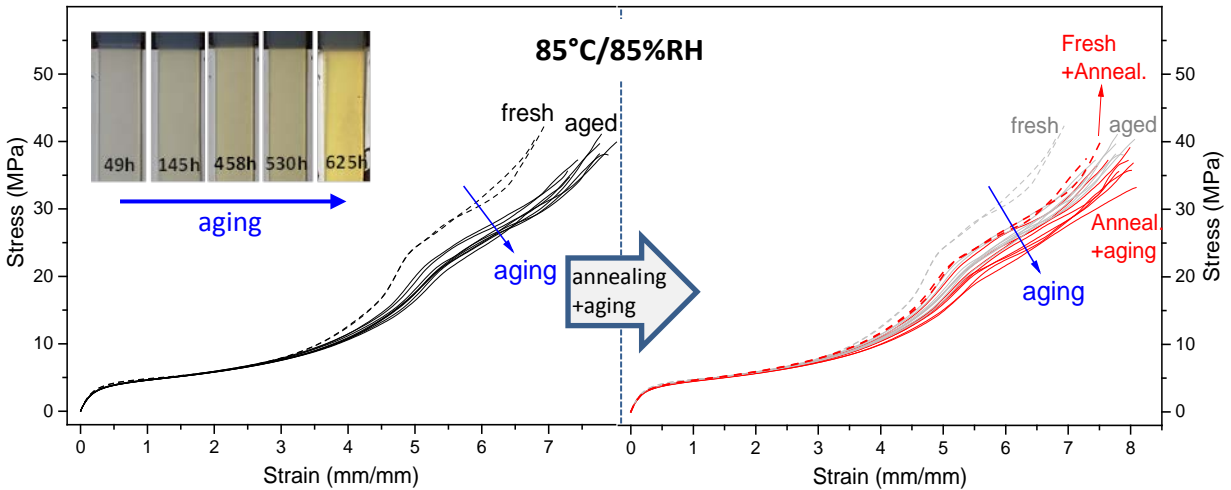


Figure 75. Strain-stress curves for fresh TPU strips hygrothermally aged at 85°C/85%RH. Curves on the right hand side display the mechanical behavior of annealed + hygrothermally aged strips.

Dependency of hygrothermal conditions on the mechanical performance of TPU

The tendency of the tensile strength (MPa) and ultimate strain (mm/mm) of specimens artificially aged at different environments after 1000 h is plotted in Figure 76. Properties of TPU strips exposed at tropical weather, 90 °C/40 %RH, are not affected by environmental stresses after aging, as indicated in the corresponding steady fitted line. Polymer strips aged at a higher temperature and lower humidity, 85 °C/40 %RH, display a similar trend in its tensile strength and ultimate strain, suggesting no thermo-oxidative decomposition of the polymer chains. Finally, the TPU specimens weathered at 85 °C/85 %RH exhibits a consistent decrease in the tensile strength, and at the same time, a slight increase in the final deformation after artificial aging.

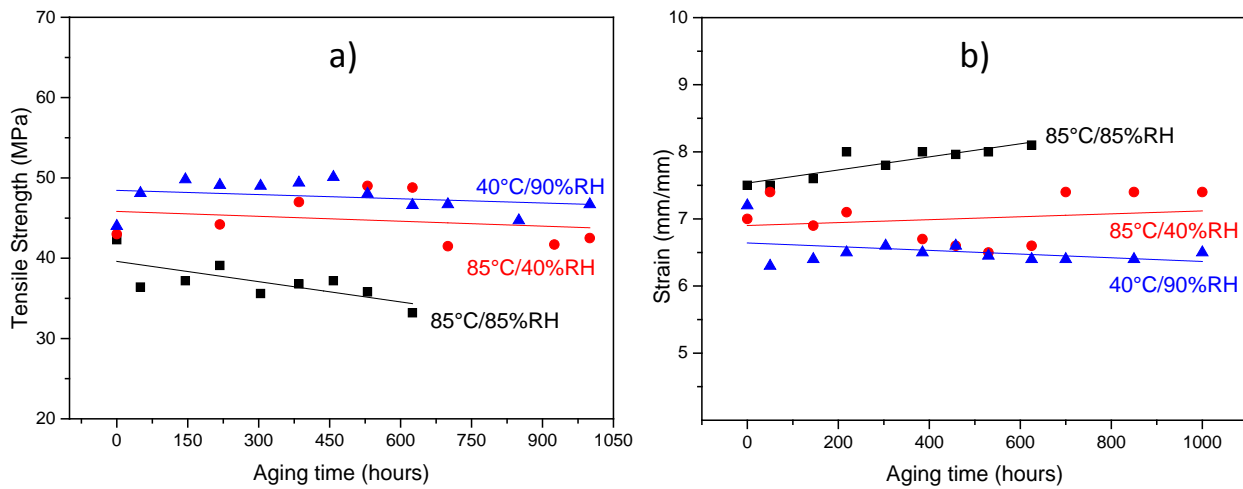


Figure 76. Dependency of a) tensile strength, and b) strain on environmental factors after accelerated aging of TPU.

The dependency of the variation of tensile strength and toughness after exposure to certain environmental conditions may suggest that the physical interactions, propitiated by the hydrogen bonds in the hard and soft phases of the polyurethane, are broken, disrupted or re-establish by water molecules that penetrate the polymer in the aging process, changing the molecular architecture and final performance [75,80]. It is evident the significance and dependence of the physical hydrogen interactions on the mechanical properties of the polymer and its influence on re-arrangement of the hard and soft segments. In [80] it is also mentioned that a thermal treatment on a segmented polyurethane, may induce a post-crosslinking reaction of residual isocyanate groups inside the TPU when water vapor penetrates it.

6.2. FAILURE MODES AT THE POLYMER-METAL JOINTS AFTER ANNEALING AND AGING

Artificially aging of hybrid specimens was conducted in different environments to establish the failure modes accurately and, subsequently, determine the lifetime of the part. Samples were taken out from the weathering cabinet after approximately three days of exposure, that is after 50, 145, 218, 304, 385, 458, 530, 625, 700, 775, 850, 925 and 1000 hours. A summary of all hybrid specimens subjected to artificial aging was displayed in detail in Figure 32; and the hygrothermal aging parameters and the corresponding methods for the analysis of failure modes is introduced in Figure 77.

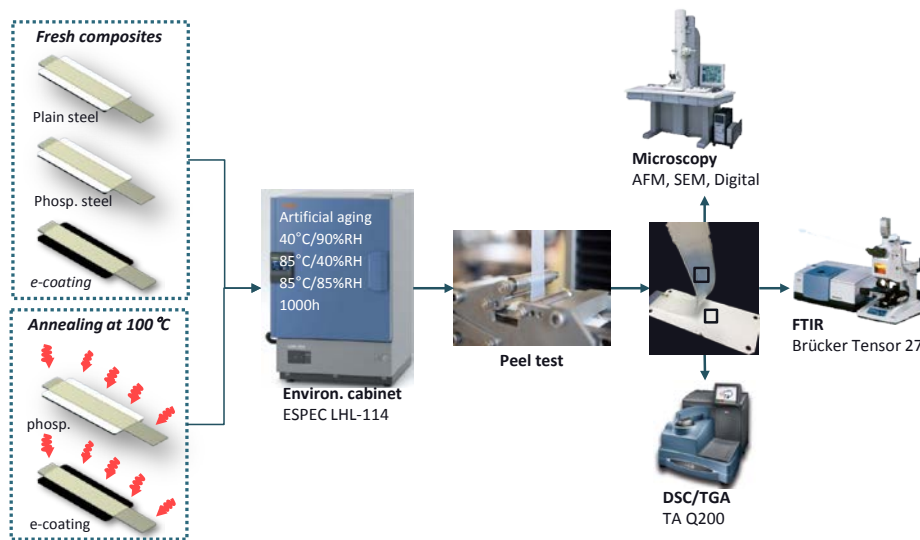


Figure 77. Path for the analysis of failure modes after artificial aging of polymer-metal composites

TPU Adhesion on Coated Metal Substrates Artificially Aged at 40 °C/90 %RH

The practical adhesion force (N) of TPU on steel substrates, measured in the peel tests in Figure 78 was conducted on hybrids after aging at tropical conditions. Plots in *a)* and *b)* indicate the adhesion of the injected polymer on the in-house coat, and on the e-coat respectively after certain exposure times. As a general remark, one can clearly observe that annealed hybrids, in red, deliver higher bonding forces, especially on samples where the polymer was overmolded on e-coat substrate. Thermally untreated composites (in black curves), processed on the in-house coat, exhibit much better and steadier adhesion strength to those prepared on e-coat.

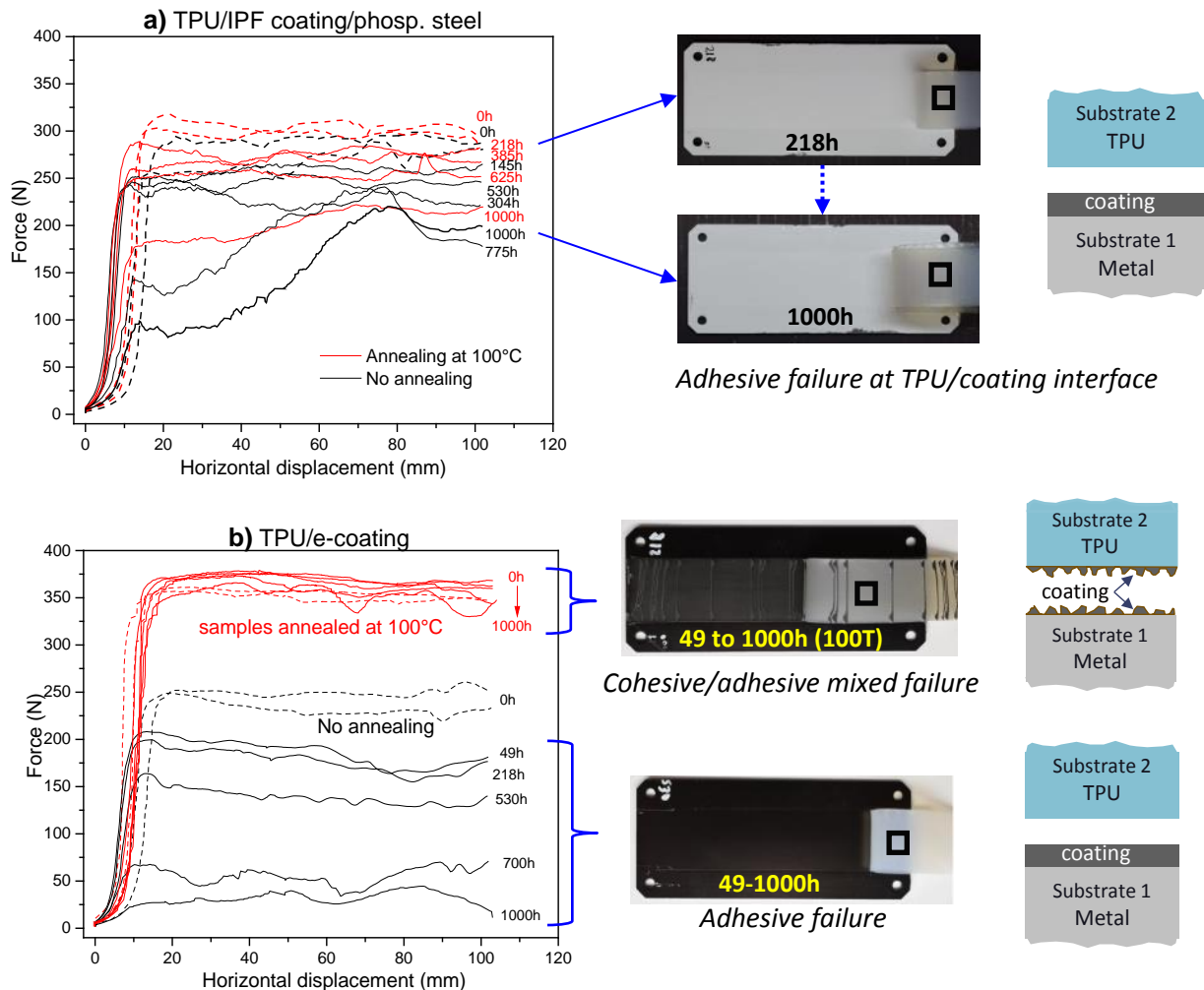


Figure 78. Adhesion force of TPU on metal substrate after artificial aging at certain exposure times at 40 °C/90 %RH, and corresponding failure modes of *a)* IPF coat and *b)* e-coat samples. Red curves indicate peeling forces of annealed hybrids at 100 °C.

TPU Adhesion on Coatings on Metal Substrates Artificially Aged at 85 °C/40%RH

For thermally treated specimens aged at 85 °C/40 %RH there is also steadier and higher adhesion forces, similar to the previous case. However, reduction of mechanical bonding between the TPU and the adhesive promoters is faster than in the specimens subjected to lower temperature and relatively high humidity (40 °C / 90 %RH) environments. After just 49 hours of exposure, the practical adhesion drops approximately 100 N for specimens prepared both in in-house and e-coat substrates, as illustrated in Figure 79. Samples subjected to longer exposure times, i.e. 145-1000 h, exhibit practically no adhesion and it is even more notorious in TPU overmolded on e-coat. The durability of fresh and aged composites prepared with the in-house coating is again better and steadier than samples overmolded on the e-coat. Nevertheless, for the electrophoretic-coated specimens that were heat treated at 100 °C for 20 hours, and hygrothermally aged, the bonding forces are significantly higher when compared to the samples treated with the in-house coat.

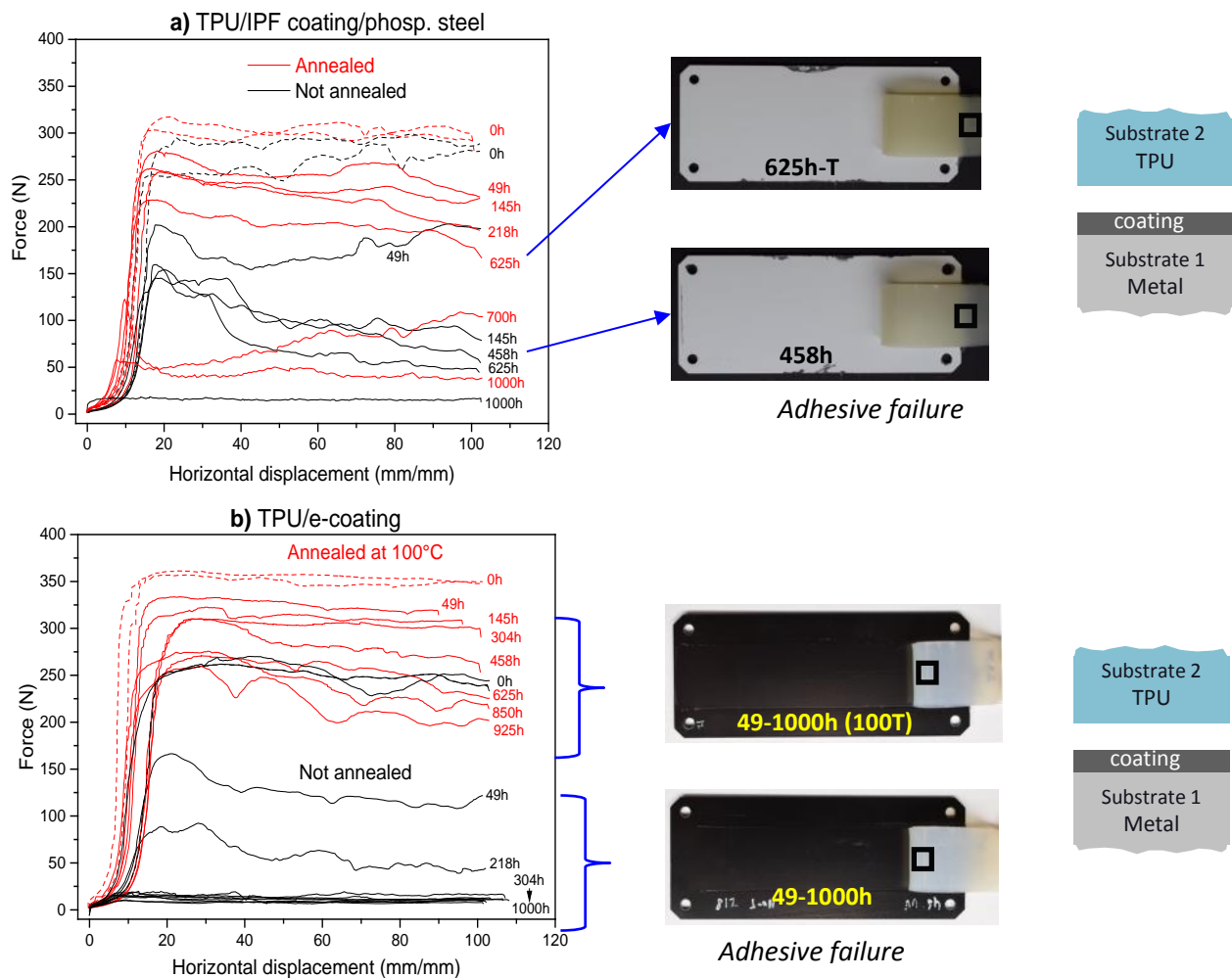


Figure 79. Adhesion force of TPU on metal substrate after artificially aging at certain exposure times at 85°C/40%RH, and corresponding failure modes of a) IPF coating and b) e-coating. Red curves indicate annealed hybrids at 100 °C.

TPU Adhesion on Coatings on Metal Substrates Artificially Aged at 85 °C/85 %RH

For the set of samples artificially aged at the most severe environment, as in Figure 80, it was found that just after 50 hours of exposure, the bonding forces of hybrids prepared with both adhesive promoters drop sharply. The failure mode was purely adhesive at the TPU/coating interface for all cases, indicating that the physical and chemical interactions between the TPU and the coatings are significantly affected by these specific environmental conditions.

The failure mode on the overmolded specimens on plain steel, Figure 80 a), was due to a combination of corrosion on the metal surface and delamination of the polymer from the substrate. The failure mode of hybrids prepared on the in-house polyester-based coat, as in Figure 80 b), was purely adhesive at the TPU/coating interface. For annealed specimens, bonding forces are higher than samples without it. None of the specimens prepared on the polyester-based coat failed at the coating/metal contact surface, suggesting a strong bond between the metal plate and the adhesive layer.

Adhesion strength of TPU on e-coat steel is higher than in the previous cases as seen in c), especially for annealed hybrids at 100 °C -highlighted in red curves-. There was a relatively good adhesion, even after 625 hours, of exposure to this severe environment.

The debonding of TPU from the plain steel sheets, as pictured in part a) of Figure 80, is giving a critical approach to the failure modes of the component. It was clearly seen that diffusion of water vapor was faster from the edge of the metal sheet that is in contact with the TPU, as indicated by orange arrows. An explanation for this specific diffusion path is due to a higher superficial area at the metal/polymer edges. Those edges contain microvoids and superficial cracks that facilitate water diffusion through the interface. It is also noticed that water diffusion in specimens prepared on plain steel oxidized the metal sheet. The failure mode of composites prepared on phosphated and e-coat steel (which are corrosion inhibitor layers) is distinctly adhesive at the polymer/coating interface. Diffusion is faster at the interlayers and destruction of physical/chemical interactions between the polymer and coatings occurred rapidly, as displayed in part b) and c) of the figure below.

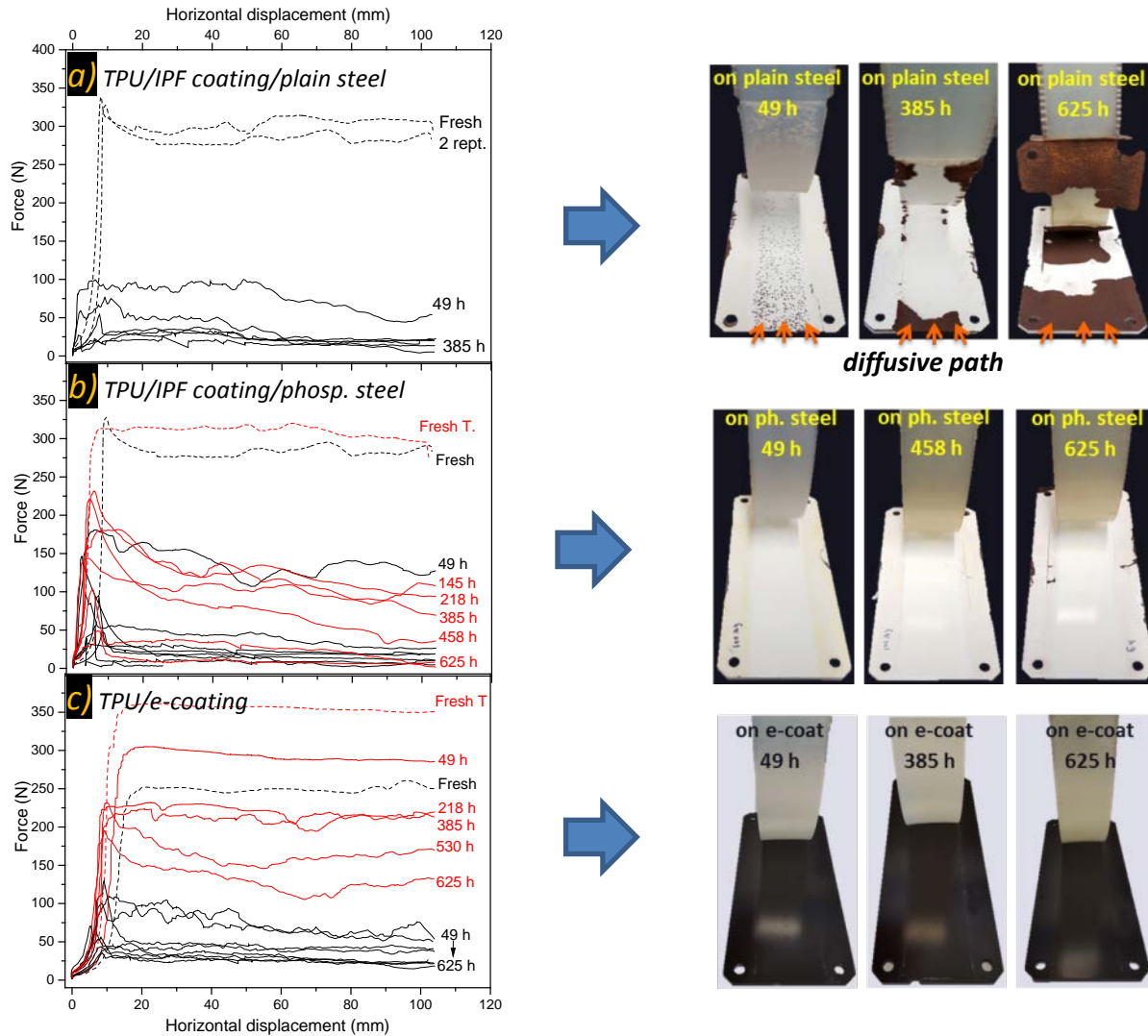


Figure 80. Adhesion force after aging at 85 °C/85 %RH of TPU-metal composites prepared on different metal substrates: a) TPU/IPF coating/plain steel, b) TPU/IPF coating/phosp. steel and c) TPU/e-coating. Red curves indicate peeling forces of annealed composites at 100 °C.

Annealing affects the endurance of the composite positively in all environmental conditions due to higher anchoring densities at the TPU-coating interface, as discussed in the previous chapter in numeral 5.5. The rearrangement and alignment of the hard and soft domains of TPU and water desorption at the interface make possible the increase of intermolecular bond density, forming a barrier to the diffusion of water through the interface, so the durability and stability of the hybrid part is improved.

6.3. INFLUENCE OF HYGROTHERMAL AGING ON ADHESION STRENGTH

The dependency of the adhesion force of annealed specimens after exposure at different environmental conditions is depicted in Figure 81. The Y axis displays the average adhesion force (N) obtained from the peel test of hybrids taken out from the aging cabinet after certain exposure hours (X axis). For the hybrids prepared on the in-house adhesive promoter at tropical environment, represented in the blue fitted line in Figure 81 a), there is a slightly decrease in the adhesive forces. It is relatively steady until an exposure time of 625 hours. Then, it falls to an average value of 200 N, decreasing the bonding force for around 30% after 1000 hours of exposure. In the other hand, higher temperatures are affecting more pronouncedly the physical-chemical interactions at the interfaces, as seen in the red trend line, with a rapid drop of the bonding force of hygrothermally aged specimens at a relatively high temperature and low humidity, 85 °C/40 %RH. For hybrids aged at a severe atmosphere, 85 °C/85 %RH, there is a fast decay on the endurance of the joint because the combination of high temperature and humidity speed up the diffusion process of water vapor at the interfaces.

In Figure 81 b), hybrids prepared on e-coat steel, presented a relative higher durability, particularly at tropical conditions, 40 °C/90 %RH. It is evident that adhesive energy does not decrease after 1000 hours of exposure, indicating still strong interactions between the epoxy amino compounds and the polyester urethane crosslinker of the electrophoretic layer with the TPU. For hygrothermally aged e-coated samples at high temperatures, the loss-of-adhesion tendency is similar when compared to specimens prepared on the in-house adhesive coating.

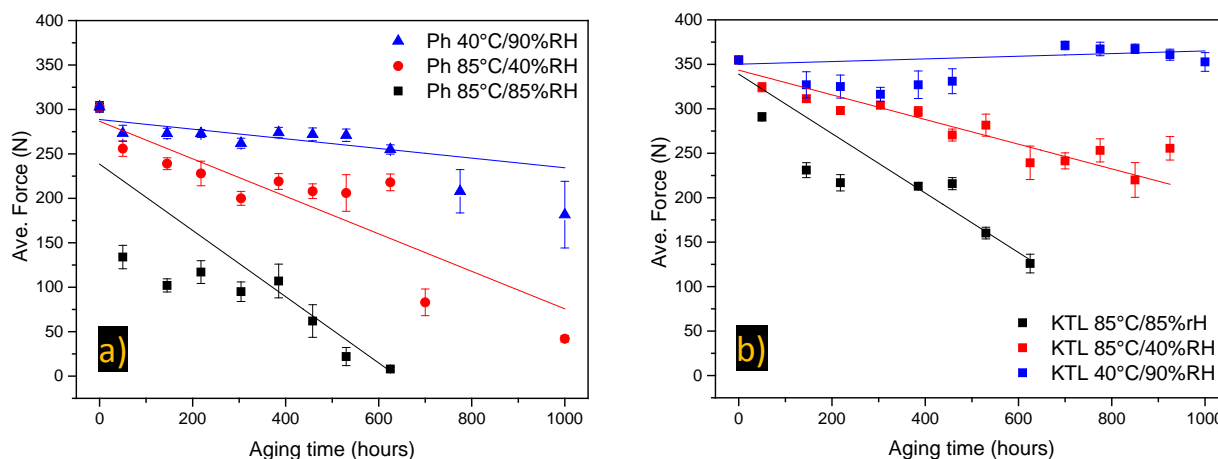


Figure 81. Influence of temperature and humidity on the adhesion force of annealed hybrids prepared with a) in-house coating on phosphatized steel and b) on e-coating steel.

6.4. THERMAL ANALYSIS OF HYGROTHERMALLY AGED TPU IN CONTACT WITH THE ADHESIVE PROMOTERS

Figure 82 and Table 17 display the heat flow, from the DSC test, of the overmolded and annealed polymer that was in direct contact with the adhesive layers. Thermographs were acquired at the first and second heating, from -80 to 230 °C at 10 K/min. In a general view, the T_g of the amorphous phase in the TPU was not affected by the artificial aging conditions and remains steady at approximately -47 °C in the first heating. At the second heating, the T_g reduces to around -40 °C for all samples, except those aged in a harsh environment (85/85) where a slightly decrease of -43 °C may suggest a plasticization of the chains due to the water vapor interactions in the amorphous domains. Endothermic peaks occurring at around 70 °C, representing the rearrangement of hard segment phases of relatively short-range [75], are changing slightly depending on the aging conditions and exposure times. Multiple endothermic peaks occurring at higher temperature ranges (120 to 210 °C) are explained by the polymorphism and rearrangement of hard segment crystallites with relatively long-range order. This reorganization of HS crystals does not seem to vary significantly after the exposure to accelerated aging conditions, even after 1000 hours, and so, there is no evidence of hydrolysis or thermal decomposition of the polymer by DSC analysis.

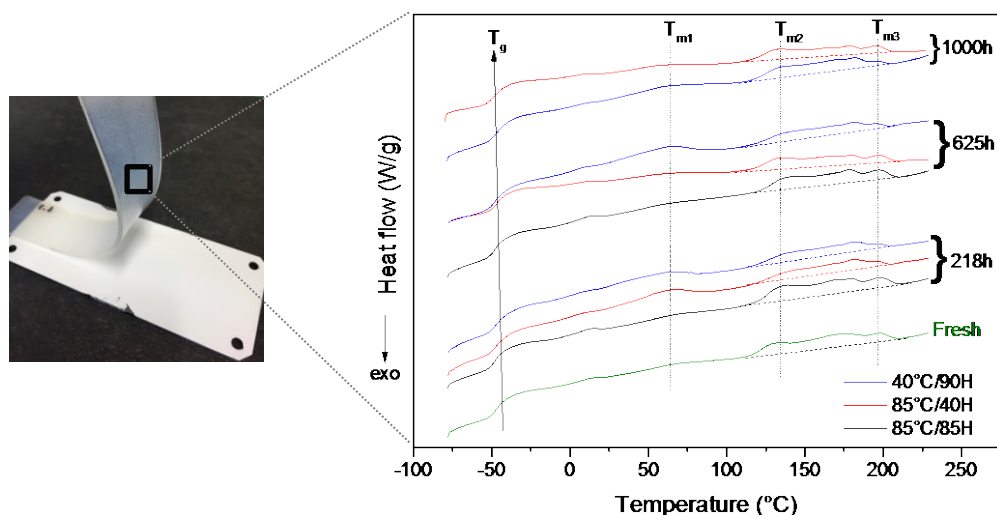


Figure 82. Thermographs of aged TPU on direct contact with the adhesive in-house coating.

exposure time (h)	40 °C/90 %RH				85 °C/40 %RH				85 °C/85 %RH			
	1st. heating		2nd. heating		1st. heating		2nd. heating		1st. heating		2nd. heating	
	Tg [°C]	Fusion enthalpy [J/g]	Tg [°C]	Fusion enthalpy [J/g]	Tg [°C]	Fusion enthalpy [J/g]	Tg [°C]	Fusion enthalpy [J/g]	Tg [°C]	Fusion enthalpy [J/g]	Tg [°C]	Fusion enthalpy [J/g]
0	-48	12.2	-41	11.1	-48	12.2	-41	11.1	-48	11.8	-41	11.4
218	-48	9.7	-40	8.0	-48	10.4	-38	7.8	-48	14.8	-42	8.9
458	-47	9.4	-40	8.5	-47	10.2	-39	9.0	-48	12.5	-43	8.0
625*	-48	8.4	-40	8.9	-47	9.6	-40	9.2	-48	11.7	-43	8.1
700	-48	11.1	-38	7.9	-46	10.9	-39	8.4	* failure of the composite by delamination of TPU and coating			
850	-46	10.7	-39	7.7	-46	10.8	-39	8.7				
1000	-46	10.8	-41	8.1	-47	10.5	-37	8.5				

Table 17. T_g and fusion enthalpy of artificially aged TPU at different environmental setups and exposure times. TPU samples were on direct contact with the adhesive in-house coating.

6.5. EFFECTS OF HYGROTHERMAL AGING AT THE TPU-STEEL INTERFACE – FTIR ANALYSIS

Influence of annealing on fresh overmolded TPU

Figure 83 shows the general “fingerprint” and description of spectral bands of freshly overmolded TPU obtained from FTIR examination. The frequency of the reflected IR beam in the inner surface is measured as Attenuated Total Reflectance (ATR) vs. wavelength number (cm^{-1}). The black and red spectra represent the fresh and annealed (100° for 20 hours) TPU strips respectively. Due to their importance in the aging process, it is necessary to highlight the spectral bands occurring between 2600 and 3500 cm^{-1} and 1750 and 1500 cm^{-1} . The first band is referred to the N-H stretching vibrations in urethane hard segments, and the second one represents carbonyl bands from the ester groups coming from urethanes and polyols, as described widely in the literature [76,81,128]. For specimens that were annealed at 100 °C, a slightly sharper band appeared at around 2800 cm^{-1} , corresponding to the stretching vibrations of CH_2 . This may indicate a re-accommodation of hard segment domains in the polymer molecular architecture, and therefore, a slight increase in the crystallinity, as it was also shown by the DSC thermographs. At a wavelength between 1625-1650 cm^{-1} a new band growths representing a strongly H-bonded urea or carbonyl stretching. Besides these slight shifts in the spectra, there is no any significant change in the molecular structure of the polymer after the post-annealing process.

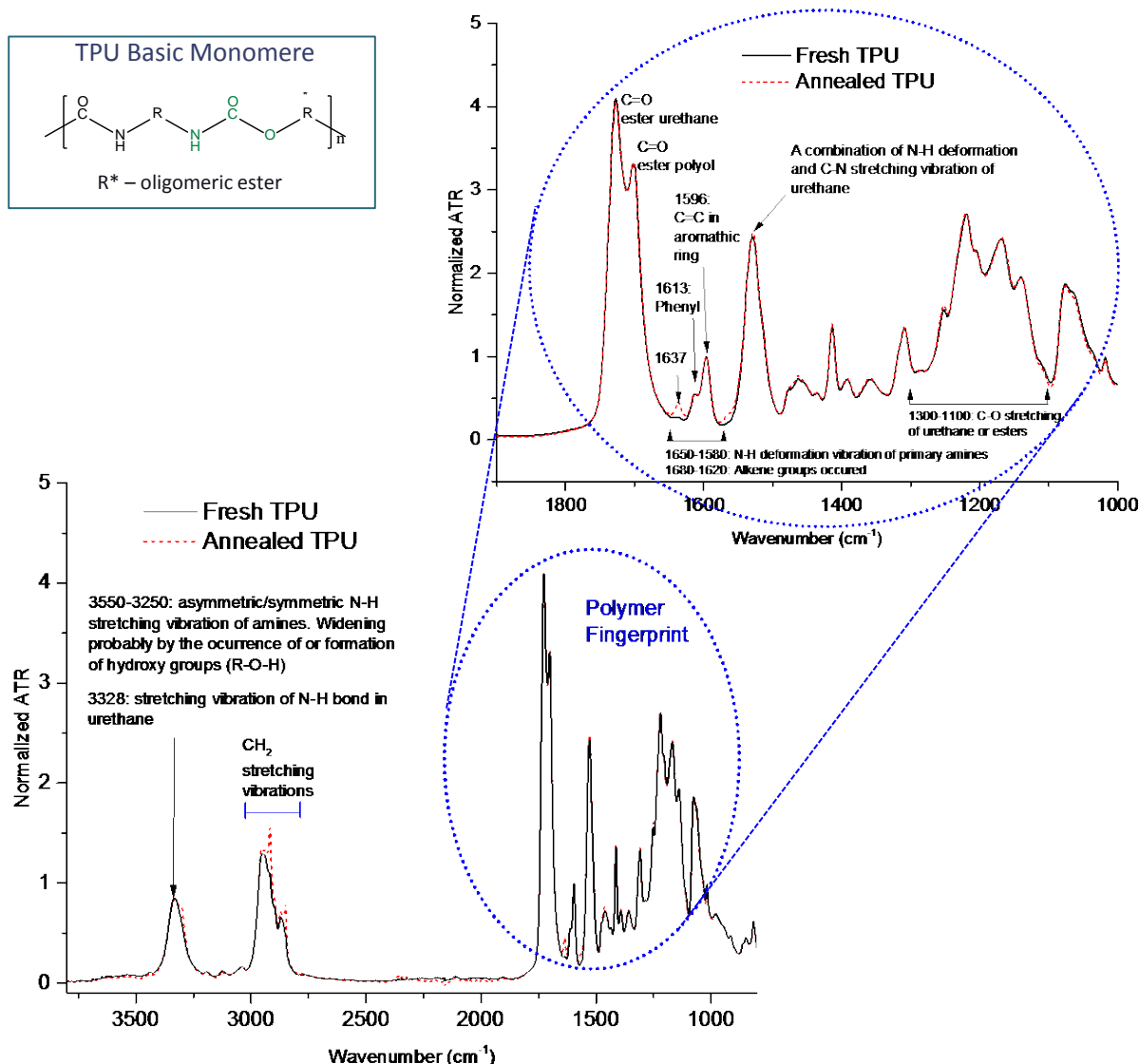


Figure 83. FTIR-ATR (Attenuated Total Reflectance) general spectra of fresh TPU and annealed at 100 °C.

Hygrothermal Aging at the TPU-Steel Joint

In Figure 84 the FTIR spectra in the range of 2700 to 3500 cm⁻¹ of annealed and aged samples at a) 40 °C/90 %RH, b) 85 °C/40 %RH and c) 85 °C/85 %RH is presented. FTIR analysis was performed on the upper-exposed surface of the overmolded polymer which is recalled here as “top”, and on the surface that was in direct contact with the coating, recalled here as “bottom”, as illustrated in Figure 41. The spectral region from 2700 to 3500 cm⁻¹ has a particular importance in the molecular analysis of the TPU because it describes stretching vibrations of the hard segments, which contains N-H groups and displays a spectra maximum at 3328 cm⁻¹ [88]. For composites aged at tropical-like weather (40 °C/90 %RH), as in

Figure 84 a), it is clear that the molecular structure of the TPU is not greatly influenced by the exposure to such environmental conditions. On the “top” exposed surface, a new small band appears between 3300 and 3330 cm^{-1} after 458 hours of exposition. This specific spectrum may be referred to the N-H new bonding with the diffused water molecules, which evidently happens at much faster rate than on the bottom surface in direct contact with the coating layer. The bands becoming sharper and narrower suggest a higher uniformity of hydrogen bonds in the N-H bonding interactions [76]. New bands also occurred between 2850 and 3000 cm^{-1} that indicate new stretching of C-H₂ and C-H interactions, also attributed to the water vapor diffusion and new physical/chemical interactions within the molecule.

Specimens that were aged at 85 °C/40 %RH and 85 °C/85 %RH, present a similar trend regarding the spectra occurring at the range from 2700 to 3500 cm^{-1} , as shown in Figure 84 b) and c). At the top surface, after just 49 hours of aging, much sharper bands appear in the range from 2800 to 3000 cm^{-1} . As explained previously, these bands belong to the C-H₂ and C-H interactions within the polymer chain. The spectrum between 3200 and 3500 cm^{-1} is also giving interesting information regarding the molecular behavior of the hard and soft segments of the TPU that are represented by the N-H stretching vibrations.

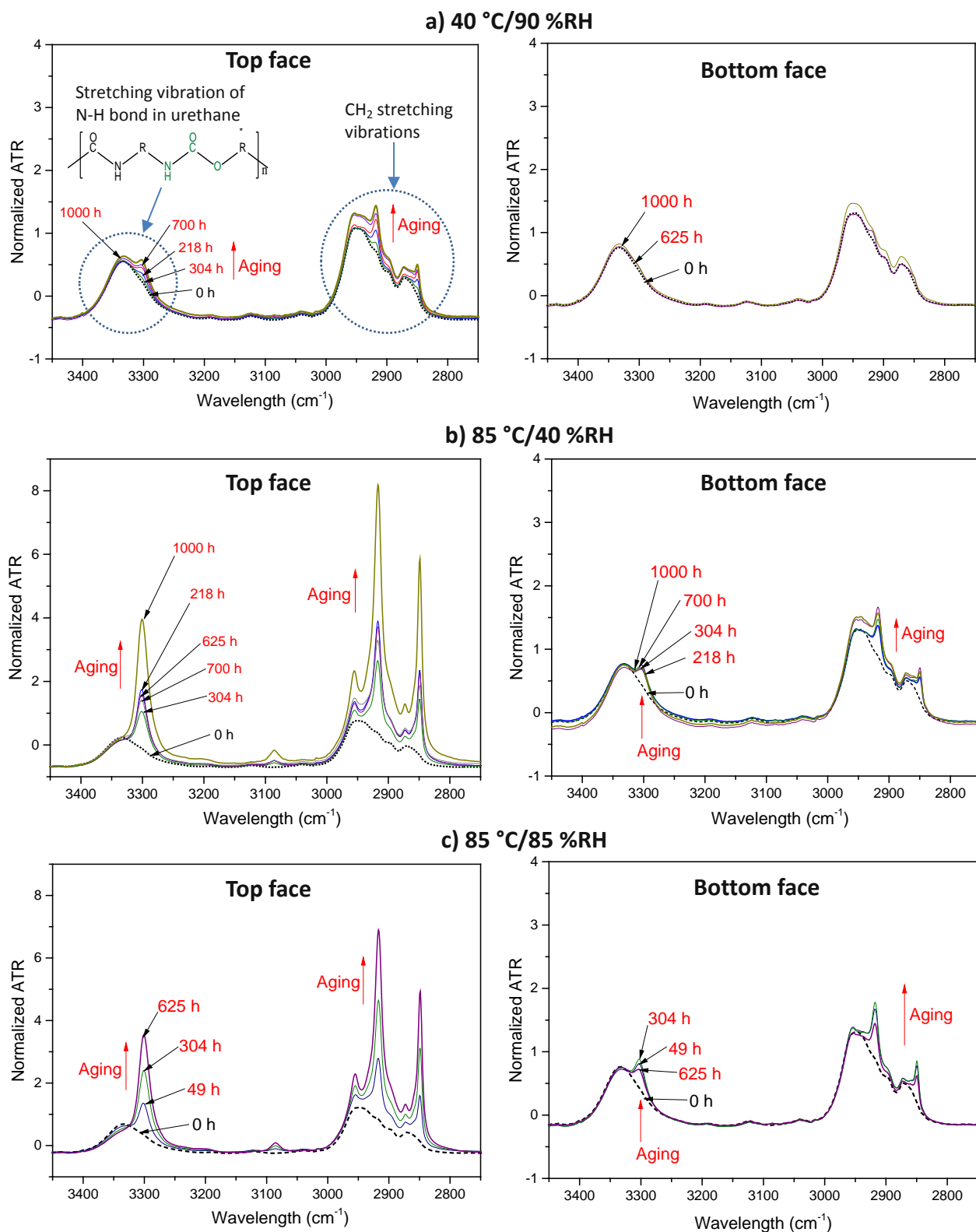


Figure 84. FTIR spectra, from 2700 - 3500 cm⁻¹, of the overmolded, annealed and aged TPU that was on direct contact with the metal substrate. Aging conditions: a) 40 °C/90 %RH, b) 85 °C/40 %RH and c) 85 °C/85 %RH. Figures to the left-hand side show the resulting spectra of “top” exposed TPU surface and, in the left, the spectra of the polymer that was in direct contact with the coating and recalled here as “bottom”.

Graphs in Figure 85 display the variation of the intensity band of the N-H stretching vibration at approximately 3300 cm⁻¹ at different environmental conditions and exposure times. At 40 °C/90 %RH, the intensity in both top and bottom surfaces is steady suggesting that molecular vibrations due to the artificial aging not be influencing the molecular structure of the polymer. On the other hand, samples exposed at 85 °C/40 %RH and 85 °C/85 %RH and examined on the top face of the TPU, show a fast increase in the intensity. In the case of overmolded strips aged at 85 °C/40 %RH, it reaches saturation after 145 hours of hygrothermal aging and remains steady until approximately 700 hours. After that time interactions of the N-H groups increase rapidly until the end of the experiment at 1000 hours. The polymer exposed to the most severe environment seems to reach saturation just after 145 hours of exposure and, subsequently, increases slightly after 458 hours.

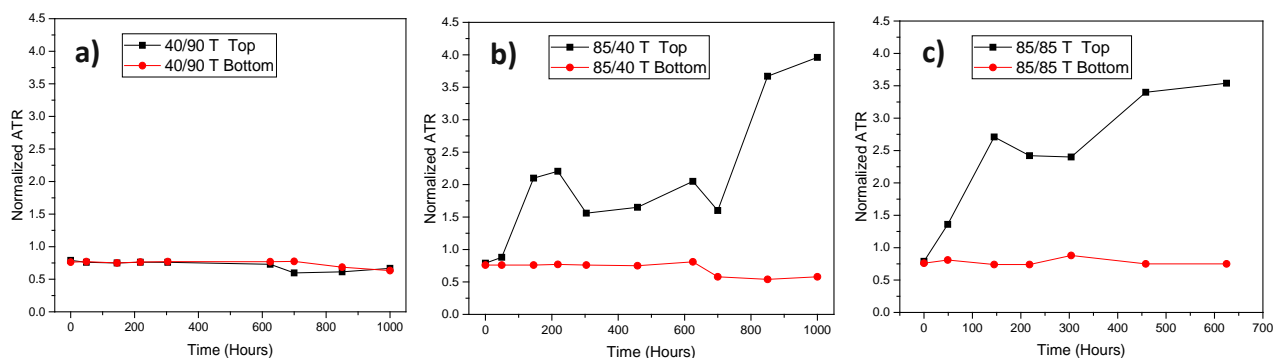


Figure 85. Normalized ATR intensities of the N-H stretching vibrations depending on aging conditions: a) 40 °C/90 %RH, b) 85 °C/40 %RH and c) 85 °C/85 %RH.

As mentioned previously, the strength of intermolecular hydrogen interactions in the TPU can be examined through the shifting or intensity variation of the spectral bands corresponding to C=O and N-H groups [88]. These interactions are illustrated in Figure 86. Generally, three types of intermolecular interactions in the TPU chains have been reported in the literature [129]. Firstly, hydrogen bonding with urethane carbonyl groups in hard segments; secondly, hydrogen with alkoxy oxygen atoms in urethane linkages between hard domains as well, and thirdly, hydrogen interactions between ether oxygen or carbonyl oxygen in soft segments or between soft and hard domains. Matsunaga et al. [129] found that density of the physical crosslinks created by the H⁺ bridging is higher within the hard phase than in soft phase.

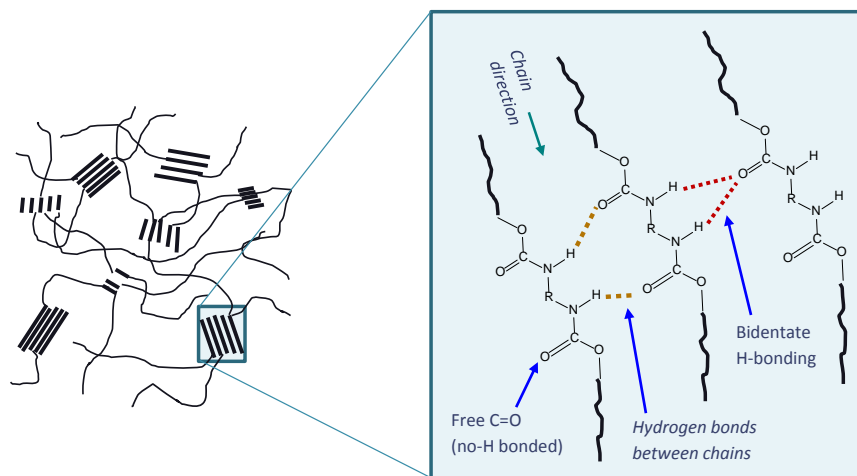


Figure 86. Sketch of TPU intermolecular bonding

Major changes in the molecular structure take place also at the polymer fingerprint spectra between 1500 and 1750 cm^{-1} , as presented in Figure 88. (C=O) Carbonyl bands at 1730 and 1702 cm^{-1} are referred first to free, non-hydrogen-bonded urethane, and secondly, to hydrogen-bonded, disorder urethane groups in the TPU chains [128]. These carbonyl bands are constant at specimens aged at 40 °C/90 %RH in both top and bottom surfaces, as displayed in Figure 88 part a). From there, it is also possible to evidence a new small spectrum occurring at 1636 cm^{-1} at the top surface that is related to an urea compound that forms an intermolecular bidentate hydrogen bonding [81]. For the rest of the spectra remain constant, with similar intensities and no shifts in wavelengths.

Composites that were environmentally stressed at 85 °C/40 %RH and 85 °C/85 %RH exhibit similar molecular interactions after aging, as seen in Figure 88 part b) and c). It is clear that at the exposed surface (top), there is a reduction of the broad carbonyl bands between 1675 and 1750 cm^{-1} , indicating a decrease in the concentration of free and hydrogen-bonded carbonyl compounds, and it is also correlated to the N-H interactions with water molecules, as it was explained in Figure 84.

A rapid and proportional increase in the intensity of the band takes place at 1636 for the specimens subjected to 85 °C/40 %RH and 85 °C/85 %RH respectively. This intermolecular bidentate hydrogen bonding, illustrated in Figure 86, could be explained by the new intermolecular interactions with water molecules, as in Figure 87.

A new band grows with aging at 1564 cm^{-1} and increases its intensity after just 49 hours of exposure in both cases, and it is especially fast-growing at the most severe environmental condition. This band is correlated in the literature to the bending of N-H groups [130]. The constant band at 1597 cm^{-1} denotes

the aromatic ring stretch from the hard segment in the main polymer chain [76], and it was taken as a reference for normalizing the ATR spectra.

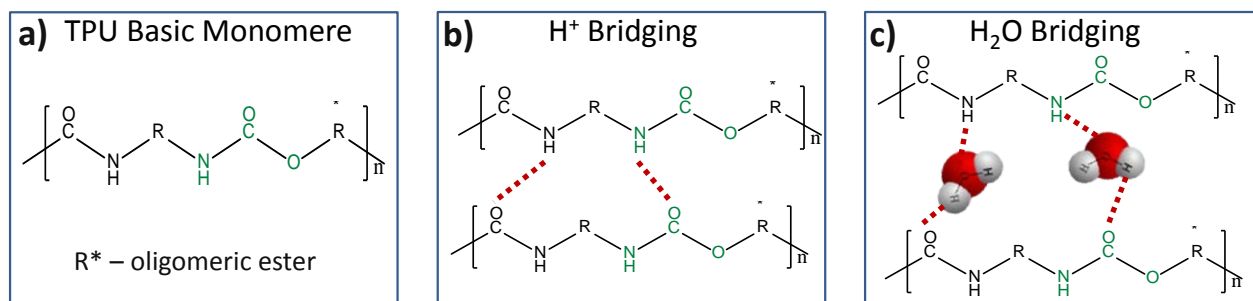


Figure 87. a) TPU basic monomer, b) expected physical interactions of hard and soft domains in fresh overmolded TPU, and c) possible water vapor bridging in the TPU urethane hard phases when aged at 85 °C/40 %RH and 85 °C/85 %RH as seen in FTIR examination at 3300 cm^{-1} .

As a summary, it is possible to conclude that for all hybrids environmentally stressed at 85 °C/40 %RH and 85 °C/85 %RH, on the top side of the polymer, there are new strong water interactions detected with the increase of the intensity of the N-H groups at 3300 cm^{-1} and a decrease in the intensity of the carbonyl bands between 1675 and 1750 cm^{-1} . This overlapping indicates strong interactions of the hard urethane segments with water molecules due to their inherent high polarity, as it is suggested in Figure 87, and corroborated by the reduction of the tensile strength of the polymer in numeral 6.1. Molecular interactions of the polymer face that are in direct contact with the coating (bottom) is not significantly affected, as depicted in the figures on the right-hand side in Figure 84 and Figure 88. However, in all cases, there is a slight increase in the band at 1636 cm^{-1} indicating that water is diffusing through the polymer even at normal environmental conditions, here at 40 °C/90 %RH.

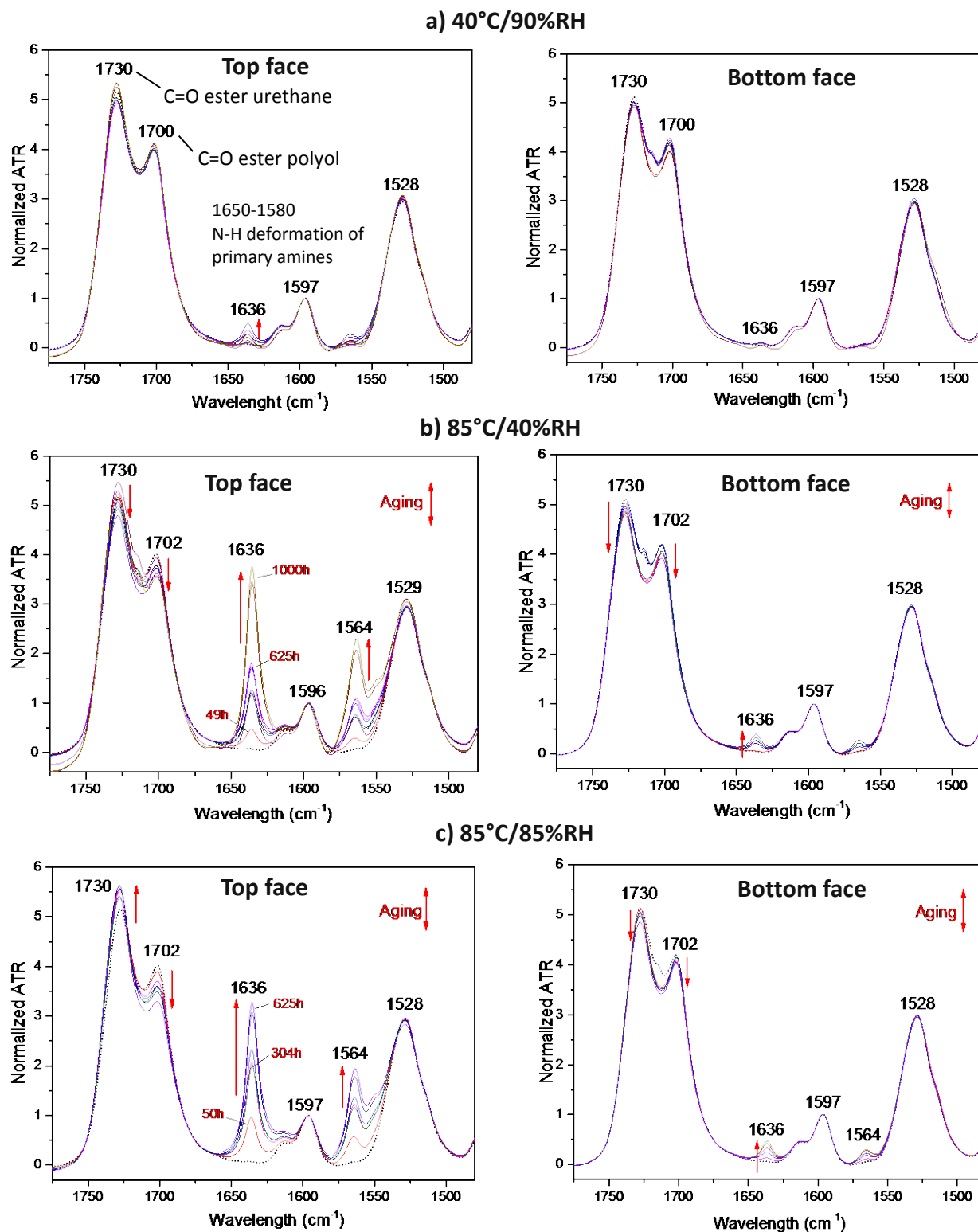


Figure 88. FTIR spectra, from 1500 - 1750 cm^{-1} , of the aged TPU that was overmolded and annealed on metal substrates. Aging conditions: a) 40°C/90%RH, b) 85°C/40%RH and c) 85°C/85%. Figures to the left hand side show the resulting spectra of “top” exposed TPU surface and, in the left, the spectra of the polymer that was in direct contact with the coating and recalled here as “bottom”.

6.6. CORROSION OF THE METAL SUBSTRATE AND EFFECTS AT THE POLYMER-METAL JOINT

Diffused water oxidized the steel surface causing blistering in the coating, as explained in numeral 2.7.3, which leads to a premature failure of the polymer-metal joint. Blistering on the intermediate polymeric coatings after hygrothermal aging was assessed through the ISO 4628 part 2 [131]. The Standard is based on visual examination of the quantity and size of blisters that is compared with well-established graphic patterns. A number of blisters, measured as density per area, is symbolized with the letter Q, which is followed by a numerical value from 1 to 5, where 1 indicates that blisters are not visible with the naked eye, and 5 designates a high density of imperfections. The size of blisters, symbolized with the letter S, remained constant after aging and is equivalent to the S2 pattern referred in the Standard. Figure 89 depicts exposed surfaces of hybrids manufactured on phosphated steel substrates aged at 85 °C/85 %RH, 85 °C/40 %RH, and 40 °C/90 %RH. Blister quantity evaluation, in the Y axis, is notorious for samples subjected to the harshest environment (85 °C/85 %RH), as exhibited in red dots. Samples exposed to lesser harmful environments, 85 °C/40 %RH and 40 °C/90 %RH, did not exhibit blistering or superficial damage meaning a good resistant of the coatings to weathering. As a measure of quality, the Standard recommends recoating or replacement of the part when the exposed layer has a value higher than Q2.

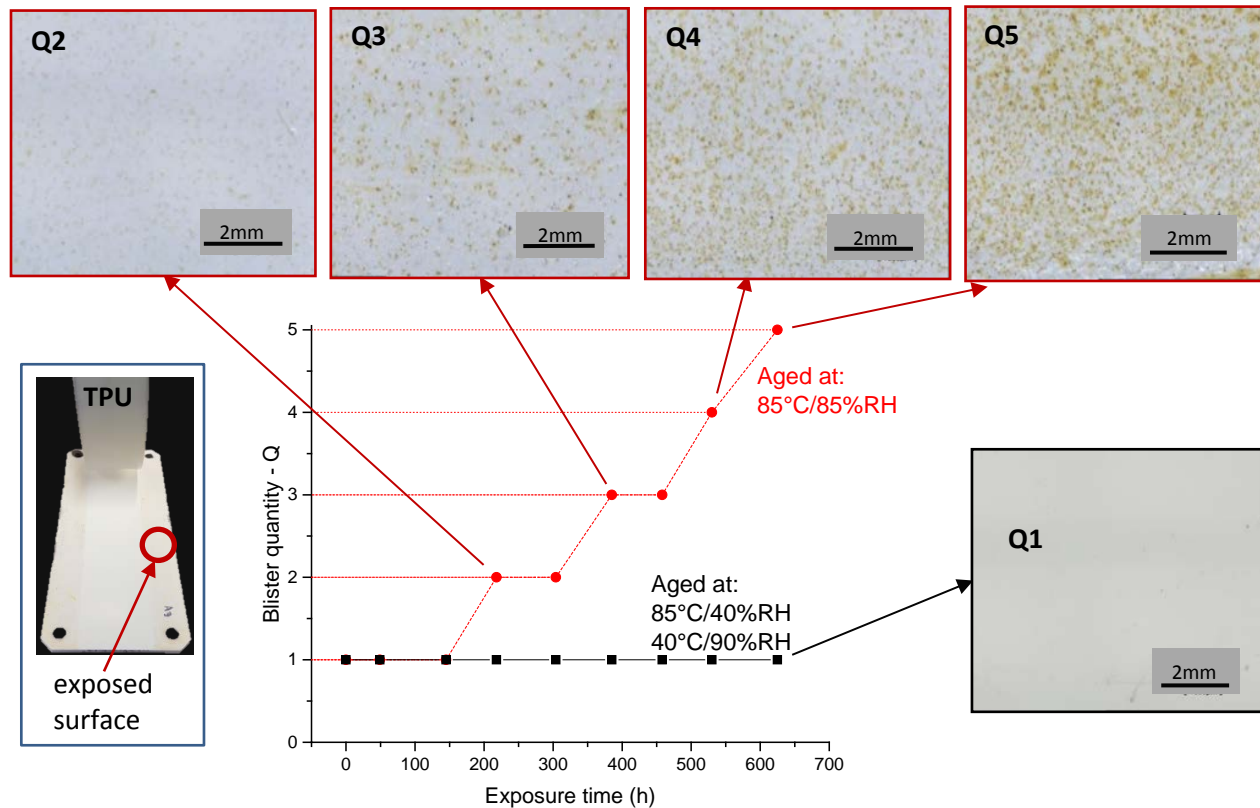


Figure 89. Determination of blister quantity, from Q2 to Q5, for the aged in-house coating on phosphated steel following the ISO 4628-2. Red dots show specimens aged at 85 °C/85 %RH and black dots represent samples aged at 85 °C/40 %RH and 40 °C/90 %RH. The surface evaluated is indicated in the left-hand side picture.

In the same way, a determination of the quantity of blisters was performed on the surface that was in direct contact with the overmolded TPU on plain and phosphated steel substrates, as illustrated in Figure 90. From there, it is well defined the increase in blister density, in particular on the surface of the unprotected steel, designated in triangular symbols. The quantity of blisters on the in-house coating on phosphated substrates stabilizes after 304 hours of exposure and remains steady through the end of the test. Blisters were not detected on hybrids exposed to less severe conditions (85 °C/40 %RH and 40 °C/90 %RH), as indicated by black dots with a Q1 quantity denomination.

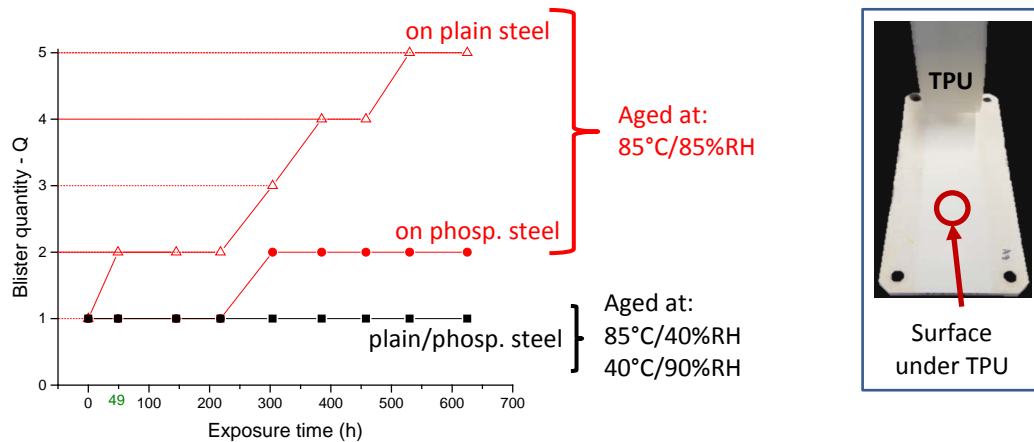


Figure 90. Blister densities under the TPU overmolded on pre-coated plain and phosphated steel sheets aged at 85 °C/85 %RH. Surface evaluated is indicated in the right-hand side picture.

A summary of a microscopic evaluation of the surfaces that were in direct contact with the overmolded TPU is displayed in Figure 91. It is evident the adverse effects of steel oxidation on the coating when subjected to the harshest atmosphere (85 °C/85 %RH). The small and homogeneous rusting points confirm that water vapor is diffusing through the overmolded polymer, as it was also detected by FTIR analysis. Hybrid parts subjected to the other environmental conditions, i.e. 85 °C/40 %RH and 40 °C/90 %RH, did not deteriorate even after 1000 hours of exposure, as highlighted by the blue dotted line.

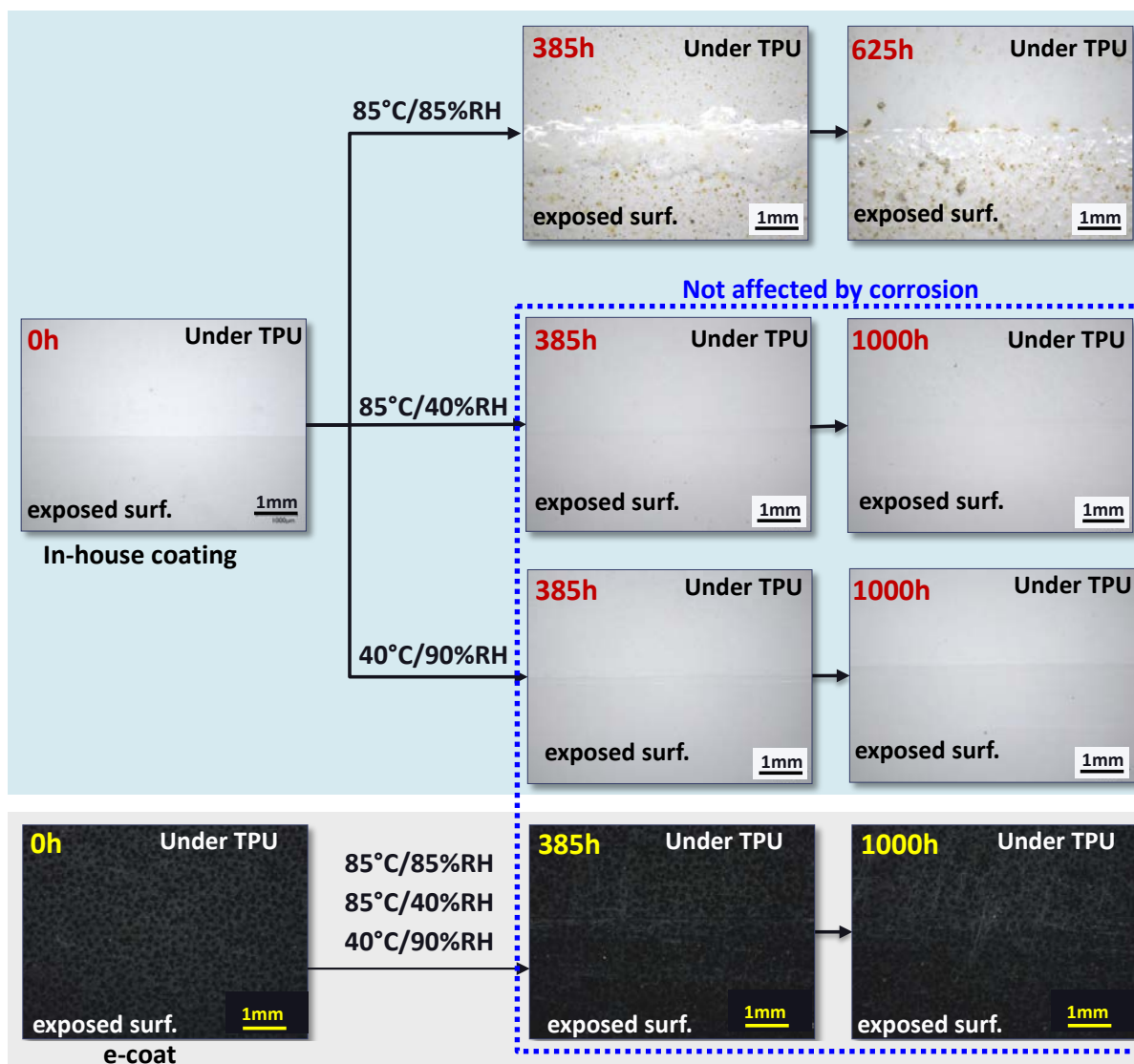
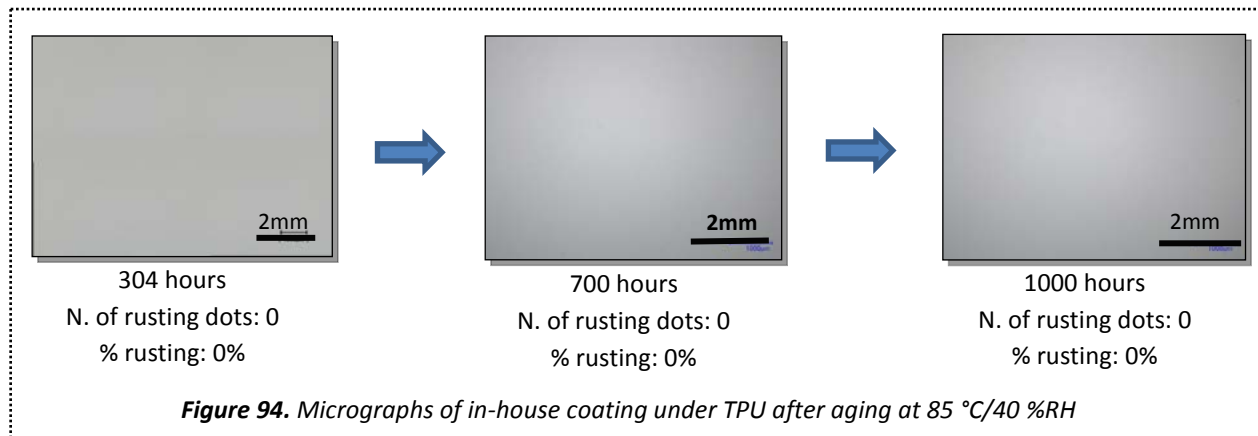
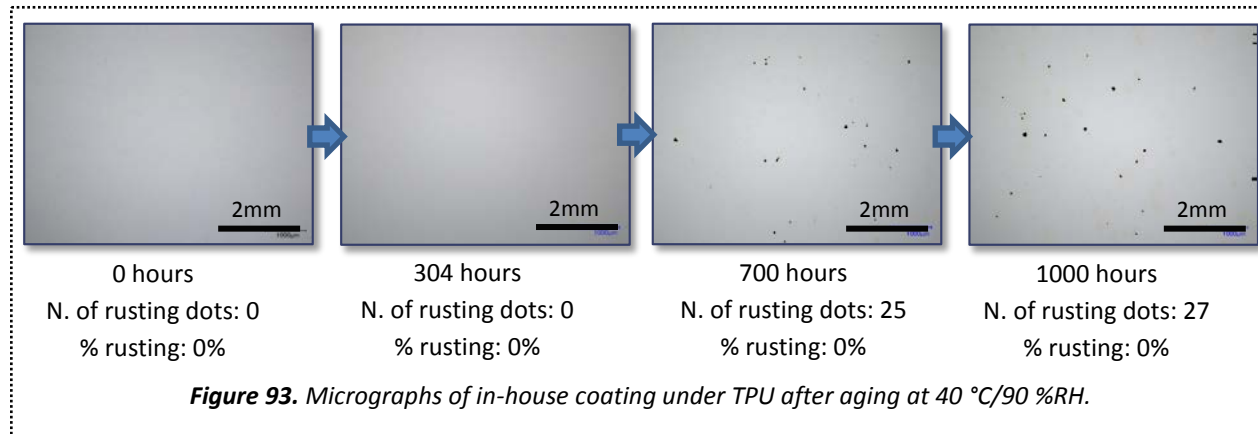
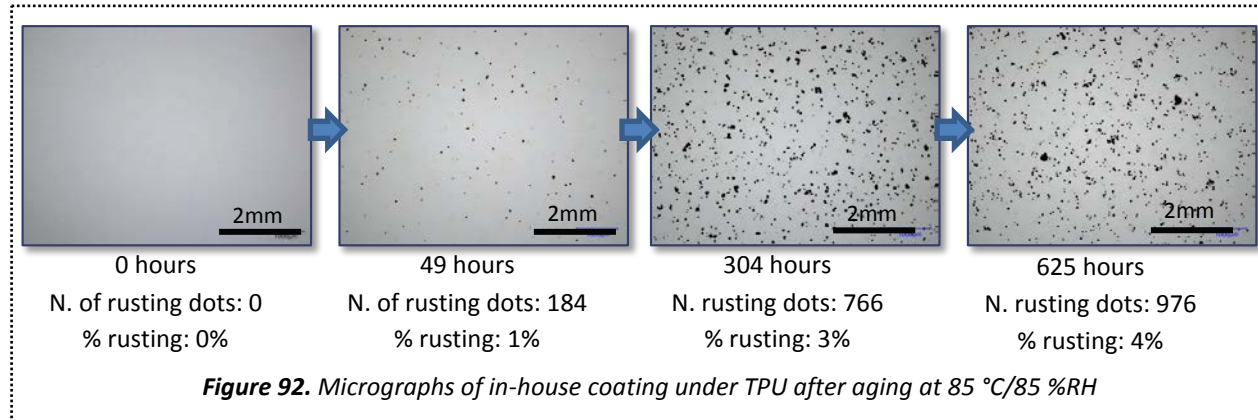


Figure 91. Digital microscopy images of composites prepared with different substrates and exposed to different environmental conditions.

The level of rusting on the coating that was underneath the TPU was evaluated microscopically using specialized software that counts the number and percentage of corrosion dots by color contrast on the surface. Figure 92 to Figure 94 display surfaces underneath the overmolded TPU with the number of rusting dots and the corresponding percentages of the corroded area. It is distinctly seen that there are rusting spots formed, presumably, by water vapor diffused from the outside through the polymer/coating interface. They are homogeneously distributed on the surface and easily detectable in the aged hybrid under the most severe conditions, as in Figure 92. Some corrosion dots were also measured at 40 °C/90 %RH, after 700 hours of exposure, as indicated in Figure 93. Due to the low relative humidity, specimens subjected to 85 °C/40 %RH do not exhibit rusting on the surfaces even after 1000 hours, as depicted in Figure 94.



An in-depth SEM-XDS examination of the effects of corrosion on the exposed face and underneath the film after osmotic blister formation is presented in Figure 95. The deposits of a corrosion product consisting of Fe and Zn adhered to the coating were detected by XDS and depicted in part b). The exposed surface in part a) exhibits pinholes with the corrosion product, which contains only Fe. Pinholes suggest that discontinuities within the coating, like pores, facilitate the diffusion of water vapor to the steel surface, which subsequently oxidized the metal and induced premature failure due to delamination at the coating-metal interface.

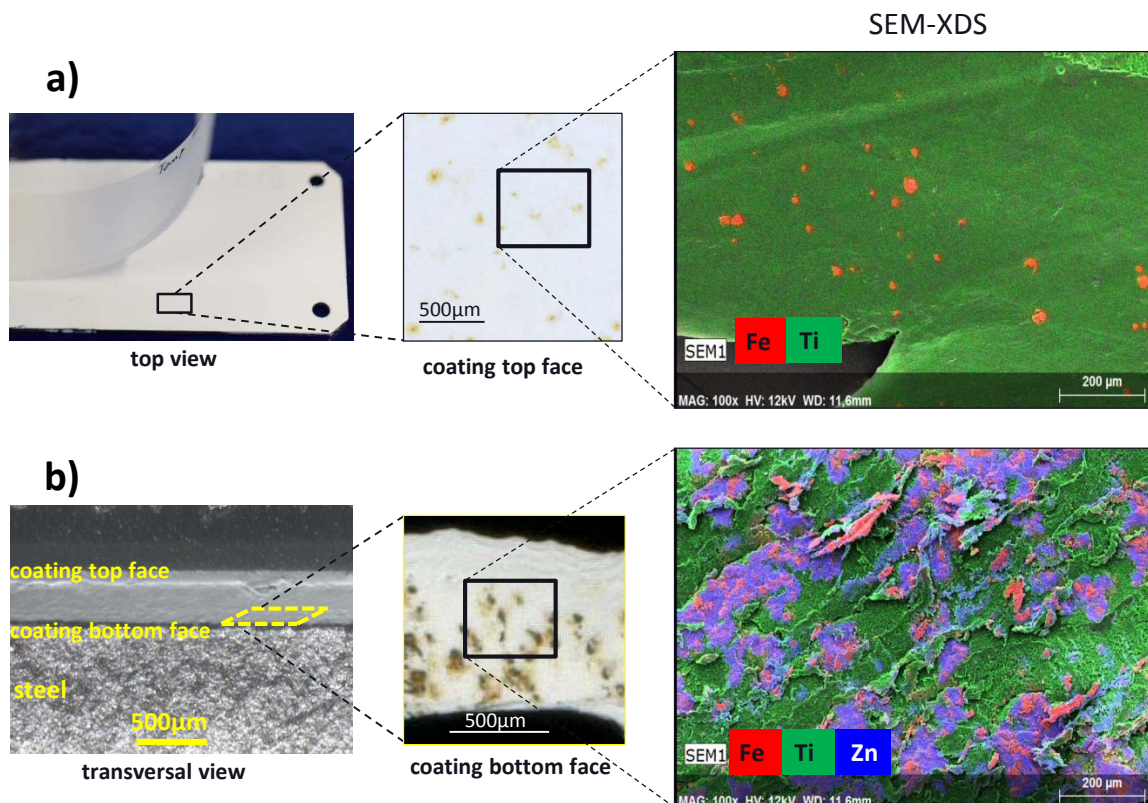


Figure 95. Digital microscopy and SEM-XDS analysis of effects of corrosion on coating after 49 h of exposure to a harsh atmosphere: 85 °C/85 %RH. a) Imaging on the exposed surface showing orange-like Fe pinholes. b) under-coating condition after osmotic blister formation showing deposits of the oxidized steel consisting of Fe and Zn.

6.6.1. Thermal Properties of Hygrothermally-Aged Adhesive Coatings

A DSC analysis was conducted on the coatings to evaluate the effect of environmental stresses on their durability. Samples for thermal evaluation were obtained by scratching the respective surface under the overmolded TPU after weathering. Figure 96 exhibits thermographs of the second heating cycle, from - 80 to 230 °C, after 625 hours of exposure at 85 °C/85 %RH. T_g increases with aging time indicating sensibility to a harsh hygrothermal environment, reaching a glass transition temperature of 55 °C at the end of the test. The increase of this physical property may be explained by the growth of the crosslinking density as a consequence of high temperature and humidity, as reported in the literature [132], and may also suggest degradation due to thermolysis or hydrolysis of the organic coating. No exothermic cure peaks were detected in any sample, indicating a fully cured system. Table 18 summarizes the trends of T_g of the TPU and the thermosetting coatings applied on the metal substrate. Similarly, one can follow a slight increase in the transition temperature in the other hygrothermal conditions. It seems that the in-house coating is mostly affected by temperature than humidity as presented in samples aged at 85 °C/40 %RH with a rapid increase in the T_g , which stabilizes at 42 °C after 218 hours of exposure. Hybrids

environmentally stressed at 40 °C/90 %RH had a rather steady T_g at around 40 °C. Examination of e-coat was more complex because the glass temperature could not be detected at the second heating cycle and significant variations were observed in the first heating. This is in part attributed to the difficulties in the preparation of the sample due to quite small and inhomogeneous flakes removed from the surface.

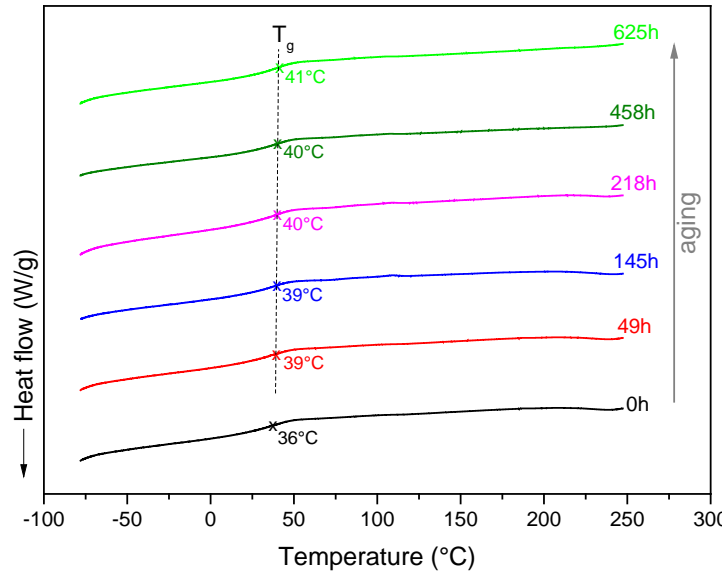


Figure 96. Second heating DSC thermographs, under N_2 , of the in-house coating after accelerated aging at 85°C/85%RH. Substrate is phosphatized steel.

Expo. time [h]	85 °C/85 %RH - T_g [°C]			85 °C/40 %RH - T_g [°C]			40 °C/90 %RH - T_g [°C]		
	e-coat (epoxy-based)	in-house (polyester-based)	TPU	e-coat (epoxy-based)*	in-house (polyester-based)	TPU	e-coat (epoxy-based)*	in-house (polyester-based)	TPU
0	57	36	-41	63	35	-41	63	35	-41
218	55	40	-42	67	42	-38	69	37	-40
458	55	40	-43	52	43	-39	61	34	-40
625**	56	41	-43	58	43	-40	58	36	-40
700	**Experiment stopped due to failure of samples			59	41	-39	57	37	-38
850				61	41	-39	64	36	-39
1000				52	41	-37	56	36	-41

* T_g of e-coating was detected at first heating step, not detectable at second heating.

Table 18. T_g of TPU, in-house and e-coat at the TPU-Coating joint at different environmental conditions.

6.7. CHAPTER SUMMARY

Researching on the aging of polymer-metal hybrids was conducted individually for each component. The analysis of the first material, the overmolded TPU, evidenced a steady behavior regarding mechanical properties, in particular for TPU stripes aged at 40 °C/90 %RH, and 85 °C/40 %RH. Tensile strength and ultimate strain remain steady after 1000 hours of exposure to those conditions. On the other hand, environmental stresses at a severe atmosphere, i.e. 85 °C/85 %RH, ended up with a slight drop in the tensile strength and a proportional increase in the ultimate deformation of the polymer just after 625 hours of exposure, as exhibited in numeral 6.1 of the current chapter. Catastrophic failure of the polymer did not occur in any of the different artificial environments, as it was referred by Hoikkanen et al. [64]. Thermal analysis on the aged TPU that was in direct contact with the adhesive promoters reveals negligible changes in the T_g , demonstrating that hygrothermal external conditions did not plasticize the polymer nor altered the amorphous continuous domains of the thermoplastic elastomer. The heat of fusion also remained relatively invariant, suggesting that there were not compromising effects in the hard segments and crystalline domains, as displayed in Figure 82 and Table 17. A detailed examination of the overmolded thermoplastic polyurethane on the surface that was exposed to the atmosphere and also underneath the surface that was in direct contact with the in-house and e-coat adhesion promoters, after the peel test, was performed by FTIR. From there, it is evident that water vapor is diffusing through the TPU, as the IR spectra changed from the top to the bottom faces. At the TPU bottom surface on direct contact with the metal substrates, there are very few variations in the spectrum; however, the rising of new bands proposes new intermolecular interactions within the polymer chains that could be explained by polar interactions from water molecules.

The lifetime of the hybrid was significantly affected by temperature and humidity especially at 85 °C/40 %RH and 85 °C/85 %RH, where the adhesion of the TPU to the metal sheet drops sharply just after 49 hours of exposure to the most severe environment. For this reason, the weathering test was stopped after 625 hours. For the other aging conditions, samples were exposed to 1000 hours.

The sharp drop in the bond strength occurs due to the fast diffusion of water vapor at the polymer-coating interface destroying the physical-chemical interactions, as illustrated in Figure 87. In the other hand, annealed hybrids at 100 °C for 20 hours, exhibited a much better performance in the long term, particularly in specimens overmolded on e-coat substrates. The better long-term performance of thermally treated hybrids may be attributed to the denser physical-chemical interactions at the TPU-metal interface, as it was explained in section 5.5.

From the summarized results, it could be concluded that progressive failure of the composite is strongly dependent on diffusion, mainly through the TPU or by the joint edges, as observed in the micrographs of coatings after the hygrothermal aging. One can consider that diffusion of water vapor may hydrolyze any of the materials that take part in the hybrid: the overmolded polymer, the intermediate coating, and/or the metal substrate. Hydrolysis of TPU, coating and/or metal sheet is controlled by diffusion and the time for hydrolysis, t_H , is determined as [133–135]:

$$t_H = \frac{1}{k} \rightarrow k = k_0 \exp \frac{-E_H}{RT} \quad \text{Equation 3. Time for hydrolysis}$$

Where k is the reaction hydrolysis rate, k_0 is the pre-exponential factor, E_H is the activation energy, and R and T are the gas constant and temperature in K, respectively. Similarly, the diffusion of water vapor into the polymer-coating interface may be calculated experimentally by [133,135]:

$$t_D = \frac{L^2}{D} \rightarrow D = D_0 \exp \frac{-E_D}{RT} \quad \text{Equation 4. Diffusion of water through the polymer}$$

Where D is the diffusion coefficient at a certain temperature, T ; and D_0 is the pre-exponential diffusion factor.

Figure 97 concludes the failure mechanisms observed in the polymer-metal composites used in this work. Failure in specimens prepared on corrosion-protected substrates and subjected to normal environmental stresses (40 °C/90 %RH and 85 °C/40 %RH), took place due to water diffusion through the TPU and hybrid joint edges. Subsequently, a destruction of polymer-coating interactions at the interface, clearly suggesting that t_D is much faster, particularly in the interface [80] than hydrolysis of the TPU or coatings, designated as t_H . On the other hand, failure in the unprotected plain steel occurred by a fast oxidation process of the steel surface that consequently decomposed the adhesive coating by blistering, as pictured in Figure 97 b). It is apparent that t_H is faster on the metal substrate than the IPF coating and the TPU.

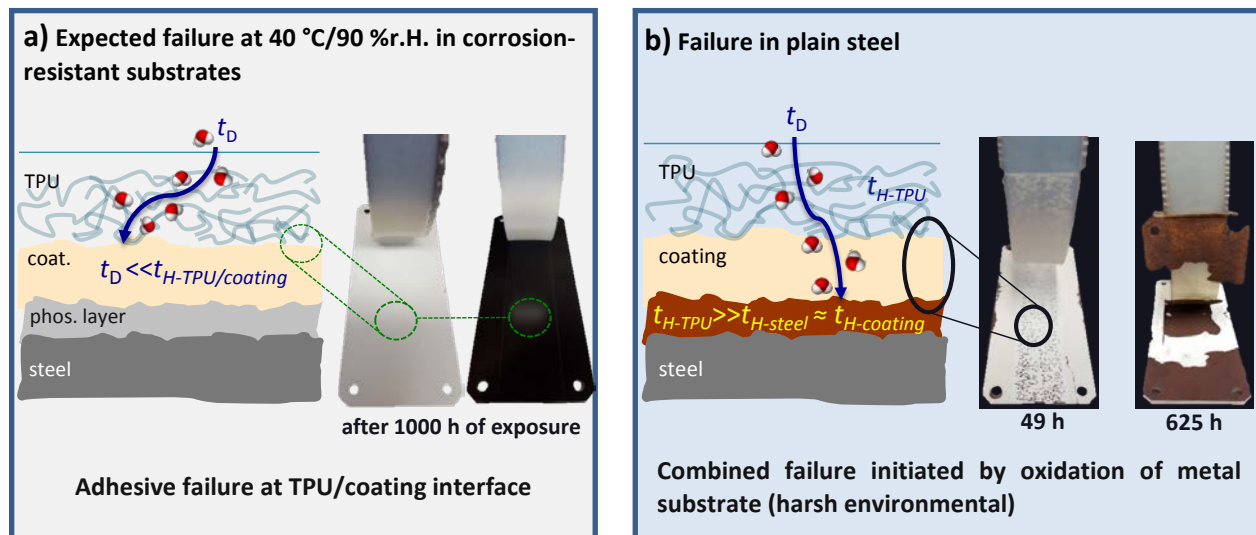


Figure 97. Failure mechanisms in the polymer-metal composites using as substrate a) a corrosion-resistant metal, and b), a plain steel.

7. DURABILITY AND LIFETIME PREDICTIONS OF THE POLYMER-METAL COMPOSITE

7.1. PERMEATION AND DIFFUSION

7.1.1. Influence of Annealing on the Diffusion of Water Vapor in TPU: Water Uptake

Water absorption examination was conducted on single TPU strips subjected to different hygrothermal aging conditions. Samples were weighted before the artificial aging process and removed from the chamber after certain exposure times. The mass of the strips was measured again and, subsequently, cut to proceed to the tensile test. Samples aged at 40 °C/90 %RH presented the highest water uptake, reaching saturation at around 0.75% of gain weight after 625 hours of exposure, as depicted in Figure 98. However, after 925 hours, the weight increased again, reaching a maximum at 0.84% of its initial mass. In the other hand, specimens hygrothermally aged at a relatively high temperature and low humidity, i.e. 85 °C/40 %RH, did not show a saturation limit, and their gain in weight is steady at around 0.3% after 1000 hours of aging. Strips exposed to the most severe environment showed a similar tendency than those exhibited by the specimens at 40 °C/90 %RH, with a saturation maximum at 0.7% in weight gain after 1000 hours. The examination of water uptake at different environmental situations suggests that the TPU is sensible to absorb humidity independently (or to a lesser extent) to the surrounding temperature, as evidenced in the strips aged at 85 °C/40 %RH, where the water absorption was much lower than in the other cases.

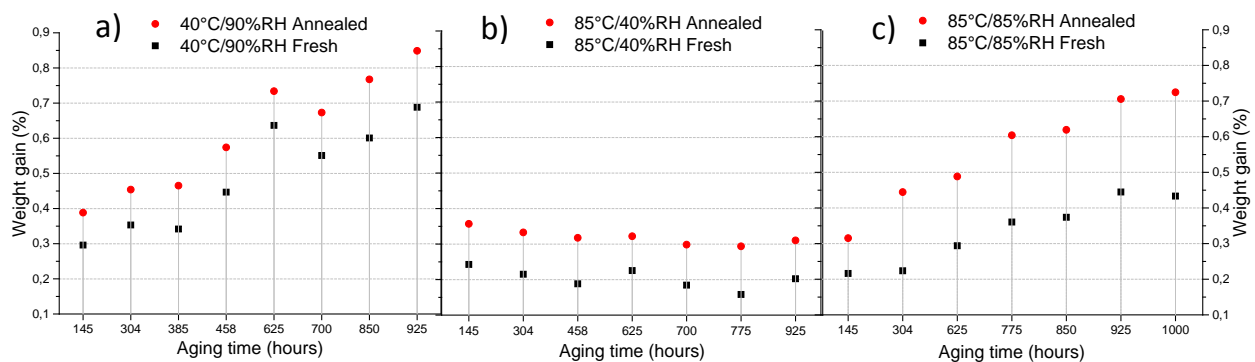


Figure 98. Water uptake of TPU after hygrothermal aging at a) 40°C/90%RH, b) 85°C/40%RH and c) 85°C/85%RH.

It is evident also that water uptake is higher for the annealed specimens, as depicted in red dots in Figure 98. Boubakri et al. [88] faced a similar tendency in a polyester-based TPU that was dried for 48 hours at 70 °C and then it was immersed in water at 70 °C for six months. Boubakri assumed that drying the TPU speeds up the kinetics of water absorption because water vapor molecules induce relaxation in the macromolecular architecture by destroying intermolecular H bridging, with a later re-arrangement of the

structure and a subsequent increase in the free volume. Mondal et al. [136] also corroborate that water absorption into the thermoplastic elastomer implies the conformation of free volume which persists in the structure and it will depend on the thermal history of the polymer. It is necessary to elucidate that despite the high water uptake registered for the polymers exposed to high humidity, 40 °C/90 %RH, the mechanical properties were not significantly affected, as already discussed in section 6.1.

7.1.2. Influence of Annealing on Permeation of Gasses in TPU

In order to understand how fast water vapor penetrates and ruptures the physical-chemical interactions at the polymer-coating-metal joints, permeation rates of different gasses through the TPU were examined. The test consists of two parts: first, an evacuation stage where the sample is under vacuum inside the permeation cell for a certain time to draw the gasses that are contained already in the specimen. The second stage is the permeation measurement, where the respective gas is filled from the top chamber, and then, the difference of pressures is measured in the bottom part of the cell as illustrated in Figure 99.

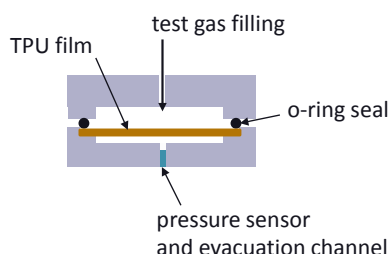


Figure 99. Schematic representation of the permeation cell.

It was found, after several trials, that the optimal evacuation period for the 300 μm TPU film was 24 hours. This long evacuation time is mainly attributed to the relatively high thickness of the sample and the corresponding time required to draw all gasses already inside the polymer. For the second stage, the time of gas flowing through the polymer film depends on the tested gas: for samples in which permeation of O_2 and N_2 were evaluated, the steady state occurred after approximately 1 hour after the filling stage. For TPU films under CO_2 , the steady state occurred after minimum 5 hours of filling time; as displayed in Figure 100, which plots the gas transmission rate, $\text{GTR} (\text{cm}^3/(\text{m}^2 \times 24\text{h} \times \text{bar}))$ vs. permeation time (h). The increase in pressure inside the sample for films permeating CO_2 refers to an increase in the solubility gradient within the TPU film. The solubility of CO_2 in most plastics is higher than other gasses [6], meaning that it is stored continuously inside the polymer. Consequently, less gas leaves the film and the GTR value will decrease over time without reaching a steady state, as it is observed with permeation

experiments with N₂ and O₂. In the case of permeation of CO₂ through the TPU film, one can assume that it is a competition between solubility and diffusion within the polymer structure.

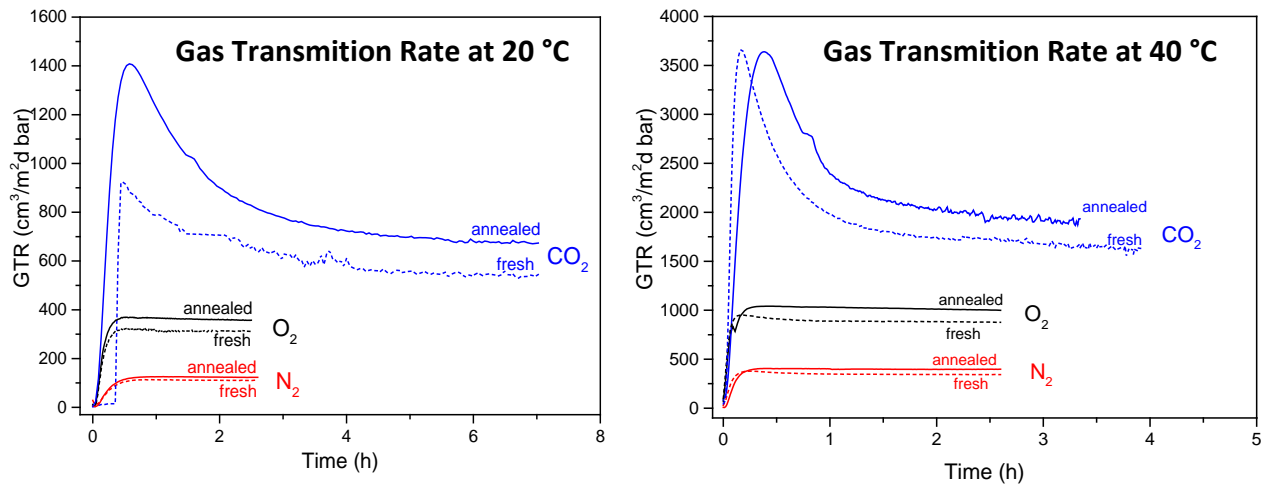


Figure 100. Gas transmission Rate (GTR) of different gases through the TPU film at 20 °C and 40 °C

Table 19 summarizes the GTR at steady state, the solubility and diffusion coefficients of the respective gasses through the TPU film. Permittivity parameters of CO₂ could not be calculated precisely because the GTR never reached a steady state.

	20 °C						40 °C					
	O ₂		N ₂		CO ₂		O ₂		N ₂		CO ₂	
	Fresh	T100	Fresh	T100	Fresh	T100	Fresh	T100	Fresh	T100	Fresh	T100
GTR [cm ³ /m ² d*bar]	313	361	112	121	538	665	832	1020	349	398	1690	1920
Solubility [cm ³ /cm ³ *bar]	0.024	1.6E-02	1.2E-02	1.1E-02	N/A	N/A	3.1E-02	1.2E-02	1.5E-02	1.3E-02	N/A	N/A
Diffusion coef. [cm ² /s]	4.6E-07	7.6E-07	3.2E-07	3.8E-07	N/A	N/A	9.3E-07	2.9E-06	8.1E-07	1.1E-06	N/A	N/A

Table 19. Gas Transmission Rate (GTR), solubility and diffusion gasses onto TPU film at 20 and 40 °C

From Figure 100 and Table 19 it is clear that the permeation parameters like GTR, solubility, and diffusion rate increased at a higher temperature. It is interesting to observe that permeation of gasses through the annealed specimens is slightly faster than in fresh polymer films, and it is in accordance with the high water absorption in the thermally treated strips, displayed in Figure 98.

These small differences in the permeation rates for annealed and fresh samples may be correlated to the re-arrangement of hard and soft phases in the polymer, which seems to affect the diffusion of water

vapor molecules through the polymer strip. As explained in the literature [6,12,129], diffusion takes place much faster in amorphous domains of the polymer than in packed and crystalline regions because of the higher free volume of the disordered phase and the weaker intermolecular interactions. From that point of view, the evaluation of diffusion and solubility of the gasses into the polymer may indicate that rearrangement of hard and crystalline phases in annealed films are increasing the free volume in the amorphous regions. Matsugana et al. [129] in an extensive work, points out that the soft phase plays the major role in diffusion through a TPU, regardless the molecular arrangements of soft and hard combinations. They found that the higher permeability values are correlated to the lengthening of amorphous domains, and the diffusion coefficients of the TPU examined, depended on the chain length of the soft segments. It was also announced that solubility is independent of the chemical structure of the hard segments. In this work, the apparent increase in the free volume of annealed samples was also observed in the water uptake examination after artificial aging of the polymer: thermally treated strips absorbed in all cases more water than the fresh thermoplastic elastomer. It is expected that water uptake depends proportionally on the configuration of the amorphous regions. The increase of free volume of disorder domains in the annealed polymeric strips may be ascribed to weaker interactions of hydrogen bonds with the ester or carbonyl oxygen between soft and hard segments, as seen as well in the FTIR examination in section 6.5.

7.1.3. Water Vapor Diffusion in the Polymer-Metal Composite

As it was demonstrated in chapter 6.7, water diffuses from the outer face of the TPU to the polymer-coating interface causing a premature failure in the composite. In order to determine the diffusion coefficient of water into the TPU, an absorption test was conducted on fresh and annealed strips 2 mm thick that were cut at 7.6 cm x 2.5 cm, and immersed in distilled water at 40 °C, 60 °C, and 85 °C until reaching saturation. The water absorption test was conducted following the ISO 62. Figure 101 illustrates water absorption tendency in the fresh and annealed TPU specimens at different temperature baths. As also observed with gas permeation, annealed specimens appear to uptake more water than fresh strips, corroborating also the announcements of Matsugana described in the previous numeral.

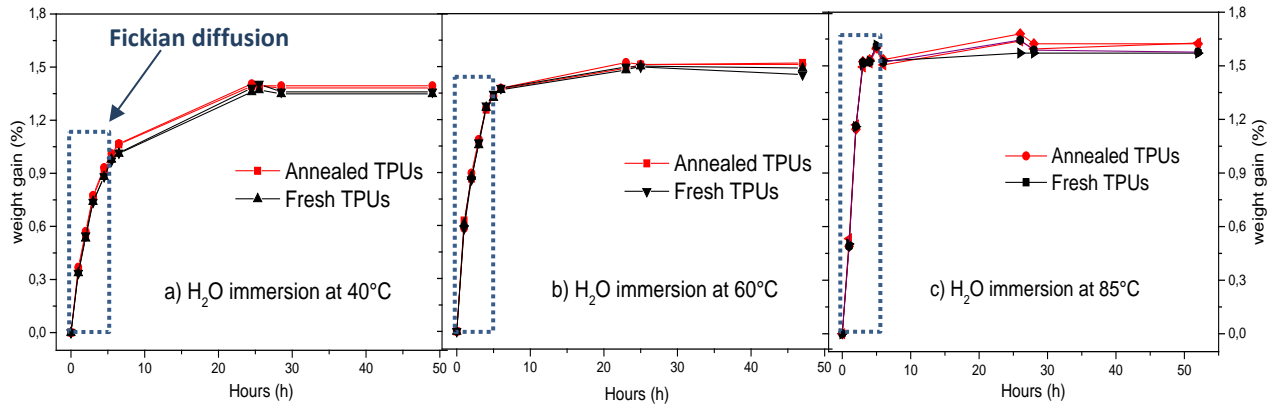


Figure 101. Time dependency of water absorption at a) 40°C, b) 60°C and c) 85°C in fresh and annealed TPU strips.

It has been demonstrated in the literature [88,137,138] that water sorption in polymers follows Fickian diffusion in the initial absorption stage as shown in Figure 101. Diffusion in that stage is represented in Equation 5 following Fick's second law [137,138]:

$$\frac{M_t}{M_{max}} = 1 - \sum_{n=0}^{\infty} \frac{8}{(2n+1)^2\pi^2} \exp\left[\frac{-D(2n+1)^2\pi^2 t}{4L^2}\right] \quad \text{Equation 5. Fickian diffusion}$$

Where D is the diffusion coefficient, L is the thickness of the sample, M_{max} is the equilibrium intake value of the diffusing water at an infinite time, and M_t is the water absorbed at a certain uptake time t . When $M/M_{max} \leq 0.6$; Equation 5 is simplified to [137,138]:

$$\frac{M_t}{M_{max}} = \frac{4}{L\sqrt{\pi}} \sqrt{D} (\sqrt{t}) \quad \text{Equation 6. Simplified diffusion in the initial absorption stage}$$

Diffusion coefficients in Table 20 were calculated experimentally from the water absorption rate as a function of immersion time, as displayed in Figure 101 and following Equation 6. They are in good agreement with Boubakri et al. [87,88] who investigated water diffusion in a specific type of ester-based TPU. It is also evidenced that molecular motion inside the annealed polymer is slightly faster than in fresh specimens.

	40 °C		60 °C		85 °C	
	Fresh	Annealed	Fresh	Annealed	Fresh	Annealed
Equilibrium H ₂ O intake [wt. %], M_{max}	1.35	1.38	1.51	1.51	1.58	1.63
Diff. coef. [cm ² /s]	2.2E-07	2.3E-07	3.5E-07	3.7E-07	5.7E-07	5.8E-07

Table 20. Equilibrium uptake and D of H₂O in fresh and annealed TPU at different immersion temperatures.

7.1.4. Diffusion Time of Water Vapor and Lifetime Estimations

Assuming an scenario where the composite does not have any other kind of external influence like UV radiation, contaminants or mechanical loads, the time water travels through the TPU and reacts with the metal substrate can be predicted assuming the Arrhenius expression [6] in Equation 7; where D is the rate at which atoms diffuse through the polymer film, expressed in cm^2/s ; D_0 is the temperature-independent preexponential, also in cm^2/s ; E_D is the activation energy required for diffusion, in J/mol ; R is the gas constant, $8,31 \text{ J/mol-K}$; and T is the absolute temperature in K .

$$D = D_0 \exp \frac{-E_D}{RT}$$

Equation 7. Arrhenius expression for Diffusion

The experimental values of the Arrhenius parameters at different temperatures are plotted in Figure 102. It displays the $\ln D$ of water in fresh and annealed TPUs (from Table 20), versus the reciprocal of the absolute temperature. From the corresponding slopes of the fitting lines, the activation energy of the diffusion process, E_D , is estimated. The E_D may be defined as the energy required to generate motion of one mole of molecules of water, so a large E_D translates into a smaller D , as the one computed for the fresh TPU.

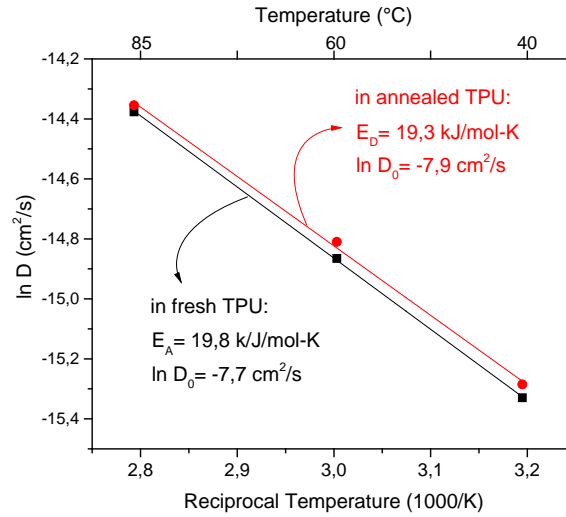
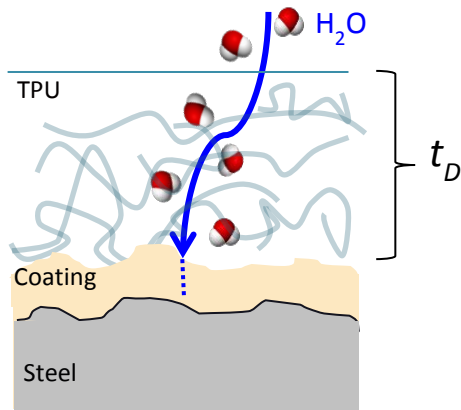


Figure 102. Experimental diffusion parameters of H_2O in fresh and annealed TPU strips at 40, 60 and 85 °C.

The time of diffusion, t_D , in function of the sample thickness, as sketched in Figure 103, can be determined from the simplified diffusion parameters, and it is presented in Equation 8 [6,133]. Where L is the thickness of the film and D , the diffusion coefficient of the respective element into the polymer.



$$t_D = \frac{L^2}{D}$$

Equation 8. Characteristic time of diffusion

Figure 103. Schematic representation of time of diffusion, t_D

Table 21 summarized the corresponding t_D , calculated from Equation 8, required for the water molecules to pass through the fresh and annealed, 2 mm thick, polymer strips. It is evident that water diffusion is faster at higher temperatures, taking only 19 hours to reach the polymer-coating interface when immersed to 85 °C; at tropical weather, i.e. 40 °C, it would take around 49 h to do so.

	Strips immersed at 40°C		Strips immersed at 60°C		Strips immersed at 85°C	
	H_2O		H_2O		H_2O	
	Fresh	Annealed	Fresh	Annealed	Fresh	Annealed
	D [cm ² /s]	D [cm ² /s]	D [cm ² /s]	D [cm ² /s]	D [cm ² /s]	D [cm ² /s]
t_D [h]	50	49	32	30	19	19
t_D [d]	2.1	2.0	1.3	1.3	0.8	0.8

Table 21. Diffusion of water through a, 2 mm thick, fresh and annealed TPU strip immersed at different temperatures.

Similarly, Table 22 resumes the required time for O_2 and N_2 molecules to pass through the 2 mm thick TPU strip. However, the lesser polarity of those gasses makes diffusion at the TPU-coating interface less harmful than that of water molecules. t_D values were estimated from the Diffusion coefficients, in Table 19, obtained by the permeation test described in numeral 7.1.2.

	Permeation test at 20°C				Permeation test at 40°C			
	O_2		N_2		O_2		N_2	
	Fresh	Anneal.	Fresh	Anneal.	Fresh	Anneal.	Fresh	Anneal.
D [cm ² /s]	4.6E-07	7.6E-07	3.2E-07	3.8E-07	9.3E-07	2.9E-06	8.1E-07	1.1E-06
t_D [h]	24	15	35	29	12	4	4	10
t_D [d]	1.0	0.6	1.4	1.2	0.5	0.2	0.6	0.4

Table 22. Required time for O_2 and N_2 molecules to pass through a 2 mm fresh and annealed TPU film at 20°C/40°C.

7.2. CHAPTER SUMMARY

Water uptaken by the polymer, measured as weight gain (Figure 98 and Figure 101), indicates an increase of the free volume in the amorphous domains. The increase in weight was higher in samples annealed at 100 °C due to a rearrangement of soft and hard segments in the TPU molecular architecture, as it was also detected by DSC analysis in chapter 5.1.3. In accordance to permeation and water immersion tests (listed in Table 20 and Table 21), the diffusion of gasses and H₂O through the TPU was faster for heat treated specimens when compared to samples without treatment. However, adhesion forces in annealed hybrids were significantly higher after hygrothermal aging. These results suggest that polar H₂O molecules diffusing from the outside into the heat treated polymer are rather stored in the larger free volume than diffused through the whole specimen until to the interface. Water molecules likely interact with the free carbonyl and urethane groups contained in the polyurethane backbone, and so diffusion rate of H₂O towards the polymer-coating interface is lowered. On the other hand, diffusion of O₂ and N₂, measured in the permeation test is faster in annealed samples because of the larger free volume in the polymer structure and the relatively smaller size and less polarity of gasses when compared to H₂O molecules [6].

Diffusion coefficient values in Table 21 are related to the diffusion rates of the hygrothermally aged hybrids, specifically for those subjected to high humidity values, i.e. 40 °C/90 %RH and 85 °C/85 %RH. Figure 104 a) recalls a premature failure of the composite due to oxidation on the plain (unprotected) steel substrate. Corrosion occurred by the rapid water diffusion into the polymer-metal interface of specimens subjected to the harshest environment: 85 °C/85 %RH after 48 h. The diffusion time, t_D , from the immersion test, was estimated at around 19 hours, as listed in Table 21. For samples hygrothermally aged at tropical climate, the first blistering was observed after 218 h of exposure, as in Figure 104 b). t_D from the immersion test at similar conditions, i.e. water at 40 °C, was estimated at 50 h. On the other hand, premature failure of specimens that were prepared on corrosion-protected steel sheets (phosphated and e-coat), took place at the polymer-coating interface in a purely adhesive mode. However, adhesion strength of hybrids prepared on unprotected and corrosion-protected steel substrates decays similarly after hygrothermal aging at similar exposure times, as exhibited in the peel test in Figure 105. That proves that diffusion destroys physical-chemical interactions at the polymer-coating interface faster than oxidation at the metal substrate.

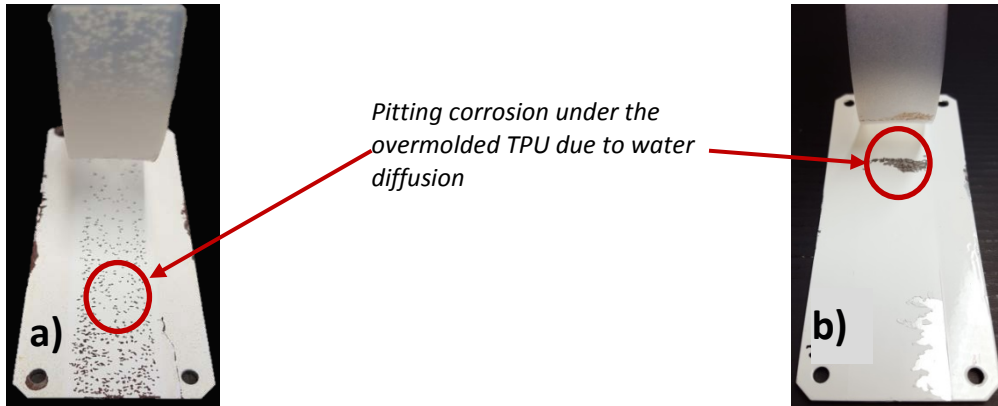


Figure 104. a) H_2O diffusion and debonding of TPU from the steel substrate after 49 h of exposure at 85°C/85%RH. b) H_2O diffusion and debonding of TPU from the steel substrate after 218 h of exposure at 40°C/90%RH.

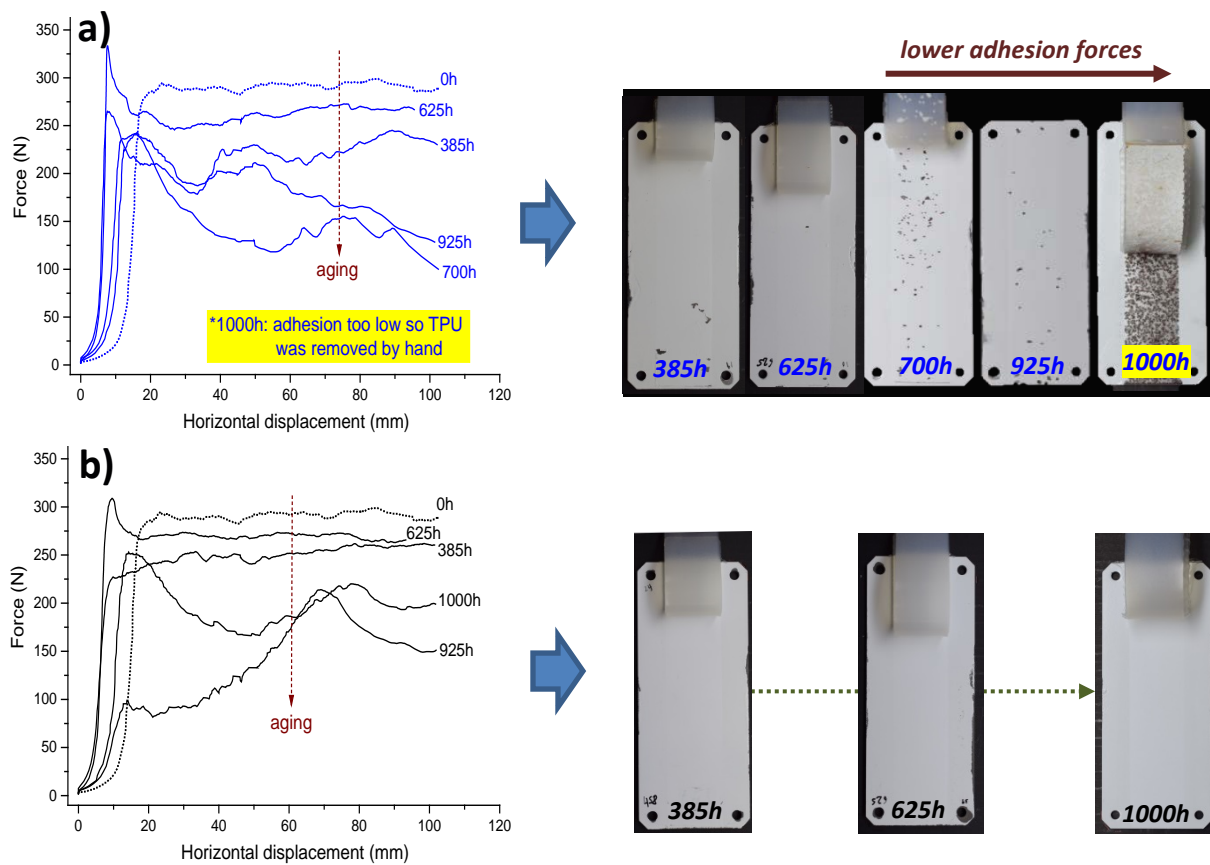


Figure 105. Adhesion force of TPU overmolded and aged at 40°C/90%RH on: a) plain steel substrate, where it is clear the oxidation of the metal due to rapid diffusion of water. b) Phosphated steel substrate: diffusion caused debonding at the polymer-coating interface.

Although diffusion time of H_2O through TPU could be calculated assuming a Fickian model, as seen in Table 22, the time that water molecules need to interact and destroy the interfacial bonds at the polymer-coating and coating-metal joints is rather complex to calculate due to the several physical-chemical and electro-chemical processes that occur also on the steel surface. In future works, it is necessary to investigate adhesion and corrosion properties in shorter time ranges so diffusion parameters and lifetime estimations may be predicted more accurately.

From this chapter, it is evident that durability of the hybrid part depends on a greater extent on the diffusion rate of water vapor through the TPU, and it is also an engineering requirement that the metal substrate had a corrosion-protection layer to increase the durability and lifetime of the composite.

8. DURABILITY AND LIFETIME OF POLYURETHANE-METAL JOINTS UNDER THERMAL LOADS

The growing demand for hybrid composites as structural components in the automotive, aerospace, medical and military applications may require long-term stability under thermal stresses. Only a little information is found in the literature about specific uses and its correlation with the lifetime and degradation process at the organic/inorganic interfaces [64,98,105]. A full understanding of the long-term performance of bonded structures is required to use these products in engineering and industrial applications. Natural aging tests are time-consuming [88,104,105], expensive and therefore not applicable for development. In real applications, the temperature is higher at the proximity to the metal substrate; therefore, the boundary between steel and polymer suffers the highest thermal stress and a collapse of the structure starting at this boundary is most likely.

Thermogravimetric (TGA) measurements allow fast investigation of thermal decomposition with rather small probes in the range of few milligrams, and so a little piece of polyurethane in the proximity of the steel surface is necessary for the investigation, as illustrated in Figure 106.

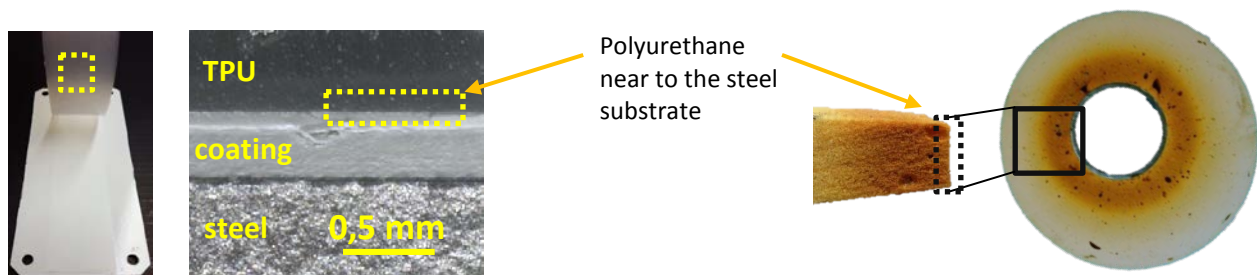


Figure 106. Polyurethane specimens in proximity to the metal substrate used in this work for TGA analysis.

From TGA data, kinetic parameters of thermal decomposition of the polymer were evaluated through the Flynn-Wall-Ozawa, Friedman, and Chang methods. Tests were conducted at three different heating rates, 5, 10 and 15 K/min and different kinetic parameters were obtained, such as the activation energy, reaction order and the pre-exponential factor [139,140]. These parameters are useful to predict the lifetime of the polymer that is in direct contact with the metal substrate. It is, in consequence, another purpose of this chapter to evidence the validity of TGA-based lifetime predictions on artificially aged polyurethane near to the polymer-metal interface assuming a continuous operation work at certain temperatures.

8.1. CASE I: DURABILITY AND LIFETIME OF OVERMOLDED TPU ON STEEL SUBSTRATES

8.1.1. Thermogravimetric Analysis of Aged TPU

In order to simplify explanations and discussion in this chapter, the decomposition kinetics analysis will be presented in detail for samples hygrothermally aged at tropical climates, i.e. 40 °C/90 %RH. In Figure 107, a typical TGA degradation curve -under N₂- of fresh and aged TPU exhibits a sharp degradation step, which starts at around 300 °C with a constant decay until losing around 96% of its weight at 450 °C. Thermal degradation of hygrothermally aged specimens shifted slightly to lower temperatures. As reported in literature [139,140], thermal decomposition takes place due to scission of primary bonding in three main pathways: first, at lower temperatures -at around 300 °C- the degradation of urethane linkages; second, at higher temperatures the isocyanate, alcohol and amine groups disappear; and finally, aromatic rings are removed near to 400 °C.

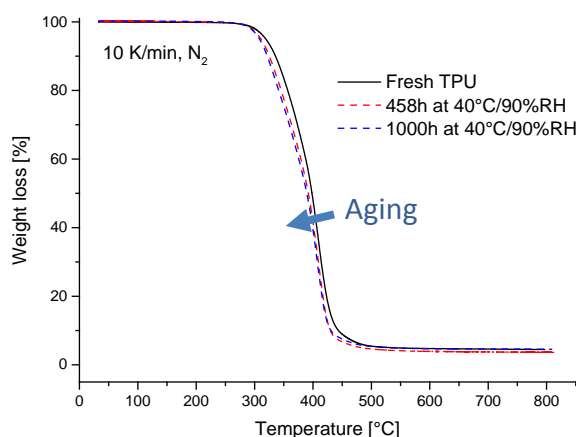


Figure 107. Characteristic TGA diagram, at 10 K/min under N₂, of fresh and aged TPU near to the steel surface.

8.1.1.1. Kinetic parameters of thermal decomposition

The Ozawa-Flynn-Wall (OFW) experimental method, expressed in Equation 9, has been widely used to determine the activation energy from thermogravimetric data. It is derived from the basic kinetic equation for heterogeneous chemical reactions and therefore has a wide application in thermal decomposition investigations [107,108,140].

$$\frac{d \log \beta}{d \frac{1}{T}} \cong \left(\frac{0,457}{R} \right) x E_A$$

Equation 9. Activation Energy from Ozawa-Flynn-Wall

Where β is the constant heating rate, T is the absolute temperature, R the gas constant and E_A the activation energy. The OFW method requires thermogravimetric data at different heating rates so that the E_A can be calculated more accurately.

Figure 108 a) displays TGA curves of a fresh TPU near to the steel surface heated at 5, 10, 15 K/min; under N_2 . As expected, higher heating rates shift the onset of decomposition to higher temperatures due to slower reaction rates [141]. Figure 108 b) shows the logarithm of heating rates vs. reciprocal absolute temperatures at 95, 90, 80 and 70% residual weight values. Additionally, the best fitting was determined for samples whose coefficient of determination, R^2 , was closer to 1, as displayed in the red line at 5% conversion.

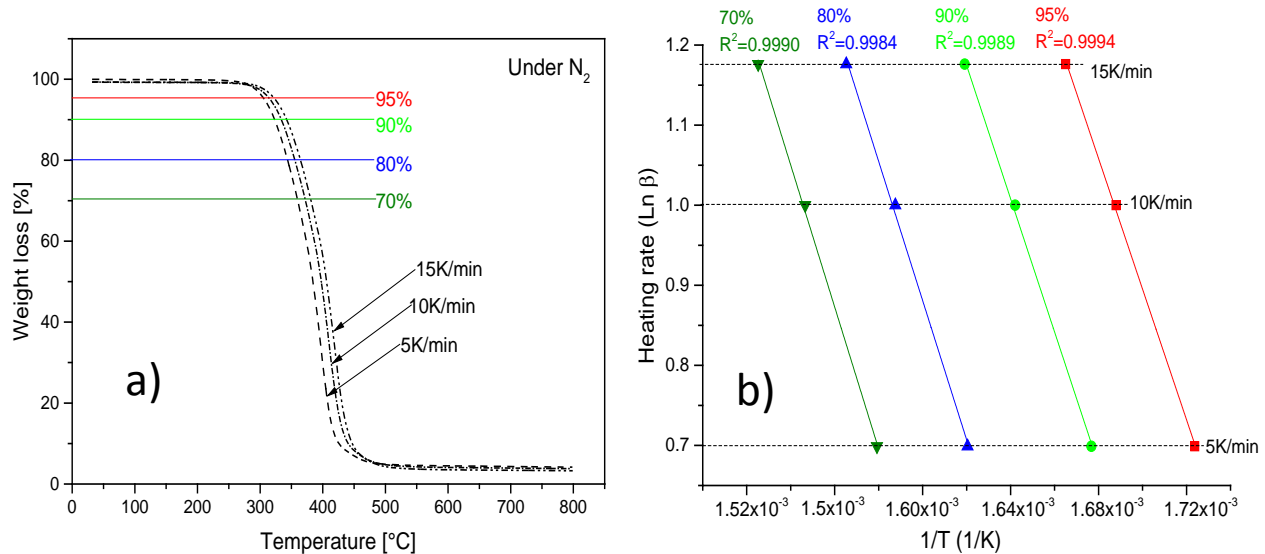


Figure 108. a) TGA curves of fresh TPU near to the steel surface heated at different rates, under N_2 . b) Logarithm of heating rate vs. reciprocal absolute temperature using same conversion data as in a). The best coefficient of determination, R^2 , was obtained by a residual weight of 95% as seen in the red fitting.

The characteristic slopes of fresh and aged TPU (until 1000 hours of exposure at 40 °C/90 %RH) at different weight fractions are presented in Figure 109. It is evident that fitted lines of the aged polymer are shifted to the right, and their slopes are slightly lower when compared to the fresh sample, indicating a decrease in the E_A . In Table 23, the apparent activation energies calculated from the slopes in Figure 108 b) and using Equation 9, indicate that the polymer degradation is getting less temperature dependent due to aging. However, after 458 h of exposure, the E_A stabilizes suggesting that the reaction rate of chemical reactions and physical processes of thermal decomposition in the polymer is steady even after 1000 h of hygrothermal aging.

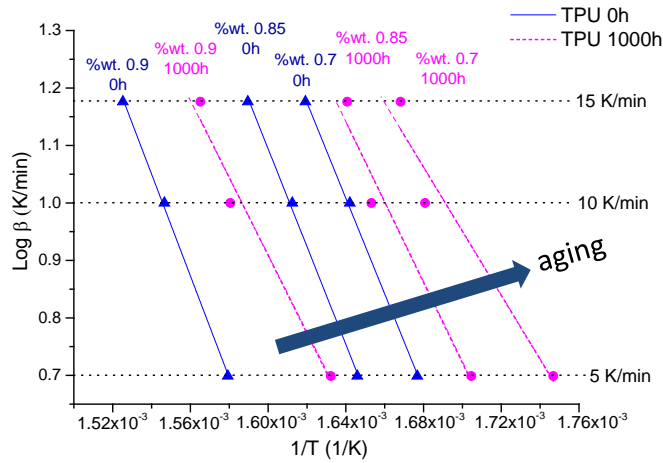


Figure 109. OFW method for the determination of the E_A of the thermal decomposition stage. Blue continuous lines indicate the slopes of the fresh TPU and purple dotted ones represent aged samples at 1000 hours.

Calculated Activation Energies, E_A , by OFW [KJ/mol]			
Weight fraction	Fresh 0 hours	Aged at 458 hours	Aged at 1000 hours
0,90	151	116	101
0,85	155	119	134
0,7	161	124	123
E_A Average	156	120	119

Table 23. Calculated E_A following Ozawa-Flynn-Wall in three different weight fractions.

Additionally, the Chang and Friedman methods were used to having a better idea about the decomposition kinetics in the artificially aged samples. The experimental approach is followed by the kinetic equation of solid decomposition [96,142,143]:

$$\frac{d\alpha}{dt} = kf(\alpha)$$

Equation 10. Kinetic decomposition

Where $d\alpha/dt$ is the variation in the weight loss of the sample after a certain time, t ; k is the reaction rate constant from Arrhenius, and $f(\alpha)$ is proportional to the amount of available material during decomposition: $f(\alpha) = (1-\alpha)^n$, where n is the decomposition reaction order. After some rearrangements and replacing $f(\alpha)$ and k from the Arrhenius equation, the kinetic decomposition can be represented as:

$$\frac{d\alpha}{dt} = A \exp\left(-\frac{E_A}{RT}\right)(1-\alpha)^n$$

Equation 11.

Where A , E_A , R , and T are the pre-exponential factor, activation energy, gas constant and temperature from the Arrhenius expression for a determine degradation system. After taking logarithms of Equation 11, the Friedman method can be expressed as:

$$\ln\left(\frac{d\alpha}{dt}\right) = \ln A + n \ln(1-\alpha) - \frac{E_A}{RT}$$

Equation 12. Friedman method

Experimentally, the E_A / R value is the slope of the $\ln(d\alpha/dt)$ vs. $1/T$ and the reaction order, n , can be obtained from the slope $-E_A / (nR)$, from the plot of $\ln(1-\alpha)$ vs. $1/T$, as described in the Chang method in Equation 13:

$$\frac{\ln\left(\frac{d\alpha}{dt}\right)}{(1-\alpha)^n} = \ln A - \frac{E_A}{RT} \quad \text{Equation 13. Chang method}$$

From Chang approach, the E_A and pre-exponential factor A can be determined by plotting $\ln(d\alpha/dt)/(1-\alpha)^n$ vs $1/T$. The reaction order, n , is determined as the best-fitted value of the decomposition step from the TGA curve, as shown in Figure 108 b).

The experimental slope from Chang method is depicted in Figure 110, where the computed E_A from the aged polymer is lower than that obtained from the untreated sample, as it was also demonstrated by OWF and Friedman analysis and tabulated in Table 23.

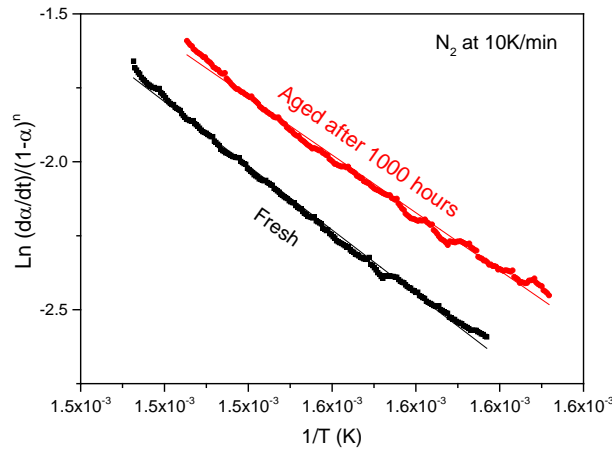


Figure 110. Degradation kinetics by Chang method for fresh and aged TPU at 1000 hours. Best fitting occurred between 85% and 60% of weight loss.

A summary of the kinetic parameters of thermal decomposition of the three different approaches is displayed in Table 24. The lower E_A calculated for the pre-aged samples may be explained by the scission of polymer chains that possibly occurred during the isothermal aging [107].

Although the different TGA decomposition kinetic parameters result in different values of apparent E_A in the range of 154 kJ/mol (for the fresh TPU) to 68 kJ/mol (for the pre-aged polymer), all three methods show the same tendency. In these cases, the E_A is smaller than that of fresh samples just after 625 h of exposure when it stabilizes. As presented in Figure 109 and Table 23, the apparent E_A not only depends on the time of pre aging, but also on the conversion value chosen for calculation. Considering that in the

case of artificial aging the degradation processes take place before the sample was investigated in TGA, a shift to lower temperatures as shown in Figure 109 could be expected due to pre-aging.

Sample	Test atmosphere	OFW	Chang	Friedman
		E_A [kJ/mol]	E_A [kJ/mol] / n / $\ln A$	E_A [kJ/mol] / n / $\ln A$
Fresh	N ₂	156	121/1.7/21	93/9.2/35
625h	N ₂	120	108/1.3/18	67/4.2/25
1000h	N ₂	119	118/1.8/21	68/4.4/24
Fresh	O ₂	165	154/3/27	138/11.3/40
625h	O ₂	162	151/3.2/27	104/8/22
1000h	O ₂	78	147/3.1/26	148/12.3/28

Table 24. Different decomposition kinetics parameters calculated from OFW, Chang and Friedman for fresh and hygrothermally aged, 40°C/90%RH, TPU on the steel surface at 10 K/min.

In any case, the aim of applying different kinetic decomposition methods is to evaluate the E_A , which is the key parameter for lifetime predictions. Based on experiments performed at elevated temperatures, a lower E_A transfers into a shorter lifetime. Therefore, the lowest determined E_A should represent the most conservative prediction.

8.1.1.2. Durability of TPU subjected to continuous operation temperatures

Lifetime prediction of polymeric systems based on thermogravimetric data has been analyzed widely in the literature [87,107,108,139]. Lifetime can be approximated from the integration of the Arrhenius expression as demonstrated elsewhere [107] and it is interpreted as follows:

$$t_f = \frac{1 - 0,95^{1-n}}{A(1-n)} \exp\left(\frac{E_A}{RT}\right) \text{ when } n \neq 1 \quad \text{Equation 14. Lifetime prediction}$$

Decomposition kinetic parameters required for Equation 14 were determined experimentally following the Chang method. Activation energies were closer to the values found in the literature [104,108] and those calculated by OFW. On the other hand, kinetic parameters evaluated by Friedman differed significantly from Chang and OFW, as enlisted in Table 24.

Figure 111 exhibits the predicted lifetime of the fresh and pre-aged TPU near to the steel surface at certain continuous operation temperatures (COT). Estimations were calculated from Equation 14, using kinetic parameters of solid decomposition from Chang approach -under O₂-, as indicated in Table 24.

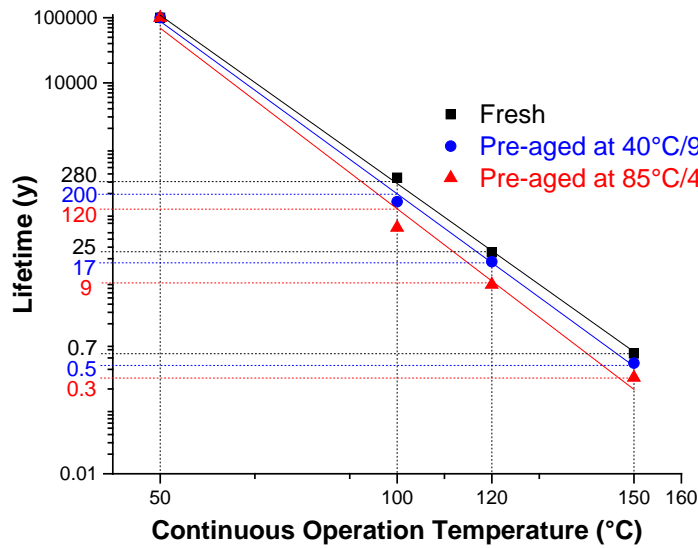


Figure 111. Lifetime estimations (in years) of fresh and hygrothermally pre-aged TPU exposed to certain continuous operation temperatures.

The predicted service lifetime for the polymers, as in Figure 111, depends on the pre-aging conditions: specimens pre-aged 1000 h at higher temperatures (85 °C/40 %RH), exhibit a faster lifetime decay when subjected to different operation temperatures. If it is exposed to a continuous operation temperature (COT) of 150 °C, it will last just 0.3 years. The fresh polymer under the same conditions would endure around 0.7 years, and TPU pre-aged for 1000h to a lower temperature, 40 °C/90 %RH, will last eventually for around half a year. Estimated lifetime of TPU subjected to lower constant temperatures have an exponential growth in their durability. For example, pre-aged composites at 85 °C/40 %RH subjected to a COT of 100 °C, would have a lifetime of around 60 years. In the other hand, composites hygrothermally pre-aged at 40 °C/90 %RH would last for more than 150 years. Durability of fresh and pre-aged TPUs exposed to lower COTs, as in real engineering applications ($T \approx 50$ °C), presented an hypothetical unlimited lifetime. The determined values of E_A show that durability of the TPU is definitely more affected by temperature than humidity at the conditions described in this work. E_A 's of pre-aged specimens, and especially those subjected to higher temperature, were lower when compared to the fresh polymer. All three kinetic of degradation for solid decomposition approaches showed the same tendency: lower E_A transfers into a shorter lifetime. However, further investigation and validation for reliable prediction is still a requirement at long term applications.

8.1.2. Thermogravimetric Analysis of Coatings in Contact with TPU

TGA examination for the in-house and e-coat layers was performed in a TGA Q5000 of TA Instruments, from room temperature to 800 °C, under N₂ and O₂ at three different heating rates: 5, 10 and 15 K/min. Figure 112 illustrates the approximate surface from where the samples were obtained for analysis. Surfaces that were in direct contact with the TPU were scratched until approximately 3 mg of material was extracted. It is hard to obtain more than that amount due to the proximity of coating to the metal.

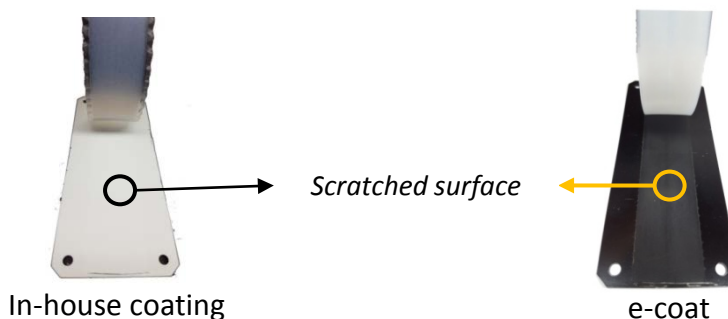


Figure 112. Illustration of surfaces where specimens were obtained for TGA

8.1.2.1. Thermogravimetric analysis of the in-house coating in contact with the TPU

Figure 113 a) presents typical TGA curves normalized of the in-house coating and his derivative curve, DTG, at 10k/min under N₂. Decomposition diagrams are rather complex exhibiting two main degradation steps, attributed to the thermosetting nature of the layer, which consists of low molecular weight polyester chains crosslinked with urethane molecules, as it was discussed in numeral 3.2.2. The derivative curve show clearly the multi-step decomposition process, where the first reaction step is observed at around 280 °C and stopped at 325 °C, with a maximum rate of mass loss at 300 °C. A second decomposition step begins at 325 °C and finishes at approx. 420 °C with a maximum reaction rate at around 350 °C. The residue mass is about 32% after decomposition, which could proceed from carbonized products. Figure 113 b) presents the thermal degradation behavior of in-house coatings that were pre-aged at 40 °C/90 %RH for 625 and 1000h; similarly to the TPU, the decomposition temperatures shifted slightly to the left.

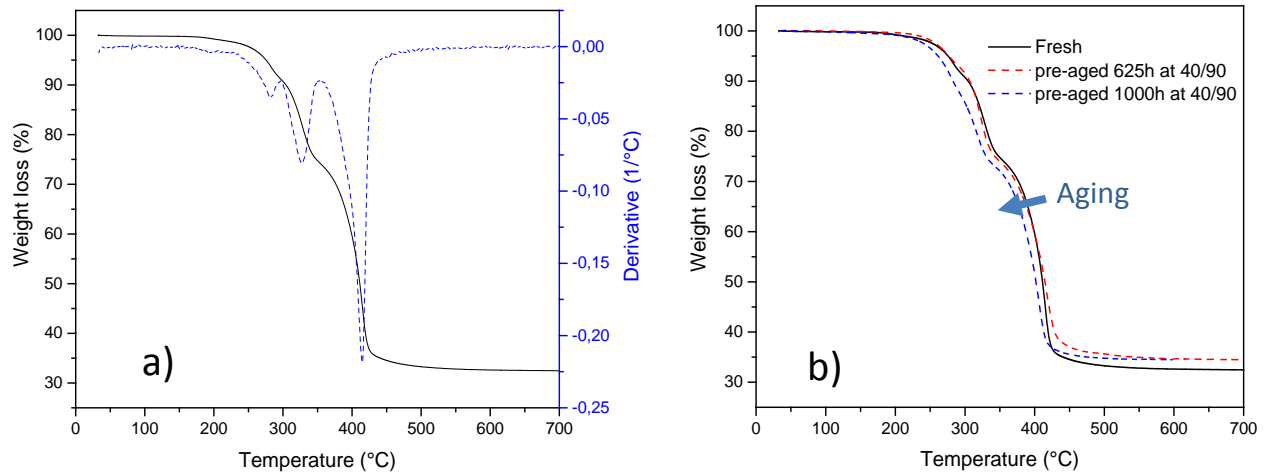


Figure 113. a) Typical TGA with DTGA of fresh in-house coating at different service temperatures, 10K/min. b) TGA curves of aged coatings at 40 °C/90 %RH. N₂.

8.1.2.2. Kinetic parameters of thermal decomposition of in-house coating and durability

Decomposition kinetics parameters for the in-house coating after pre-aging at 85 °C/40 %RH and 40 °C/90 %RH are presented in Table 25. Parameters were computed from TGA data (under N₂ and O₂, at 10 K/min) and using the Chang method. The resulting E_A and pre-exponential factor, $\ln A$, seem in good agreement when compared with previous works in thermosetting polyurethanes from Li et al. [108]. Lower E_A transfers into a shorter lifetime, as observed in pre-aged specimens after 625 h of exposure. Therefore, the lowest determined E_A should represent the most conservative prediction. On the other hand, reaction order values, n , differed significantly from 85 °C/40 %RH to 40 °C/90 %RH and also from the values obtained by Li in [108]. These significant deviations in the kinetic parameters, which could be explained by the complexity of the decomposition process of the cured-thermosetting coating, make lifetime calculations unreliable, as seen in specific samples in Table 26.

Sample	85 °C/40 %RH		40 °C/90 %RH	
	Test atmosphere	E_A [kJ/mol]/ n /ln A	Test atmosphere	E_A [kJ/mol]/ n /ln A
Fresh	N ₂	153/17/30	N ₂	153/17/30
625h	N ₂	113/7/21	N ₂	142/13/28
1000h	N ₂	101/8/19	N ₂	122/12/23
Fresh	O ₂	105/11/20	O ₂	105/11/20
625	O ₂	87/9/16	O ₂	103/9/20
1000h	O ₂	86/8/16	O ₂	94/10/18

Table 25. Decomposition kinetics parameters for the in-house coating after pre-aging at 85 °C/40 %RH and 40 °C/90 %RH. Parameters were calculated from TGA data, under N₂ and O₂, at 10 K/min using Chang method.

Pre-aging exposure time [h]	Estimated lifetime [y] at certain continuous operation temperatures					
	Pre-aging condition: 85 °C/40 %RH			Pre-aging condition: 40 °C/90 %RH		
	50 °C	100 °C	150 °C	50 °C	100 °C	150 °C
Fresh	22	0.1	2.2E-03	22	0.12	2.0E-03
625	2	2.7E-2	9.6E-04	17	0.1	1.9E-3
1000	4	2.0E-2	7.3E-04	5	4.2E-2	1.2E-3

Table 26. Estimated lifetime for the in-house coating after pre-aging at 85 °C/40 %RH and 40 °C/90 %RH. Estimations were calculated from kinetic parameters from Chang method under O_2 .

8.1.2.3. Thermogravimetric analysis of e-coat in direct contact to the TPU

Figure 114 shows typical TGA curves of e-coat and his derivative curve (DTG) at 10 k/min under N_2 . The DTG curve displays a one step in decomposition process; the degradation reaction under N_2 started at around 200 °C and stopped at 550 °C, with a maximum rate of mass loss around 330 °C. The residue mass is about 28% after decomposition.

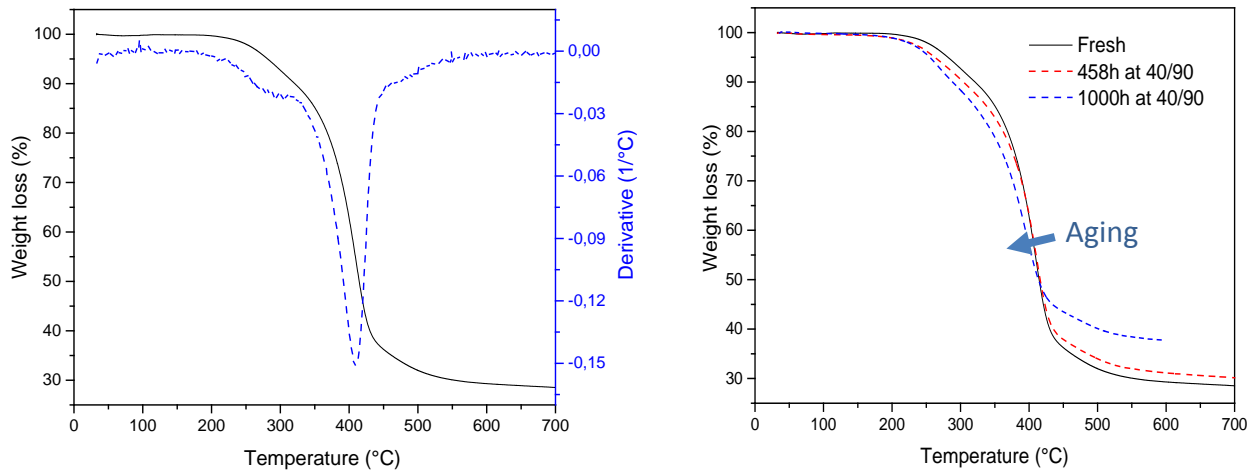


Figure 114. a) Typical TGA with DTG of fresh e-coating at 10K/min under N_2 . b) TGA curves of fresh and aged e-coat.

8.1.2.4. Kinetic parameters of thermal decomposition and durability of e-coat

e-coat specimens prepared for TGA were difficult to obtain due to subtle and dispersed flakes that could have extracted out of the surface. However, kinetics decomposition parameters calculated with Chang method under N_2 and O_2 , pre-aged at 85 °C/40 %RH and 40 °C/90 %RH are listed in Table 27. From there, lifetime calculations are summarized in Table 28. Similarly, as in the in-house coating, kinetic parameters of solid decomposition had significant deviations for specific samples and therefore lifetime calculations are inconsistent and, therefore unreliable. It suggests that the complex thermal decomposition process of thermosetting-cured-coatings makes difficult the kinetic examination process

by Chang method. As a matter of fact, no further discussions of lifetime predictions on adhesive coatings will be held.

Sample	85 °C/40 %RH		40 °C/90 %RH	
	Test atmosphere	E_A [kJ/mol]/n/ln A	Test atmosphere	E_A [kJ/mol]/n/ln A
Fresh	N ₂	110/19/22	N ₂	110/19/20
625h	N ₂	76/9/13	N ₂	47/6/6
1000h	N ₂	118/23/29	N ₂	100/19/19
Fresh	O ₂	108/19/20	O ₂	110/19/22
625	O ₂	68/12/11	O ₂	89/13/15
1000h	O ₂	143/20/34	O ₂	114/20/23

Table 27. Estimated kinetics parameters calculated with Chang method for fresh and pre-aged e-coat at 40 °C/90 %RH under N₂ and O₂.

Pre-aging exposure time [h]	Estimated lifetime [y] at certain continuous operation temperatures					
	Pre-aging condition: 85 °C/40 %RH			Pre-aging condition: 40 °C/90 %RH		
	50°C	100°C	150°C	50°C	100°C	150°C
Fresh	27	0.1	1.6E-3	27	0.1	1.6E-3
625	1	1.0E-2	6.3E-4	5	6.0E-2	2.2E-3
1000	0.7	2.0E-3	2.1E-5	45	0.1	2.0E-3

Table 28. Estimated lifetime for the e-coat after pre-aging at 85 °C/40 %RH and 40 °C/90 %RH. Estimations were calculated from kinetic parameters from Chang method under O₂.

8.2. CASE II: DURABILITY AND LIFETIME OF RIGID PUR IN DIRECT CONTACT WITH A STEEL DISTRICT HEAT PIPE. FAILURE ANALYSIS AND VALIDATION OF THE TGA METHOD

In order to validate the TGA investigations conducted on the hybrid described in section 8.1, a failure analysis was performed on rigid polyurethane (PUR) near to the metal interface of an insulating district heat pipe. The polymer-metal composite consists of a steel tube surrounded by a rigid and thick PUR layer for thermal isolation purposes. Artificial aging, mechanical tests, thermogravimetric (TGA) and surface analysis were conducted to determine the failure mechanisms of the composite interface and then, predict the lifetime. From the TGA data, OFW, Chang and Friedman methods were applied to identify parameters of the kinetics of degradation and predict the life cycle of the product. Chang analysis gave the best approach when compared to previous results attained by mechanical tests.

This section was pre-published as “Failure Analysis and durability of preinsulating district heat pipes”, *Polym Adv Technol.* 2018;29:1048-1055 [144].

8.2.1. Materials and Methods

8.2.1.1. Materials

The general setup of a district heat pipe is shown in Figure 115. It consists of a main service steel tube, which is in charge of transporting hot water; an isolating rigid polyurethane (PUR) material surrounds this metal pipe approximately 50 mm thick, which is sometimes encircled by a thin diffusion barrier film of EVOH or aluminum. Typically, pipes to end users have a dimension of e.g. DN50/160 whereas transport pipes have dimensions DN 800 or larger. Such pipes have an expected time of use of 30 years or more. In order to allow an accelerated aging and an adequate gas exchange, a High-Density Polyethylene (HDPE) film was used instead of the standard casing, as seen in Figure 115 b).

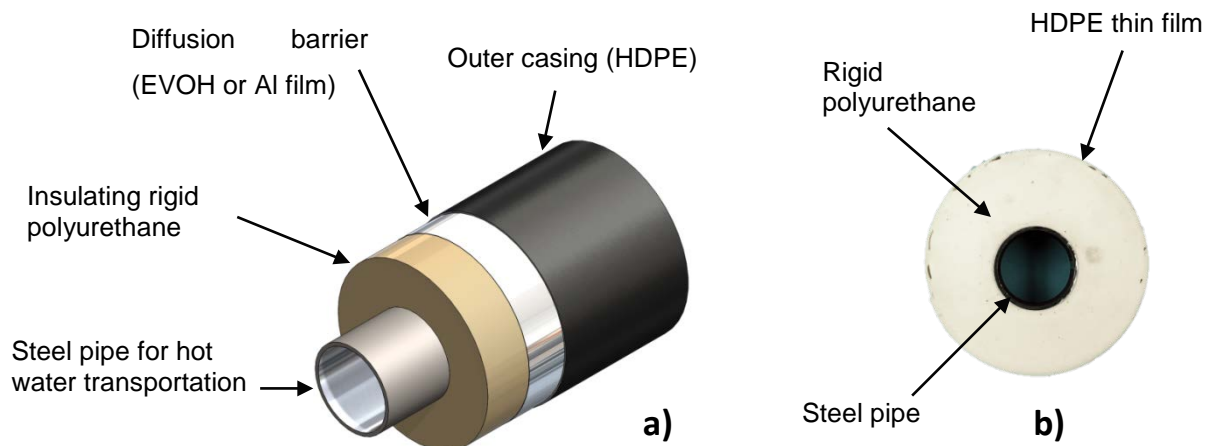


Figure 115. a) General setup of a district heat pipe. b) Frontal view of a specimen used in this research.

8.2.1.2. Methods

Artificial Aging

Samples were subjected to different temperatures on the inner (steel), and outer surfaces of the PUR, 180 °C, and 60 °C respectively, to accelerate the aging process of the polymer near to the metal interface. These temperatures were intended to be higher than those measured at real working conditions: 120 °C at the inner and 30 °C at the outer surface [145]. The internal and external temperatures were selected according to the estimated air intrusion depicting a lifetime of thirty years within the estimated testing time according to [104]. Figure 116 illustrates the experimental setup for the artificial aging at different internal and external temperatures. The temperature-controlled chamber was tightly closed with a steel-end cup, so no air intake was allowed.



Figure 116. Artificial aging setup at different external and internal temperatures.

Mechanical test

The shear strength was determined similarly to the standard DIN EN 253. A universal testing machine, FPZ 100, with a load cell of 10 kN at 23 °C and 50% relative humidity, was used. The speed test was setup to 5 mm/min. The specimen was taken from assemblies of conventional production from which transversal section had to be cut to be at least five times the thickness of the insulation [145]. In Figure 117, a sketch of the setup of the axial applied load. The speed of the testing machine was 5 mm/min, and the shear strength was calculated as follows in Equation 15.

$$\tau_{axial} = \frac{F_{axial}}{L \times d \times \pi}$$

Equation 15. Shear strength calculation

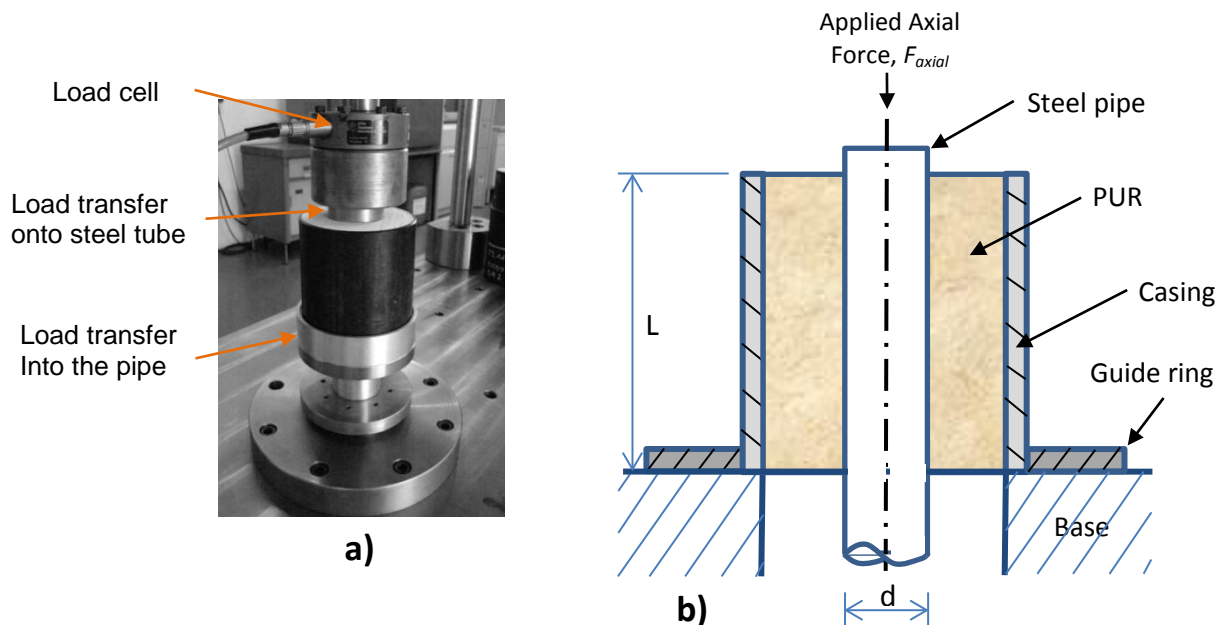


Figure 117. a) Mechanical test setup for the determination of the shear strength, b) transversal cut representation of the shear strength applied to the assembled pipes.

Thermogravimetric analysis

The TGA experiment was performed by a TGA Q5000 of TA Instruments, from room temperature to 800 °C, under air and nitrogen, at four different heating rates: 2, 5, 10 and 20 K/min. Small samples of PUR were cut near the steel pipe at a maximum of 2 to 5 mm from the metal wall, as depicted in Figure 118. For determination of the degradation kinetics parameters, Ozawa-Flynn-Wall, Chang, and Friedman thermal methods were used, and subsequently, lifetime was estimated.

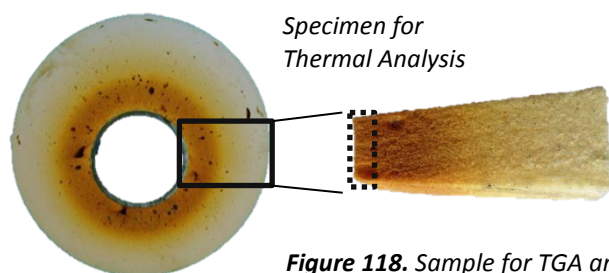


Figure 118. Sample for TGA analysis

8.2.2. Results and Discussion

8.2.2.1. Analysis of the Interfacial Surface

In order to evaluate the aging behavior of the polymer close to the interface, it was necessary to understand the composition and structure of the PUR and the adhesion mechanisms at the metal interface. First, the PUR is a closed-cell rigid polyurethane foam, which consists of a polyol with an additional mixture of catalyst, stabilizer, and blowing agent; and an aromatic isocyanate component

which contains the polymeric diphenylmethane diisocyanate MDI. The porous polymer is produced from the high amount of crosslinks which configure a three-dimensional network and high molecular weight material [91,96,146–148]. A SEM micrograph from the specimen used in this work is in Figure 119.

In-situ polymerization of the rigid foam facilitates the adhesion to the metal substrate using the strong interactions between the polar and functional groups of the polymer and the metallic ions at the surface of the steel [46]. However, Dillingham and Moriarty [116] demonstrated in an extensive work, that adhesion of isocyanate-based polymers to steel is more complex due to the existence of covalent metal oxide-urethane linkages in the interface. The covalent bonds can explain the excellent strength and durability of isocyanate-based adhesives and coatings.

Additionally, to physical and chemical bonds, it has been widely demonstrated in the literature [47,48,52,56,64,149–152] that a high roughness on the metal substrate favors the adhesion because of the large superficial area. The measured average roughness R_a by confocal microscopy on samples was around 3.2 μm .

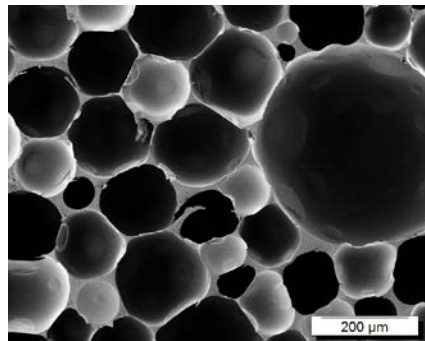


Figure 119. Morphology of a fresh PUR specimen.

8.2.2.2. Mechanical Evaluation of Artificial Aged Samples

Extensive investigations on the mechanical strength of artificially aged pipes, also related to this work [10, 28], have shown in detail discrepancies in the lifetime predictions on the naturally old pipes. Figure 120 exhibits the axial shear strength ratio and the visual aspect of the artificial aging of assemblies subjected to an inside and outside temperatures of 180 °C and 60 °C after different exposure times. After 250 hours, the shear strength drops approximately to 50% and remains constant up to around 2000 hours.

The decay of strength after 2000 hours is due likely to oxidative degradation that destroys PUR in direct contact with the steel pipe. In several cases, a molten-like residue was found on the steel surface, as seen in Figure 121. The specimen exposed to 3150 hours is entirely damaged at the interface, meaning

that the debonding occurred between 2500 and 3150 hours of artificial aging. The dotted line shows a clear tendency of the decay of strength of the assembled pipes at the failure time after 2000 h of exposure.

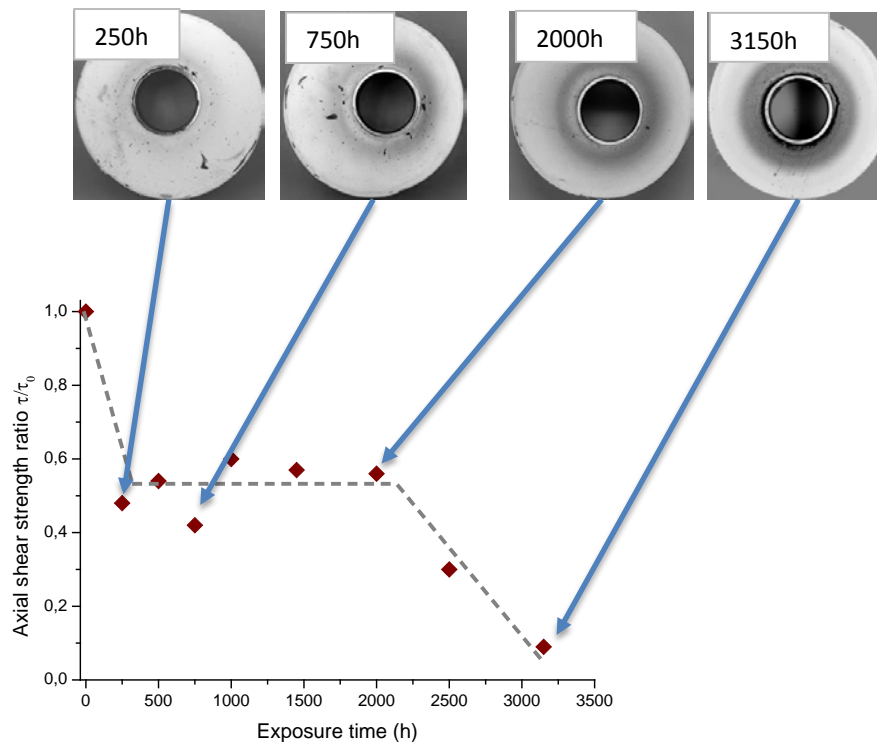


Figure 120. Axial shear strength ratio of samples exposed at inner and outer temperatures of 180°C and 60°C, respectively. Upper pictures show the condition of the composites after certain exposure times.

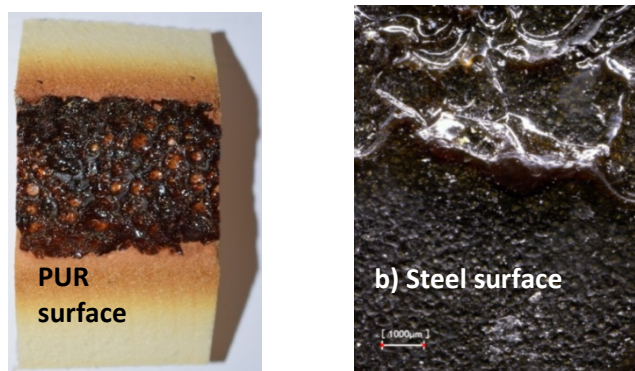


Figure 121. Failure surface after an artificial aging time of 3150 hours at a) PUR surface and b) metal surface.

Performing the mechanical test after artificial aging at different temperatures allows determining apparent activation energy of 95 kJ/mol [105]. Based on these results, an estimated time of use of 30 years at about 110 °C was calculated for the pipes covered only by a HDPE film, whereas for pipes with a standard casing thickness of 3 mm at 135 °C of continuous operating temperature is evaluated [153]. Due to the necessity of artificial aging, the testing time following the EN253 is time-consuming (24000 h

testing), expensive and therefore not applicable for development. The temperature in both cases, accelerated and natural aging is highest in proximity to the steel pipe. Therefore, the boundary between steel and polyurethane suffers the highest thermal stress. A collapse of the structure starting at this boundary is most likely.

8.2.2.3. Thermogravimetric analysis of rigid PUR near to the steel surface

In Figure 122 a characteristic TGA diagram of rigid polyurethane under air atmosphere from a fresh and artificially aged specimens exhibiting two main degradation steps: the first one starting at around 250 °C, with a constant decay until around 350 °C and 55% of weight loss. After 450 °C, a second decomposition begins. The TGA curves of aged specimens shifted to lower temperatures indicating that the non-isothermal behavior of PUR changed because of the isothermal artificial aging. This temperature shifting may be attributed to initial scission of polymer chains during thermal pre-aging which ended up with the PUR degradation at low temperature [91,141].

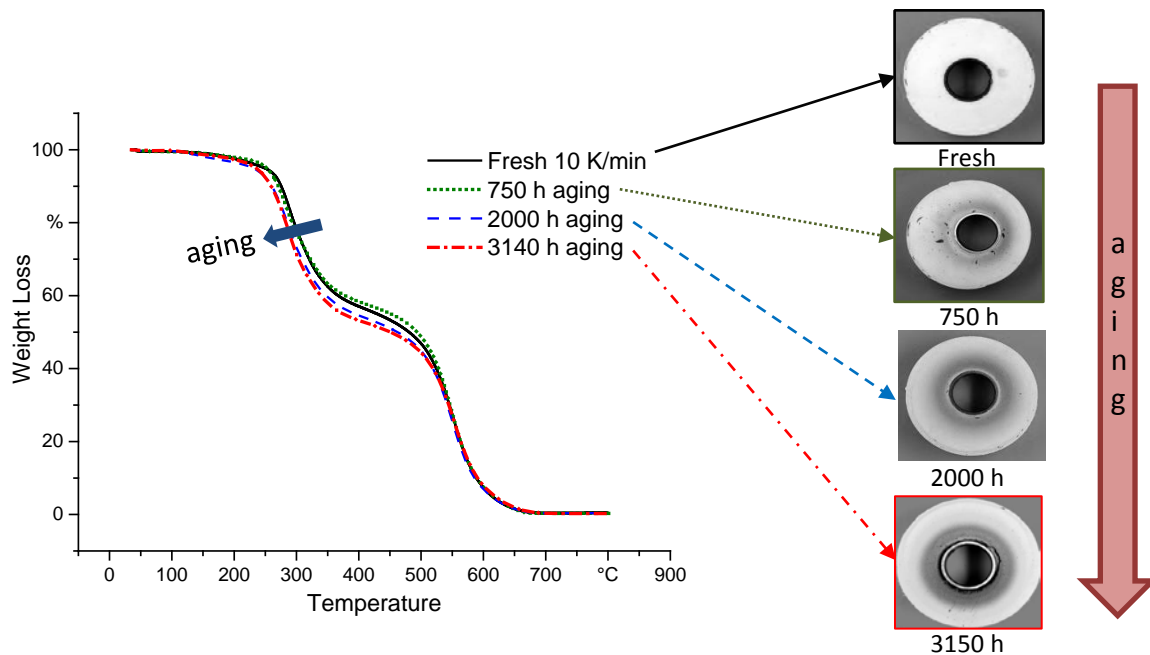


Figure 122. Typical TGA diagram, under O₂, of fresh and aged rigid PUR near to the steel surface.

8.2.2.4. Kinetic parameters of thermal decomposition

Figure 123 a) displays the TGA curves of fresh PUR near to the steel surface heated at 2, 5 10, 15 K/min. As seen in the TPU analysis, higher heating rates shift the onset of decomposition to higher temperatures due to slower reaction rates [141]. In Figure 123 b), and following the OFW kinetic decomposition method explained in 8.1.1.1., the logarithm of heating rates vs. reciprocal absolute temperatures at 95, 90, 80 and 70% of residual weight. Additionally, the best fitting was determined for samples whose coefficient of determination, R^2 , was closer to 1, as displayed in the red line at 80% of residual weight.

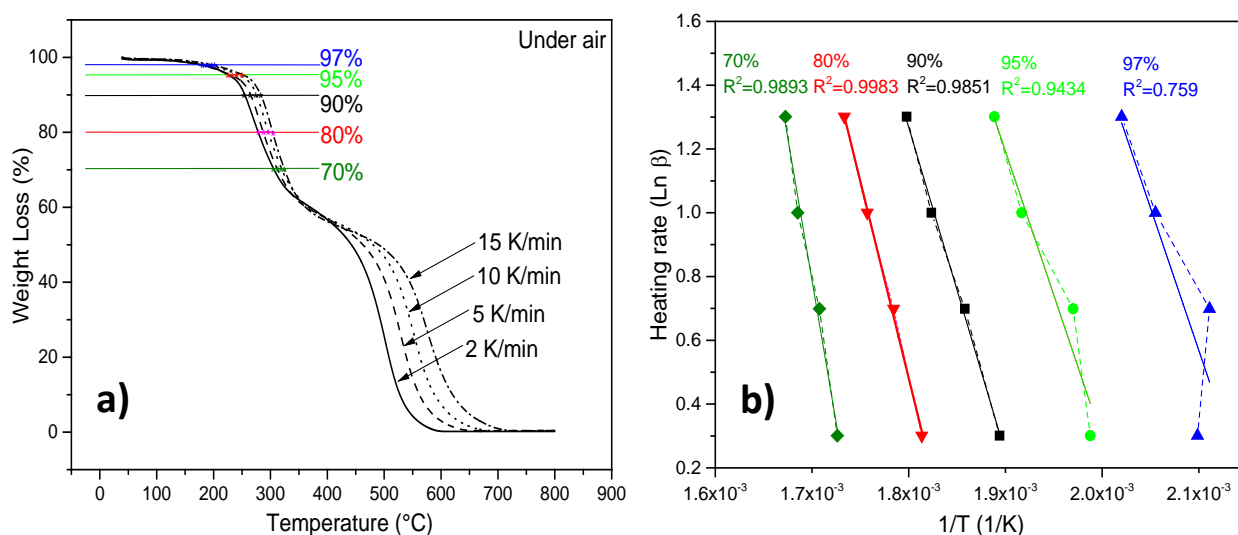


Figure 123. a) TGA analysis at 4 heating rates of fresh PUR near to the steel. b) Log of heating rate vs. reciprocal temperature using same data as in a). The best coefficient of determination, R^2 , was obtained by a residual weight of 80% as seen in the red line.

The characteristic slopes of the fresh and aged PUR after 2500 hours of exposure and different weight fractions for the first decomposition step are represented in Figure 124, where it is clear that the apparent activation energy decreases. In Table 29, the apparent E_A calculated from the slopes of Figure 123, and Equation 9 [154,155] indicate that the polymer degradation is getting less temperature dependent due to aging.

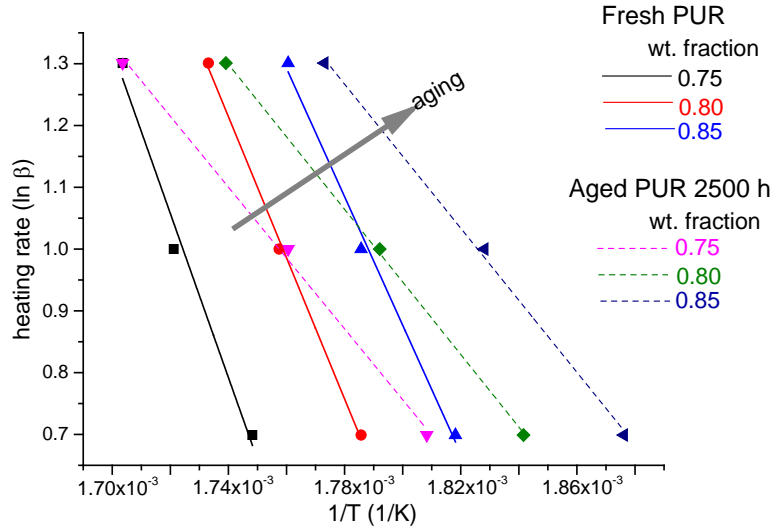


Figure 124. OFW method for determination of E_a at first decomposition stage. Continuous lines indicate the slopes of the fresh or unaged PUR and dotted ones represent aged samples at 2500 hours.

Calculated Activation Energies, E_a , by OFW [kJ/mol]					
Weight fraction	Fresh sample	Aged at 750 hours	Aged at 2000 hours	Aged at 2500 hours	Aged at 3150 hours
0,85	192	148	126	114	128
0,8	235	147	129	111	139
0,75	245	176	145	115	147
E_a Average	224	156	133	113	138

Table 29. Calculated activation energies following Ozawa-Flynn-Wall.

Adopting the Friedman method described in Equation 12, Figure 125 shows the slopes of a fresh and an artificially pre-aged sample after 2500 hours. The calculated E_A for the aged sample, listed in Table 30, is slightly lower than the one from the unaged PUR, indicating that the temperature dependency is shifting to lower values when compared to the unaltered sample.

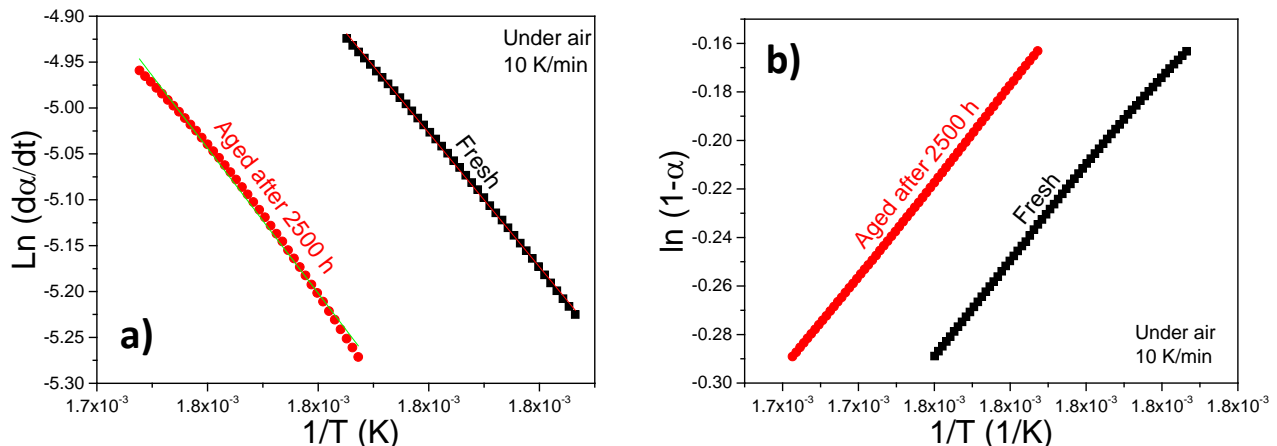


Figure 125. Friedman method showing in a) $\ln(da/dt)$ vs. $1/T$ and b) $\ln(1-\alpha)$ vs. $1/T$ for fresh PUR, in red, and artificially aged samples at 2500 h in black.

The experimental slope from the Chang method, described in Equation 13, is depicted in Figure 126, where the computed E_A from the pre-aged polymer is lower than that obtained from the fresh specimen, as it was also demonstrated by the OFW and Friedman analysis in Figure 124 and Figure 125.

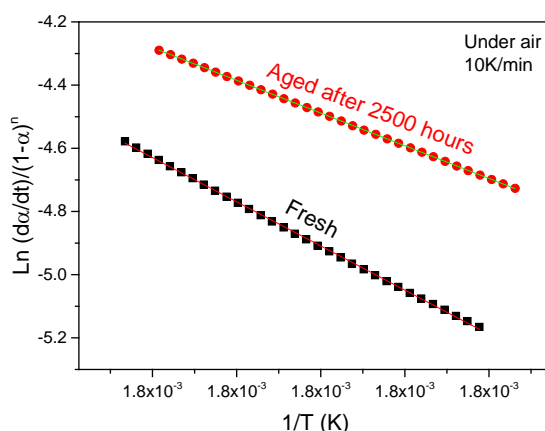


Figure 126. Degradation kinetics through Chang method for fresh and aged samples at 2500 hours, at 10K/min.

A summary of the kinetic parameters of thermal decomposition of the three methods is displayed in Table 30.

		OFW	Chang			Friedman		
	Sample	Ea [kJ/mol]	Ea [kJ/mol]	lnA	n	Ea [kJ/mol]	lnA	n
	Fresh	224	148	27.3	4.5	82	30.9	5.0
Pre-aged PUR	750 hours	157	144	26.8	5.0	81	30.8	5.5
	2000 hours	133	142	26.9	5.6	60	21.8	4.4
	2500 hours	113	108	18.9	3.1	61	22.0	3.9
	3150 hours	138	142	26.6	3.9	60	21.9	3.3

Table 30. Different Decomposition Kinetics Parameters calculated from the OFW, Chang and Friedman method for Rigid PUR on the Steel Surface at 10 K/min.

Similar to the results obtained from the TPU examination, the different kinetic decomposition analysis of PUR near to the steel surface, give different values of apparent E_A in the range of 224 kJ/mol to 82 kJ/mol. OFW, Friedman, and Chang exhibit the same tendency if pre-aged samples are used for the calculation. In these cases, the apparent activation energy is smaller than that of fresh specimens. As also demonstrated in the TPU decomposition analysis in section 8.1.1., the determined apparent E_A not only depends on the time of pre-aging but also on the conversion value chosen for calculation, as

evinced in Figure 124 and Table 29. It is also worth to mention that decomposition kinetics of rigid polyurethane is a complex phenomenon including parallel and follow up reactions [108,156,157] that cannot be easily interpreted in detail by the kinetics of solid decomposition. Finally, the loss of mechanical strength does not follow a linear dependency as depicted in Figure 124, and it is agreed on that behavior according to [10] and [105].

8.2.2.5. Lifetime Predictions of Rigid PUR Adhered to the Steel Pipe

Thermal decomposition reactions in rigid polyurethane are much more complex than in the thermoplastic urethane because it contains physical and chemical blowing agents and thermo-oxidative and hydrolysis-sensitive bonds; additionally, its degradation depends on the chemical structure of the isocyanates, oligomer polyols, and chain extenders that form their molecules [4,6,27]. For these reasons, Nolte [157] concluded that the real decomposition of rigid expanded polyurethane in district heat pipes occurred after a mass loss of 16 to 18% until failure. In this work, it is assumed that lifetime, t_o , is the time when the foam decreases its weight by 20%. Therefore, modifying slightly Equation 14, we have that:

$$t_f = \frac{1 - 0,80^{1-n}}{A(1-n)} \exp\left(\frac{E_a}{RT}\right) \text{ when } n \neq 1 \quad \text{Equation 16. Lifetime predictions for rigid PUR}$$

Additionally, the best fitting, obtained from the OFW, as seen in Figure 123, occurred for specimens whose residual weight was 80%. The best fitting was determined for samples whose coefficient of determination, R^2 , was closer to 1, as in Figure 123 b).

Decomposition kinetic parameters required for Equation 16 were determined experimentally after TGA analysis - under O_2 - and following Chang method. As occurred with the lifetime estimations of TPU, E_a obtained by Chang analysis were closer to the values found in the literature [104,108] and comparable to activation energies by OFW. On the other hand, kinetic parameters evaluated by Friedman differed significantly from Chang and OFW methods, as listed in Table 30.

Figure 127 exhibits the predicted lifetime, calculated from Equation 16, of the unaged PUR near to the steel surface. The predicted service life for the composite that was exposed to 180 °C is 0.1 years; which is a good approximation to the experimental test of the specimens that were artificially aged at that temperature and, then, subjected to a mechanical shear test, whose outcomes are shown in Figure 120.

Heat district pipes working at lower service temperatures have an exponential growing in their durability, as seen for the samples exposed to a continuous service temperature of 110 °C, they could last more than 100 years working in that condition. PUR-metal composites that are subjected to service temperatures around 120 °C have a theoretical lifetime of nearly 40 years, which approximates to the values dictated by the Standard EN253 [104,145], where the time frame of the part is predicted at around 30 years.

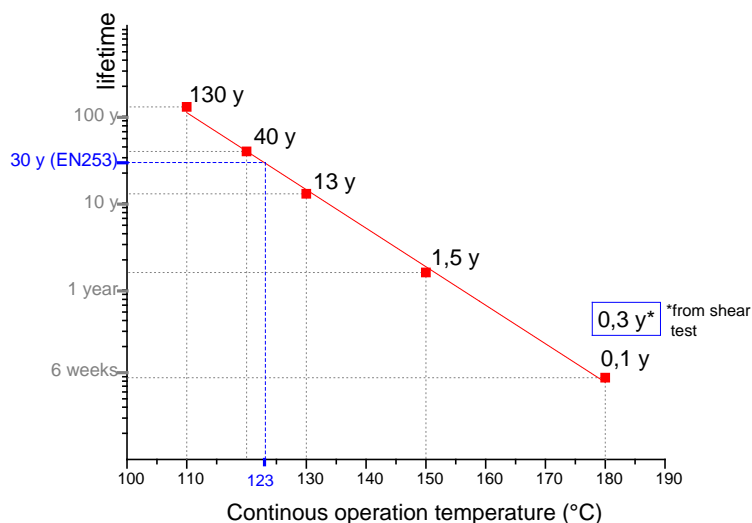


Figure 127. Estimated lifetime, of rigid PUR near to the steel surface at different service temperatures. The value with the (*) was obtained from a sample that was artificially aged at 180 °C and tested mechanically.

The lifetime predictions of the artificially aged heat district pipes at a constant temperature of 180 °C are presented in Table 31. Specimens were taken out from the chamber after 750, 2000, 2500 and 3150 hours of exposure, and the PUR near to the steel pipe was evaluated under TGA. Lifetime predictions were calculated following the Chang method as described above. The lifespan for the unaged sample, assuming that it works at a continuous service temperature of 180 °C, was predicted at 876 hours. From the mechanical evaluation, the pipe failed after an exposure time between 2500 and 3150 hours, indicating the end of the artificial aging test and referred to 100% of the total exposure time. Specimens that were removed from the aging chamber after 750 hours (24% of total exposure time), the remaining lifetime was calculated for another 613 hours, which is equivalent to the 70% of the total life cycle of the heat district pipe. In the same way, PUR evaluated after 2000 and 2500 hours (63% and 79% of exposure time respectively), have an additional lifespan of 350 and 88 hours for the respective exposure times. The remaining lifetime of the sample that was aged 3150 hours was predicted in 17 hours, which is equivalent to the 2% of its total life cycle. Despite the considerable variation between the predicted total lifespan of the unaged PUR -determined in 876 hours-, and the experimental values -near to 3150 hours-,

it is possible to evidence a correlation between the percentages of the experimental exposure time and the percentages of the remaining predicted lifetime, showed both in grayscale in Table 31.

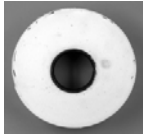

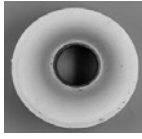
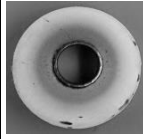
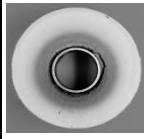

Artificial Aging at a Continuous Temperature of 180°C					
					
					
Exposure Time [Hours]	0	750	2000	2500	3150 (near to failure)
Exposure time [%]	0	24	63	79	100
Remaining lifetime [hours] predicted after exposure to respective hours	876	613	350	88	17
Remaining lifetime [%]	100	70	40	10	2

Table 31. Artificial aging at a constant temperature of 180 °C and different exposure times. The corresponding lifetime predictions were calculated following the Chang method.

8.3. CHAPTER SUMMARY

Accelerated aging was used to correlate lifetime predictions through the analysis of the kinetics of degradation using TGA experiments and mechanical tests. Important kinetic degradation data and lifetime predictions can be calculated from thermal analysis. In this chapter it was demonstrated that the Chang method, which requires only one heating rate per sample, showed comparable results with those obtained from another, reliable but more time consuming, methods like the OFW, which requires at least three heating rates per sample.

Lifetime estimations calculated from Chang analysis exhibited reasonable values for polyurethane-based polymers. Although there is not enough information in the literature about the long-term durability of TPU, the results obtained for the rigid PUR were approximated to previous experimental aging test, and they could be correlated in good agreement to the Standard EN 253. On the other hand, the corresponding kinetic parameters for the adhesive coatings in the hybrid composite, estimated by Chang and Friedman, were not reliable enough. That suggests that kinetics of degradation for solid decomposition of cured polymers cannot be estimated accurately due to their molecular complexity. Nevertheless, hygrothermally pre-aged polyurethanes and coatings exhibited a shorter lifecycle when they are subjected to different continuous operation temperatures. Lower lifetimes under thermal stresses of rigid and thermoplastic polyurethanes and adhesive promoters as well, are correlated to the lower activation energies detected by Chang, OFW, and Friedman methods.

From the lifetime estimations, as presented in Figure 111 and Figure 127, there is evidence suggesting that durability of polyurethane-based polymers is largely influenced by the combination of environments with high temperatures and certain degree of humidity. However, the combination of high humidity and temperature, i.e. 40 °C/90%RH, which is normally found in tropical environments, resulted in less harmful effects in the durability of the polymers when it was compared to the thermoplastic polyurethane subjected to a relative high temperature and low humidity (85 °C/40 % RH).

It is also worth to mention that accurate lifetime prediction for polymeric systems is, in most of the cases, a rather difficult task due to a number of variables involved in the service operational conditions, such as corrosion on the metal substrate, unexpected variations in humidity and temperature, quality of raw materials, environmental exposure, among others. However, it was evidenced that TGA is a primary tool to predict lifetime, especially for the thermoplastic and thermosetting polyurethanes, although results showed large deviations for some specific samples.

9. RELEVANT CONCLUSIONS AND OUTLOOK

- PART I. ADHESION AND ANNEALING

Adhesion of TPU on the steel substrate using the in-house and e-coat adhesive promoters was successful due to the contribution of new physical-chemical and mechanical interactions at the polymer-coating interface. Overmolding of the TPU on the pre-coated metal sheets triggered functional groups on surface producing strong joints between the TPU and the adhesive promoter. It is assumed that molecular interactions at TPU/e-coat interfaces are similar to those occurring at the TPU/in-house hybrid, which takes place between the TPU urethane reactive NH groups and at urethane and OH polar groups of both adhesive promoters.

The increase of the practical adhesive force in the hybrid after annealing at 100 °C for 20 hours occurs by the combination of two contributions: first, the rearrangement of the long-range hard segment crystallites of the TPU, as it was measured by the widening of the melting enthalpy in DSC analysis. This is also correlated with the higher tensile strength observed in the single TPU strips after annealing at the same temperature. The alignment of the hard segment crystals in the direction of processing increased the adhesion strength of the polymer to the substrate due to higher shearing stresses required to remove the polymer from the substrate. Annealing at lower temperatures did not represent a significant change in the mechanical or thermal properties.

The second contribution of annealing to interfacial adhesion is assigned to the increase of the anchoring density at the hybrid joints. As exhibited in the peel test, the outstanding adhesion and stability of the joints after the thermal treatment took place, due to desorption of water molecules at the polymer-coating interface, as it was correlated to the weight reduction of single components after the same treatment. Water desorption occurred on both substrates, but was particularly high in the e-coat steel: this could be attributed to the highly polar epoxy-based matrix -as detected in XPS- that facilitates water adsorption. Desorption, nevertheless, increased intermolecular adhesive forces at hybrid joints, with a consequent improvement of durability and stability, even after hygrothermal aging. Failure modes in hybrids switched from purely adhesive at the TPU-coating interface to a cohesive failure of the coating after annealing at 100 °C. It is also likely that homogeneity of the coat increases anchoring density between the TPU and coating.

- **PART II. HYGROTHERMAL AGING AND DURABILITY**

Hygrothermal aging of single TPU stripes evidenced a steady behavior in terms of its ultimate strength-strain. Catastrophic failure of the polymer did not occur in any of the different artificial environments, as it was reported by Hoikkanen et al. [64]. Thermal analysis of the overmolded TPU in direct contact with the intermediate layers showed negligible changes in the T_g , indicating that hygrothermal external conditions did not plasticized the polymer nor altered the amorphous domains. The heat of fusion also remained relatively invariant, suggesting no compromising effects in the crystalline domains.

On the other hand, adhesion strength of hybrids was significantly affected by accelerated aging at specimens subjected to 85 °C/40 %RH and 85 °C/85 %RH. In the latter condition, the adhesion dropped sharply just after 49 hours of exposure and so the weathering test was stopped just after 625 hours of exposure. For the other hygrothermal environments, samples were subjected to 1000 hours. The rapid drop of adhesion strength indicated that water vapor diffuses faster at the polymer-coating joint destroying intermolecular forces. Annealed hybrids exhibited a much better performance because of the apparent increased in the anchoring density at the joint interface. Specimens subjected to tropical conditions, i.e. 40 °C/90 %RH, indicated a stable and reliable performance in terms of adhesion until the end of the experiment at 1000 hours.

It is conclusive that progressive failure of the composite is strongly dependent on water diffusion rather than temperature decomposition, as it was detected by FTIR and observed in the micrographs on the aged hybrid surfaces. Diffusion to the hybrid dissimilar interfaces was much faster than the hydrolysis of the individual components. Another important consideration is that aging on hybrids manufactured on plain steel oxidized readily the metal surface with a subsequent destruction of the polyester-based coat that was applied on top of the steel. For that reason, it is strongly recommended to use an anti-corrosive superficial treatment on the metal substrates additionally to the phosphated conversion layer to improve durability and life cycle of the hybrid part.

- **PART III. DURABILITY AND LIFETIME: PERMEATION AND DIFFUSION**

Water uptake of TPU was higher in annealed samples indicating a rearrangement of hard and soft segments of the polymer. Annealing is likely changing the distribution of intermolecular hydrogen bonds within the hard and crystalline domains favoring for tighter and stronger bonds. This also goes with a decrease of intermolecular H bonding distances, and a corresponding increase of free volume in the amorphous domains. Permeation of N₂, O₂ and CO₂ gases through a TPU film was also faster for the heat-treated samples. However, adhesion forces in annealed hybrids were significantly higher, so it is

proposed that polar H₂O molecules diffusing into the annealed TPU, were rather stored in the larger free volume than diffused throughout the thermoplastic elastomer. On the other hand, permeation of gases was faster because of their relative small size and reduced polarity, so they moved easily through the larger free volume in the polymer structure.

Diffusion time of H₂O in TPU was successfully calculated and correlated to additional immersion tests that are not presented in this work. However, precise calculations of the time required for destruction of interactions at hybrid interfaces is rather complex due to the physical-chemical and electro-chemical processes that may happen also at the steel surface; additionally, it was found that diffusion at the joint edges occurred simultaneously.

- **PART IV. DURABILITY AND LIFETIME: THERMAL LOADS**

Accelerated aging was used to correlate lifetime predictions through the analysis of the kinetics of degradation using TGA experiments and mechanical tests. Important kinetic degradation data and lifetime predictions have been calculated from thermal analysis. In this work, the Chang method, which requires only one heating rate per sample, showed comparable results with those obtained from other methods like the OFW. Lifetime estimations for TPU and rigid PUR based on Chang analysis, exhibited reasonable values.

Although there is not enough information in the literature about long-term durability of TPU, results obtained for rigid PUR were approximated to previous experimental aging tests; additionally, the predicted lifetime could be correlated in a good agreement to the Standard EN 253. On the other hand, the corresponding kinetic parameters for the adhesive coatings in the hybrid composite, estimated by Chang and Friedman, were not reliable enough. That suggests that kinetics of degradation for solid decomposition of cured thermosetting polymers cannot be estimated by this means due to its molecular complexity.

The calculated values of the activation energy evidence that durability of the polyurethane-based polymers is definitely affected by temperature and humidity at the conditions described in this work. Lifecycle is directly related to the kinetic parameters determined experimentally from TGA experiments, especially the activation energy, E_A . This kinetic parameter for pre-aged specimens, and particularly for those subjected to higher temperature conditions, were lower when compared to the fresh polymer. All three TGA methods evaluated showed the same tendency, meaning that lower E_A transfers into a shorter lifetime.

It is also worth to mention that accurate lifetime predictions for polymeric systems is, in most of the cases, a rather difficult task due to the amount of variables involved in the service operational conditions, such as corrosion on the substrate, unexpected variations in humidity and temperature, quality of raw materials, environmental exposure, among others. Nonetheless, it was demonstrated that TGA analysis is a primary tool to predict lifetime for thermoplastic and thermosetting polyurethanes, although results showed large deviations for some specific samples. This demonstrates that further investigation for reliable prediction is still a requirement.

OUTLOOK

- It is interesting to perform more detailed experiments in order to isolate variables and determine in the most precisely manner the direct contributions on adhesion from the TPU strength and from the physical-chemical and mechanical interactions at the polymer-coating interface.
- Although diffusion time of H₂O through TPU could be calculated, the time that water molecules take to interact and destroy the bonds at the polymer-coating and coating-metal interfaces is rather complex due to the several physical-chemical and electro-chemical processes that take place also at the steel surface and require further detailed research. In future works it is necessary to investigate adhesion and corrosion properties in shorter time ranges, so diffusion parameters and lifetime estimations may be predicted more accurately.
- Other methods should be reviewed in order to calculate precisely the kinetics of degradation for solid decomposition of crosslinked and cured polymers. In this work, it was not possible to determine the apparent activation energies for the adhesive promoters by the Chang, Friedman nor OFW method due to the impossibility of extracting enough material from the coated surface.
- Further research is necessary in order to evaluate durability of hybrids exposed to low temperature environments to clearly identify the effects at material and joint level. Additionally, an investigation of the combined effect of UV radiation with temperature and humidity is required to have a better idea on the failure modes at the polymer-metal interface under such environments.

10. REFERENCES

- [1] M. Hoikkanen, Injection Moulded Thermoplastic Elastomer – Metal Hybrids. PhD Thesis, Tampere University of Technology, 2012.
- [2] K. Martinsen, S.J. Hu, B.E. Carlson, Joining of dissimilar materials, *CIRP Ann. - Manuf. Technol.* 64 (2015) 679–699. doi:10.1016/j.cirp.2015.05.006.
- [3] S.T. Amancio-Filho, J.F. dos Santos, Joining of Polymers and Polymer – Metal Hybrid Structures : Recent Developments and Trends, *Polym. Eng. Sci.* 49 (2009) 1461–1476. doi:10.1002/pen.
- [4] M. Fischer, Prüfung und Qualitätssicherung beim Mehrkomponenten-spritzgießen. Projektarbeit, 2013.
- [5] A. Puentes-Parodi, I. Kuehnert, Effects of Annealing on the Bonding Properties of Polymer-Metal Hybrids, in: *ANTEC® 2016 -Society Plast. Eng., Indianapolis*, 2016: pp. 591–595.
- [6] W.D. Callister, *Materials Science*, 7th ed., John Wiley & Sons, Ltd, 2007.
- [7] M. Ashby, H. Shercliff, D. Cebon, *Materials: Engineering, Science, Processing and Design*, 2007.
- [8] F.C. Campbell, *Structural Composite Materials*, American Society of Materials, 2010.
- [9] M. Grujicic, V. Sellappan, L. Mears, X. Xuan, N. Seyr, M. Erdmann, et al., Selection of the spraying technologies for over-coating of metal-stampings with thermo-plastics for use in direct-adhesion polymer metal hybrid load-bearing components, *J. Mater. Process. Technol.* 198 (2008) 300–312. doi:10.1016/j.jmatprotec.2007.07.011.
- [10] J.F. Shackelford, W. Alexander, *Materials Science and Engineering Handbook*, 3rd ed., CRC Press, 2001.
- [11] American Society of Materials, *Metals Handbook - Desk Edition*, ASM International, 2001. doi:10.1017/CBO9781107415324.004.
- [12] C.A. Harper, *Modern Plastics Handbook*, McGraw-Hill, 1999.
- [13] M. Grujicic, V. Sellappan, M. a. Omar, N. Seyr, A. Obieglo, M. Erdmann, et al., An overview of the polymer-to-metal direct-adhesion hybrid technologies for load-bearing automotive components, *J. Mater. Process. Technol.* 197 (2008) 363–373. doi:10.1016/j.jmatprotec.2007.06.058.
- [14] LANXESS Energizing Chemistry, *Plastic/Metal Hybrid Technology*, (2015). <https://techcenter.lanxess.com/scp/americas/en/innoscp/tech> (accessed April 3, 2017).
- [15] Dow Automotive Systems, *Structural Bonding of Lightweight Cars*, (2015) 12. <http://msdssearch.dow.com/PublishedLiteratureDOWCOM/> (accessed March 12, 2017).
- [16] Basf, *PUR Elastogran Technical Sheet BASF*, (2014) 10. <http://www.polyurethanes.basf.de/pu/solutions/de/> (accessed December 12, 2017).
- [17] Evonik Resource Efficiency GmbH, *VESTAMELT® Hylink Adhesion Promoter*, (2016) 2. <http://adhesives-sealants.evonik.com/sites/lists/RE/DocumentsAC/> (accessed March 15, 2017).
- [18] R.D. Leaversuch, *Plastic-Metal Hybrids Make Headway On and Off the Road*, *Plast. Technol.* (2003). <http://www.ptonline.com/articles/plastic-metal-hybrids-make-headway-on-and-off-the-road> (accessed May 3, 2017).
- [19] Inovon, *Metal-Plastic Composites*, (2015). <http://www.inovan.de/prym/proc/docs/0H0I004R2.html> (accessed May 3, 2017).

-
- [20] LANXESS, PLASTIC/METAL Hybrid Technology, (2005) 8.
<https://techcenter.lanxess.com/scp/americas/en/docguard/> (accessed May 3, 2017).
 - [21] H.M. Wong, K.W.K. Yeung, K.O. Lam, V. Tam, P.K. Chu, K.D.K. Luk, et al., A biodegradable polymer-based coating to control the performance of magnesium alloy orthopaedic implants., *Biomaterials*. 31 (2010) 2084–96. doi:10.1016/j.biomaterials.2009.11.111.
 - [22] M. Grujicic, V. Sellappan, S. Kotrika, G. Arakere, A. Obieglo, M. Erdmann, et al., Suitability analysis of a polymer–metal hybrid technology based on high-strength steels and direct polymer-to-metal adhesion for use in load-bearing automotive body-in-white applications, *J. Mater. Process. Technol.* 209 (2009) 1877–1890. doi:10.1016/j.jmatprotec.2008.04.050.
 - [23] G. Lucchetta, F. Marinello, P.F. Bariani, Aluminum sheet surface roughness correlation with adhesion in polymer metal hybrid overmolding, *CIRP Ann. - Manuf. Technol.* 60 (2011) 559–562. doi:10.1016/j.cirp.2011.03.073.
 - [24] M. Grujicic, Injection over molding of polymer-metal hybrid structures, *Am. J. Sci. Technol.* 1 (2014) 168–181.
 - [25] I. Kühnert, S. Druwen, Hard-soft material composites: Processing and adhesive strength test, *TPE Mag.* 4 (2015) 272–275.
 - [26] J.-H. Kweon, J.-W. Jung, T. Kim, J. Choi, D. Kim, Failure of carbon composite-to-aluminum joints with combined mechanical fastening and adhesive bonding, *Compos. Struct.* 75 (2006) 192–198.
 - [27] J.R. Vinson, Mechanical fastening of polymer composites, *Polym. Eng. Sci.* 29 (2004) 1332–1339.
 - [28] D.W. Oplinger, *Mechanical Fastening and Adhesive Bonding - Handbook of Composites*, Springer, 1998.
 - [29] J.A. Speck, *Mechanical Fastening, Joining, and Assembly*, CRC Press, 1997.
 - [30] H. Mizukoshi, H. Okada, Fatigue Properties of Mechanical Fastening Joints, *Mater. Sci. Forum.* 242 (1997) 231–242.
 - [31] O. Dos Santos Ferreira, a. Stevens, C. Schrauwen, Quantitative comparison of adhesion in metal-to-plastic systems, *Thin Solid Films*. 517 (2009) 3070–3074. doi:10.1016/j.tsf.2008.11.117.
 - [32] UK Composites Association, *Adhesive bonding - A guide to best practice*, (2013).
<http://www.compositesuk.co.uk/Information/Tools/AdhesivesToolkit.aspx> (accessed May 10, 2016).
 - [33] UK Composites Association, *Adhesive bonding of composites*, (2013).
<http://www.compositesuk.co.uk/LinkClick.aspx?fileticket=RwPAVyA0UNA%3D&tabid=111&mid=550> (accessed May 3, 2017).
 - [34] Kaysun Corporation, *Overmolding Fundamentals Report*, 2016.
 - [35] GLS Total TPE Solutions, *Overmolding Guide*, 11 (2004) 30.
http://www.polyone.com/files/resources/Overmold_Design_Guide.pdf (accessed May 3, 2017).
 - [36] L. Hudacek, How to Optimize Adhesion in Hard-Soft Overmolding, *Plast. Technol.* (2004).
<http://www.ptonline.com/articles/how-to-optimize-adhesion-in-hard-soft-overmolding> (accessed May 3, 2017).
 - [37] P. Kah, R. Suoranta, J. Martikainen, C. Magnus, *Techniques for Joining Dissimilar Materials : Metals and Polymers*, 36 (2014) 152–164.
 - [38] M. Troughton, *Handbook of Plastics Joining. A Practical Guide*, 2nd ed., William Andrew Inc., 2008.

- doi:10.1017/CBO9781107415324.004.
- [39] S.J. Marshall, S.C. Bayne, R. Baier, A.P. Tomsia, G.W. Marshall, A review of adhesion science., *Dent. Mater.* 26 (2010) e11–6. doi:10.1016/j.dental.2009.11.157.
 - [40] A.J. Kinloch, Review: the science of adhesion, *J. Mater. Sci.* 15 (1980) 2141–2166.
 - [41] S.M. Goushegir, Friction Spot Joining of Polymer-Metal Hybrid Structures, (2015) 1–4. www.hzg.de/institutes_platforms/materials_research/materials_mechanics/advanced_metal_polymer_structures/techniques/ (accessed May 3, 2017).
 - [42] L. Blaga, Friction Riveting, (2015) 2. www.hzg.de/institutes_platforms/materials_research/materials_mechanics/advanced_metal_polymer_structures/techniques/ (accessed May 1, 2017).
 - [43] J. Lindsay, Bonding of Rubber, in: *Rubber to Met. Bond.*, Rapra Technology Limited, 1997: p. 1.
 - [44] M. Rooke, Elastomer to Substrate Bonding, in: *Rubber to Met. Bond.*, Rapra Technology Limited, 1997: p. 4.
 - [45] M.M. Chehimi, J.F. Watts, An XPS study of the steel-aromatic moisture-cured urethane interface, *J. Adhes. Sci. Technol.* 6 (1992) 377–393. doi:10.1163/156856192X00205.
 - [46] J. Gaehde, J. Friedrich, R. Gehrke, J. Sachse, Adhesion of Polyurethane to Surface-modified Steel, *J. Adhes.* 6 (2012) 569–586. doi:10.1163/156856192X00403.
 - [47] B. Escaig, Binding metals to polymers. A short review of basic physical mechanisms, *J. Phys. IV.* 3 (1993) 753–761. doi:10.1051/jp4:19937120.
 - [48] G. Ramarathnam et. al., Joining of Polymers to Metal, *Weld. Res. Suppl.* (1992) 483–490.
 - [49] D.A. Dillard, A. V Pocius, Fundamentals of stress transfer in bonded systems, in: *Mech. Adhes.*, Elsevier, 2002: pp. 1–44.
 - [50] D.E. Packham, *Handbook of Adhesion*, 2nd ed., John Wiley & Sons, Ltd, Chichester, UK, 2005. doi:10.1002/0470014229.
 - [51] A. Baldan, Adhesively-bonded joints and repairs in metallic alloys, polymers and composite materials: Adhesives, adhesion theories and surface pretreatment, *J. Mater. Sci.* 39 (2004) 1–49. doi:10.1023/B:JMSC.0000007726.58758.e4.
 - [52] C. Boiziau, G. Lecayon, Adhesion of polymers to metals: A review of the results obtained studying a model system, *Surf. Interface Anal.* 12 (1988) 475–485.
 - [53] A. Baldan, Adhesion phenomena in bonded joints, *Int. J. Adhes. Adhes.* 38 (2012) 95–116. doi:10.1016/j.ijadhadh.2012.04.007.
 - [54] A. Pizzi, K.L. Mittal, *Handbook of Adhesive Technology*, 2nd ed., Marcel Dekker, 2003. doi:10.1201/9780203904046.
 - [55] P. a. Fabrin, M.E. Hoikkanen, J.E. Vuorinen, Adhesion of thermoplastic elastomer on surface treated aluminum by injection molding, *Polym. Eng. Sci.* 47 (2007) 1187–1191. doi:10.1002/pen.20801.
 - [56] J.F. Silvain, J.J. Ehrhardt, An overview on metal/PET adhesion, *Thin Solid Films.* 236 (1993) 230–235. doi:10.1016/0040-6090(93)90675-F.
 - [57] C. Ochoa-Putman, U.K. Vaidya, Mechanisms of interfacial adhesion in metal–polymer composites – Effect of chemical treatment, *Compos. Part A Appl. Sci. Manuf.* 42 (2011) 906–915.

- doi:10.1016/j.compositesa.2011.03.019.
- [58] D.E. Packham, Surface energy, surface topography and adhesion, *Int. J. Adhes. Adhes.* 23 (2003) 437–448. doi:10.1016/S0143-7496(03)00068-X.
 - [59] M.S. Islam, L. Tong, P.J. Falzon, Influence of metal surface preparation on its surface profile, contact angle, surface energy and adhesion with glass fibre prepreg, *Int. J. Adhes. Adhes.* 51 (2014) 32–41. doi:10.1016/j.ijadhadh.2014.02.006.
 - [60] E. Sarlin, E. Heinonen, J. Vuorinen, M. Vippola, T. Lepistö, Adhesion properties of novel corrosion resistant hybrid structures, *Int. J. Adhes. Adhes.* 49 (2014) 51–57. doi:10.1016/j.ijadhadh.2013.12.009.
 - [61] C. Hopmann, J. Wunderle, A. Neus, P. Ochotta, K. Bobzin, C. Schulz, et al., Influence of surface treatment on the bond strength of plastics/metal hybrids, *Zeitschrift Kunststofftechnik*. 11 (2015).
 - [62] J. Cognard, Some recent progress in adhesion technology and science, *Comptes Rendus Chim.* 9 (2006) 13–24. doi:10.1016/j.crci.2004.11.016.
 - [63] Department of Chemistry of Purdue University, London Dispersion Forces, (2015). <https://www.chem.purdue.edu/gchelp/liquids/disperse.html> (accessed February 3, 2017).
 - [64] M. Hoikkanen, M. Honkanen, L. Frisk, M. Vippola, T. Lepistö, J. Vuorinen, Metal–thermoplastic urethane hybrids in environmental exposure, *Int. J. Adhes. Adhes.* 35 (2012) 21–26. doi:10.1016/j.ijadhadh.2012.01.024.
 - [65] E. Sarlin, M. Hoikkanen, L. Frisk, J. Vuorinen, M. Vippola, T. Lepistö, Ageing of corrosion resistant steel/rubber/composite hybrid structures, *Int. J. Adhes. Adhes.* 49 (2014) 26–32. doi:10.1016/j.ijadhadh.2013.12.008.
 - [66] H. Vakili, B. Ramezanzadeh, R. Amini, The corrosion performance and adhesion properties of the epoxy coating applied on the steel substrates treated by cerium-based conversion coatings, *Corros. Sci.* 94 (2015) 466–475. doi:10.1016/j.corsci.2015.02.028.
 - [67] X. Jiang, X. Qiang, M.H. Kolstein, F.S.K. Bijlaard, Experimental investigation on mechanical behaviour of FRP-to-steel adhesively-bonded joint under combined loading - Part 2: After hygrothermal ageing, *Compos. Struct.* 125 (2015) 687–697. doi:10.1016/j.compstruct.2014.12.040.
 - [68] ASM International, *ASM Handbook Volume 13A: Corrosion: Fundamentals, Testing, and Protection*, 2004.
 - [69] European Commission, *Surface Treatment of Metals and Plastics - Reference Document*, 2006.
 - [70] International Lead Zinc Research Organization, *Zinc Phosphate Treatments for Painted Galvanized & Galvannealed Sheet Products - Report*, 2003.
 - [71] American Society of Materials, *ASM Handbook Volume 5: Surface Engineering*, ASM International, 1994.
 - [72] CathoCare by BASF, *Grundlagen der Elektrotauchlackierung-Kundenschulung*, Münster, 2009.
 - [73] Huntsman, *A guide to thermoplastic polyurethanes (TPU)*, (2010) 1–25. http://www.huntsman.com/portal/page/portal/polyurethanes/Media Library/global/files/guide_tpu.pdf (accessed May 3, 2017).
 - [74] H.J. Qi, M.C. Boyce, *Stress-Strain Behavior of Thermoplastic Polyurethane - Report*, 2004.
 - [75] G. Pompe, a. Pohlers, P. Pötschke, J. Pionteck, Influence of processing conditions on the multiphase structure of segmented polyurethane, *Polymer (Guildf)*. 39 (1998) 5147–5153. doi:10.1016/S0032-3861(97)10350-0.

- [76] Z.S. Petrović, J. Ferguson, Polyurethane elastomers, *Prog. Polym. Sci.* 16 (1991) 695–836. doi:10.1016/0079-6700(91)90011-9.
- [77] Y.J. Li, T. Gao, J. Liu, K. Linliu, C.R. Desper, B. Chu, Multiphase Structure of a Segmented Polyurethane - Effects of Temperature and Annealing, *Macromolecules*. 25 (1992) 7365–7372. doi:10.1021/ma00052a045.
- [78] F. Piana, J. Pionteck, Composite s Scien ce and Techn ology Effect of the melt processing conditions on the conductive paths formation in thermoplastic polyurethane / expanded graphite (TPU / EG) composites, *Compos. Sci. Technol.* 80 (2013) 39–46. doi:10.1016/j.compscitech.2013.03.002.
- [79] A. Frick, A. Rochman, Characterization of TPU-elastomers by thermal analysis (DSC), *Polym. Test.* 23 (2004) 413–417. doi:10.1016/j.polymertesting.2003.09.013.
- [80] O. Klæusler, S. Clauss, L. Luebke, J. Trachsel, P. Niemz, Influence of moisture on stress-strain behaviour of adhesives used for structural bonding of wood, *Int. J. Adhes. Adhes.* 44 (2013) 57–65. doi:10.1016/j.ijadhadh.2013.01.015.
- [81] I. Yilgor, E. Yilgor, I.G. Guler, T.C. Ward, G.L. Wilkes, FTIR investigation of the influence of diisocyanate symmetry on the morphology development in model segmented polyurethanes, *Polymer (Guildf)*. 47 (2006) 4105–4114. doi:10.1016/j.polymer.2006.02.027.
- [82] H. Munkert, F. Voigts, L. Wegewitz, H. Palkowski, W. Maus-Friedrichs, The interaction of epoxy adhesives with steel surfaces, *Materwiss. Werksttech.* 44 (2013) 36–43. doi:10.1002/mawe.201300051.
- [83] R.A. Pethrick, Design and ageing of adhesives for structural adhesive bonding - A review, *Proc. Inst. Mech. Eng. Part L J. Mater. Des. Appl.* 229 (2014) 349–379. doi:10.1177/1464420714522981.
- [84] M. Honkanen, M. Hoikkanen, M. Vippola, J. Vuorinen, T. Lepistö, Metal–Plastic Adhesion in Injection-Molded Hybrids, *J. Adhes. Sci. Technol.* 23 (2009) 1747–1761. doi:10.1163/016942409X12489445844435.
- [85] ASM International, *ASM Handbook Volume 13: Corrosion*, ASM International, 1992.
- [86] H. Aglan, M. Calhoun, L. Allie, Effect of UV and Hygrothermal Aging on the Mechanical Performance of Polyurethane Elastomers, *J. Appl. Polym. Sci.* 108 (2008) 558–564. doi:10.1002/app.
- [87] A. Boubakri, N. Haddar, K. Elleuch, Y. Bienvenu, Impact of aging conditions on mechanical properties of thermoplastic polyurethane, *Mater. Des.* 31 (2010) 4194–4201. doi:10.1016/j.matdes.2010.04.023.
- [88] A. Boubakri, K. Elleuch, N. Guermazi, H.F. Ayedi, Investigations on hygrothermal aging of thermoplastic polyurethane material, *Mater. Des.* 30 (2009) 3958–3965. doi:10.1016/j.matdes.2009.05.038.
- [89] U. Braun, E. Lorenz, M. Maskos, Investigation of the durability of poly(ether urethane) in water and air, *Int. J. Artif. Organs.* 34 (2011) 129–133. doi:10.5301/IJAO.2011.6408.
- [90] M. Herrera, G. Matuschek, a. Kettrup, Thermal degradation of thermoplastic polyurethane elastomers (TPU) based on MDI, *Polym. Degrad. Stab.* 78 (2002) 323–331. doi:10.1016/S0141-3910(02)00181-7.
- [91] Simon J. et al., Thermal Stability of Polyurethanes, *Chromatographia*. 25 (1988) 99–106. doi:10.1007/BF02259024.
- [92] BASF, Thermoplastic Polyurethane Elastomers (TPU). Elastollan-Material Properties, (2011) 1–44. http://www.polyurethanes.basf.de/pu/solutions/en/function/conversions:/publish/content/group/Arbeitsgebiete_und_Produnkte/Thermoplastische_Spezialelastomere/Infomaterial/elastollan_verarbeitung_en.pdf (accessed April 10, 2017).
- [93] ISO International, ISO 4628:2016, Paints and varnishes — Evaluation of degradation of coatings — Designation of quantity and size of defects, and of intensity of uniform changes in appearance, 2016.

-
- [94] E. Petrie, Osmotic Blisters in Coatings and Adhesives, *Mater. Today*. (2011). <http://www.materialstoday.com/metal-finishing/features/osmotic-blisters-in-coatings-and-adhesives/> (accessed December 23, 2016).
 - [95] C.H. Hare, Blistering of Paint Films on Metal, Part 1: Osmotic Blistering, *J. Prot. Coatings Linings*. (1998) 45–63.
 - [96] X. Yang, D. Tallman, S. Croll, G. Bierwagen, Morphological changes in polyurethane coatings on exposure to water, *Polym. Degrad. Stab.* 77 (2002) 391–396. doi:10.1016/S0141-3910.
 - [97] N. Guerhazi, K. Elleuch, H.F. Ayedi, P. Kapsa, Aging effect on thermal, mechanical and tribological behaviour of polymeric coatings used for pipeline application, *J. Mater. Process. Technol.* 203 (2008) 404–410. doi:10.1016/j.jmatprotec.2007.10.062.
 - [98] A. Puentes-Parodi, M. Gedan-Smolka, A. Leuteritz, I. Kuehnert, Artificial Aging and Failure Modes of TPU-Metal Hybrid Composites, in: 32nd, Int. Conf. Polym. Process. Soc., Polymer Processing Society, Lyon, France, 2016: pp. 113–114.
 - [99] M. Heshmati, R. Haghani, M. Al-Emrani, Effects of moisture on the long-term performance of adhesively bonded FRP/steel joints used in bridges, *Compos. Part B Eng.* 92 (2016) 447–462. doi:10.1016/j.compositesb.2016.02.021.
 - [100] R. Leger, A. Roy, J.C. Grandidier, A study of the impact of humid aging on the strength of industrial adhesive joints, *Int. J. Adhes. Adhes.* 44 (2013) 66–77. doi:10.1016/j.ijadhadh.2013.02.001.
 - [101] R. a. Gledhill, a. J. Kinloch, Environmental Failure of Structural Adhesive Joints, *J. Adhes.* 6 (2006) 315–330. doi:10.1080/00218467408075035.
 - [102] R. Leger, A. Roy, J.C. Grandidier, A study of the impact of humid aging on the strength of industrial adhesive joints, *Int. J. Adhes. Adhes.* 44 (2013) 66–77.
 - [103] T.S. Williams, H. Yu, P.-C. Yeh, J.-M. Yang, R.F. Hicks, Atmospheric pressure plasma effects on the adhesive bonding properties of stainless steel and epoxy composites, *J. Compos. Mater.* 48 (2012) 219–233. doi:10.1177/0021998312470150.
 - [104] Ingenieurgesellschaft für Energie-technik und FernwärmeChemnitz mbH, IMA Materialforschung und Anwendungstechnik, Leibniz Institut für Polymerforschung, Zeitstandfestigkeit von Kunststoffmantelrohren, 2011. doi:10.1017/CBO9781107415324.004.
 - [105] A. Leuteritz, K.-D. Döring, T. Lampke, I. Kuehnert, Accelerated ageing of plastic jacket pipes for district heating, *Polym. Test.* 51 (2016) 142–147. doi:10.1016/j.polymertesting.2016.03.012.
 - [106] A. Puentes-Parodi, I. Kuehnert, A. Leuteritz, Degradation (Kinetics) and Lifetime Predictions of Rigid Polyurethane for Preinsulated Steel Pipes, in: 31st, Int. Conf. Polym. Process. Soc., Polymer Processing Society, Jeju Island, South Korea, 2015: p. 763.
 - [107] P.K. Roy, Thermal degradation studies of LDPE containing cobalt stearate as pro-oxidant, *EXPRESS Polym. Lett.* 1 (2007) 208–216. doi:10.3144/expresspolymlett.2007.32.
 - [108] X.-B. Li, H.-B. Cao, Y. Zhang, Thermal degradation kinetics of rigid polyurethane foams blown with water, *J. Appl. Polym. Sci.* 102 (2006) 4149–4156. doi:10.1002/app.24379.
 - [109] H. Wang, X. Tao, E. Newton, Thermal degradation kinetics and lifetime prediction of a luminescent conducting polymer, *Polym. Int.* 53 (2004) 20–26. doi:10.1002/pi.1279.
 - [110] ArcelorMittal, Cold Rolled Steel Technical Sheet for Drawing and Forming, (2010) 1–3. https://flatsteel.arcelormittalsa.com/fspcatalogue/DataSheets/UnCoated/Web_datasheet_b3.1.pdf

- (accessed May 4, 2017).
- [111] National Technical University KhPI, European Steel and Alloy Grades / Numbers Searchable Database, (n.d.). <http://www.steelnumber.com/en/> (accessed April 10, 2017).
 - [112] BASF, Thermoplastic Polyurethane Elastomers (TPU) Processing Recommendations, (2011) 28. http://www.polyurethanes.basf.de/pu/solutions/en/function/conversions:/publish/content/group/Arbeitsgebiete_und_Produnkte/Thermoplastische_Spezialelastomere/Infomaterial/elastollan_verarbeitung_en.pdf (accessed May 4, 2017).
 - [113] BASF, Thermoplastic Polyurethane Elastomers (TPU). Elastollan - Product Range, (2011). http://www.polyurethanes.basf.com/pu/solutions/en/function/conversions:/publish/content/group/News_und_Medien/Spezialelastomere/Thermoplastic_Polyurethane_Elastomers_Product_Range_EN.pdf (accessed May 4, 2017).
 - [114] M.J. Thies, Comparison of tribo and corona charging methods: How they work and the advantages of each, in: Powder Coat. Proc., 1994: pp. 235–251.
 - [115] M. Zimmermann, Haftungsuntersuchung an Kunststoff – Kunststoff – Verbindungen: Optimierung des Montagespritzgießprozesses und der Prüfmethode - Master Thesis, 2013.
 - [116] G. Dillingham, C. Moriarty, The Adhesion of Isocyanate-based Polymers to Steel, J. Adhes. 79 (2003) 269–285. doi:10.1080/00218460390148149.
 - [117] Verein Deutscher Ingenieure, Standard VDI 2199 - Testing the Adhesion of thermoplastic Elastomers (TPE) on Substrates, 2014.
 - [118] G. Paumier, Dynamic contact angle measurement, (2008). https://en.wikipedia.org/wiki/Contact_angle#/media/File:Dynamic_contact_angle_measurement.svg (accessed January 6, 2017).
 - [119] International Electrotechnical Commission, Standard IEC 61340-5-1, 2016.
 - [120] N. Birkner, Q. Wang, How an FTIR Spectrometer Operates, (2016) 1–8. http://chem.libretexts.org/Core/Physical_and_Theoretical_Chemistry/Spectroscopy/Vibrational_Spectroscopy/Infrared_Spectroscopy/ (accessed December 15, 2016).
 - [121] Materials Evaluation and Engineering, Fourier Transform-Infrared Spectroscopy, in: Handb. Anal. Methods Mater., Materials Evaluation and Engineering, Inc, 2014: pp. 19–20.
 - [122] Brugger GmbH, Brugger GDP-C Instructions Manual, 2013.
 - [123] Y. Yuan, R. Lee, Contact Angle and Wetting Properties, in: G. Bracco, B. Holst (Eds.), Surf. Sci. Tech., Springer Series in Surface Sciences, 2013.
 - [124] XPS Casa Software, XPS Spectra, (2013) 1–77. http://www.casaxps.com/help_manual (accessed August 29, 2017).
 - [125] C.M. Brunette, S.L. Hsu, W.J. MacKnight, Hydrogen-Bonding Properties of Hard-Segment Model Compounds in Polyurethane Block Copolymers, Macromolecules. 15 (1982) 71–77. doi:10.1021/ma00229a014.
 - [126] R. King, Additives: Polyolefin Discoloration, Plast. Technol. (2017). <http://www.ptonline.com/articles/additives-polyolefin-discoloration> (accessed September 20, 2017).
 - [127] K. Bruckmoser, K. Resch, Investigation of Ageing Mechanisms in Thermoplastic Polyurethanes by Means of IR and Raman Spectroscopy, Macromol. Symp. 339 (2014) 70–83. doi:10.1002/masy.201300140.

-
- [128] I. Yilgor, E. Yilgor, Structure-Morphology-Property Behavior of Segmented Thermoplastic Polyurethanes and Polyureas Prepared without Chain Extenders, *Polym. Rev.* 47 (2007) 487–510. doi:10.1080/15583720701638260.
 - [129] K. Matsunaga, K. Sato, M. Tajima, Y. Yoshida, Gas Permeability of Thermoplastic Polyurethane Elastomers, *Polym. J.* 37 (2005) 413–417. doi:10.1295/polymj.37.413.
 - [130] R.M. Silverstein, G.C. Bassler, T.. Morrill, *Spectrometric Identification of Organic Compounds*, 4th ed., John Wiley and Sons, 1981.
 - [131] ISO International, ISO 4628-2, Paints and varnishes — Evaluation of degradation of coatings — Designation of quantity and size of defects, and of intensity of uniform changes in appearance — Part 2: Assessment of degree of blistering, 2016.
 - [132] W.J. Sichina, *Characterization of epoxy resins using DSC - PerkinElmer Instruments*, 2000.
 - [133] V. Bellenger, M. Ganem, B. Mortaigne, J. Verdu, Lifetime prediction in the hydrolytic ageing of polyesters, *Polym. Degrad. Stab.* 49 (1995) 91–97. doi:10.1016/0141-3910(95)00049-R.
 - [134] P. Le Gac, D. Choqueuse, D. Melot, B. Melve, L. Meniconi, Life time prediction of polymer used as thermal insulation in offshore oil production conditions: Ageing on real structure and reliability of prediction, *Polym. Test.* 34 (2014) 168–174. doi:10.1016/j.polymertesting.2014.01.011.
 - [135] P.Y. Le Gac, D. Choqueuse, D. Melot, Description and modeling of polyurethane hydrolysis used as thermal insulation in oil offshore conditions, *Polym. Test.* 32 (2013) 1588–1593. doi:10.1016/j.polymertesting.2013.10.009.
 - [136] S. Mondal, J.L. Hu, Z. Yong, Free volume and water vapor permeability of dense segmented polyurethane membrane, *J. Memb. Sci.* 280 (2006) 427–432. doi:10.1016/j.memsci.2006.01.047.
 - [137] H.L. Frisch, “Diffusion in polymers” edited by J. Crank and G. S. Park, Academic Press, London and New York, 1968; 452 pg, *J. Appl. Polym. Sci.* 14 (1970) 1657–1657. doi:10.1002/app.1970.070140623.
 - [138] L. Li, Y. Yu, Q. Wu, G. Zhan, S. Li, Effect of chemical structure on the water sorption of amine-cured epoxy resins, *Corros. Sci.* 51 (2009) 3000–3006. doi:10.1016/j.corsci.2009.08.029.
 - [139] J. Rychlý, A. Lattuat-Derieux, B. Lavédrine, L. Matisová-Rychlá, M. Malíková, K. Csomorová, et al., Assessing the progress of degradation in polyurethanes by chemiluminescence and thermal analysis. II. Flexible polyether- and polyester-type polyurethane foams, *Polym. Degrad. Stab.* 96 (2011) 462–469. doi:10.1016/j.polymdegradstab.2011.01.012.
 - [140] R. Gonçalves, J. Rocco, K. Iha, Thermal Decomposition Kinetics of Aged Solid Propellant Based on Ammonium Perchlorate - AP/HTPB Binder, in: *Appl. Calorim. a Wide Context - Differ. Scanning Calorimetry, Isothermal Titration Calorim. Microcalorim.*, INTECH, 2013: pp. 325–342. doi:10.2514/6.2008-4969.
 - [141] B. Gornicka, L. Gorecki, TGA/DTG/DSC investigation of thermal ageing effects on polyamide-imide enamel, *J. Therm. Anal. Calorim.* 101 (2010) 647–650. doi:10.1007/s10973-010-0883-9.
 - [142] M.E. Brown, *Kinetic Analysis of Isothermal Data*, in: *Introd. to Therm. Anal. Tech. Appl.*, 2nd ed., Springer, 2001. doi:10.1180/minmag.1989.053.373.29.
 - [143] P.P. Kalbende, M. V Tarase, A.B. Zade, Preparation , Characterization and Thermal Degradation Studies of p-nitrophenol Based Copolymer, *Hindawi Publ. Corp.* 2013 (2013) 1–9.
 - [144] A. Puentes-Parodi, M. Gehde, A. Leuteritz, I. Kuehnert, Failure analysis and durability of preinsulating district heat pipes, *Polym. Adv. Technol.* (2017) 1–8. doi:10.1002/pat.4216.

- [145] European Committee for Standardization, EN 253 European standard for district heat pipes, 2009.
- [146] Hunstman, PUR Pipe Insulation Fact Sheet Hunstmann, (2015) 1–16. <http://www.huntsman.com/polyurethanes/> (accessed May 5, 2017).
- [147] Bayer Materials Science, PUR Mondur Technical Sheet Bayer, (2015) 1–2. www.polyurethanes.covestro.com/ (accessed May 2, 2017).
- [148] Logstor, District Heating and Cooling, (2015). www.logstor.com (accessed May 2, 2017).
- [149] J.P. Wightman, T.D. Lin, H.F. Webster, Surface chemical aspects of polymer/metal adhesion, *Int. J. Adhes. Adhes.* 12 (1992) 133–137. doi:10.1016/0143-7496(92)90043-U.
- [150] J. D. Venables, Review Adhesion and durability of metal-polymer bonds, *J. Mater. Sci.* 19 (1984) 2431–2453. doi:10.1007/BF00550796.
- [151] K. Ramani, B. Moriarty, Thermoplastic Bonding to Metals Via Injection Molding for Macro-Composite Manufacture, *Polym. Eng. Sci.* 3 (1998) 1–7. doi:10.1002/pen.10253.
- [152] A.L. Gasparin, C.H. Wanke, R.C.R. Nunes, E.K. Tentardini, C. a. Figueroa, I.J.R. Baumvol, et al., An experimental method for the determination of metal–polymer adhesion, *Thin Solid Films.* 534 (2013) 356–362. doi:10.1016/j.tsf.2013.03.018.
- [153] AGFW Forschung und Entwicklung, AGFW, Technisches Handbuch Qualitätssicherung für zukünftige Kunststoffmantelrohrsysteme, 2017.
- [154] J.H. Flynn, L.A. Wall, A quick, direct method for the determination of activation energy from thermogravimetric data, *Polym. Lett.* 4 (1966) 323–328. doi:10.1002/pol.1966.110040504.
- [155] T. Ozawa, Kinetic Analysis of Derivative Curves in Thermal Analysis, *J. Therm. Anal. Calorim.* 2 (1970) 301–324.
- [156] J. Lefebvre, S. Duquesne, V. Mamleev, M. Le Bras, R. Delobel, Study of the kinetics of pyrolysis of a rigid polyurethane foam: use of the invariant kinetics parameters method, *Polym. Adv. Technol.* 14 (2003) 796–801. doi:10.1002/pat.397.
- [157] H. Haferkamp, K. Nolte, T. Winkler, Forschungsvorhaben Alterungsverhalten von PUR-Hartschaum gedämmten Fernwärmeleitung, 1982.
- [158] G.T. Howard, Biodegradation of polyurethane: a review, *Int. Biodeterior. Biodegradation.* 49 (2002) 245–252. doi:10.1016/S0964-8305(02)00051-3.
- [159] Logstor, District heat pipes for high temperatures, (2016). <https://www.sks-online.com/en/products/pre-insulated-tubes/logstor-en/logstor-high-temperatures/> (accessed August 26, 2016).
- [160] Power Chemical Corporation, Silane Coupling Agent, (1999). powerchemical.net (accessed August 29, 2016).
- [161] Amtec Consultants, Amtec Guide to Coating Failures & Coating Breakdown, (2015). amteccorrosion.co.uk (accessed February 3, 2017).
- [162] The Bernasek Lab - Princeton University, ATR-FTIR, (2016). <http://chemists.princeton.edu/bernasek/atr-ftir> (accessed December 15, 2016).